Optogenetic Regulation of Membrane-Associated Proteins

By

Anna Isabella Wurz

May, 2024

Director of Dissertation: Robert M. Hughes, Ph.D.

Major Department: Chemistry

ABSTRACT

Optogenetics has emerged as a powerful tool for controlling cellular processes with light. Two optogenetic approaches were designed using the flavin-containing photoreceptor Cryptochrome 2 (Cry2) from *Arabidopsis thaliana* that control protein function and target distinct cellular events. These approaches focus on the membrane-bound receptor tyrosine kinase, Eph receptor, and a membrane-associated protein, Inverse Bin, Amphiphysin, and Rvs (I-BAR). Eph receptors are crucial for cell-cell communication, proliferation, and migration. A light-activated EphA1 receptor (EphA1Cry2) was created by fusing Cry2 to the intracellular domains of EphA1 receptor, enabling blue light-dependent oligomerization and auto-phosphorylation of the receptor. Key cell signaling targets were identified and characterized in response to light-stimulated EphA1Cry2 activation. The optogenetic regulation of Eph receptor RTK signaling without the need for external ligand binding promises to be an effective means of controlling individual Eph receptor-mediated activities and creates a path forward for the identification of new Eph-dependent functions. The second developed optogenetic approach

involved membrane remodeling light-gated tools called CRY-BARs; this optogenetic system combines the membrane-binding affinity of the I-BAR domain, a negative membrane-curvature generating domain, with the homo-oligomerizing capability of Cry2. Using immortalized cell lines and primary neuron cultures, the CRY–BAR optogenetic tool evokes membrane dynamic changes associated with cellular activity. Moreover, ezrin was shown to act as a relay between the plasma membrane and the actin cytoskeleton and therefore is an important mediator of CRY-BARs' switch function. CRY–BARs hold promise as a useful addition to the optogenetic toolkit to study membrane remodeling in live cells. Overall, these optogenetic approaches offer precise spatial and temporal control over cellular signaling and membrane dynamics, opening up new possibilities for studying cellular functions and developing novel therapeutic strategies.

Optogenetic Regulation of Membrane-Associated Proteins

A Dissertation

Presented to the Faculty of the Department of Chemistry

East Carolina University

In Partial Fulfillment of the Requirements for the Degree

Doctorate of Philosophy in Interdisciplinary Doctoral Program in Biology, Biomedicine, and Chemistry

By

Anna Isabella Wurz

May, 2024

Director of Dissertation: Robert M. Hughes, Ph.D.
Dissertation Committee Members:
Colin Burns, Ph.D.
Eli Hvastkovs, Ph.D.
Hun Lim, Ph.D.
Erzsebet Szatmari, Ph.D.
Jitka Virag, Ph.D.

ACKNOWLEDGEMENTS

I would like to thank my family, especially my parents, for their constant encouragement and belief in me throughout my academic and professional career; my friends, old and new, that have kept me sane with their humor and love; my fellow lab mates, committee members, the IDPBBC community, Dr. Ariane Peralta, and the chemistry department for their continuous support and assistance throughout my time here at ECU; and especially Dr. Hughes for being the best PI and mentor that I could have asked for (indeed, no words can truly express my gratitude).

I would like to dedicate this dissertation to the memory of:

Rowe Garrett, my grandfather

Dr. Keith Holmes

Butterscotch the Bunny, beloved companion and lab mascot

~ In the ability to dream is the possibility to achieve ~

TABLE OF CONTENTS

TITLE PAGE i

COPYRIGHT PAGE ii

ACKNOWLEDGMENTS iii

LIST OF TABLES vi

LIST OF FIGURES viii

CHAPTER 1: REVIEW OF LITERATURE 1

Optogenetics 1

Cryptochrome 12

Eph Receptors 18

Optogenetic Applications 27

BAR domains 31

Optogenetic Applications 38

References 45

CHAPTER 2: OPTOGENETIC REGULATION OF EPHA1 RTK ACTIVATION AND SIGNALING 56

Introduction 56

Materials and Methods 60

Results and Discussion 66

References 113

CHAPTER 3: CRY-BARS: VERSATILE LIGHT-GATED TOOLS FOR THE REMODELING OF MEMBRANE ARCHITECTURES 123

Introduction 123

Materials and Methods 126
Results and Discussion 131
References 154
CHAPTER 4: CONCLUSION 158
References 161
APPENDIX I: IACUC APPROVAL LETTER FOR CHAPTER 3 162
APPENDIX II: SUPPORTING INFORMATION FOR CHAPTER 2 163
APPENDIX III: SUPPORTING INFORMATION FOR CHAPTER 3 187

LIST OF TABLES

1. Table 2.1. Comparison of significant upregulated and downregulated genes 89
2. Table 2.2. Significant DEGs of interest for PMb-EphA1Cry2Δ light condition compared to its dark condition..... 92
3. Table 2.3. Top up-regulated DEGs by Log2FoldChange for PMb-EphA1Cry2Δ light condition compared to Cry2olig light condition..... 94
4. Table 2.4. Top down-regulated DEGs by Log2FoldChange for PMb-EphA1Cry2Δ light condition compared to Cry2olig light condition..... 95
5. Table 2.5. Significant DEGs of interest for PMb-EphA1Cry2Δ light condition compared to Cry2olig light condition..... 97
6. Table 2.6. Top upregulated DEGs by Log2FoldChange for PMb-EphA1Cry2Δ light condition compared to ephrinA1-stimulated condition 99
7. Table 2.7. Top downregulated DEGs by Log2FoldChange for PMb-EphA1Cry2Δ light condition compared to ephrinA1-stimulated condition 101
8. Table 2.8. Significant DEGs of interest by Log2FoldChange for PMb-EphA1Cry2Δ light condition compared to ephrinA1-stimulated condition 103
9. Table AII.1. Primer sequences used for construct design..... 164
10. Table AII.2. Sample sequencing statistics and mapping sequence reads to reference human genome..... 172
11. Table AII.3. The top downregulated and the two upregulated significant DEGs for Cry2olig light condition compared to its dark condition 183
12. Table AII.4. Significant DEGs for no transfection light condition compared to its dark condition 183

13. Table AII.5. Ontological process names, the genes associated with each process, and the adjusted p-values for each process of PMb-EphA1Cry2Δ dark vs. light condition 184
14. Table AII.6. Ontological process names, the number of genes associated with each process, and the adjusted p-values for each process of PMb-EphA1Cry2Δ light vs. Cry2olig light conditions 184
15. Table AII.7. Ontological process names, the number of genes associated with each process, and the adjusted p-values for each process of PMb-EphA1Cry2Δ light vs. ephrinA1-stimulated conditions 185

LIST OF FIGURES

1. Figure 1.1: Overview of optogenetic applications 2
2. Figure 1.2: Schematic of a phytochrome-Pif optogenetic system 6
3. Figure 1.3: Examples of LOV domain optogenetic systems 11
4. Figure 1.4: Active site of Cryptochrome 2 from *Arabidopsis thaliana* 13
5. Figure 1.5: Schematic of Cry2-CIBN association and Cry2-Cry2 clustering 15
6. Figure 1.6: Schematic of the signaling outcomes of Eph receptors and ephrin 20
7. Figure 1.7: Schematic of cis-interactions between Eph receptors and membrane-associated receptors 23
8. Figure 1.8: Optogenetic EphB2 receptor 29
9. Figure 1.9: BAR protein structures and their membrane curvature 33
10. Figure 1.10: Design of opto-FBAR and opto-IBAR constructs 39
11. Figure 1.11: Examples of other optogenetic designs using non-enzymatic proteins 43
12. Figure 2.1: Schematic of Eph receptor and ephrin bi-directional signaling 57
13. Figure 2.2: Schematic of EphA1Cry2 constructs 67
14. Figure 2.3: Optogenetic clustering of EphA1Cry2 constructs 70
15. Figure 2.4: Analysis of EphA1Cry2 tyrosine phosphorylation 73
16. Figure 2.5: ERK phosphorylation in response to EphA1Cry2Δ activation 77
17. Figure 2.6. ERK-KTR translocation in response to EphA1Cry2Δ activation. 79
18. Figure 2.7: Akt phosphorylation in response to EphA1Cry2Δ activation 83
19. Figure 2.8. Akt-KTR translocation in response to EphA1Cry2Δ activation 84
20. Figure 2.9. mRNA sequencing experiment and workflow 87
21. Figure 2.10. Gene ontology analysis for PMb-EphA1Cry2Δ light vs. dark conditions .. 91

22. Figure 2.11. Gene ontology analysis for PMb-EphA1Cry2Δ light vs. Cry2olig light condition 94
23. Figure 2.12. Gene ontology analysis for PMb-EphA1Cry2Δ light vs. ephrinA1-stimulated conditions 99
24. Figure 2.13. Optogenetic clustering of transfected N2a cells 105
25. Figure 3.1: I-BAR schematic and construct design 132
26. Figure 3.2: Light-activated responses of CRY-BAR constructs 135
27. Figure 3.3: Analysis of light-activated responses of CRY-BAR constructs 137
28. Figure 3.4: Reversible light-activated membrane remodeling with CRY-BAR 141
29. Figure 3.5: Localized light activation of membrane remodeling with CRY-BAR 142
30. Figure 3.6: Light activation of N-terminal I-BAR-Cry2 fusions 143
31. Figure 3.7: CRY-BAR activation linked to ezrin 145
32. Figure 3.8: CRY-BAR activation and cell thickness 146
33. Figure 3.9: Coalescence of actin-rich protrusions after CRY-BAR activation 147
34. Figure 3.10: CRY-BAR plasma membrane recruitment in neurons 150
35. Figure 3.11: Localized light activation of CRY-BAR in neurons 152
36. Figure AII.1: Spatiotemporal light activation of EphA1Cry2 constructs 163
37. Figure AII.2: Cell rounding assay in response to EphA1Cry2 light activation 165
38. Figure AII.3: Cell rounding assay in response to EphA1Cry2 light activation 167
39. Figure AII.4: mCherry expression of EphA1Cry2 constructs 168
40. Figure AII.5: Additional graphs for ERK-KTR C/N change analysis 169
41. Figure AII.6: Additional graphs for Akt-KTR C/N change analysis 170
42. Figure AII.7: Comparison of ERK-KTR and Akt-KTR C/N change 171

43. Figure AII.8: RNA sequencing data for PMb-EphA1Cry2Δ dark vs. light control condition 173
44. Figure AII.9: RNA sequencing data for transfected PMb-EphA1Cry2Δ light vs. Cry2olig light condition 175
45. Figure AII.10: RNA sequencing data for transfected PMb-EphA1Cry2Δ light vs. no transfection with ephrinA1-stimulated control condition 177
46. Figure AII.11: RNA sequencing data for transfected Cry2olig dark vs. light control condition 179
47. Figure AII.12: RNA sequencing data for 'No Transfection' dark vs. light control condition 181
48. Figure AIII.1: CRY-BAR construct design and expression 187
49. Figure AIII.2: Temporal relationship of Cry2-mCh-IBAR and Ezrin-GFP 188
50. Figure AIII.3: Global activation of CRY-BAR in hippocampal neurons 190
51. Figure AIII.4: Dark localization of Cry2-mCh-IBAR and CIB-GFP-CAAX 191

CHAPTER 1

Review of Literature

Optogenetics

Optogenetics is a burgeoning field involving light stimulation of a protein or protein fusion to control its function and signaling (**Fig. 1.1**) (De Mena et al., 2018). Beginning with studies of light-induced neuronal activity (Williams & Deisseroth, 2013), optogenetics has evolved to include experiments such as spatial gradient shaping (Beco et al., 2018), protein condensate disruption (Hernández-Candia et al., 2021), and gene regulation (Hughes, 2018; Konermann et al., 2013). Using light as an exogenous stimulus has significant benefits when working with live cells, as it eliminates the need for chemical induction or ligand stimulation and provides superior spatial and temporal control of molecular processes (De Mena et al., 2018; Kramer et al., 2021). Due to the prolific research and design of different optogenetic tools, a database called Optobase has been developed as a way for researchers to collect, organize, and search-enable these tools (Kolar et al., 2018).

Many classes of optically active proteins have been utilized as optogenetic tools. Rhodopsins are a large family of light-sensitive proteins found in microbes (type I) and animals (type II) that regulate ionic potential within a cell (Joshi et al., 2019; Koyanagi & Terakita, 2014). Phytochromes, light-oxygen-voltage (LOV) sensors, and cryptochromes make up the family of photoreceptors that engage in light-stimulated dimerization (De Mena et al., 2018; Rost et al., 2017). This section will briefly review commonly implemented optogenetic systems used in cell-based research with a special focus on Cryptochrome, the blue light-activated photoreceptor utilized in Chapters 2 and 3.

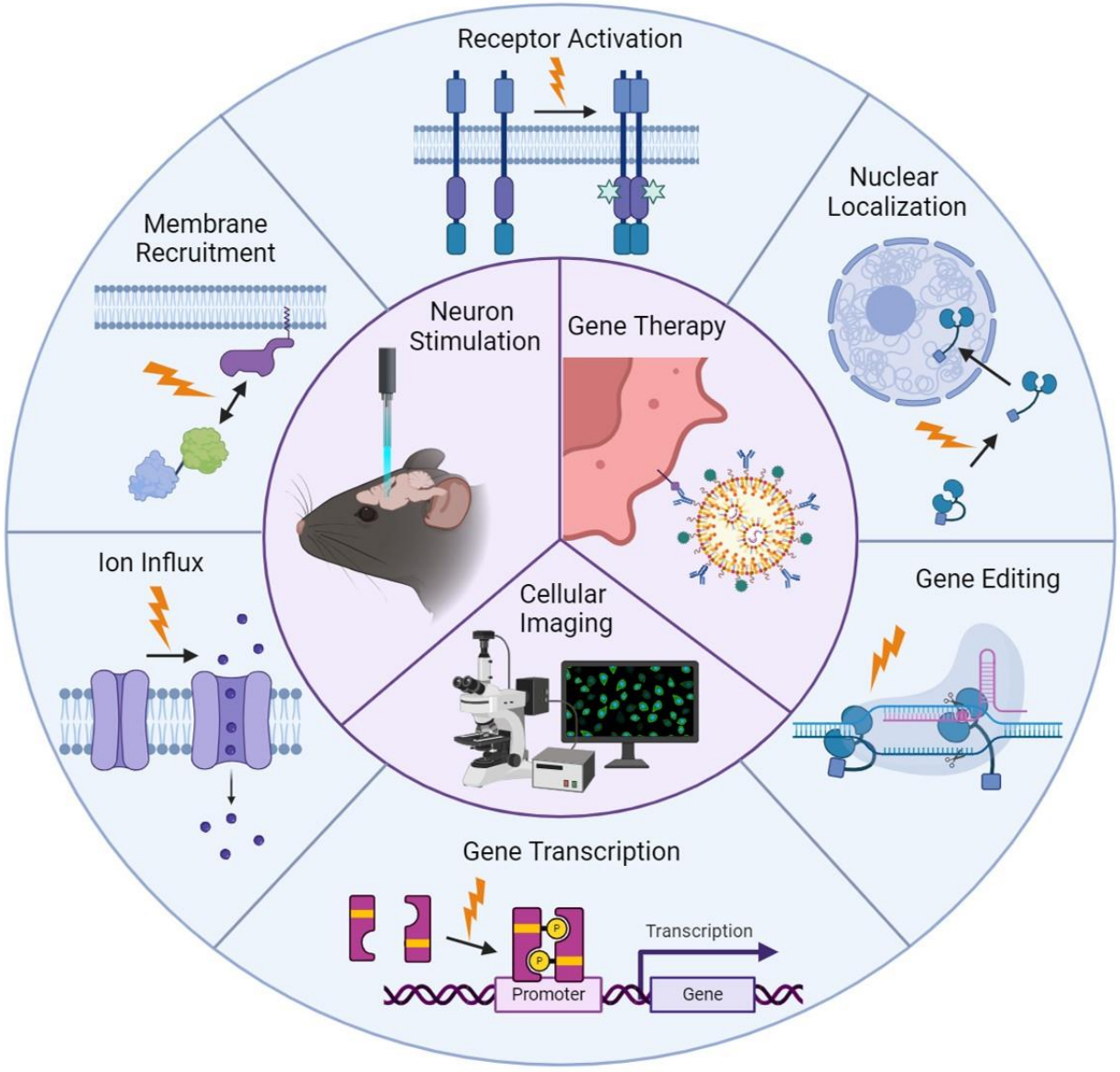

Figure 1.1. *Overview of optogenetic applications. An array of optogenetic tools using proteins have been designed to control cellular processes, such as membrane recruitment, receptor activation, nuclear localization, gene editing, gene transcription, and ion influx through light-gated ion channels. These tools can be implemented for fluorescent imaging of cells, gene therapy through viral vectors, and neuronal stimulation of mice brains (Williams & Deisseroth, 2013). Created with biorender.com.*

Rhodopsins

Rhodopsins, commonly shortened to opsins, are expressed in all organisms and can detect and respond to light. Type I microbial rhodopsins optically regulate ion channel activity directly and have been used to control neuronal membrane potentials (Deisseroth, 2015; Mattis et al., 2011). Type II rhodopsins found in animals are G-protein coupled receptors (GPCR) that indirectly regulate ionic potential important for optical signaling (Koyanagi & Terakita, 2014). Both types of rhodopsins contain seven transmembrane α-helices and a chromophore, retinal, tethered to the C-terminal helix. Upon light stimulation, the retinal undergoes isomerization that activates the opsin through a conformational change (Joshi et al., 2019).

Channel rhodopsins (ChR), a type I rhodopsin, have been extensively used in optogenetics due to their ability to produce action potentials across a membrane in response to light (Deisseroth & Hegemann, 2017). One of the first studies using optogenetic ChR involved expression of ChR carried by lentivirus into the lateral hypothalamus of mice brains. Light stimulation with an optical fiber produced a change in actin potential within neurons that produced a wakefulness behavioral effect in sleeping mice (Adamantidis et al., 2007). Many optimizations to ChR have been used to regulate not only neurons, but also myocytes, with light, including red-light sensitive opsins that are excited in cells deep inside tissues; however, more studies will have to further optimize expression levels and light intensity in order to fully take advantage of these naturally optically active tools (Karathanos et al., 2016).

Different kinds of Type II animal opsins have different sensitivities to various wavelengths of light, and each have a different efficiency of stimulation, where both depend on the opsin's photochemical properties (Koyanagi & Terakita, 2014). Gq-coupled opsins are considered bistable pigments and are stably reversible to their dark state after light activation.

Some opsins are considered bleaching pigments, as the opsin releases its chromophore in response to light stimulation and effectively is bleached (no longer active). The irreversibility of the bleaching pigments has been hypothesized to be attributed to the large conformational change of the opsin, correlating to a larger efficiency in downstream signaling, but conversely preventing structural stability and therefore reversibility (Koyanagi & Terakita, 2014). Modified opsins can be expressed in animals to overcome this bleaching effect, such as the bleach-resistant opsin from box jellyfish, "JellyOp," that produces photosensitive and reversible receptor activity (Bailes et al., 2012).

Manipulation of opsin structure has led to increased light sensitivity and efficiency of signal transduction within the field of optogenetics. Factors including the class of opsin and the organism the opsin comes from are important when selecting an optogenetic switch, as the sensitivity to the range of wavelengths and the kinetics of light activation could vary. In one study, step-function opsins were used since their light-activated ion channels stay open for about 30 minutes (Gong et al., 2020). Optical stimulation of opsins has been of interest in therapies relating to heart disease, such as ventricular fibrillation (Boyle et al., 2018; Karathanos et al., 2016), and neurodegenerative diseases, such as Alzheimer's disease (Deisseroth, 2015).

Phytochromes

Found in plants and bacteria, phytochromes can activate and heterodimerize with its binding partner, phytochrome interacting factor (Pif), in response to red and near-infrared light, controlling transcription and protein localization and signaling, similar to other optogenetic systems (De Mena et al., 2018; Lehtinen et al., 2022). By itself, phytochrome consists of dimers; its photo-sensing N-terminal domain interacts with a bilin chromophore, and its functional C-terminal domain binds with cGMP. Bacterial phytochromes bind with biliverdin Ixα (BV), while phytochromes from plant and cyanobacteria bind phytochromobilin (PΦB) and phycocyanobilin (PCB) (Chernov et al., 2017). To become active, red-light stimulation induces a conformational change in phytochrome from its inactive form (Pr) into its active form (Pfr). Heterodimerization of Pfr with Pif leads to an optogenetic system that can modulate the protein-protein interactions of transcription factors (Chernov et al., 2017; De Mena et al., 2018). This system is unique in that near-infrared light stimulation reverses heterodimerization through the absorption of a photon by phytochrome (**Fig. 1.2**) (De Mena et al., 2018). The kinetics of activation and deactivation are very fast, in the range of milliseconds (Björling et al., 2016), thus many studies with phytochrome-protein fusions have been designed (Chernov et al., 2017).

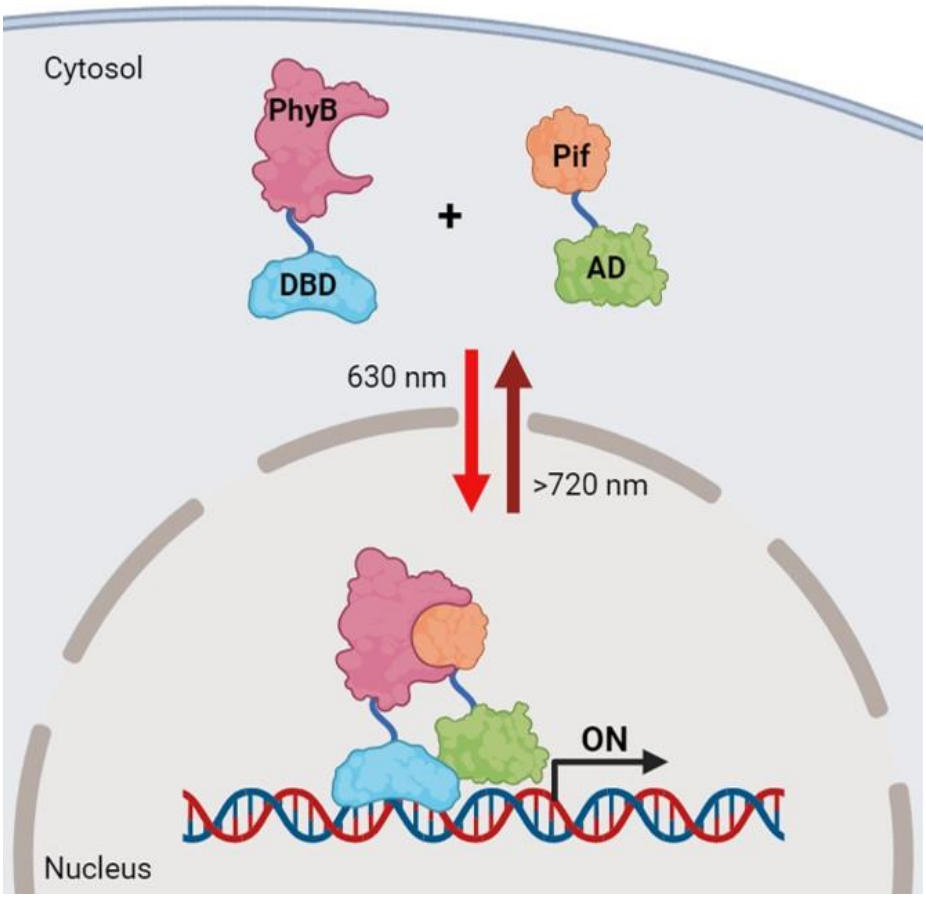

Figure 1.2*: Schematic of a phytochrome-Pif optogenetic system. PhyB and Pif are individually fused to a transcription factor (DNA-binding domain (DBD) and transcriptional activation domain (AD), respectively). Upon red light stimulation at 630 nm, PhyB and Pif heterodimerize, bringing the two transcription factors together to induce gene transcription. Upon near-infrared light stimulation > 720 nm, the PhyB-Pif heterodimer breaks apart, ending transcription (De Mena et al., 2018). Created with biorender.com.*

Of the five members of the phytochrome family (A-E), phytochrome B (PhyB) is most used in optogenetic systems (Chernov et al., 2017). The first study of a PhyB-Pif system utilized a fusion of PhyB to a Gal4 DNA-binding domain (DBD) and a fusion of Pif3 to a GAL4 transcriptional activation domain (AD), expressed in yeast. Red light exposure, in conjunction with the inclusion of PCB in medium, induced clonal growth in a two-hybrid assay and a significant increase in LacZ reporter gene expression. LacZ expression was reversed upon far-red light exposure (Shimizu-Sato et al., 2002). This system has been used for recruitment of proteins to the plasma membrane, first described by Toettcher et. al. in 2011 (Toettcher et al., 2011). PhyB is tethered to the plasma membrane by a CAAX sequence and a protein of interest fused to Pif allows for the protein to be associated with the plasma membrane upon light exposure. Several studies have utilized this design, such as recruitment of a polarity protein to a zebrafish embryo's epithelium (Buckley et al., 2016) and recruitment of a mitotic cyclin to different organelles to control cell cycle progression (X. Yang et al., 2013). Applying this to protein signaling, Toettcher et. al. adapted their Phy-Pif system to recruit a RasGEF, Son of Sevenless (SOS), to Ras. Under red light exposure, a SOS-Pif fusion was recruited to membrane-tethered PhyB-CAAX through PhyB-Pif interactions. Membrane-adjacent SOS was then able to activate membrane-bound Ras, resulting in activation of the MAPK/ERK pathway, reversible with far-red light (Toettcher et al., 2013).

In addition to heterodimerization using PhyB, bacterial phytochromes can undergo homodimerization through BV photoisomerization. A study utilizing this design describes the fusion of a human phosphodiesterase and the photosensory domain of a bacterial phytochrome. Similar to PhyB, red light stimulation induced the phosphodiesterase activity of hydrolyzing cAMP and cGMP by six-fold, and exposure to far-red light ceased hydrolysis (Gasser et al., 2014).

Another study fused the photosensory domain of cyanobacterial phytochrome 1 and two separate tyrosine kinase domains to take advantage of phytochrome's homodimerizing ability to activate the receptor kinase domain. MAPK/ERK signaling pathway was then activated in response to red light and deactivated with far-red light (Reichhart et al., 2016).

Utilizing red and far-red light for optogenetic activation provides the advantage of the light penetrating deep into tissue, whereas visible light can only affect the surface of tissues or thin layers of cells (N. Yu et al., 2019). This has led to advances in noninvasive technology since tissue is effectively transparent to infrared/near-infrared light and does not have to be directly exposed to tissue, as opposed to visible light that might require LED insertion into body parts,[1] such as the brain (N. Yu et al., 2019). Interestingly, IR light systems have been shown to exhibit lower phototoxicity and less extraneous scattering as visible light systems (Kaberniuk et al., 2021).

LOV domains

Light-Oxygen-Voltage (LOV) domains are flavin-containing domains part of the Period-ARNT-Singleminded (PAS) domain family and are found in bacteria, fungus, and plants (Pudasaini et al., 2015). Several different types of LOV domains exist, but for all, the central mechanism of action occurs on the flavin chromophore and the cysteine in the GXNCRFLQ motif. Blue light absorption at 450 nm excites the flavin, generating a radical which induces a covalent linkage between the flavin and cysteine (Iwata et al., 2002; Pudasaini et al., 2015). LOV domains have been exploited in optogenetics for their blue-light sensitivity, and depending on the type of optogenetic system of interest, utilizing different kinetic parameters can afford a multitude of options for the system. Fast protein activation kinetics requires intense light but that also means rapid on/off control of protein function. Slower stimulation kinetics affords the benefit of less intense light but a decreased control of optogenetic function (Zoltowski et al., 2009).

Two mechanisms of LOV domain photo activation have been utilized for optogenetic systems: signal transduction and dimerization (Flores-Ibarra et al., 2023). The first, signal transduction, involves the LOV domain and an effector protein tethered together by a helical linker. In the dark, the close association with the LOV domain inhibits the effector from signal transduction. Upon blue light stimulation, the conformational change associated with the LOV domain assists in unfolding of the helical linker, allowing the effector to physically move away from the LOV domain and undergo signal transduction (Pudasaini et al., 2015). An example of this describes the design of a light-inducible nuclear export system (LEXY) by Niopek et. al. (Niopek et al., 2016). LEXY-tagged proteins of interest were exported out of the nucleus in response to blue light through the sequestration of the nuclear export receptor, CRM1. In this

design, the C-terminal Jα helix of *As*LOV2 was modified with a nuclear export signal (NES). Under dark conditions, the NES is tightly secured next to the LOV domain, rendering it inactive. Upon blue light exposure, the Jα helix unwinds, allowing CRM1 to bind to the NES and export the LOV domain out of the nucleus. To prevent nuclear export, LEXY was tethered to chromatin via a H2B histone anchor. Blue light stimulation resulted in CRM1 binding to exposed NES and sequestration of CRM1 to chromatin (**Fig. 1.3A**) (Niopek et al., 2016).

Many optogenetic designs have explored the ability of LOV domains to homo- and/or hetero-dimerize. Briefly, heterodimerization systems have coupled LOV domains or LOV-based peptides to certain proteins that can bind to complementary proteins or DNA binding domains to mediate a multitude of various cellular processes (Nagasawa et al., 2023). Glozter et al. developed a system coined tunable light-inducible dimerization tags (TULIPs) using a synthetically designed interaction between AsLOV2 domain and a PDZ domain. This interaction is stimulated by light; therefore, the system has the ability to recruit protein of interests to cellular localizations (**Fig. 1.3B**) (Oakes et al., 2017; Strickland et al., 2012). Another popular system utilizing AsLOV2 domain involves its fusion to *E. coli* SsrA peptide, which shares similarities in sequence to the LOV domain's Jα helix. With light, SsrA can then bind to adaptor protein, SspB, promoting localization or cellular signaling (Guntas et al., 2015; Johnson et al., 2017). Opposed to light-induced association, LOVTRAP undergoes light-induced dissociation of phototropin 1 LOV2 domain with Z-domain-derived affibody (Zdk1). In dark conditions, Zdk1 binds LOV2 with high affinity and light stimulation interrupts this interaction, enabling a protein-Zdk1fusion to be released (H. Wang et al., 2016). Some LOV domains can homo-dimerize with itself, similar to cryptochromes; these systems are useful for activating receptor

tyrosine kinases through auto-phosphorylation (Khamo et al., 2019a), which will be further described later in this chapter.

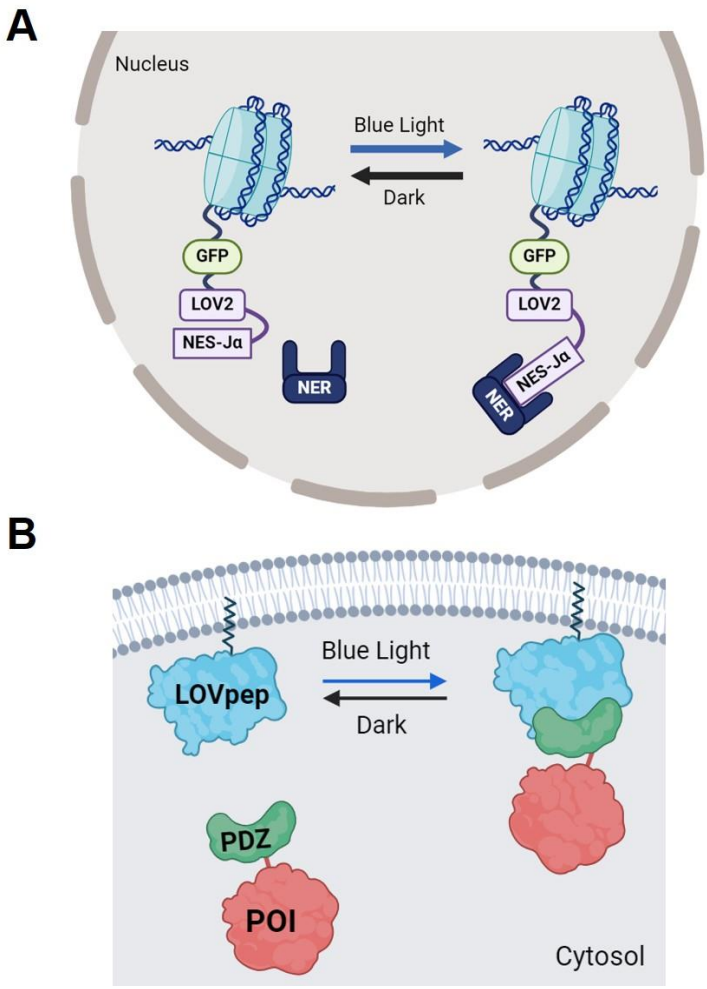

Figure 1.3. *Examples of LOV domain optogenetic systems.* ***(A)*** *Regulation of nuclear transport of a nuclear export receptor (NER) through a NES-modified LOV domain. NES-LOV2-GFP is tethered to a histone core. Upon blue light illumination, NES is exposed, allowing NER binding and sequestration (Niopek et al., 2016).* ***(B)*** *Recruitment of a protein of interest (POI) to the plasma membrane via membrane-tethered LOVpep and PDZ interaction (Oakes et al., 2017). Created with biorender.com.*

Cryptochrome

Cryptochromes are blue light-dependent photoreceptors that are genetically similar to photolyases (Kennedy et al., 2010). The family of cryptochromes are naturally found in plants and some animals and absorbs blue light (430-490 nm) using its chromophore, flavin (Che et al., 2015; Kennedy et al., 2010). Cryptochromes have a photolyase homology region (PHR), in addition to a second domain, the cryptochrome C-terminal extension (CCE), that is unique to cryptochromes. The PHR domain at the N-terminus binds to the chromophore, flavin adenine dinucleotide (FAD), which absorbs blue light and acts as the catalytic cofactor (H. Liu et al., 2008). Although still not fully understood, it has been postulated that the electrons within FAD are excited by blue-light photons and this results in electron shuttling and subsequent conformational changes in the protein (Schwinn et al., 2020; X. Yu et al., 2010). For full-length cryptochromes, this conformational change can lead to phosphorylation and activation of the protein into the open form, which can then bind and interact with signaling proteins to regulate transcription and translation (X. Yu et al., 2010). Although cryptochromes share homology to photolyases, they do not repair DNA like photolyases. Instead, their function in plants include flowering control and fruit development; functions in both plants and animals include magnetoreception and circadian rhythm (H. Liu et al., 2008; X. Yu et al., 2010).

The residues that non-covalently bind the flavin in the PHR domain (LLDAD) are highly conserved throughout all cryptochromes in species (H. Liu et al., 2008). The residues that are proposed to be involved in electron transfer are three tryptophan (W) residues near the flavin binding site (**Fig. 1.4**) (Solov'yov et al., 2014). A light-stimulated redox reaction involving a disulfide bond has also been hypothesized to induce conformational changes in the protein. For phosphorylation of cryptochromes, ATP binds in the FAD-binding site of the PHR domain,

which transfers electrons from ATP to the flavin upon photoexcitation. This electron transfer might facilitate phosphorylation of serine residues by ATP (Brautigam et al., 2004).

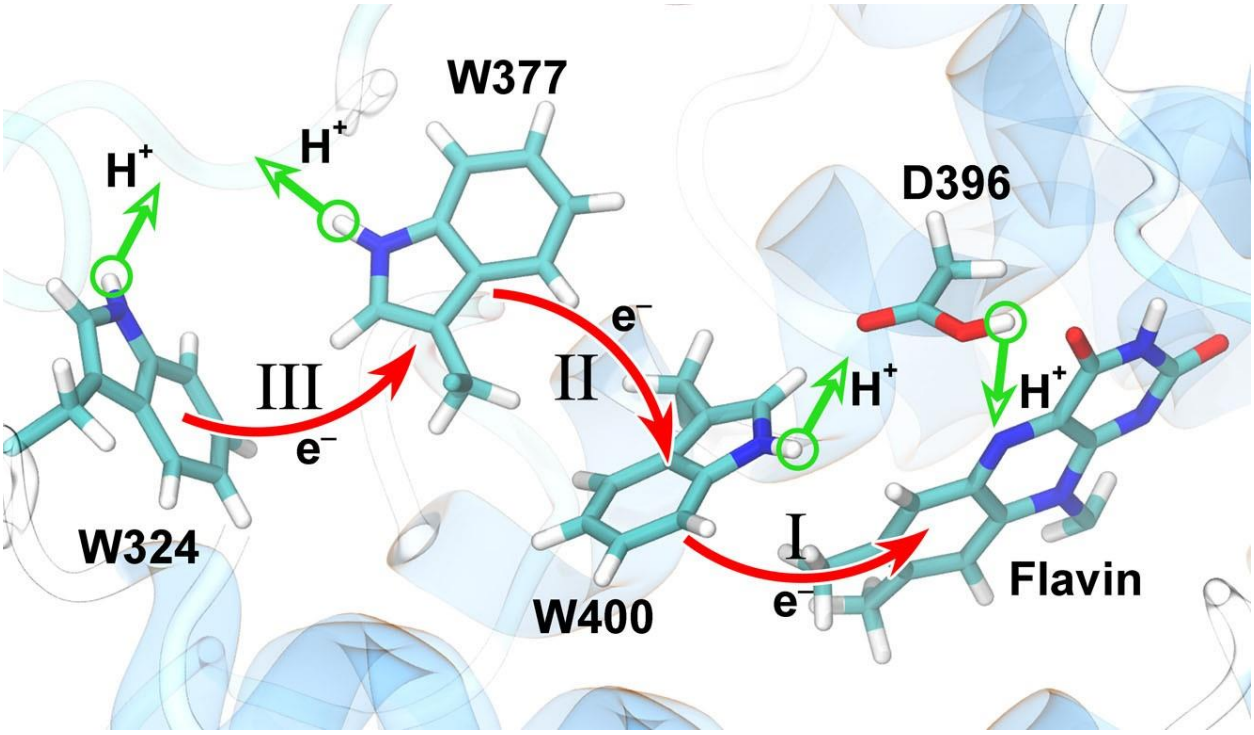

Figure 1.4. *Active site of Cryptochrome 2 from Arabidopsis thaliana. Photoexcitation induces electron transfer (red) from (I) flavin to W400, (II) $W400^{\cdot+}$ to W377, and (III) $W4377^{\cdot+}$ to W324. Proton transfer (green) occurs at D396 and the three W residues. Reused with permission by Scientific Reports, CC BY-NC-ND 3.0, https://creativecommons.org/licenses/by-nc-nd/3.0/ (Solov'yov et al., 2014).*

Detailed mechanisms into cryptochrome oligomerization are also not fully understood, even though this light-dependent protein has been used in numerous optogenetic systems and the focal point of many optogenetic switches (X. Yu et al., 2010). Positively-charged residues (K2, K5, K6) on the N-terminal PHR domain mediates light-dependent cryptochrome and CIB1

heterodimerization. C-terminal CCE domain also contains positively-charged residues (R487, R489) that mediate cryptochrome homodimerization, in addition to a negatively-charged residue (E490) that suppresses dimerization (Duan et al., 2017). The negative charged residue on the C-terminus reduces oligomerization but does not completely prevent clustering. Moreover, larger clusters of cryptochrome have been shown to take longer to dissociate than smaller clusters, indicating there may be stabilizing interactions in the protein structure that promote oligomerization (Duan et al., 2017). Many design details should be considered when proposing optogenetic switches involving cryptochromes. For many optogenetic systems, cryptochrome 2 (Cry2) from *Arabidopsis thaliana* is utilized as the light-sensitive switch (Hughes, 2018). This dynamic, versatile protein has been used in a multitude of experiments, including but not limited to gene expression and transcriptional control (Hernández-Candia & Tucker, 2020), reversible protein-protein interactions and signaling (Che et al., 2015; Duan et al., 2017), inhibition of protein signaling (Bugaj et al., 2015), and protein condensate dissociation (Hernández-Candia et al., 2021).

As cryptochrome can homo-oligomerize with itself (**Fig. 1.5A**), many different mutants have been developed to control and manipulate this oligomerization ability (Kramer et al., 2021; Taslimi et al., 2014a). In most optogenetic designs with Cry2, the PHR domain is used since this region is where most monomer interaction occurs (Kennedy et al., 2010a; Kramer et al., 2021). In some designs, increasing the clustering ability of Cry2 is desirable if efficient protein-protein interaction is the goal. The Cryolig mutant has greater clustering ability compared to wildtype Cry2 and has been used in many different optogenetic switches (Kramer et al., 2021; Taslimi et al., 2014). By mutating a negatively charged residue to a neutral residue (E490G), repulsion of the Cry2 monomers decreased (Taslimi et al., 2014). A more positively charged C-terminus

further increases homodimerization ability, such as the case in Cry2high, a E490R mutant. In the same study, reduced clustering of Cry2 was achieved by adding negatively charged residues (EED) to the C-terminus of Cry2 (Cry2low) (Duan et al., 2017). A weaker clustering ability might be more optimal for some designs, as larger clusters resulting from better oligomerization take longer to dissociate. If constructs are membrane-bound, some high background clustering in the dark from overexpression of constructs can hinder control of the optogenetic switch (Duan et al., 2017).

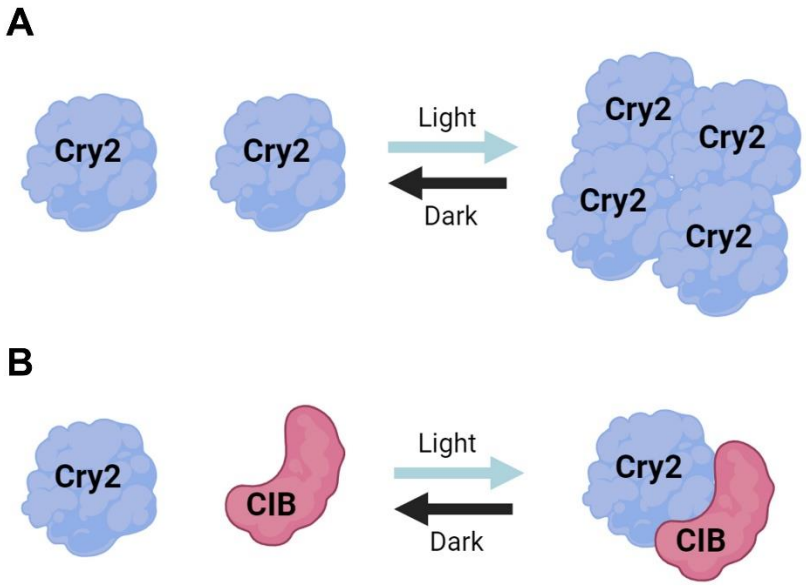

Figure 1.5. *Schematic of* ***(A)*** *Cry2-Cry2 homo-oligomerization and* ***(B)*** *Cry2-CIB hetero-oligomerization before and after blue light stimulation and the reversible dissociation of oligomerization in the dark. Created with biorender.com.*

Another study by Park et al. mentions that quaternary structure and conjugation of the fluorescent protein (FP) tagged to Cry2 can affect the clustering of Cry2 (Park et al., 2017). Conjugation of the FP tagged to the C-terminus of Cry2 showed a larger clustering effect than that at the N-terminus of Cry2. In the same study, a 9-residue peptide added to the C-terminus of Cry2 also increased clustering. The 7^{th} amino acid of the peptide, Leucine, was determined to play a critical role in increased clustering due to its hydrophobicity. From there, they determined that the Phenylalanine at position 507 of Cry2 was also crucial for efficient clustering due to its hydrophobicity (Park et al., 2017). The size of the FP also affects clustering, as a large, bulky FP fused to Cry2 can prevent Cry2 interactions and optimal clustering due to steric hindrance (Duan et al., 2017; Park et al., 2017). Another consideration is the finding that Cry2, modified to tether to the membrane, rapidly clusters better than the cytosolic Cry2. Plasma membrane-bound Cry2 has been shown to have slower clustering dynamics than Cry2 on the ER membrane, which can be contributed to protein and lipid concentration of the membranes (Che et al., 2015). To disrupt Cry2 homo-oligomerization, a rapamycin-based chemically inducible dissociation can be utilized with a fusion of Cry2 and FKBP-rapamycin binding (FRB) domain (Hernández-Candia et al., 2021). Cry2-FRB forms clusters after light stimulus by Cry2 interactions, but co-expressed with the FRB ligand, FK506-binding protein (FKBP), rapamycin induces binding of FKBP to the FRB domain of Cry2-FRB and disrupts the fusion clusters into monomers (Hernández-Candia et al., 2021). This method of Cry2 cluster dissociation can be used immediately after light-activated cluster formation and eliminates the requirement for post-light relaxation in the dark in order to reverse clustering, which can take up to 30 minutes (Duan et al., 2017; Hernández-Candia et al., 2021).

In addition to homo-oligomerization, blue light stimulation initiates Cry2 hetero-dimerization with its binding partner, Cryptochrome-interacting basic helix-loop-helix protein 1 (CIB1 or CIB), that is tethered to the plasma membrane (**Fig. 1.5B**) (Kramer et al., 2021). A common truncation of CIB1, CIBN, contains only the first 170 amino acids and lacks the nuclear localization sequence; this mutant exhibits lower background association of Cry2 in the dark and does not contain the basic helix-loop-helix domain that binds DNA (Kennedy et al., 2010). A complication with this optogenetic approach is that Cry2 can also homodimerize; before and after light stimulation, this can cause undesirable clusters to form in the cytosol instead of recruitment to the membrane. Additionally, light stimulation results in homo- and hetero-dimerization, and each association cannot be separated if co-expressed (Che et al., 2015). In order to block Cry2 clustering but retain Cry2-CIB interactions, the Cry2-FRB fusion was recruited to the membrane by interaction with CIB1 under light stimulation, but upon rapamycin induction, FKBP ligand associated with FRB and disrupted Cry2-Cry2 interactions but not the Cry2-CIB1 interaction. Even though this method involves transfection and overexpression of three different protein fusions, it is a novel way of maintaining membrane interactions while also tightly controlling the signaling of receptor proteins (Hernández-Candia et al., 2021). Extensive reviews of these optogenetic designs have enumerated the different uses of Cry2 and its optimizations in various regulatory techniques (De Mena et al., 2018; Hughes, 2018; Kramer et al., 2021; X. Yu et al., 2010). These have all given way to many options for using effective and controllable Cry2 in optogenetic switches.

Eph Receptors

Receptor tyrosine kinases (RTK) are transmembrane proteins that transduce critical signaling pathways within cells to regulate cell communication, growth, development, and mobility (Hubbard & Miller, 2007). Erythropoietin-producing hepatocellular carcinoma (Eph) receptors are the largest family of receptor tyrosine kinases with 14 types classified into two groups, type A and type B (D. Arvanitis & Davy, 2008). The type of receptor is determined by which type of ligand it binds: EphA (A1-A8, A10) receptors bind ephrinA (A1-5), and EphB (B1-4, 6) receptors bind ephrinB (B1-3). EphrinA is tethered to the membrane extracellularly by a glycosylphosphatidylinositol (GPI) anchor; ephrinB contains an extracellular binding domain, a transmembrane sequence, and an intracellular PDZ-binding motif (L.-Y. Liang et al., 2019). When a cell moves close to a neighboring cell, the ephrin on one cell can bind to the Eph receptor on the other cell via its ligand binding domain (LBD), also referred to as a globular domain. The Eph receptor's N-terminal LBD, cysteine-rich region (CRD), and two consecutive fibronectin type-III domains are part of the receptor's extracellular portion, followed by a transmembrane region (TM). The intracellular portion of the receptor consists of the juxtamembrane region (JM), tyrosine kinase domain (KD), sterile α-motif domain (SAM), and the C-terminal PDZ-binding motif (D. Arvanitis & Davy, 2008; Hughes & Virag, 2020; L.-Y. Liang et al., 2019; J. S. Yang et al., 2018).

Membrane-bound Eph receptors on one cell are activated by binding to ephrin on a neighboring cell (**Fig. 1.6**). Ephrin ligands have different affinities to its receptor, depending on the types of each ligand and receptor. In its inactive form, an Eph receptor is in a conformation where the kinase domain interacts with the JM region, shielding the tyrosine residues within the KD from interacting with adjacent receptors (Himanen et al., 2010; Wiesner et al., 2006). Upon

ephrin binding, the activated Eph receptor dimerizes with another ephrin-Eph receptor heterocomplex. In fact, structural studies have shown that Eph receptors can form high-order oligomers of active dimers (Himanen et al., 2010). Next, the receptor interactions promote the phosphorylation of tyrosine residues in the JM region by ATP, and then the dissociation of the JM from the kinase domain allows for the tyrosine residue in the kinase domain to be phosphorylated. The kinase domain is then activated to phosphorylate downstream signaling proteins (Himanen et al., 2010; Nievergall et al., 2012; Wiesner et al., 2006). In high receptor concentrations, activated ephrin-Eph receptor clusters can recruit unbound Eph receptors to these high-order clusters, and these unbound clustered receptors can still be phosphorylated and induce downstream signaling in the absence of ligand binding (Wimmer-Kleikamp et al., 2004). In studies using exogenous ephrin treatments, pre-clustered ephrin using the immunoglobulin Fc (ephrin-Fc) is required to activate Eph receptors; monomeric ephrin is not sufficient to produce receptor clustering (Davis et al., 1994).

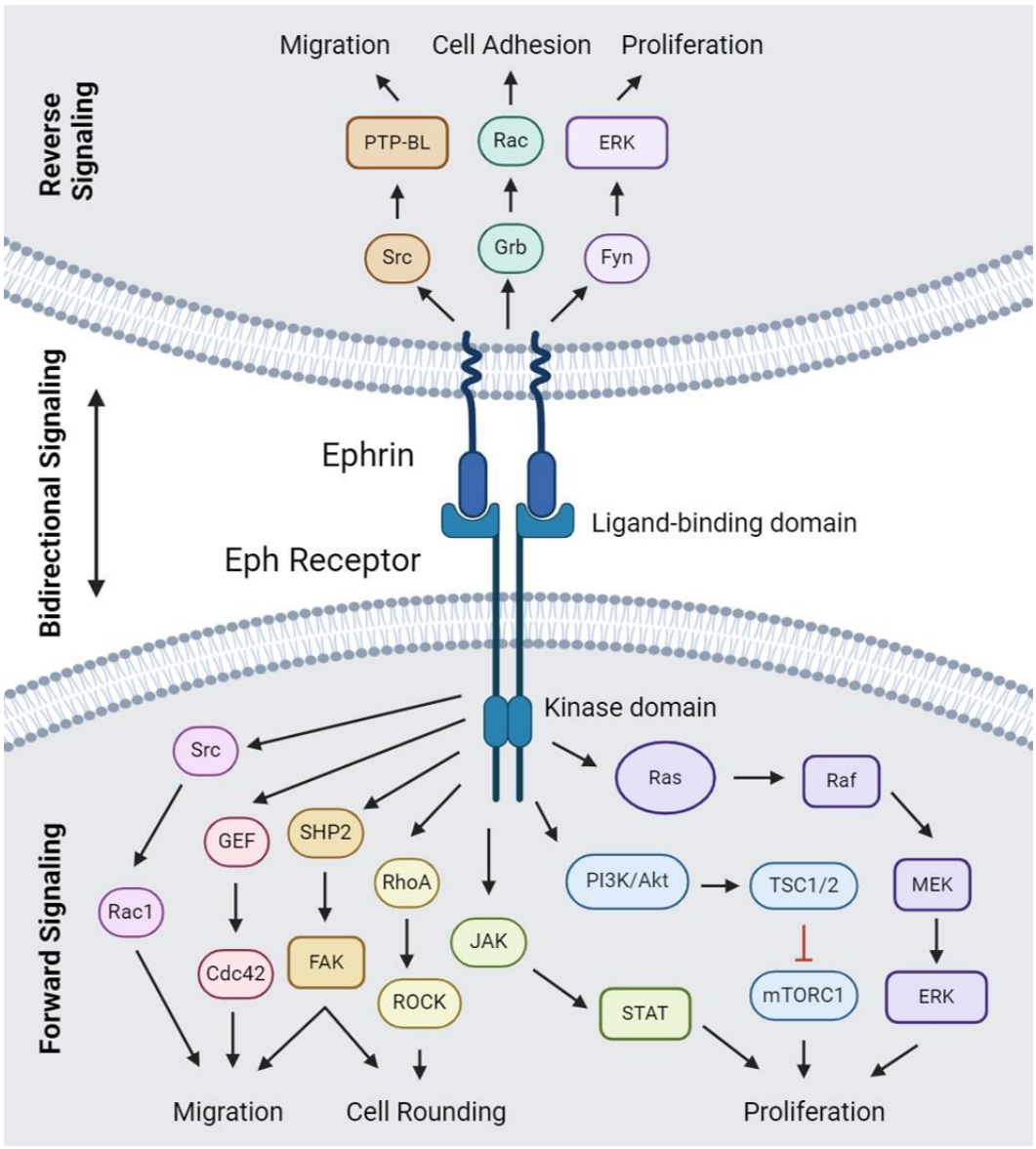

Figure 1.6. *Schematic of the signaling outcomes of Eph receptor and ephrin. The main structural domains of Eph receptor are the ligand-binding domain and the kinase domain. Eph receptors are activated and dimerize upon binding to ephrin ligand, inducing forward signaling of various pathways. Ephrins also undergo reverse signaling upon receptor binding. Forward signaling pathways lead to processes such as cell migration, cell rounding, and proliferation. Reverse signaling can induce cell migration, cell adhesion, and proliferation. Created with biorender.com.*

Although Eph/ephrin signaling crosstalk has been studied extensively, elucidating the role of each receptor has been difficult. First, each of 14 types of Eph receptors mediates different, and sometimes the same, signaling cascades as the other Eph receptors. Both EphA2 and EphA4 receptors regulate the MAPK signaling pathway and focal adhesion kinase (FAK) (D. Arvanitis & Davy, 2008). EphA2 receptor and EphB1 have been shown to upregulate Rac1, while EphB6 has been shown to downregulate Rac1 in T cells (Pasquale, 2010). Second, Eph receptor expression profiles are specific to cell type. For example, EphA2 expression is high in angiogenic vascular cells and cardiac progenitor cells, but expression is low in embryonic quiescent vascular cells (Barquilla & Pasquale, 2015). EphA1 receptor has almost no expression in human embryonic kidney (Hek) cells (Yamazaki et al., 2009), but CD4+ T lymphocytes readily express EphA1 receptor (Aasheim et al., 2005). EphB receptors are highly expressed in red and white blood cells and in dendritic cells (Darling & Lamb, 2019). Third, a single ephrin ligand has promiscuous binding to more than one Eph receptor. EphrinA5 can bind to either EphA2 or EphA4 but the resulting biological effect is different. Activated EphA2 promotes cell adhesion, but EphA4 activation induces cell de-adhesion and rounding (Y. Wang et al., 2018). Some types of Eph receptors have the ability to bind different types of ephrins. While most Eph receptors bind the ligand to their complementary class (A or B), EphA4 can bind ephrinB, and EphB2 receptor can bind ephrinA5 (Pasquale, 2010). This promiscuity introduces difficulty *in vitro* and *in vivo* to ensure that only the receptor of interest is activated and no other receptors.

To add more complexity to Eph/ephrin signaling, Eph receptors not only homo-dimerize with themselves, but they can also interact in a *cis* fashion with other membrane-bound proteins and receptors. Cis-interaction between Eph and ephrin, dimerization of two different types of Eph receptor, and interactions between Eph and other RTKs can occur and lead to different

signaling outcomes (D. Arvanitis & Davy, 2008; L.-Y. Liang et al., 2019). *Cis*-interaction between an ephrin and Eph receptor has been shown to inhibit Eph receptor activation. In retinal axons, EphA3 and ephrinA5 cis-interactions prevents EphA3 tyrosine phosphorylation and silences forward signaling (Carvalho et al., 2006). Another Eph receptor crosstalk includes the ability of an Eph receptor to dimerize with a different type of Eph receptor. Different types of EphA receptors, such as ephrinA5-activated EphA3 and EphA4, can heterodimerize to produce the same cellular response, for example growth cone collapse in spinal motor neurons (Marquardt et al., 2005). Other cis-interactions with Eph receptors include dimerization with another membrane-associated receptor. Eph receptors have been show to interact with growth factor receptors, chemokine receptors, integrins, and NMDA receptors (**Fig. 1.7**) (D. Arvanitis & Davy, 2008; Cecchini & Cornelison, 2022). In neural progenitor cells, treatment with ephrinA1 stimulated an interaction between EphA4 and platelet-derived growth factor receptor β (PDGFRβ) that promoted proliferation and differentiation of the cells (Q. Chen et al., 2020). Another study found that EphB receptors associate with NMDA receptors without the requirement for EphB activation (Dalva et al., 2000). Further studies elucidated the role of EphB interactions with NMDAR; in mature neurons, EphB2 regulates NMDAR localization levels at synapses and has the ability to bind and phosphorylate NMDAR (Nolt et al., 2011).

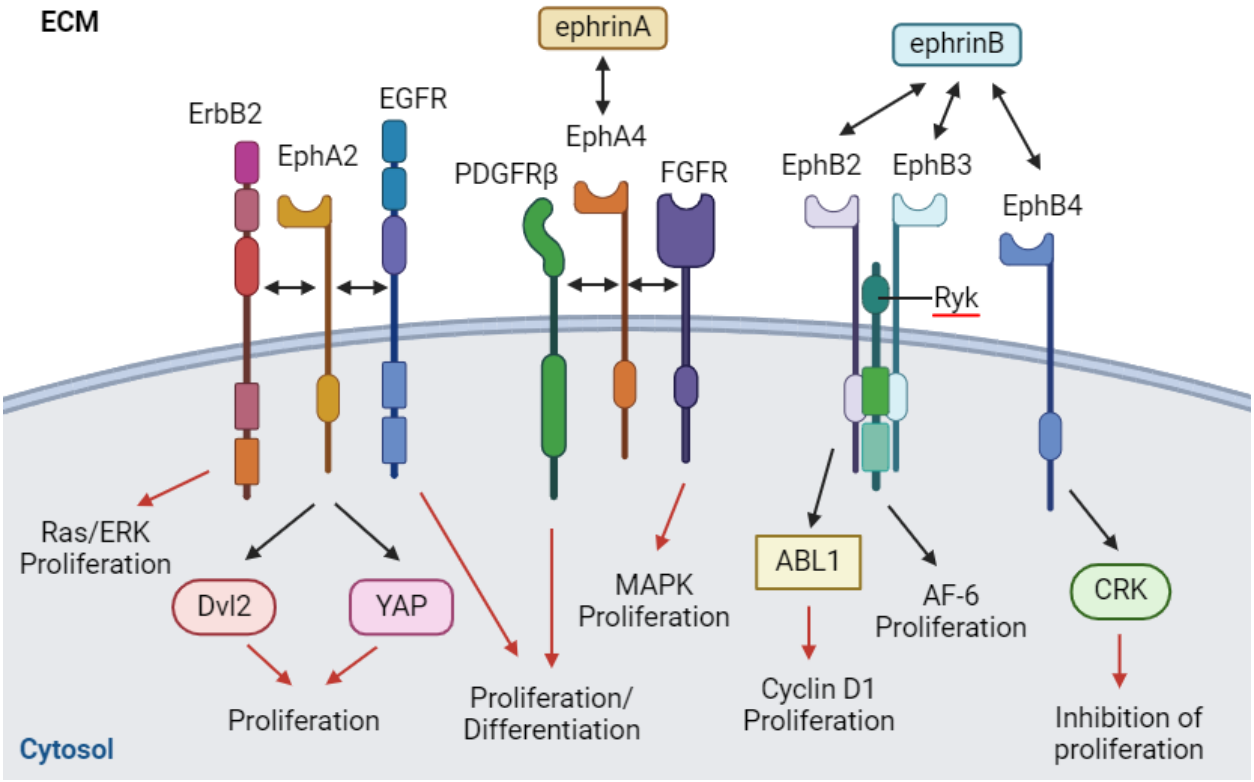

Figure 1.7. *Schematic of cis-interactions between Eph receptors and membrane-associated receptors. EphA2 receptors can interact with other proteins along the plasma membrane, such as epidermal growth factor receptor (EGFR) and Erb2, to promote proliferation in a ephrin-independent manner. EphA4 receptors interact with platelet-derived growth factor receptor β (PDGFRβ) and fibroblast growth factor receptors (FGFR) for ephrinA-dependent upregulation of proliferation. EphrinB-mediated activation of EphB receptors can either promote proliferation or inhibit proliferation depending on type of receptor interaction (Cecchini & Cornelison, 2022). Created with biorender.com.*

Another factor to consider when studying Eph receptor signaling is that endocytosis and degradation of activated ephrin-Eph receptor complexes can abolish forward and reverse signaling within the cell (Ieguchi & Maru, 2019). For ephrinA and Eph receptors, this can affect the signaling due to the metalloprotease ADAM10/12 (Ieguchi et al., 2014; Ieguchi & Maru, 2019). When ephrinA binds to EphA receptor, ADAM12 cleaves the membrane-bound section of ephrinA, severing the cell-cell link. This mechanism is thought to promote cell de-adhesion by cleaving the Eph/ephrin connection and additionally inducing endocytosis of the Eph/ephrin complex, which signals downstream targets to reduce protrusion formation and increase cell retraction (Ieguchi et al., 2014; Ieguchi & Maru, 2019). Taking these factors into account along with the consideration that the ephrin/Eph regulatory mechanism is yet to be fully understood, the relationship between Eph receptor and the activation of its cascade of signaling does not seem to be linear but could be closer to a feedback loop of signaling (Nievergall et al., 2012).

Eph forward signaling is of particular interest in the biochemical community due to the diverse downstream pathways that are initiated by Eph activation. Phosphorylated tyrosine residues on the kinase domain interact with Src Homology 2 (SH2) domain proteins, leading to signal activation of many different pathways (Gucciardo et al., 2014). Unsurprisingly, mutations of all classes of Eph and ephrins can lead to various diseases including many types of cancer. Due to the importance of these pathways on cell growth, replication, and development, Eph receptor signaling have been extensively studied (Barquilla & Pasquale, 2015). Eph receptors and ephrins play a critical role in heart development and angiogenesis; recent studies have shown that since Eph receptors mediate cardiomyocyte communication between epithelial tissues, controlling Eph/ephrin signaling (O'Neal et al., 2013). Eph receptors are also crucial for

neurogenesis and neuronal repair (Klein, 2009), leukocyte migration as part of immune response (Darling & Lamb, 2019), and actin cytoskeleton remodeling (Gucciardo et al., 2014).

Many Eph receptor signaling cascades include, but are not limited to, Rho GTPase, ERK/MAPK, Rac1, Cdc42, and FAK (**Fig. 1.6**). Some of these signaling proteins are upregulated or downregulated depending on the type of Eph receptor and the type of cell (Gucciardo et al., 2014; J. S. Yang et al., 2018). ERK/MAPK signaling pathway regulates cell proliferation, and both EphA and EphB receptors have been shown to promote ERK phosphorylation and subsequently cell proliferation (Pasquale, 2010; Pratt & Kinch, 2002). One of the main functional endpoints of Eph receptor activation is ECM reorganization (cell migration and adhesion), which includes the modulation of proteins such as integrin, actin, and focal adhesions. EphA2 receptor activation, found to produce cell rounding and de-adhesion, has been shown to dephosphorylate and inactivate focal adhesion kinase (FAK), a kinase that recruits ECM proteins to the membrane. From these studies, FAK and integrin activation are inhibited by EphA2 receptor, resulting in cell rounding and migration (Miao et al., 2000). RhoA is another common signaling target of EphA receptors, such as EphA1 receptor. RhoA is activated by phosphorylation either directly or indirectly as a result of ephrinA1-induced EphA1 receptor activation, and the RhoA effector, ROCK, is subsequently activated by the active RhoA-GTP (Yamazaki et al., 2009). This pathway results in cell de-adhesion and rounding. In general, RhoA/ROCK has also been implicated in ECM reorganization involving ezrin, radixin, and moesin (ERM) proteins, which mediate the association of actin to the plasma membrane (Hartmann et al., 2015). Other signaling pathways of interest that lead to ECM reorganization are the PI3K/Akt, Rac1, Cdc42, FAK, and Grb4 (Pasquale, 2010). ECM proteins are regulated by

many other proteins other than the Eph receptor, but overexpression of Eph receptors in the cell can yield insights into the outcome of receptor activation.

Optogenetic Applications

As described above, studying Eph receptor activation and signaling can be a daunting task, as expression and signaling crosstalk differ for each Eph receptor in different cell types and even in different stages of development. Endogenous or over-expressed Eph receptors can be stimulated with exogenous ephrin-Fc, an engineered clustered form of ephrin, to activate receptors and produce downstream signaling (Davis et al., 1994; Yamazaki et al., 2009). To simplify the complex web of signaling pathways, optogenetic activation of specific Eph receptors will more precisely delineate Eph signaling outcomes, leading to a better understanding of the impacts of Eph-dependent cell signaling cascades (Locke et al., 2017). Optogenetics uses light to control protein function and cell signaling; photoactivation of cell signaling pathways provides exceptional spatiotemporal control and can bypass the need for small molecule activation of cell signaling pathways, such as ephrin ligands. Light-activated experimental approaches improve precision while lowering toxic effects of traditional experimental approaches (Hughes, 2018; Rost et al., 2017). Through optogenetics, regulating the activation and signaling of Eph receptors would allow scientists to control receptor signaling outcomes that are unique to each receptor that are otherwise up-regulated or down-regulated in certain diseases, such as cancer, heart disease, and neurodegenerative diseases (Hughes & Virag, 2020).

A study in optogenetic EphB2 receptors have exploited reversible Cry2 clustering to activate Eph receptors and downstream signaling pathways without the need for Eph-to-ephrin binding (Locke et al., 2017). The lack of the requirement for ligand-binding activation is convenient as optogenetic clustering via Cry2 serves as the artificial activation mechanism. In this case, the extracellular domains of the Eph receptor are not necessary in the construct; although the cysteine-rich domain and the fibronectin type III domains have been found to

promote clustering of wildtype Eph receptors, the clustering ability of the Cry2 is more than sufficient to produce receptor activation and cellular response (Locke et al., 2017). The difference in the biological effect of clustering between wildtype Eph receptors and an opto-Eph construct is the presence of reverse signaling. Activation without the ligand means that no reverse signaling can occur, and the absence of the ligand-binding domain ensures no extraneous ephrin signaling upon receptor clustering. Locke et al. showed that their OptoEphB2 construct exhibited superior tyrosine phosphorylation through clustering and auto-phosphorylation of the kinase domains upon blue light exposure, with little to no dark background phosphorylation (**Fig. 1.8B**) (Locke et al., 2017). Their construct consisted of an N-terminal c-Src derived myristoylation domain, replacing the wild-type transmembrane domain, tethered to the intracellular domain of EphB2. Cry2olig and the fluorescent protein mCherry were then tethered to the C-terminus of EphB2 (**Fig. 1.8A**). They had found that the wild-type Cry2 did not generate high-order clusters required for receptor activation, so they utilized the highly-oligomerizing Cry2 mutant Cry2olig for its clustering ability. In Hek293 cells, their construct clustered readily upon blue light (**Fig. 1.8C**) and exhibited cell rounding. They also expressed their construct in neurons, and blue light activation of OptoEphB2 produced an increase in filopodial protrusions along dendrites (Locke et al., 2017). The same team then used OptoEphB2 to study memory formation in mice, as EphB2 has been expressed in the area of the brain where the site of fear conditioning memory is active, the lateral amygdala (LA), and has been associated with fear memory formation. OptoEphB2 was expressed in the LA via an adeno-associated virus and upon light stimulation, downstream phosphorylation of Src increased and fear conditioning behavioral studies showed an enhancement of long-term memory formation (Alapin et al., 2018).

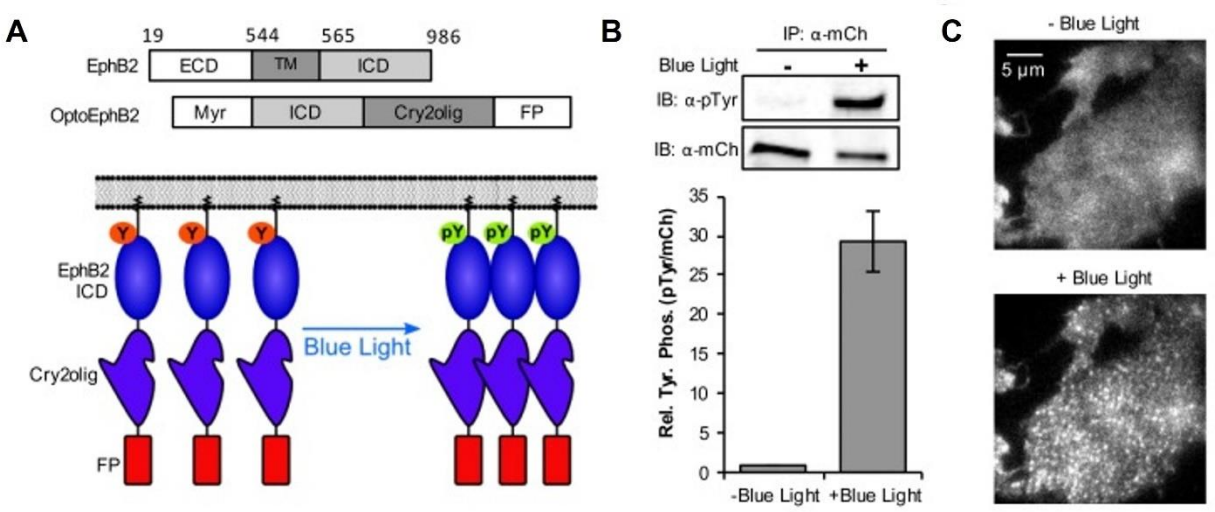

Figure 1.8. *Optogenetic EphB2 receptor.* ***(A)*** *Schematic of OptoEphB2 construct design and activation in response to blue light.* ***(B)*** *Quantitation of tyrosine phosphorylation in OptoEphB2 immunoprecipitates of Hek293 cell lysates.* ***(C)*** *TIRF image of Hek293 cells expressing OptoEphB2 before blue light exposure (top) and three 250 ms pulses of blue light 4.5 seconds apart (bottom). Reused with permission by Biology Open, CC BY 3.0, https://creativecommons.org/licenses/by/3.0/ (Locke et al., 2017).*

As of 2024, OptoEphB2 is currently the only optogenetic Eph receptor described in the literature, aside from our EphA1Cry2 constructs further detailed in Chapter 2. Similar optogenetic designs have been applied to other receptor tyrosine kinases and share similarity with OptoEphB2 construct design. For example, the intracellular domains of a murine FGFR were tethered to the plasma membrane using a myristoylation domain, and the phytochrome CPH1 was fused to the C-terminus of the receptor. Red light stimulation induced homodimerization of CPH1 and activation of FGFR, leading to MAPK/ERK pathway signaling (Reichhart et al., 2016). Another design using a LOV-domain incorporates the intracellular

domains of a RTK fused C-terminal to the LOV-domain (Grusch et al., 2014). Seven different LOV-domains were tested with FGFR and found that the VfAU1 from *V. frigida* produced the best signaling response from FGFR that was additionally spatially and temporally controllable. Two other RTKs, EGFR and rearranged during transfection (RET), were also tested with VfAU1 and found to induce similar signaling output upon blue light stimulation (Grusch et al., 2014).

A unique way of clustering RTKs is to fuse Cry2 not to the receptor, but to a SH2 domain that can bind to the receptor. Bugaj et al. fused Cry2 to the SH2 domain of PLC-γ, and under blue light stimulation, clustering of the SH2 domains enhanced binding of the domain to endogenous RTKs, activating the receptors (Bugaj et al., 2015). This approach would be useful to study a RTK activity in cells with high expression of the a particular RTK of interest; however, activation may not be specific as SH2 domains have promiscuous binding to other RTKs. Another way of clustering RTK that is more specific is to utilize Cry2-CIB hetero-oligomerization is a two-part system. Described by Duan et al., the intracellular domains of TrkA were fused N-terminal with Cry2-mCherry to create a cytosolic construct. CIB1 was tethered to the plasma membrane to recruit the receptor domains to the membrane. Under blue light stimulation, the cytosolic Cry2-TrkA would be recruited to the membrane via Cry2-CIB1 interactions and also cluster via Cry2-Cry2 oligomerization, activating the receptor (Duan et al., 2018). While this approach has more control of receptor activation, the system still requires co-transfection of the Cry2 and CIB1 constructs. Fusing Cry2 to the intracellular domains of a RTK seems to be the simplest design to induce receptor dimerization while still maintaining spatiotemporal light activation.

BAR domains

Bin/amphiphysin/Rvs (BAR) domain proteins are a large group of proteins containing a BAR domain that generate membrane-curvature of the plasma membrane and intracellular organelles. BAR domains are named for three of its proteins within the family: Bin1, amphiphysin 2 (a splice variant of Bin1), and Rvs (membrane-associated yeast proteins) (Stanishneva-Konovalova et al., 2016). The proteins in the BAR family (simply called BAR proteins in this review) share a functional commonality of membrane association and subsequent membrane shaping due to the presence of the BAR domain; therefore, they are critical for membrane morphology and dynamics. The BAR domain itself consists of a dimer of curved helices that is attributed to its ability to curve membranes; in fact, positively charged residues are present on the outside curved areas which assist in the domain binding to membranes (Antonny, 2011; Salzer et al., 2017; Simunovic et al., 2015). BAR domains generate membrane curvature by association of these positively charged residues with negatively charged phospholipids on the membrane. The biological result of BAR domain-membrane association varies depending on the length, curvature, and the binding affinity of the helices within the domain (Simunovic et al., 2015), in addition to BAR protein interactions with other proteins. These interactions, stimulated by BAR protein recruitment to the membrane, assist in actin cytoskeletal rearrangement and structure formation. Src homology 3 (SH3) domains commonly found in BAR proteins interact with proline-rich regions within actin-associated proteins including dynamin and actin assembly factors (Carman & Dominguez, 2018). Some actin assembly factors that interact with BAR proteins include nucleation promoting factors of the Arp2/3 complex, formins, Wiskott-Aldrich syndrome protein (WASP), WASP family verproline-homologous protein (WAVE), vasodilator-stimulated phosphoprotein (VASP), and VASP-family proteins. Some BAR proteins also

regulate cytoskeletal remodeling through direct or indirect interactions with the Rho GTPases Rac1 and Cdc42 (Carman & Dominguez, 2018).

BAR domains generate positive membrane curvature through the interaction between two monomers, each a coiled-coil of three kinked antiparallel α-helices (Peter et al., 2004). The monomers interact through mainly hydrophobic residues, and the resulting dimer resembles a crescent shape. Due to its shape and the positively charged residues on its concave surface (the inside of the crescent), these domains generate positive curvature when bound to membranes (**Fig. 1.9A**) and therefore possess the ability to form invaginations within a cell (Stanishneva-Konovalova et al., 2016). The function of many BAR proteins is the formation of contacts between synapses and processes for signal transduction in neurons. In neurons, amphiphysins play a role in endocytosis, but in muscle cells, they help form and stabilize T-tubules (E. Lee et al., 2002). Amphiphysin from *Drosophila* houses its BAR domain between residues 35 and 240 (**Fig 1.9B**) (Salzer et al., 2017); residues N-terminal and C-terminal to this domain are disordered. The N-terminal residues (1-26) have been proposed to form an amphipathic helix, and the proteins that contain this helix on the end of the BAR domain has been coined N-BAR (Peter et al., 2004). Proteins that contain a N-BAR domain also include endophilin and sorting nexins (Peter et al., 2004; Simunovic et al., 2015). Endophilins additionally contain a Src homology 3 (SH3) domain that interacts with other proteins in a variety of regulatory processes (**Fig. 1.9B**). Endophilin A modulates endocytosis, and endophilin B1 activates cell apoptosis through interactions with Bax and subsequent release of cytochrome C (L.-Q. Yang et al., 2023). Sorting nexins (SNX) assist in trafficking proteins during endocytosis and proteolysis. A portion of SNXs contain BAR domains (SNX-BAR) essential for trafficking proteins from endosomes to

the *trans*-Golgi network or the plasma membrane as part of the endo-lysosomal pathway (Hanley & Cooper, 2020).

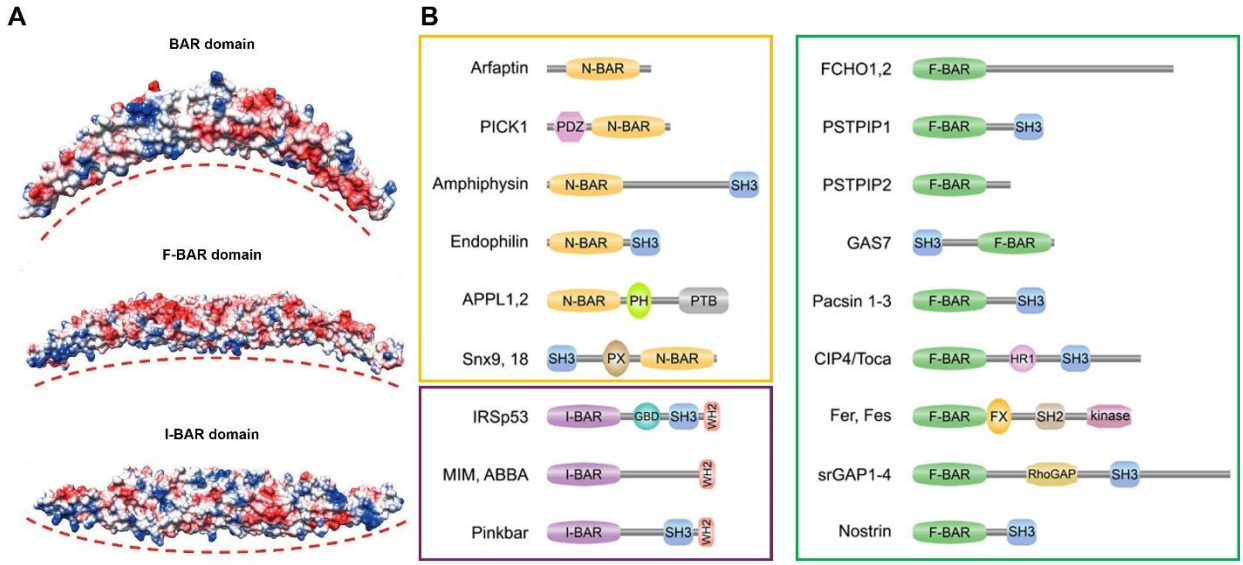

Figure 1.9. *BAR protein structures and their membrane curvature.* ***(A)*** *The BAR/N-BAR and F-BAR domains generate positive membrane curvature upon membrane binding. I-BAR domains induce negative membrane curvature. Positively charged residues are colored in blue, and negatively charged residues are in red. Reused with permission by Acta Naturae, Copyright ® 2016 Park-media Ltd., CC BY 4.0 https://creativecommons.org/licenses/by/4.0/ (Stanishneva-Konovalova et al., 2016).* ***(B)*** *Yellow box: Domains of select N-BAR proteins. Purple box: Domains of select I-BAR proteins. Green box: Domains of select F-BAR protein. Reused with permission by Cellular and Molecular Life Sciences, CC BY 4.0 https://creativecommons.org/licenses/by/4.0/ (Salzer et al., 2017).*

F-BAR, short for FCH-BAR, proteins also generate positive membrane curvatures and are crucial for the curvatures of cellular structures such as filopodia and lamellipodia; these structures are in turn critical for cell mobility and migration (Stanishneva-Konovalova et al., 2016). The BAR domain of F-BAR proteins lies C-terminal to the far N-terminal FES/CIP4 Homology (FCH) region, named for its presence in the FES and CIP4 proteins. In contrast to the classical BAR domains, F-BAR domain monomers are comprised of five α-helices that yield an elongated, shallower crescent shape than the BAR dimer (**Fig. 1.9A**) (Shimada et al., 2007; Zhao et al., 2011). Many F-BAR proteins contain C-terminal SH3 domains as well, which have been found to bind proline-rich proteins associated with the actin cytoskeleton, specifically Wiskott-Aldrich syndrome protein (WASP) and WASP family verproline-homologous protein (WAVE) (**Fig. 1.9B**) (S. Liu et al., 2015; Salzer et al., 2017). F-BAR proteins such as CIP4 and FBP17 mediate actin polymerization at the membrane and can even interact with dynamin to initiate scission of vesicles during endocytosis (S. Liu et al., 2015). CIP4, FBP17, and other F-BARs can also selectively bind phosphoinositides for prejudice to certain membrane regions (Stanishneva-Konovalova et al., 2016). The protein Nervous Wreck (Nwk) functions differently than other F-BAR proteins; instead of forming invaginations or tubules, Nwk induces membrane scallops or ridges by deforming the edges around actin filaments through positive curvature, resulting in protrusions (Becalska et al., 2013).

Inverse BAR domains (I-BAR) are structurally similar to BAR domains in that they also contain a dimer with monomers of three α-helices (Stanishneva-Konovalova et al., 2016). Unlike BAR domains but similar to F-BAR domains, the I-BAR dimer shape is less curved, and since positively charged residues lie on the convex surface (outside of curve), I-BAR domains generate negative membrane curvature (**Fig. 1.9A**) (Zhao et al., 2011). Due to its convex structure, I-BAR

proteins form membrane protrusions instead of invaginations. The I-BAR domain itself strongly binds phosphoinositides within membrane regions, specifically phosphatidylinositol 4,5-bisphosphate (PIP_2). I-BAR domain mechanism of action to form tubular structures involves binding to PIP_2 and subsequent clustering of PIP_2 through oligomerization of the BAR domains (Nepal et al., 2021; Saarikangas et al., 2009). Additionally, I-BAR proteins contain a WASP-homology 2 (WH2) domain that interact with actin monomers to seed actin polymerization mediated by Arp2/3 (**Fig. 1.9B**) (Saarikangas et al., 2011; Zhao et al., 2011). I-BAR domains were first discovered in the proteins missing-in-metastasis (MIM) and insulin receptor kinase substrate p53 (IRSp53). All five I-BAR proteins participate in protrusion formation, e.g. filopodia and lamellipodia, emphasizing their role in cytoskeletal reorganization (Zhao et al., 2011). IRSp53 has been shown to form complexes with Cdc42 and Eps8, an actin bundling and capping protein, to induce filopodia formation (Scita et al., 2008). It also interacts with Rac through its I-BAR domain and the WAVE complex through its SH3 domain to induce actin nucleation during lamellipodia formation (Miki et al., 2000). Actin-bundling protein with BAIAP2 homology (ABBA) proteins are also involved in lamellipodia formation through Rac1 interactions, especially in the processes of glial cells (D. Zheng et al., 2010). MIM proteins share close homology to ABBA proteins and are critical for membrane ruffling, filopodia, and actin stress fibers (Saarikangas et al., 2011; Zhao et al., 2011). Membrane ruffling is modulated by the phosphorylation of central tyrosine residues by Src kinase and interaction with cortactin. In cilia formation and maintenance, MIM is implicated in Sonic hedgehog (Shh) signaling and Gli-mediated transcription (Bershteyn et al., 2010; Saarikangas et al., 2011). In neurons, MIM is integral in the formation and elongation of protrusions on dendritic spines (Saarikangas et al., 2015). An interesting I-BAR protein named planar intestinal and kidney specific BAR domain

protein (Pinkbar) does not form protrusions like other I-BAR domains, but instead creates planar sheet-like assemblies at the membrane. These proteins are mainly expressed in intestinal and kidney epithelial cells and are thought to stabilize the planar membrane at cell-cell junctions. Enrichment of Pinkbar in Rab13 vesicles further suggests that Pinkbar is trafficked by these vesicles to intercellular junctions in order to sculpt and bolster the structural integrity of these junctions (Pykäläinen et al., 2011).

Upon the discovery and subsequent investigations into BAR proteins, researchers have sought an answer to an important question of how do BAR domains sense and generate membrane curvature. Initial generation of membrane curvature starts with binding of BAR domains to the membrane via electrostatic interactions. N-BAR proteins can generate asymmetric curvature through insertion of its amphipathic helix directly into the membrane (Peter et al., 2004). Initial propagation then continues with the incorporation of more BAR proteins to the membrane, forming a scaffold through interactions of the BAR domains with the membrane and with each other. Propagation continues until a threshold is reached: for N-BAR domains, 20% surface density is required before protrusion formation can occur (Simunovic et al., 2015). F-BAR domains bind to flat membrane surfaces and interact with each other laterally to form flat scaffolds, which then arrange into helices alongside tubule formation (Shimada et al., 2007). I-BAR domains have been shown to both sense and generate negative membrane curvature, depending on concentration. I-BAR proteins at low concentration can sense pre-existing curved membranes and then recruit I-BAR and other proteins for propagation; whereas at high concentration of protein, the proteins oligomerize and actively propagate curvature (Breuer et al., 2019; Zhao et al., 2011). I-BAR scaffolds recruit actin for filament and tubule formation; therefore, their role in protrusion formation is transient after curvature propagation.

Conversely, the insertion of N-BAR's amphipathic helix into the membrane stabilizes its interaction with membrane, allowing for persistence of membrane curvature needed for tubule and liposome formation (Peter et al., 2004).

Optogenetic Applications

Few optogenetic investigations have explored light-regulated membrane-binding proteins, and only one study has engineered optogenetic BAR proteins (Jones et al., 2020). Jones et al. designed two opto-BAR constructs using a F-BAR domain and an I-BAR domain with iLID and SsrA/SspB as the light-dependent switch for membrane recruitment (**Fig. 1.10A**). For the F-BAR construct design, SspB and tdTOM was fused N-terminal to the F-BAR domain (residues 1-288) of FBP17 (tdTom-SspBmicro-FBP17BAR). To induce membrane recruitment of F-BAR, phototropic 1 LOV2 domain was tethered to the plasma membrane via a CAAX box at the N-terminus, tagged with EGFP, and fused C-terminal to SsrA (iLID-EGFP-CAAX). In the dark, opto-FBAR is cytosolic, but upon blue light stimulation, SsrA releases from the LOV domain and is available to bind to SspB, recruiting F-BAR to the membrane for association. In COS7 African green monkey kidney cells, light-activated opto-FBAR produced membrane tubules characteristic of FBP17. Previously, they had integrated full-length FBP17 into the construct but observed membrane tubule formation in the dark as FBP17 has a higher affinity to membranes than the F-BAR domain alone. Using only the F-BAR domain in their construct showed minimal dark background activation and a robust response in only 10 seconds of blue light stimulation (Jones et al., 2020).

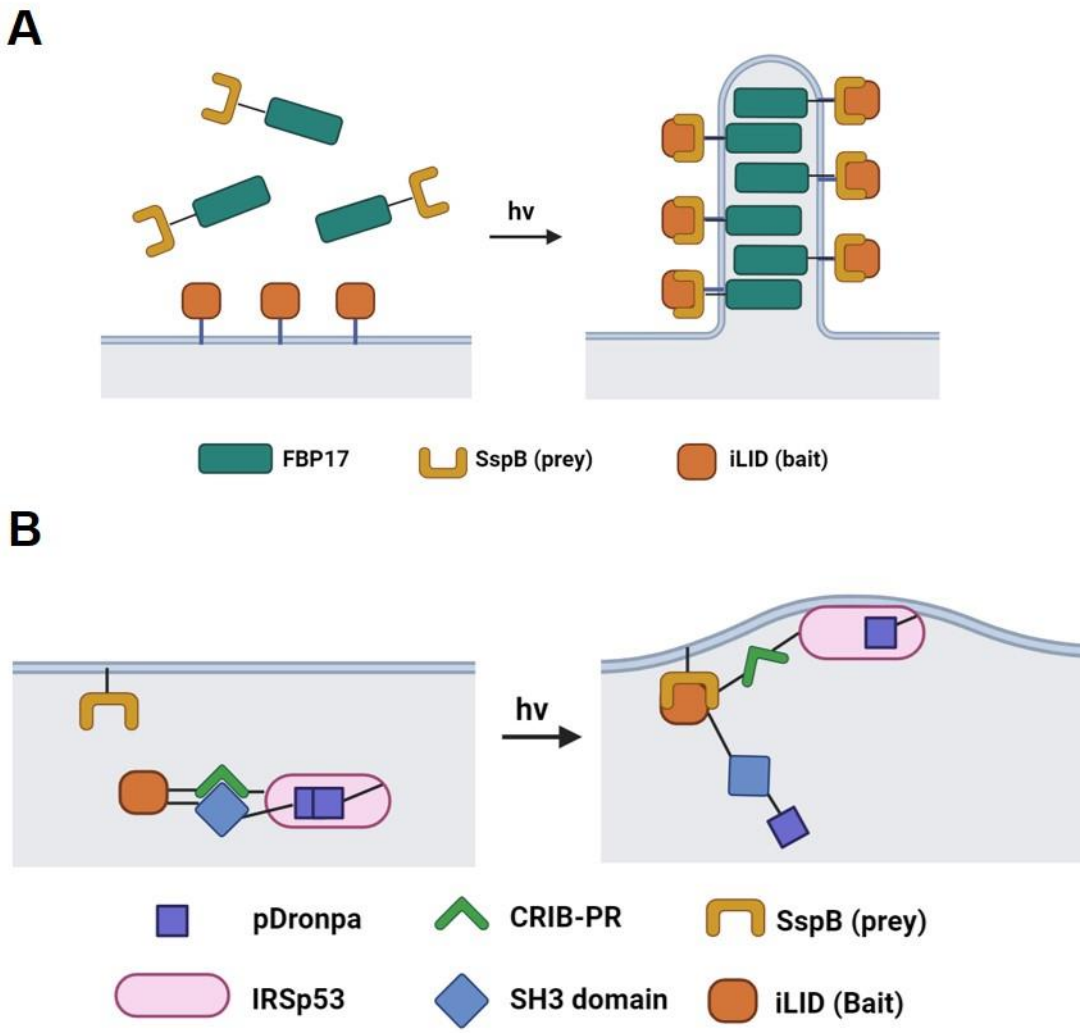

Figure 1.10. *Design of opto-FBAR and opto-IBAR constructs.* ***(A)*** *Opto-FBAR is recruited to the plasma membrane upon blue light stimulation via SspB (prey) and iLID (bait) interactions. FBAR proteins then cluster and generate positive membrane curvature.* ***(B)*** *Opto-IBAR is photo-caged by pdDronpa1in the dark, but is released with blue light, allowing iLID and SspB interactions. IRSp53 binds to the membrane and induces negative membrane curvature (Jones et al., 2020). Created with biorender.com.*

After the success of their opto-FBAR construct, Jones et al. attempted the same construct design with the I-BAR domain of IRSp53 (residues 1-300) in order to induce negative membrane curvature in response to light; however, their initial construct strongly associated with the plasma membrane and formed protrusions in the absence of light. Another design replaced residues 300-370 of IRSp53 with iLID (IRSp53(hv)) to remove the 14-3-3 binding sites contributing to auto-inhibition of IRSp53. To remedy this, a caging system was implemented using photo-dissociable dimeric Dronpa 1 (pdDronpa1). In the dark, the two monomers of pdDronpa1 interact with each other forming a dimer; light stimulation triggers dissociation of the monomers. By inserting IRSp53(hv) between the monomers of pdDronpa1 (pdDronpa1-IRSp53(hv)-pdDronpa1), the domains of IRSp53 responsible for membrane association were caged in the dark, cytosolic and unable to bind membranes. With SspB tethered to the plasma membrane, light illumination released IRSp-53(hv) from the dpDronpa1 photocage and allowed the construct to bind SspB at the membrane (**Fig 1.10B**). Transfected U2OS cells illuminated with light produced rapid and robust filopodial-like protrusions that increased in number and length when compared to the dark state. Additionally, they found that their opto-IBAR colocalized with actin at the site of these protrusions, either through direct interactions or protein associations (Jones et al., 2020).

An optogenetic approach designed by Redchuk et al. directly controls actin localization through fusing a light-dependent switch directly to actin itself (Redchuk et al., 2020). In this system, intrabodies coupled with the iRIS system were used to regulate actin recruitment to the membrane and subsequent polymerization (**Fig. 1.11A**). Intrabodies (iB) are antibodies that bind to proteins within the cell and have been primarily used in knockdown studies of proteins. The dual-light controlled system iRIS utilizes the *As*LOV2 domain with a nuclear localization sequence (NLS) attached to its Jα helix. The phytochrome-interacting protein QPAS1 and a

GFP-labeled iB that binds actin (iB(actin)) were fused to the N-terminal end of *As*LOV2-NLS. In dark conditions, the actin-iRIS construct was localized to the cytosol and formed actin fibers. After blue light exposure, the NLS attached to *As*LOV2 was released, and the construct was translocated to the nucleus. Upon red light exposure, the QPAS1 protein within the actin-iRIS construct was recruited to the plasma membrane via interaction with a membrane-tethered phytochrome BphP1 (BphP1-CAAX) (Redchuk et al., 2020). Although this approach may seem complicated, the ability to regulate actin localization spatially and temporally by three modes with only a two-plasmid co-transfection and light as the stimulus is relatively non-invasive and does not involve enzymatic processes, maintaining the metabolic integrity of the cell.

Other similar approaches have used light-activated heterodimers to recruit non-enzymatic proteins to the plasma membrane. Although GFP has no regulatory or enzymatic function, recruitment of GFP to the plasma membrane in high concentrations can cause membrane perturbations, such as changes in curvature and surface tension (Meshik et al., 2019). Using the iLID system, opto-GFP was recruited and localized to the plasma membrane with light to one side of a macrophage (**Fig. 1.11B**). Lateral accumulation of opto-GFP polarized the cell by inducing membrane curvature and reducing tension at the membrane. In response, the macrophage migrated in the opposite direction of light-stimulated GFP localization. Migration was proposed to be a result of integrin β1 activation, in addition to actin recruitment, at the sites of light exposure as a result of opto-GFP's mechanical forces on the membrane (Meshik et al., 2019).

Another approach uses the I-BAR domain-interacting protein, ezrin, as its protein of interest. Ezrin is part of the ezrin-radixin-moesin (ERM) protein family and as an actin-to-membrane linking protein, plays a role in cell mobility and polarity (Tsai et al., 2018). Like I-

BAR domains, ezrin's N-terminal FERM domain binds to PIP_2. In the cytosol, ezrin adopts a closed conformation where the FERM domain interacts with its C-terminal ERM association domain (C-ERMAD). Upon FERM binding to PIP_2, C-ERMAD is phosphorylated, dissociates with FERM, and the C-ERMAD actin-binding site is accessible (Bretscher et al., 1995). Although found *in vitro* that ezrin cannot sense negative membrane curvature, it does interact with I-BAR domains for recruitment to negatively curved membranes (Tsai et al., 2018). Opto-ezrin has been designed for use in studying micro-ridges present in motile cilia (Yasunaga et al., 2022). In order to underline the importance of ezrin in ciliogenesis, the C-ERMAD domain of ezrin was fused to PhyB, and the FERM domain of ezrin was fused with its binding partner, Pif (**Fig. 1.11C**). In multiciliated cells undergoing maturation, exposure to 660 nm red light during the stages of ciliogenesis maintained cilia structure and function due to the fidelity of ezrin domain presence. In contrast, far red-light exposure at a later developmental stage dissociated the two ezrin domains, resulting in the disruption of rootlet tilting and polarity (Yasunaga et al., 2022). This study provides a unique approach to investigating the role of membrane linker proteins in later stages of development without disrupting earlier developmental stages.

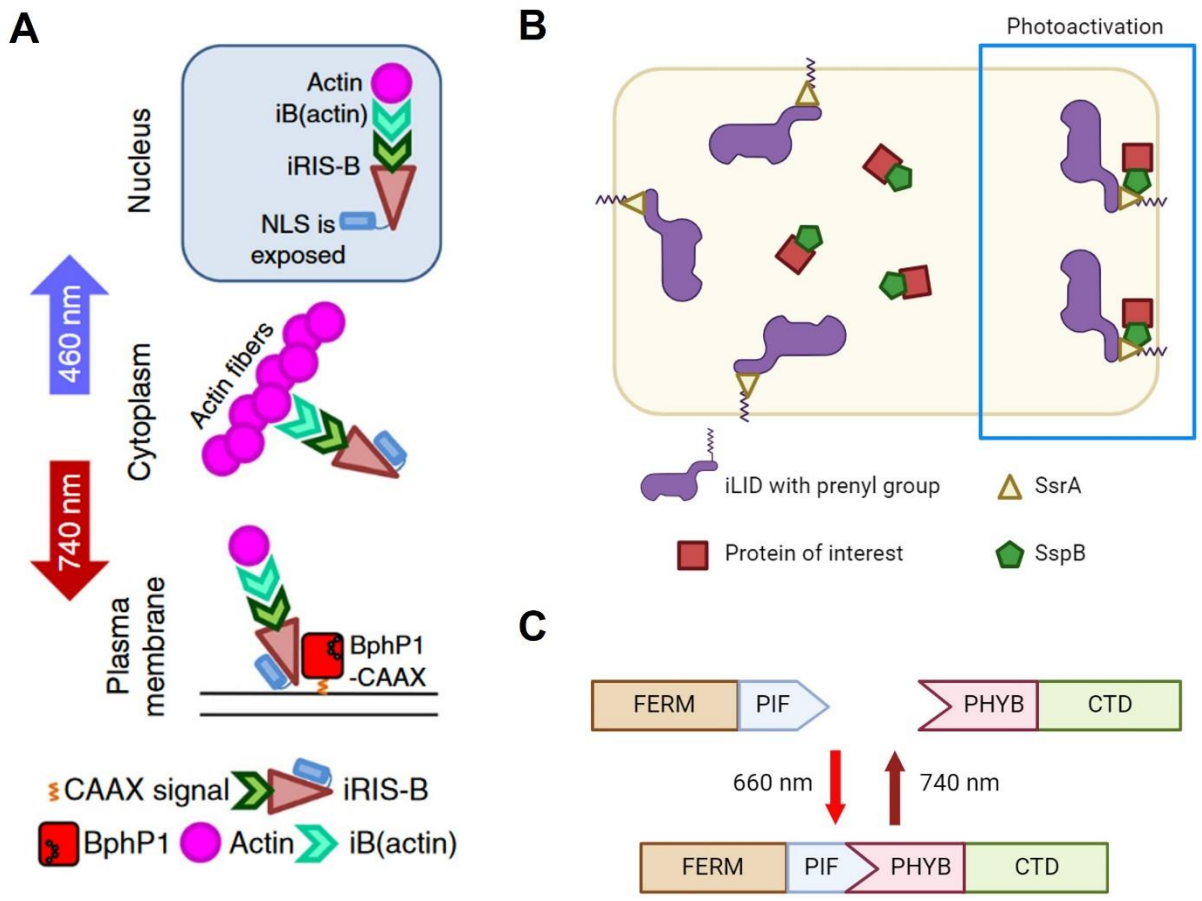

Figure 1.11. *Examples of other optogenetic designs using non-enzymatic proteins.* ***(A)*** *Opto-actin, or iB(actin)-iRIS, forms actin fibers in the cytosol when in the dark. Blue light (460 nm) exposes NLS and opto-actin is translocated to the nucleus. Red light (740 nm) induces heterodimerization of QPAS1 to BphP1-CAAX, localizing actin to the plasma membrane. Reused with permission by Nature Communications, CC BY 4.0, https://creativecommons.org/licenses/by/4.0/ (Redchuk et al., 2020).* ***(B)*** *Blue light activation on one side of cell leads to lateral recruitment of a protein of interest to the lit side as a result of iLID-SsrA and SspB-CAAX interactions (Meshik et al., 2019). Created with biorender.com.* ***(C)*** *Pif fused to the FERM domain of ezrin interacts with PhyB fused to the C-terminal of ezrin (CTD) in the presence of red light (660 nm), reconstituting ezrin function. Far red light (740 nm)*

causes dissociation of Pif-PhyB interaction and breaks apart the ezrin domains, knocking down ezrin function (Yasunaga et al., 2022). Created with biorender.com.

References

Aasheim, H.-C., Delabie, J., & Finne, E. F. (2005). Ephrin-A1 binding to CD4+ T lymphocytes stimulates migration and induces tyrosine phosphorylation of PYK2. *Blood*, *105*(7), 2869–2876. https://doi.org/10.1182/blood-2004-08-2981

Adamantidis, A. R., Zhang, F., Aravanis, A. M., Deisseroth, K., & de Lecea, L. (2007). Neural substrates of awakening probed with optogenetic control of hypocretin neurons. *Nature*, *450*(7168), 420–424. https://doi.org/10.1038/nature06310

Alapin, J. M., Dines, M., Vassiliev, M., Tamir, T., Ram, A., Locke, C., Yu, J., & Lamprecht, R. (2018). Activation of EphB2 Forward Signaling Enhances Memory Consolidation. *Cell Reports*, *23*(7), 2014–2025. https://doi.org/10.1016/j.celrep.2018.04.042

Antonny, B. (2011). Mechanisms of membrane curvature sensing. *Annual Review of Biochemistry*, *80*, 101–123. https://doi.org/10.1146/annurev-biochem-052809-155121

Arvanitis, D., & Davy, A. (2008). Eph/ephrin signaling: Networks. In *Genes and Development* (Vol. 22, Issue 4). https://doi.org/10.1101/gad.1630408

Bailes, H. J., Zhuang, L.-Y., & Lucas, R. J. (2012). Reproducible and sustained regulation of Gαs signalling using a metazoan opsin as an optogenetic tool. *PloS One*, *7*(1), e30774. https://doi.org/10.1371/journal.pone.0030774

Barquilla, A., & Pasquale, E. B. (2015). Eph receptors and ephrins: Therapeutic opportunities. In *Annual Review of Pharmacology and Toxicology* (Vol. 55). https://doi.org/10.1146/annurev-pharmtox-011112-140226

Becalska, A. N., Kelley, C. F., Berciu, C., Stanishneva-Konovalova, T. B., Fu, X., Wang, S., Sokolova, O. S., Nicastro, D., & Rodal, A. A. (2013). Formation of membrane ridges and scallops by the F-BAR protein Nervous Wreck. *Molecular Biology of the Cell*, *24*(15), 2406–2418. https://doi.org/10.1091/mbc.E13-05-0271

Beco, S. de, Vaidžiulytė, K., Manzi, J., Dalier, F., Federico, F. di, Cornilleau, G., Dahan, M., & Coppey, M. (2018). Optogenetic dissection of Rac1 and Cdc42 gradient shaping. *Nature Communications*, *9*(1). https://doi.org/10.1038/s41467-018-07286-8

Bershteyn, M., Atwood, S. X., Woo, W.-M., Li, M., & Oro, A. E. (2010). MIM and Cortactin Antagonism Regulates Ciliogenesis and Hedgehog Signaling. *Developmental Cell*, *19*(2), 270–283. https://doi.org/10.1016/j.devcel.2010.07.009

Björling, A., Berntsson, O., Lehtivuori, H., Takala, H., Hughes, A. J., Panman, M., Hoernke, M., Niebling, S., Henry, L., Henning, R., Kosheleva, I., Chukharev, V., Tkachenko, N. V., Menzel, A., Newby, G., Khakhulin, D., Wulff, M., Ihalainen, J. A., & Westenhoff, S. (2016). Structural photoactivation of a full-length bacterial phytochrome. *Science Advances*, *2*(8), e1600920. https://doi.org/10.1126/sciadv.1600920

Boyle, P. M., Karathanos, T. V., & Trayanova, N. A. (2018). Cardiac Optogenetics: 2018. *JACC. Clinical Electrophysiology*, *4*(2), 155–167. https://doi.org/10.1016/j.jacep.2017.12.006

Brautigam, C. A., Smith, B. S., Ma, Z., Palnitkar, M., Tomchick, D. R., Machius, M., & Deisenhofer, J. (2004). Structure of the photolyase-like domain of cryptochrome 1 from Arabidopsis thaliana. *Proceedings of the National Academy of Sciences of the United States of America*, *101*(33), 12142–12147. https://doi.org/10.1073/pnas.0404851101

Bretscher, A., Gary, R., & Berryman, M. (1995). Soluble ezrin purified from placenta exists as stable monomers and elongated dimers with masked C-terminal ezrin-radixin-moesin association domains. *Biochemistry*, *34*(51), 16830–16837. https://doi.org/10.1021/bi00051a034

Breuer, A., Lauritsen, L., Bertseva, E., Vonkova, I., & Stamou, D. (2019). Quantitative investigation of negative membrane curvature sensing and generation by I-BARs in filopodia of living cells. *Soft Matter*, *15*(48), 9829–9839. https://doi.org/10.1039/C9SM01185D

Buckley, C. E., Moore, R. E., Reade, A., Goldberg, A. R., Weiner, O. D., & Clarke, J. D. W. (2016). Reversible Optogenetic Control of Subcellular Protein Localization in a Live Vertebrate Embryo. *Developmental Cell*, *36*(1), 117–126. https://doi.org/10.1016/j.devcel.2015.12.011

Bugaj, L. J., Spelke, D. P., Mesuda, C. K., Varedi, M., Kane, R. S., & Schaffer, D. V. (2015). Regulation of endogenous transmembrane receptors through optogenetic Cry2 clustering. *Nature Communications*, *6*. https://doi.org/10.1038/ncomms7898

Carman, P. J., & Dominguez, R. (2018). BAR domain proteins-a linkage between cellular membranes, signaling pathways, and the actin cytoskeleton. *Biophysical Reviews*, *10*(6), 1587–1604. https://doi.org/10.1007/s12551-018-0467-7

Carvalho, R. F., Beutler, M., Marler, K. J. M., Knöll, B., Becker-Barroso, E., Heintzmann, R., Ng, T., & Drescher, U. (2006). Silencing of EphA3 through a cis interaction with ephrinA5. *Nature Neuroscience*, *9*(3), 322–330. https://doi.org/10.1038/nn1655

Cecchini, A., & Cornelison, D. D. W. (2022). Eph/Ephrin-Based Protein Complexes: The Importance of cis Interactions in Guiding Cellular Processes. *Frontiers in Molecular Biosciences*, *8*, 809364. https://doi.org/10.3389/fmolb.2021.809364

Che, D. L., Duan, L., Zhang, K., & Cui, B. (2015). The Dual Characteristics of Light-Induced Cryptochrome 2, Homo-oligomerization and Heterodimerization, for Optogenetic Manipulation in Mammalian Cells. *ACS Synthetic Biology*, *4*(10). https://doi.org/10.1021/acssynbio.5b00048

Chen, Q., Song, H., Liu, C., Xu, J., Wei, C., Wang, W., & Han, F. (2020). The Interaction of EphA4 With PDGFRβ Regulates Proliferation and Neuronal Differentiation of Neural Progenitor Cells in vitro and Promotes Neurogenesis in vivo. *Frontiers in Aging Neuroscience*, *12*, 7. https://doi.org/10.3389/fnagi.2020.00007

Chernov, K. G., Redchuk, T. A., Omelina, E. S., & Verkhusha, V. V. (2017). Near-Infrared Fluorescent Proteins, Biosensors, and Optogenetic Tools Engineered from Phytochromes. *Chemical Reviews*, *117*(9), 6423–6446. https://doi.org/10.1021/acs.chemrev.6b00700

Dalva, M. B., Takasu, M. A., Lin, M. Z., Shamah, S. M., Hu, L., Gale, N. W., & Greenberg, M. E. (2000). EphB receptors interact with NMDA receptors and regulate excitatory synapse formation. *Cell*, *103*(6), 945–956. https://doi.org/10.1016/s0092-8674(00)00197-5

Darling, T. K., & Lamb, T. J. (2019). Emerging roles for Eph receptors and ephrin ligands in immunity. In *Frontiers in Immunology* (Vol. 10, Issue JULY). https://doi.org/10.3389/fimmu.2019.01473

Davis, S., Gale, N. W., Aldrich, T. H., Maisonpierre, P. C., Lhotak, V., Pawson, T., Goldfarb, M., & Yancopoulos, G. D. (1994). Ligands for EPH-related receptor tyrosine kinases that require membrane attachment or clustering for activity. *Science (New York, N.Y.)*, *266*(5186), 816–819. https://doi.org/10.1126/science.7973638

De Mena, L., Rizk, P., & Rincon-Limas, D. E. (2018). Bringing Light to Transcription: The Optogenetics Repertoire. *Frontiers in Genetics*, *9*, 518. https://doi.org/10.3389/fgene.2018.00518

Deisseroth, K. (2015). Optogenetics: 10 years of microbial opsins in neuroscience. *Nature Neuroscience*, *18*(9), 1213–1225. https://doi.org/10.1038/nn.4091

Deisseroth, K., & Hegemann, P. (2017). The form and function of channelrhodopsin. *Science (New York, N.Y.)*, *357*(6356), eaan5544. https://doi.org/10.1126/science.aan5544

Duan, L., Hope, J. M., Guo, S., Ong, Q., François, A., Kaplan, L., Scherrer, G., & Cui, B. (2018). Optical Activation of TrkA Signaling. *ACS Synthetic Biology*, *7*(7), 1685–1693. https://doi.org/10.1021/acssynbio.8b00126

Duan, L., Hope, J., Ong, Q., Lou, H. Y., Kim, N., McCarthy, C., Acero, V., Lin, M. Z., & Cui, B. (2017). Understanding CRY2 interactions for optical control of intracellular signaling. *Nature Communications*, *8*(1). https://doi.org/10.1038/s41467-017-00648-8

Flores-Ibarra, A., Maia, R. N. A., Olasz, B., Church, J. R., Gotthard, G., Schapiro, I., Heberle, J., & Nogly, P. (2023). Light-Oxygen-Voltage (LOV)-sensing Domains: Activation Mechanism and Optogenetic Stimulation. *Journal of Molecular Biology*, 168356. https://doi.org/10.1016/j.jmb.2023.168356

Gasser, C., Taiber, S., Yeh, C.-M., Wittig, C. H., Hegemann, P., Ryu, S., Wunder, F., & Möglich, A. (2014). Engineering of a red-light–activated human cAMP/cGMP-specific phosphodiesterase. *Proceedings of the National Academy of Sciences*, *111*(24), 8803–8808. https://doi.org/10.1073/pnas.1321600111

Gong, X., Mendoza-Halliday, D., Ting, J. T., Kaiser, T., Sun, X., Bastos, A. M., Wimmer, R. D., Guo, B., Chen, Q., Zhou, Y., Pruner, M., Wu, C. W.-H., Park, D., Deisseroth, K., Barak, B., Boyden, E. S., Miller, E. K., Halassa, M. M., Fu, Z., … Feng, G. (2020). An Ultra-

Sensitive Step-Function Opsin for Minimally Invasive Optogenetic Stimulation in Mice and Macaques. *Neuron*, *107*(1), 38-51.e8. https://doi.org/10.1016/j.neuron.2020.03.032

Grusch, M., Schelch, K., Riedler, R., Reichhart, E., Differ, C., Berger, W., Inglés-Prieto, Á., & Janovjak, H. (2014). Spatio-temporally precise activation of engineered receptor tyrosine kinases by light. *The EMBO Journal*, *33*(15), 1713–1726. https://doi.org/10.15252/embj.201387695

Gucciardo, E., Sugiyama, N., & Lehti, K. (2014). Eph- and ephrin-dependent mechanisms in tumor and stem cell dynamics. In *Cellular and molecular life sciences: CMLS* (Vol. 71, Issue 19). https://doi.org/10.1007/s00018-014-1633-0

Guntas, G., Hallett, R. A., Zimmerman, S. P., Williams, T., Yumerefendi, H., Bear, J. E., & Kuhlman, B. (2015). Engineering an improved light-induced dimer (iLID) for controlling the localization and activity of signaling proteins. *Proceedings of the National Academy of Sciences*, *112*(1), 112–117. https://doi.org/10.1073/pnas.1417910112

Hanley, S. E., & Cooper, K. F. (2020). Sorting Nexins in Protein Homeostasis. *Cells*, *10*(1), 17. https://doi.org/10.3390/cells10010017

Hartmann, S., Ridley, A. J., & Lutz, S. (2015). The function of rho-associated kinases ROCK1 and ROCK2 in the pathogenesis of cardiovascular disease. In *Frontiers in Pharmacology* (Vol. 6, Issue NOV). https://doi.org/10.3389/fphar.2015.00276

Hernández-Candia, C. N., Pearce, S., & Tucker, C. L. (2021). A modular tool to query and inducibly disrupt biomolecular condensates. *Nature Communications*, *12*(1). https://doi.org/10.1038/s41467-021-22096-1

Hernández-Candia, C. N., & Tucker, C. L. (2020). Optogenetic Control of Gene Expression Using Cryptochrome 2 and a Light-Activated Degron. *Methods in Molecular Biology (Clifton, N.J.)*, *2173*, 151–158. https://doi.org/10.1007/978-1-0716-0755-8_10

Himanen, J. P., Yermekbayeva, L., Janes, P. W., Walker, J. R., Xu, K., Atapattu, L., Rajashankar, K. R., Mensinga, A., Lackmann, M., Nikolov, D. B., & Dhe-Paganon, S. (2010). Architecture of Eph receptor clusters. *Proceedings of the National Academy of Sciences*, *107*(24), 10860–10865. https://doi.org/10.1073/pnas.1004148107

Hubbard, S. R., & Miller, W. T. (2007). Receptor tyrosine kinases: Mechanisms of activation and signaling. *Current Opinion in Cell Biology*, *19*(2), 117–123. https://doi.org/10.1016/j.ceb.2007.02.010

Hughes, R. M. (2018). A compendium of chemical and genetic approaches to light-regulated gene transcription. In *Critical Reviews in Biochemistry and Molecular Biology* (Vol. 53, Issue 5). https://doi.org/10.1080/10409238.2018.1487382

Hughes, R. M., & Virag, J. A. I. (2020). Harnessing the power of eph/ephrin biosemiotics for theranostic applications. In *Pharmaceuticals* (Vol. 13, Issue 6). https://doi.org/10.3390/ph13060112

Ieguchi, K., & Maru, Y. (2019). Roles of EphA1/A2 and ephrin-A1 in cancer. In *Cancer Science* (Vol. 110, Issue 3). https://doi.org/10.1111/cas.13942

Ieguchi, K., Tomita, T., Omori, T., Komatsu, A., Deguchi, A., Masuda, J., Duffy, S. L., Coulthard, M. G., Boyd, A., & Maru, Y. (2014). ADAM12-cleaved ephrin-A1 contributes to lung metastasis. *Oncogene*, *33*(17), 2179–2190. https://doi.org/10.1038/onc.2013.180

Iwata, T., Tokutomi, S., & Kandori, H. (2002). Photoreaction of the Cysteine S−H Group in the LOV2 Domain of *Adiantum* Phytochrome3. *Journal of the American Chemical Society*, *124*(40), 11840–11841. https://doi.org/10.1021/ja020834c

Johnson, H. E., Goyal, Y., Pannucci, N. L., Schüpbach, T., Shvartsman, S. Y., & Toettcher, J. E. (2017). The Spatiotemporal Limits of Developmental Erk Signaling. *Developmental Cell*, *40*(2), 185–192. https://doi.org/10.1016/j.devcel.2016.12.002

Jones, T., Liu, A., & Cui, B. (2020). Light-Inducible Generation of Membrane Curvature in Live Cells with Engineered BAR Domain Proteins. *ACS Synthetic Biology*, *9*(4), 893–901. https://doi.org/10.1021/acssynbio.9b00516

Joshi, J., Rubart, M., & Zhu, W. (2019). Optogenetics: Background, Methodological Advances and Potential Applications for Cardiovascular Research and Medicine. *Frontiers in Bioengineering and Biotechnology*, *7*, 466. https://doi.org/10.3389/fbioe.2019.00466

Kaberniuk, A. A., Baloban, M., Monakhov, M. V., Shcherbakova, D. M., & Verkhusha, V. V. (2021). Single-component near-infrared optogenetic systems for gene transcription regulation. *Nature Communications*, *12*(1), 3859. https://doi.org/10.1038/s41467-021-24212-7

Karathanos, T. V., Bayer, J. D., Wang, D., Boyle, P. M., & Trayanova, N. A. (2016). Opsin spectral sensitivity determines the effectiveness of optogenetic termination of ventricular fibrillation in the human heart: A simulation study. *The Journal of Physiology*, *594*(23), 6879–6891. https://doi.org/10.1113/JP271739

Kennedy, M. J., Hughes, R. M., Peteya, L. A., Schwartz, J. W., Ehlers, M. D., & Tucker, C. L. (2010a). Rapid blue-light-mediated induction of protein interactions in living cells. *Nature Methods*, *7*(12). https://doi.org/10.1038/nmeth.1524

Kennedy, M. J., Hughes, R. M., Peteya, L. A., Schwartz, J. W., Ehlers, M. D., & Tucker, C. L. (2010b). Rapid blue-light-mediated induction of protein interactions in living cells. *Nature Methods*, *7*(12), 973–975. https://doi.org/10.1038/nmeth.1524

Khamo, J. S., Krishnamurthy, V. V., Chen, Q., Diao, J., & Zhang, K. (Optogenetic Delineation of Receptor Tyrosine Kinase Subcircuits in PC12 Cell Differentiation. *Cell Chemical Biology*, *26*(3), 400-410.e3. https://doi.org/10.1016/j.chembiol.2018.11.004

Klein, R. (2009). Bidirectional modulation of synaptic functions by Eph/ephrin signaling. In *Nature Neuroscience* (Vol. 12, Issue 1). https://doi.org/10.1038/nn.2231

Kolar, K., Knobloch, C., Stork, H., Žnidarič, M., & Weber, W. (2018). OptoBase: A Web Platform for Molecular Optogenetics. *ACS Synthetic Biology*, *7*(7), 1825–1828. https://doi.org/10.1021/acssynbio.8b00120

Konermann, S., Brigham, M. D., Trevino, A. E., Hsu, P. D., Heidenreich, M., Cong, L., Platt, R. J., Scott, D. A., Church, G. M., & Zhang, F. (2013). Optical control of mammalian endogenous transcription and epigenetic states. *Nature*, *500*(7463). https://doi.org/10.1038/nature12466

Koyanagi, M., & Terakita, A. (2014). Diversity of animal opsin-based pigments and their optogenetic potential. *Biochimica Et Biophysica Acta*, *1837*(5), 710–716. https://doi.org/10.1016/j.bbabio.2013.09.003

Kramer, M. M., Lataster, L., Weber, W., & Radziwill, G. (2021). Optogenetic Approaches for the Spatiotemporal Control of Signal Transduction Pathways. *International Journal of Molecular Sciences*, *22*(10), 5300. https://doi.org/10.3390/ijms22105300

Lee, E., Marcucci, M., Daniell, L., Pypaert, M., Weisz, O. A., Ochoa, G.-C., Farsad, K., Wenk, M. R., & De Camilli, P. (2002). Amphiphysin 2 (Bin1) and T-Tubule Biogenesis in Muscle. *Science*, *297*(5584), 1193–1196. https://doi.org/10.1126/science.1071362

Lehtinen, K., Nokia, M. S., & Takala, H. (2022). Red Light Optogenetics in Neuroscience. *Frontiers in Cellular Neuroscience*, *15*, 778900. https://doi.org/10.3389/fncel.2021.778900

Liang, L.-Y., Patel, O., Janes, P. W., Murphy, J. M., & Lucet, I. S. (2019). Eph receptor signalling: From catalytic to non-catalytic functions. *Oncogene*, *38*(39), 6567–6584. https://doi.org/10.1038/s41388-019-0931-2

Liu, H., Yu, X., Li, K., Klejnot, J., Yang, H., Lisiero, D., & Lin, C. (2008). Photoexcited CRY2 interacts with CIB1 to regulate transcription and floral initiation in Arabidopsis. *Science (New York, N.Y.)*, *322*(5907), 1535–1539. https://doi.org/10.1126/science.1163927

Liu, S., Xiong, X., Zhao, X., Yang, X., & Wang, H. (2015). F-BAR family proteins, emerging regulators for cell membrane dynamic changes-from structure to human diseases. *Journal of Hematology & Oncology*, *8*, 47. https://doi.org/10.1186/s13045-015-0144-2

Locke, C., Machida, K., Wu, Y., & Yu, J. (2017). Optogenetic activation of EphB2 receptor in dendrites induced actin polymerization by activating Arg kinase. *Biology Open*, *6*(12). https://doi.org/10.1242/bio.029900

Marquardt, T., Shirasaki, R., Ghosh, S., Andrews, S. E., Carter, N., Hunter, T., & Pfaff, S. L. (2005). Coexpressed EphA Receptors and Ephrin-A Ligands Mediate Opposing Actions on Growth Cone Navigation from Distinct Membrane Domains. *Cell*, *121*(1), 127–139. https://doi.org/10.1016/j.cell.2005.01.020

Mattis, J., Tye, K. M., Ferenczi, E. A., Ramakrishnan, C., O'Shea, D. J., Prakash, R., Gunaydin, L. A., Hyun, M., Fenno, L. E., Gradinaru, V., Yizhar, O., & Deisseroth, K. (2011).

Principles for applying optogenetic tools derived from direct comparative analysis of microbial opsins. *Nature Methods*, *9*(2), 159–172. https://doi.org/10.1038/nmeth.1808

Meshik, X., O'Neill, P. R., & Gautam, N. (2019). Physical Plasma Membrane Perturbation Using Subcellular Optogenetics Drives Integrin-Activated Cell Migration. *ACS Synthetic Biology*, *8*(3), 498–510. https://doi.org/10.1021/acssynbio.8b00356

Miao, H., Burnett, E., Kinch, M., Simon, E., & Wang, B. (2000). Activation of EphA2 kinase suppresses integrin function and causes focal-adhesion-kinase dephosphorylation. *Nature Cell Biology*, *2*(2), 62–69. https://doi.org/10.1038/35000008

Miki, H., Yamaguchi, H., Suetsugu, S., & Takenawa, T. (2000). IRSp53 is an essential intermediate between Rac and WAVE in the regulation of membrane ruffling. *Nature*, *408*(6813), 732–735. https://doi.org/10.1038/35047107

Nagasawa, Y., Ueda, H. H., Kawabata, H., & Murakoshi, H. (2023). LOV2-based photoactivatable CaMKII and its application to single synapses: Local Optogenetics. *Biophysics and Physicobiology*, *20*(2), n/a. https://doi.org/10.2142/biophysico.bppb-v20.0027

Nepal, B., Sepehri, A., & Lazaridis, T. (2021). Mechanism of negative membrane curvature generation by I-BAR domains. *Structure (London, England: 1993)*, *29*(12), 1440-1452.e4. https://doi.org/10.1016/j.str.2021.07.010

Nievergall, E., Lackmann, M., & Janes, P. W. (2012). Eph-dependent cell-cell adhesion and segregation in development and cancer. *Cellular and Molecular Life Sciences*, *69*(11), 1813–1842. https://doi.org/10.1007/s00018-011-0900-6

Niopek, D., Wehler, P., Roensch, J., Eils, R., & Di Ventura, B. (2016). Optogenetic control of nuclear protein export. *Nature Communications*, *7*(1), 10624. https://doi.org/10.1038/ncomms10624

Nolt, M. J., Lin, Y., Hruska, M., Murphy, J., Sheffler-Colins, S. I., Kayser, M. S., Passer, J., Bennett, M. V. L., Zukin, R. S., & Dalva, M. B. (2011). EphB controls NMDA receptor function and synaptic targeting in a subunit-specific manner. *The Journal of Neuroscience: The Official Journal of the Society for Neuroscience*, *31*(14), 5353–5364. https://doi.org/10.1523/JNEUROSCI.0282-11.2011

Oakes, P. W., Wagner, E., Brand, C. A., Probst, D., Linke, M., Schwarz, U. S., Glotzer, M., & Gardel, M. L. (2017). Optogenetic control of RhoA reveals zyxin-mediated elasticity of stress fibres. *Nature Communications*, *8*(1), 15817. https://doi.org/10.1038/ncomms15817

O'Neal, W. T., Griffin, W. F., Dries-Devlin, J. L., Kent, S. D., Chen, J., Willis, M. S., & Virag, J. A. I. (2013). Ephrin-Eph signaling as a potential therapeutic target for the treatment of myocardial infarction. *Medical Hypotheses*, *80*(6). https://doi.org/10.1016/j.mehy.2013.02.024

Park, H., Kim, N. Y., Lee, S., Kim, N., Kim, J., & Heo, W. D. (2017). Optogenetic protein clustering through fluorescent protein tagging and extension of CRY2. *Nature Communications*, *8*(1), 30. https://doi.org/10.1038/s41467-017-00060-2

Pasquale, E. B. (2010). Eph receptors and ephrins in cancer: Bidirectional signalling and beyond. *Nature Reviews. Cancer*, *10*(3), 165–180. https://doi.org/10.1038/nrc2806

Peter, B. J., Kent, H. M., Mills, I. G., Vallis, Y., Butler, P. J. G., Evans, P. R., & McMahon, H. T. (2004). BAR domains as sensors of membrane curvature: The amphiphysin BAR structure. *Science (New York, N.Y.)*, *303*(5657), 495–499. https://doi.org/10.1126/science.1092586

Pratt, R. L., & Kinch, M. S. (2002). Activation of the EphA2 tyrosine kinase stimulates the MAP/ERK kinase signaling cascade. *Oncogene*, *21*(50), 7690–7699. https://doi.org/10.1038/sj.onc.1205758

Pudasaini, A., El-Arab, K. K., & Zoltowski, B. D. (2015). LOV-based optogenetic devices: Light-driven modules to impart photoregulated control of cellular signaling. *Frontiers in Molecular Biosciences*, *2*, 18. https://doi.org/10.3389/fmolb.2015.00018

Pykäläinen, A., Boczkowska, M., Zhao, H., Saarikangas, J., Rebowski, G., Jansen, M., Hakanen, J., Koskela, E. V., Peränen, J., Vihinen, H., Jokitalo, E., Salminen, M., Ikonen, E., Dominguez, R., & Lappalainen, P. (2011). Pinkbar is an epithelial-specific BAR domain protein that generates planar membrane structures. *Nature Structural & Molecular Biology*, *18*(8), 902–907. https://doi.org/10.1038/nsmb.2079

Redchuk, T. A., Karasev, M. M., Verkhusha, P. V., Donnelly, S. K., Hülsemann, M., Virtanen, J., Moore, H. M., Vartiainen, M. K., Hodgson, L., & Verkhusha, V. V. (2020). Optogenetic regulation of endogenous proteins. *Nature Communications*, *11*(1), 605. https://doi.org/10.1038/s41467-020-14460-4

Reichhart, E., Ingles-Prieto, A., Tichy, A., McKenzie, C., & Janovjak, H. (2016). A Phytochrome Sensory Domain Permits Receptor Activation by Red Light. *Angewandte Chemie International Edition*, *55*(21), 6339–6342. https://doi.org/10.1002/anie.201601736

Rost, B. R., Schneider-Warme, F., Schmitz, D., & Hegemann, P. (2017). Optogenetic Tools for Subcellular Applications in Neuroscience. In *Neuron* (Vol. 96, Issue 3). https://doi.org/10.1016/j.neuron.2017.09.047

Saarikangas, J., Kourdougli, N., Senju, Y., Chazal, G., Segerstråle, M., Minkeviciene, R., Kuurne, J., Mattila, P. K., Garrett, L., Hölter, S. M., Becker, L., Racz, I., Hans, W., Klopstock, T., Wurst, W., Zimmer, A., Fuchs, H., Gailus-Durner, V., Hrabě de Angelis, M., … Hotulainen, P. (2015). MIM-Induced Membrane Bending Promotes Dendritic Spine Initiation. *Developmental Cell*, *33*(6), 644–659. https://doi.org/10.1016/j.devcel.2015.04.014

Saarikangas, J., Mattila, P. K., Varjosalo, M., Bovellan, M., Hakanen, J., Calzada-Wack, J., Tost, M., Jennen, L., Rathkolb, B., Hans, W., Horsch, M., Hyvönen, M. E., Perälä, N., Fuchs, H., Gailus-Durner, V., Esposito, I., Wolf, E., de Angelis, M. H., Frilander, M. J., … Lappalainen, P. (2011). Missing-in-metastasis MIM/MTSS1 promotes actin assembly at intercellular junctions and is required for integrity of kidney epithelia. *Journal of Cell Science*, *124*(Pt 8), 1245–1255. https://doi.org/10.1242/jcs.082610

Saarikangas, J., Zhao, H., Pykäläinen, A., Laurinmäki, P., Mattila, P. K., Kinnunen, P. K. J., Butcher, S. J., & Lappalainen, P. (2009). Molecular mechanisms of membrane deformation by I-BAR domain proteins. *Current Biology: CB*, *19*(2), 95–107. https://doi.org/10.1016/j.cub.2008.12.029

Salzer, U., Kostan, J., & Djinović-Carugo, K. (2017). Deciphering the BAR code of membrane modulators. *Cellular and Molecular Life Sciences*, *74*(13), 2413–2438. https://doi.org/10.1007/s00018-017-2478-0

Schwinn, K., Ferré, N., & Huix-Rotllant, M. (2020). UV-visible absorption spectrum of FAD and its reduced forms embedded in a cryptochrome protein. *Physical Chemistry Chemical Physics: PCCP*, *22*(22), 12447–12455. https://doi.org/10.1039/d0cp01714k

Scita, G., Confalonieri, S., Lappalainen, P., & Suetsugu, S. (2008). IRSp53: Crossing the road of membrane and actin dynamics in the formation of membrane protrusions. *Trends in Cell Biology*, *18*(2), 52–60. https://doi.org/10.1016/j.tcb.2007.12.002

Shimada, A., Niwa, H., Tsujita, K., Suetsugu, S., Nitta, K., Hanawa-Suetsugu, K., Akasaka, R., Nishino, Y., Toyama, M., Chen, L., Liu, Z.-J., Wang, B.-C., Yamamoto, M., Terada, T., Miyazawa, A., Tanaka, A., Sugano, S., Shirouzu, M., Nagayama, K., … Yokoyama, S. (2007). Curved EFC/F-BAR-domain dimers are joined end to end into a filament for membrane invagination in endocytosis. *Cell*, *129*(4), 761–772. https://doi.org/10.1016/j.cell.2007.03.040

Shimizu-Sato, S., Huq, E., Tepperman, J. M., & Quail, P. H. (2002). A light-switchable gene promoter system. *Nature Biotechnology*, *20*(10), 1041–1044. https://doi.org/10.1038/nbt734

Simunovic, M., Voth, G. A., Callan-Jones, A., & Bassereau, P. (2015). When Physics Takes Over: BAR Proteins and Membrane Curvature. *Trends in Cell Biology*, *25*(12), 780–792. https://doi.org/10.1016/j.tcb.2015.09.005

., Domratcheva, T & Schulten, K. (2014). Separation of photo-induced radical pair in cryptochrome to a functionally critical distance. https://doi.org/10.1038/srep03845

Stanishneva-Konovalova, T. B., Derkacheva, N. I., Polevova, S. V., & Sokolova, O. S. (2016). The Role of BAR Domain Proteins in the Regulation of Membrane Dynamics. *Acta Naturae*, *8*(4), 60–69.

Strickland, D., Lin, Y., Wagner, E., Hope, C. M., Zayner, J., Antoniou, C., Sosnick, T. R., Weiss, E. L., & Glotzer, M. (2012). TULIPs: Tunable, light-controlled interacting protein tags for cell biology. *Nature Methods*, *9*(4), 379–384. https://doi.org/10.1038/nmeth.1904

Toettcher, J. E., Gong, D., Lim, W. A., & Weiner, O. D. (2011). Light Control of Plasma Membrane Recruitment Using the Phy–PIF System. In *Methods in Enzymology* (Vol. 497, pp. 409–423). Elsevier. https://doi.org/10.1016/B978-0-12-385075-1.00017-2

Toettcher, J. E., Weiner, O. D., & Lim, W. A. (2013). Using Optogenetics to Interrogate the Dynamic Control of Signal Transmission by the Ras/Erk Module. *Cell*, *155*(6), 1422–1434. https://doi.org/10.1016/j.cell.2013.11.004

Tsai, F.-C., Bertin, A., Bousquet, H., Manzi, J., Senju, Y., Tsai, M.-C., Picas, L., Miserey-Lenkei, S., Lappalainen, P., Lemichez, E., Coudrier, E., & Bassereau, P. (2018). Ezrin enrichment on curved membranes requires a specific conformation or interaction with a curvature-sensitive partner. *eLife*, *7*, e37262. https://doi.org/10.7554/eLife.37262

Wang, H., Vilela, M., Winkler, A., Tarnawski, M., Schlichting, I., Yumerefendi, H., Kuhlman, B., Liu, R., Danuser, G., & Hahn, K. M. (2016). LOVTRAP: An optogenetic system for photoinduced protein dissociation. *Nature Methods*, *13*(9), 755–758. https://doi.org/10.1038/nmeth.3926

Wang, Y., Shang, Y., Li, J., Chen, W., Li, G., Wan, J., Liu, W., & Zhang, M. (2018). Specific Eph receptor-cytoplasmic effector signaling mediated by SAM–SAM domain interactions. *eLife*, *7*, e35677. https://doi.org/10.7554/eLife.35677

Wiesner, S., Wybenga-Groot, L. E., Warner, N., Lin, H., Pawson, T., Forman-Kay, J. D., & Sicheri, F. (2006). A change in conformational dynamics underlies the activation of Eph receptor tyrosine kinases. *The EMBO Journal*, *25*(19), 4686–4696. https://doi.org/10.1038/sj.emboj.7601315

Williams, S. C. P., & Deisseroth, K. (2013). Optogenetics. *Proceedings of the National Academy of Sciences of the United States of America*, *110*(41), 16287. https://doi.org/10.1073/pnas.1317033110

Wimmer-Kleikamp, S. H., Janes, P. W., Squire, A., Bastiaens, P. I. H., & Lackmann, M. (2004). Recruitment of Eph receptors into signaling clusters does not require ephrin contact. *The Journal of Cell Biology*, *164*(5), 661–666. https://doi.org/10.1083/jcb.200312001

Yamazaki, T., Masuda, J., Omori, T., Usui, R., Akiyama, H., & Maru, Y. (2009). EphA1 interacts with integrin-linked kinase and regulates cell morphology and motility. *Journal of Cell Science*, *122*(2). https://doi.org/10.1242/jcs.036467

Yang, J. S., Wei, H. X., Chen, P. P., & Wu, G. (2018). Roles of Eph/ephrin bidirectional signaling in central nervous system injury and recovery (Review). In *Experimental and Therapeutic Medicine* (Vol. 15, Issue 3). https://doi.org/10.3892/etm.2018.5702

Yang, L.-Q., Huang, A.-F., & Xu, W.-D. (2023). Biology of endophilin and it's role in disease. *Frontiers in Immunology*, *14*, 1297506. https://doi.org/10.3389/fimmu.2023.1297506

Yang, X., Jost, A. P.-T., Weiner, O. D., & Tang, C. (2013). A light-inducible organelle-targeting system for dynamically activating and inactivating signaling in budding yeast. *Molecular Biology of the Cell*, *24*(15), 2419–2430. https://doi.org/10.1091/mbc.e13-03-0126

Yasunaga, T., Wiegel, J., Bergen, M. D., Helmstädter, M., Epting, D., Paolini, A., Çiçek, Ö., Radziwill, G., Engel, C., Brox, T., Ronneberger, O., Walentek, P., Ulbrich, M. H., & Walz, G. (2022). Microridge-like structures anchor motile cilia. *Nature Communications*, *13*(1), 2056. https://doi.org/10.1038/s41467-022-29741-3

Yu, N., Huang, L., Zhou, Y., Xue, T., Chen, Z., & Han, G. (2019). Near-Infrared-Light Activatable Nanoparticles for Deep-Tissue-Penetrating Wireless Optogenetics. *Advanced Healthcare Materials*, *8*(6), e1801132. https://doi.org/10.1002/adhm.201801132

Yu, X., Liu, H., Klejnot, J., & Lin, C. (2010). The Cryptochrome Blue Light Receptors. *The Arabidopsis Book*, *8*, e0135. https://doi.org/10.1199/tab.0135

Zhao, H., Pykäläinen, A., & Lappalainen, P. (2011). I-BAR domain proteins: Linking actin and plasma membrane dynamics. *Current Opinion in Cell Biology*, *23*(1), 14–21. https://doi.org/10.1016/j.ceb.2010.10.005

Zheng, D., Niu, S., Yu, D., Zhan, X. H., Zeng, X., Cui, B., Chen, Y., Yoon, J., Martin, S. S., Lu, X., & Zhan, X. (2010). Abba promotes PDGF-mediated membrane ruffling through activation of the small GTPase Rac1. *Biochemical and Biophysical Research Communications*, *401*(4), 527–532. https://doi.org/10.1016/j.bbrc.2010.09.087

Zoltowski, B. D., Vaccaro, B., & Crane, B. R. (2009). Mechanism-based tuning of a LOV domain photoreceptor. *Nature Chemical Biology*, *5*(11), 827–834. https://doi.org/10.1038/nchembio.210

CHAPTER 2

Optogenetic Regulation of EphA1 RTK Activation and Signaling

Introduction

Erythropoietin-producing hepatocellular carcinoma (Eph) receptors are the largest family of receptor tyrosine kinases (RTK) with 14 different types of this transmembrane protein (D. Arvanitis & Davy, 2008). Each Eph receptor includes an extracellular domain, comprising of the ligand-binding domain on the N-terminal, a cysteine-rich region, and two consecutive fibronectin type-III domains that are adjacent to the transmembrane region of the Eph receptor (**Fig. 2.1**) (Hughes & Virag, 2020) and an intracellular portion consisting of a juxtamembrane region, followed by a kinase domain, a sterile alpha motif (SAM) domain, and ending in a PDZ-binding motif at the C-terminus. Each of the two classes of Eph receptors, EphA (A1-A8, A10) and EphB (B1-5), is classified by the binding of their corresponding ligands, ephrinA and ephrinB, respectively (D. Arvanitis & Davy, 2008; L. Y. Liang et al., 2019). EphrinA and B both contain an extracellular receptor-binding domain that interacts with the ligand-binding domain on the Eph receptor; however, ephrinA is anchored to the membrane by a glycosylphosphatidylinositol (GPI) post-translational modification, and ephrinB has a transmembrane domain with an intracellular PDZ-binding motif on the C-terminus (Darling & Lamb, 2019; L. Y. Liang et al., 2019).

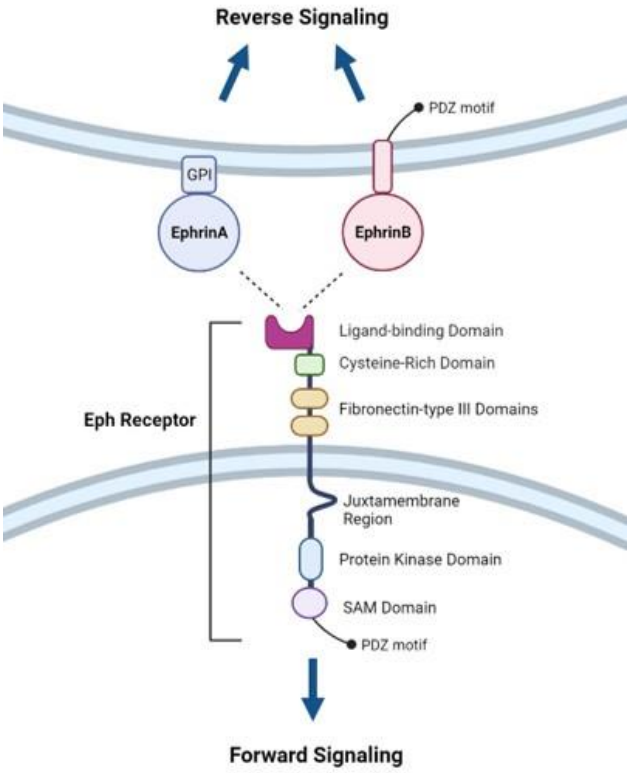

Figure 2.1. *Schematic of Eph receptor and ephrin and their bi-directional signaling. Ephrin binds to the extracellular ligand-binding domain of the Eph receptor expressed on a neighboring cell. This interaction activates reverse signaling by the ephrin ligand in one cell and forward signaling by the Eph receptor in the other cell.*

The ephrin/Eph system incorporates bi-directional signaling pathway, triggered by the binding of ephrin to the Eph's ligand-binding domain (**Fig. 2.1**)**.** Forward signaling activates kinase signaling through autophosphorylation of the tyrosine kinase domain, leading to downstream signaling. Reverse signaling is activated through cell surface displayed ephrin ligands and controls ephrin-specific pathways in the host cell. This distinctive type of signaling has implications for cell-cell communication, including cell repulsion, migration, differentiation, and proliferation (Barquilla & Pasquale, 2015; Darling & Lamb, 2019; Gucciardo et al., 2014;

Hughes & Virag, 2020; Lai & Ip, 2009; L. Y. Liang et al., 2019; Lisabeth et al., 2013). In neural development for example, forward signaling mediates axonal growth cone collapse, and reverse signaling induces growth cone survival, which in tandem can regulate migration of axons to their target destinations (Lai & Ip, 2009; Lisabeth et al., 2013).

These complex, overlapping signals make it difficult to determine the effects of individual Eph receptor activation and disentangle subsequent downstream signaling. As a result, Eph and ephrin signaling crosstalk is not completely understood, and the reports of the impacts of Eph/ephrin signaling activation are sometimes contradictory (Ieguchi & Maru, 2019). To simplify the complex web of signaling pathways, synthetic biology strategies for the control of specific Eph receptor types could more precisely delineate Eph signaling outcomes, leading to a better understanding of the impacts of Eph-dependent cell signaling cascades (Locke et al., 2017). Optogenetics comprises one such strategy that could be applied to the control of Eph receptor signaling.

In this work, we use cryptochrome 2 (Cry2), a blue light-dependent photoreceptor found in *Arabidopsis thaliana* (Kennedy et al., 2010) to create a light responsive EphA1 receptor mimic. Cry2 has been used in numerous protein fusion experiments due to its ability to homo-oligomerize in the cell cytosol in response to blue light stimulation (Bugaj et al., 2015; Hernández-Candia et al., 2021) and enables direct regulation of various cellular processes solely by control with light (Duan et al., 2017; Hughes, 2018; Kennedy et al., 2010). In prior studies of optogenetic control of Eph receptor domains, Locke et. al. described an optogenetic EphB2 receptor, named OptoEphB2, consisting of only the intracellular domains of EphB2 fused C-terminal to Cry2 and the fluorescent protein, mCherry (Locke et al., 2017). In these studies, a mutant of Cry2, Cry2olig, was used to improve light-initialized oligomerization (Taslimi et al.,

2014). For this study, EphA1 was selected as the receptor of interest due to its role in cell adhesion and migration, cancer progression, and Alzheimer's disease (Carrasquillo et al., 2011; Gucciardo et al., 2014; Ieguchi & Maru, 2019; Naj et al., 2011; Yamazaki et al., 2009). Although EphA1 was the first Eph receptor discovered in 1987 (Hirai et al., 1987), its specific function in different cell types has yet to be fully investigated (Ieguchi & Maru, 2019). Its complementary ligand, ephrinA1, has also been studied for its reverse signaling effect, which similarly promotes cell de-adhesion and migration (J. S. Yang et al., 2018). In previous studies of wild-type EphA1, ephrinA1-Fc stimulation was required to activate the receptor and produce cellular response (Yamazaki et al., 2009). To create a light-activated EphA1 that functions in the absence of ephrinA1 ligand stimulation, we coupled Cry2olig with various truncations EphA1 and investigated their ability to oligomerize and undergo RTK-dependent autophosphorylation.

Material and Methods

EphA1Cry2 construct design

Forward and reverse primers for the four EphA1 constructs were designed and amplified by PCR using human EphA1 template (P21709) (**Fig. AII.1; Table AII.1**). Construct PM-EphA1Cry2 and PM-EphA1Cry2Δ primers included a plasma membrane tether sequence at the 3' end. The amino acid sequence for PMa is MGCIKSKRKDNLNDDE (Resh, 1999; Thaa et al., 2015), and the amino acid sequence for PMb is MGSSKSKPK (Locke et al., 2017). Select regions of EphA1 (excluding the extracellular regions of IM-EphA1Cry2 construct) were cloned into Cry2olig-mCherry (Addgene: #60032) using NheI and BmtI restriction sites. The extracellular region of IM-EphA1Cry2 was cloned into Cry2olig-mCherry using BsrgI and NotI. The constructs were transformed into competent *E. Coli*, purified, and characterized via Sanger sequencing.

Cell culture preparation

HEK293T cells and Neuro2a cells were cultured in Dulbecco's Modified Eagle Medium (DMEM) (Gibco) supplemented with 10% fetal bovine serum (FBS) and 1% Penicillin/Streptomycin (PenStrep) (Gibco) in an incubator at 37°C and 5% CO_2. Cells were plated on glass-bottom dishes for imaging or 6-well plates for lysis and transfected with each construct using Calfectin (Signa Gen Laboratories). For ERK and Akt immunostaining, HEK293T cells were serum-starved in DMEM with 0.1% FBS for 2 hours prior to light exposure and lysis.

Neuro2a differentiation

Neuro2a cells were seeded at 60% confluency in 1 mL DMEM with 10% FBS and 1% PenStrep on 35 mm glass-bottom dishes. The media was replaced after 24 hours with DMEM with 1% FBS and 20 µM retinoic acid. The media was replaced daily for 3 days. On the third day, cells were transfected with either PMb-EphA1Cry2 or Cry2olig using Calfectin (Signa Gen Laboratories) in differentiation media and used for imaging the next day. Cells were serum-starved in 1x PBS for 2-4 hours prior to imaging.

Kinase translocation reporter subcloning and experiment

ERK-KTR-mNeonGreen and Akt-KTR-mTurquoise2 was subcloned from Addgene plasmid #129631 (Chavez-Abiega, 2022) into a phCMV vector (Genelantis) (**Table AII.1**). HEK293T cells were transfected with 1000 ng of KTR (ERK-KTR or Akt-KTR) or co-transfected with 1000 ng of each construct (PMb-EphA1Cry2Δ or Cry2olig) using Calfectin (Signa Gen Laboratories). The following day, cells were serum-starved with Leibovitz's L-15 medium for 1-2 hours. Cells were then incubated in 1 mL of 20 mM Hoechst 33342 nuclear stain in DPBS, washed with 1 mL DPBS, and placed back in L15 media for imaging. For ERK-KTR and Akt-KTR only cells, a 10-minute pre-stimulus period was imaged, then cells were stimulated with 500 ng/mL of epidermal growth factor (EGF).

Microscopy and image analysis

HEK293T cells and Neuro2a cells were imaged on a Leica DMi8 Live Cell Imaging System, equipped with an OKOLab stage-top live cell incubation system, LASX software, Leica HCX PL APO 63×/1.40 to 0.60 numerical objective oil objective, Lumencor LED light engine,

CTRadvanced+ power supply, and a Leica DFC900 GT camera. The mCherry channel (553 nm, 50% power, 200 ms exposure) was used for pre, during, and post-light visualization. GFP channel (480 nm, 50% power, 50 ms exposure) was used for Cry2 activation. Images were captured in 30 sec intervals.

Live-cell confocal images of HEK293T cells were collected on Zeiss LSM 700 laser scanning microscope equipped with a stage-top incubator and ZEN Black 2012 software. Images were captured on the mCherry channel (553 nm) and GFP channel (480 nm) for blue light illumination in 30 sec intervals. For ERK-KTR cell experiments, ERK-KTR was visualized on the GFP channel (5% power), and the nuclear stain was visualized on the DAPI channel (395 nm, 5% power).

Western Blotting

Transfected HEK293T cells were lysed with 1:100 HALT protease & phosphatase inhibitor (Thermo Scientific) in M-PER (Thermo Scientific) either in the dark or immediately after illumination with blue light using a homemade LED lightbox for a specified period of time. After 10 min of shaking, total cell lysates were centrifuged for 15 min at 4°C. Laemmli SDS sample buffer (Alfa Aesar) was added to supernatants and incubated at 65 °C for 10 min. Cell lysates were separated by 10% SDS-PAGE gel electrophoresis and transferred to a polyvinylidene fluoride membrane (70V for 90 min on ice). Membranes were blocked with 5% bovine serum albumin (BSA) in 1x Tris-buffered saline (TBS) with 1% Tween (TBST) for 1 hour, room temperature. Blots were then incubated with primary antibody in a 1:1000 dilution with 5% BSA in TBST overnight at 4°C: tyrosine phosphorylation using phosphotyrosine mouse monoclonal Ig pY99 (Santa Cruz Biotechnologies); mCherry expression using anti-mCherry

rabbit polyclonal Ig (Rockland Inc.); GAPDH expression using GAPDH mouse monoclonal Ig (Invitrogen); MAPK phosphorylation using phospho-p44/42 MAPK T202/Y204 rabbit monoclonal Ig (Cell Signaling Technologies); total ERK expression using p44/42 ERK1/2 rabbit monoclonal Ig (Cell Signaling Technologies); Akt phosphorylation using p-Akt T308 rabbit monoclonal Ig (Cell Signaling Technologies); total Akt using Akt (pan) rabbit monoclonal Ig (Cell Signaling Technologies). Blots were washed with TBST 3x for 5 min and incubated in corresponding secondary antibody for 1 hour room temperature: goat anti-rabbit antibody (Invitrogen) or rabbit anti-mouse antibody (Invitrogen). The membranes were again washed with TBST 3x for 5 min, incubated with a chemiluminescent substrate for 5 min, and imaged with an Azure cSeries imaging station.

Image and statistical analyses

Fiji Image J for Windows was used to analyze cell microscopy images and western blot images (Schindelin et al., 2012). Statistical significance (p values) was determined using an unpaired t-test (Welch's correction) with GraphPad Prism version 10.2.0 for Windows. Mean ± S.D. plots were constructed using GraphPad Prism version 10.2.0 for Windows, GraphPad Software, San Diego, California, USA (www.graphpad.com).

RNA Sequencing Preparation

HEK293T cells were plated on 35 mm 6-well dishes and either not transfected with construct or transfected with Cry2olig or PMb-EphA1Cry2Δ. Each transfection condition was either kept in the dark or illuminated with blue light using a homemade LED lightbox for 30 min. Separate non-transfected dishes were stimulated with 5 µL of ephrinA1-Fc (EF1-H5251; Acro

Biosystems) for 30 min. Each condition was performed in triplicate. Cells under dark conditions were trypsinized, pelleted, and lysed in the dark. Illuminated cells or cells treated with ephrinA1-Fc were trypsinized, pelleted, and lysed immediately after stimulation. RNA was purified from cells using the reagents and protocol from GeneJET RNA Purification Kit (Thermo Scientific, #K0731). Total RNA concentration was determined using Molecular Devices SpectraMax instrument. RNA samples were shipped overnight on dry ice to Azenta Life Sciences NGS, South Plainfield, New Jersey, USA (genewiz.com).

RNA Sequencing Analyses

Azenta Life Sciences analyzed RNA samples and provided differentially expressed gene counts, gene ontology data, and statistical analysis. Sequence reads were trimmed to remove possible adapter sequences and nucleotides with poor quality using fastp v.0.23.1. UMI-based de-duplication was performed using fastp v.0.23.1 simultaneously. Trimmed and de-duplicated reads were then mapped to the Homo sapiens GRCh38 with ERCC genes reference genome available on ENSEMBL using the STAR aligner v.2.5.2b. Unique gene hit counts were calculated by using featureCounts from the Subread package v.1.5.2. Only unique reads that fell within exon regions were counted.

Data from the gene hit counts was used for downstream differential expression analysis. Using DESeq2, a comparison of gene expression between the condition-defined groups of samples was performed. The Wald test was used to generate p-values and log2 fold changes. The formula for Log2 fold change of the normalized mean hit counts is:
Log2(Group 2 mean normalized counts/Group 1 mean normalized counts) = Log2FoldChange

Genes with a Benjamini-Hochberg adjusted p-value < 0.05 and absolute log2 fold change > 1 were called as differentially expressed genes for each comparison.

A gene ontology analysis was performed on the statistically significant set of genes by implementing the software GeneSCF v.1.1-p2. The goa_human GO list was used to cluster the set of genes based on their biological processes and determine their statistical significance.

Results and Discussion

Design of EphA1Cry2 constructs

Four optogenetic EphA1 receptor constructs were created and screened for their membrane localization and their light-activated clustering and RTK tyrosine autophosphorylation properties (**Fig. 2.2A**). We based the first optogenetic construct on previous optogenetic receptor designs (**Fig. 2.2A.1**) (Locke et al., 2017). This construct (PM-EphA1Cry2) contains a plasma membrane localization sequence (labeled PM) fused to the N-terminus of the intracellular protein kinase domain and SAM domain of the EphA1 receptor; Cry2olig is tethered to the C-terminus via a glycine-rich linker sequence, followed by mCherry fluorescent protein. Two separate PM localization sequences were used (denoted PMa and PMb): PMa represents a Lyn myristoylation domain with the amino acid sequence MGCIKSKRKDNLNDDE and PMb represents the membrane localization sequence MGSSKSKPK (Locke et al., 2017). The second construct (PM-EphA1Cry2Δ) is identical to the PM-EphA1Cry2 construct except the SAM domain was removed; Δ indicates the absence of the SAM domain (**Fig 2.2A.2**). The third and fourth constructs (IM-EphA1Cry2Δ and IM-EphA1Cry2) include the intermembrane (IM) region (**Fig 2.2A.3 & 4**). IM-EphA1Cry2Δ contains the intracellular protein kinase and SAM domains with the additional extracellular fibronectin type III domain (**Fig. 2.2A.3**) without the external ligand binding domain (indicated by Δ in the name). IM-EphA1Cry2 contains all intracellular and extracellular receptor domains, with Cry2olig-mCherry was fused between the intermembrane region and the protein kinase domain (**Fig. 2.2A.4**). The proposed scheme for optogenetic EphA1 receptor activation and signaling is detailed in **Figure 2.2B**: upon blue light exposure, Cry2olig-mediated oligomerization should induce RTK clustering and autophosphorylation and subsequent activation of downstream signaling.

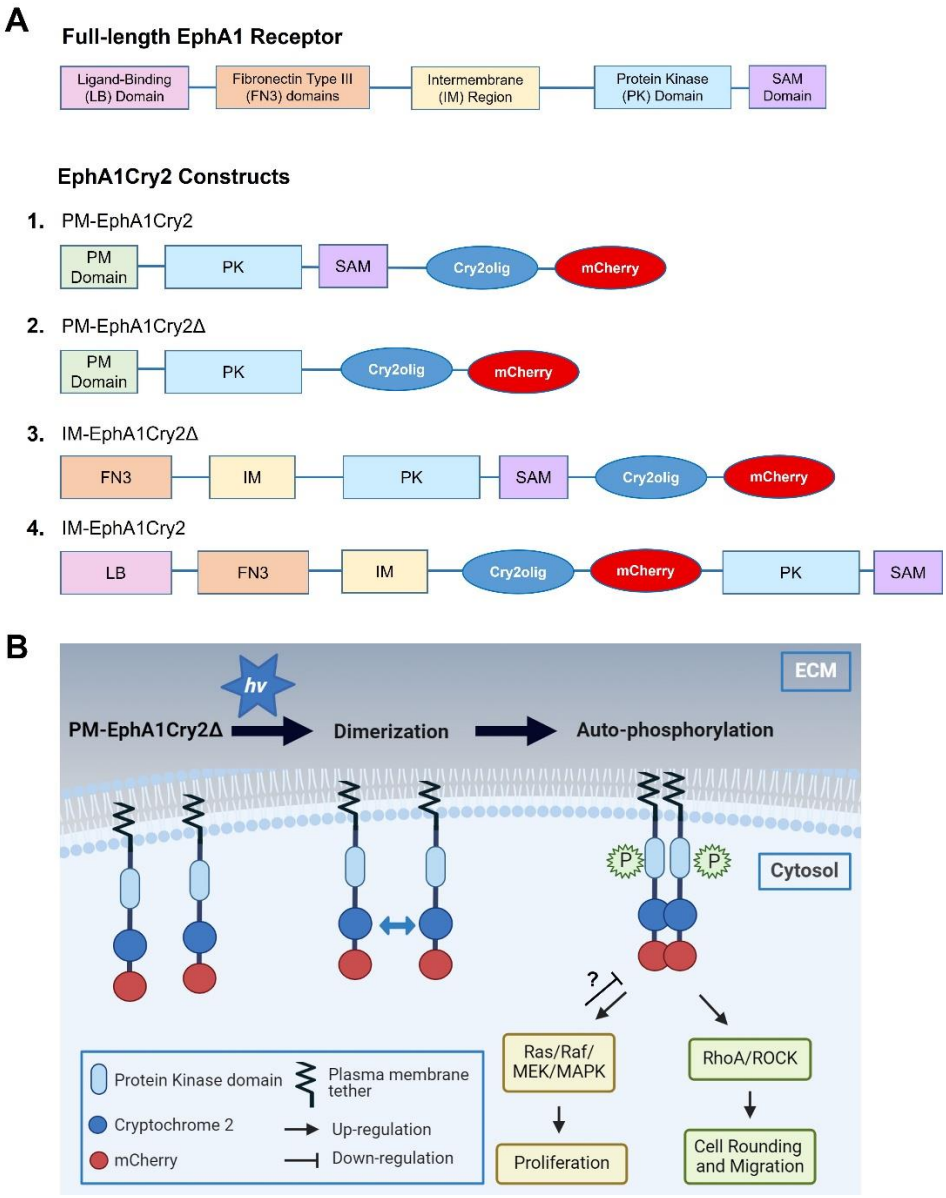

Figure 2.2 (A) *Schematic of full-length wild-type EphA1 receptor domains (top) and EphA1Cry2 constructs (bottom, labeled 1-4).* ***(B)*** *Schematic of the hypothesis of PM-EphA1Cry2 construct activation and signaling. When exposed to blue light, the constructs oligomerize via Cry2 interactions and the adjacent protein kinase domains auto-phosphorylate each other, activating downstream phosphorylation of signaling proteins that induce cell rounding and migration through the RhoA/ROCK pathway and either promote or inhibit proliferation through the Ras/Raf/MEK/MAPK pathway.*

Optogenetic EphA1 constructs were initially tested via transfection in HEK293T and subsequent activation and imaging on a widefield microscope (**Fig. 2.3A**). Hek293T cells were used for construct studies as this immortalized cell line is prolific for quick experiment turnaround. Hek293 cells were also used as the initial cell line for OptoEphB2 construct validation (Locke et al., 2017) and for other EphA1 receptor studies (Yamazaki et al., 2009). Additionally, Hek293 cells have low endogenous EphA1 receptor expression (Miao et al., 2001). For each construct, the resulting images were analyzed to determine the extent of membrane localization and light-activated clustering in response to light. As anticipated, the cytosolic Cry2olig control showed high-order clustering in the cytosol after 5 min of blue light exposure compared to the cell pre-stimulus at 0 min (**Fig. 2.3A, row 1**). By contrast, inspection of plasma membrane localization revealed that the PMa-EphA1Cry2 construct was not well localized to the plasma membrane (**Fig. 2.3A, row 2**), whereas PMa-EphA1Cry2Δ was membrane localized (**Fig. 2.3D, row 3**). To quantify membrane localization and cluster formation at the membrane upon light stimulation, the fluorescent intensity was measured at the membrane and cytosol over time of light exposure (**Fig. 2.3C**). Both the PMa-EphA1Cry2 and PMa-EphA1Cry2Δ exhibited an increase in fluorescent intensity at the membrane and a decrease in fluorescent intensity in the cytosol (**Fig. 2.3D**). Conversely, the Cry2olig control exhibited an increase in fluorescent intensity in the cytosol and a decrease in intensity at the membrane, due to recruitment and localization of Cry2 oligomers within the cytosol (**Fig. 2.3D**). Construct clustering at the membrane did improve slightly for PMb-EphA1Cry2 (**Fig. 2.3B, row 1**), but PMb-EphA1Cry2Δ construct showed a notable improvement in localization and clustering upon light exposure (**Fig. 2.3, row 2; Fig. 2.3D**) compared to PMa-EphA1Cry2Δ. Both IM-EphA1Cry2 and IM-EphA1Cry2Δ construct exhibited membrane localization but did not show visible clustering in

response to light activation (**Fig. 2.3B, row 3 & 4**). We also investigated the ability of our constructs to be activated with spatially restricted illumination and undergo dark reversion. Constructs PMa-EphA1Cry2, PMa-EphA1Cry2Δ, and PMb-EphA1Cry2Δ were confirmed to be spatially activated, and both PMa-EphA1Cry2Δ and PMb-EphA1Cry2Δ construct activation were reversible (**see Fig. AII.2 and Movie AII.1**). In addition, we performed a cell rounding assay for constructs PMa-EphA1Cry2, PMa-EphA1Cry2Δ, and PMb-EphA1Cry2Δ as previous studies have found EphA1 receptor activation promotes cell rounding (Yamazaki et al., 2009). All three constructs exhibited a decrease in cell area after light stimulation compared to the Cry2olig control (**see Fig. AII.3**). Going forward, only constructs that showed a strong membrane-adjacent light activated clustering response were selected for further analysis.

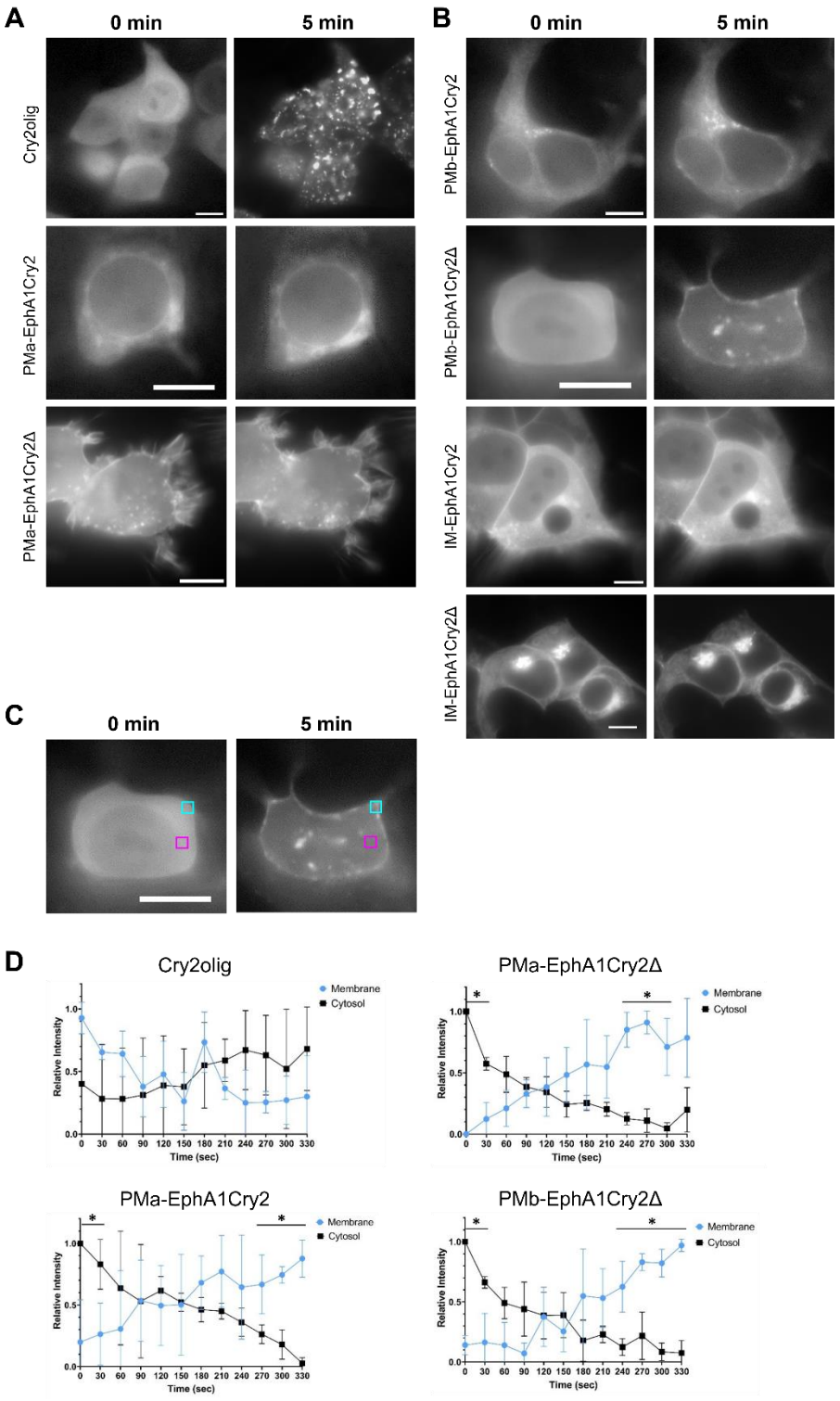

Figure 2.3. *Optogenetic clustering of EphA1Cry2 constructs. HEK293T cells were transfected with (A) Cry2olig (top row), PMa-EphA1Cry2 (middle row), or PMa-EphA1Cry2Δ (bottom*

row); and (B) PMb-EphA1Cry2 (top row), PMb-EphA1Cry2Δ (second row), IM-EphA1Cry2 (third row), or IM-EphA1Cry2Δ (bottom row). ***(A,B)*** *Widefield images of transfected cells were taken pre-illumination (0 min) and after blue light exposure (480 nm, 50 ms exposure, 30 sec intervals over 5 min). Images collected on mCherry channel (553 nm, 200 ms exposure). Scale bar: 10 µm.* ***(C)*** *Representative image of relative fluorescent intensity quantitation using regions of interest in the cytosol (magenta box, 2.5 x 2.5 µm) and at the membrane (cyan box, 2.5 x 2.5 µm) of a PMb-EphA1Cry2Δ transfected HEK293T cell.* ***(D)*** *Quantitation of the relative intensity of region of interests (C) in the cytosol (black) and at plasma membrane (blue) over 5 min (330 sec) of blue light exposure, taken every 30 sec. Data was collected for Cry2olig, PMa-EphA1Cry2, PMa-EphA1Cry2Δ, and PMb-EphA1Cry2Δ constructs using Fiji Image J and graphed using GraphPad Prism. Error bars represent standard deviation; n=3 cells taken from two separate dishes (unpaired t-test, *p < 0.05).*

Tyrosine phosphorylation in response to light activation

Next, we investigated global tyrosine phosphorylation to capture the extent of light-activated RTK activation of the selected constructs: PMa-EphA1Cry2, PMa-EphA1Cry2Δ, and PMb-EphA1Cry2Δ. Analysis of anti-phosphotyrosine (pTyr) western blots of light vs. dark conditions for PMa-EphA1Cry2, PMa-EphA1Cry2Δ, and PMb-EphA1Cry2Δ constructs showed an upward trend in phosphorylation for each construct over time compared to no change in phosphorylation for Cry2olig (**Fig. 2.3A,B**). When performing an initial comparison blot between PMa- and PMb-EphA1Cry2, we noticed very light phosphorylation bands at the molecular weight of the PMb-EphA1Cry2 construct but a dark band at around 50 kDa that was not present in the PMa-EphA1Cry2 lanes (**Fig. 2.3C**). The lower molecular weight band is most likely due to degradation of the construct; as a result, PMb-EphA1Cry2 was not investigated further. For constructs PMa-EphA1Cry2, PMa-EphA1Cry2Δ, PMb-EphA1Cry2Δ, a slight decrease in tyrosine phosphorylation was observed between the 20 min and 30 min time points and smaller error for 30 min than the 20 min time point (**Fig. 2.3B**). Based on these data, we performed a separate western blot for tyrosine phosphorylation for cells in the dark or exposed to 30 min of blue light stimulation for the three constructs in Figure 3C (**Fig. 2.3D**). Each construct exhibited a significant log fold change increase of phosphorylation after light exposure compared to the Cry2olig control (**Fig. 2.3E**). Although PMb-EphA1Cry2Δ exhibited the lowest overall phosphotyrosine band intensity, it exhibited the lowest background phosphorylation with intensities at time 0 min comparable to Cry2olig intensities (**Fig. 2.3B**) and additionally showed the largest log fold change amongst the three EphA1Cry2 constructs (**Fig. 2.3E**). As a result, PMb-EphA1Cry2Δ was selected as the lead construct for further study.

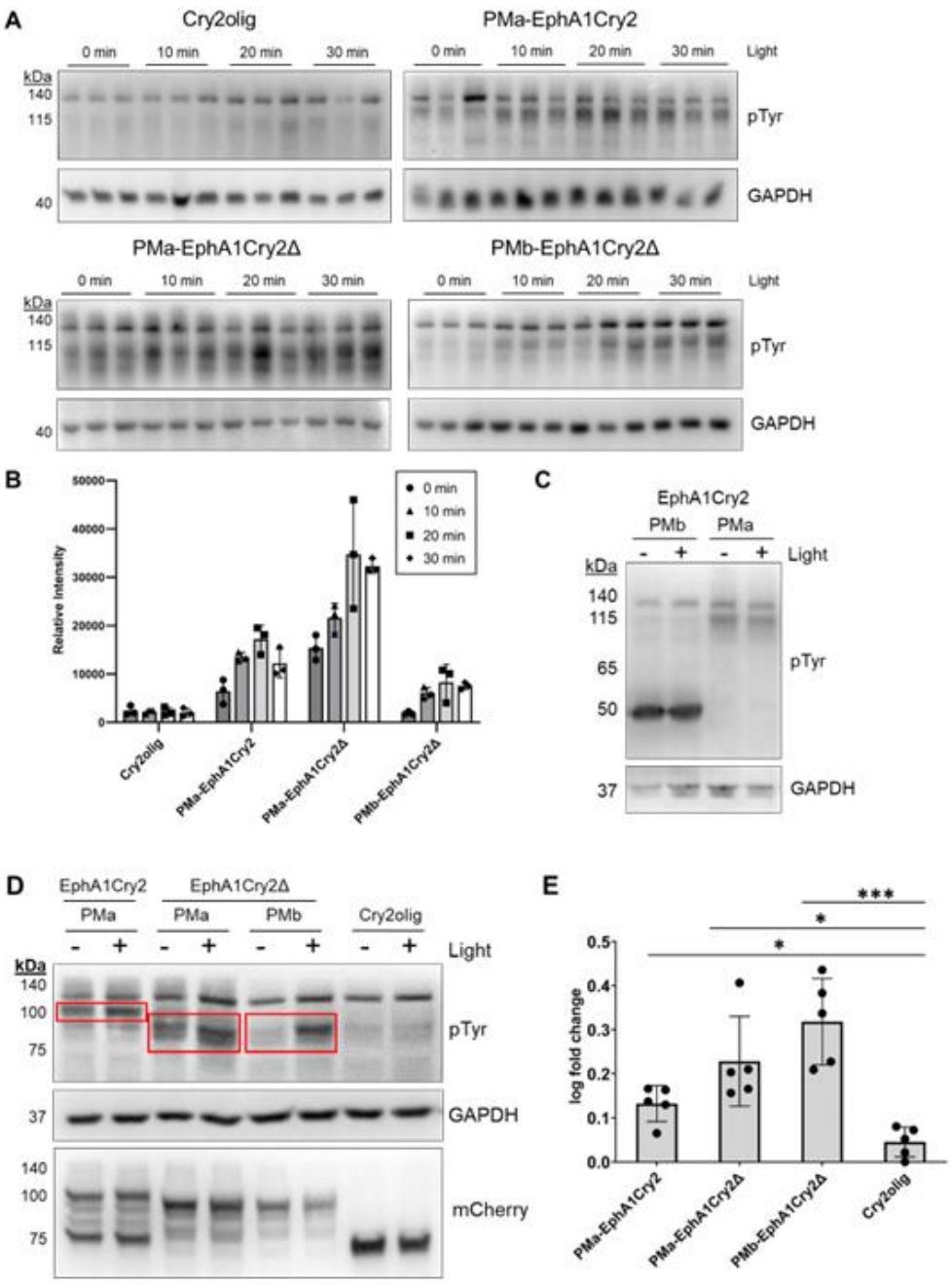

Figure 2.4. *Analysis of EphA1Cry2 tyrosine phosphorylation.* ***(A)*** *HEK293T cells were transfected with either Cry2olig, PMa-EphA1Cry2, PMa-EphA1Cry2Δ, or PMb-EphA1Cry2Δ and lysed under dark conditions (0 min light) or after exposure to either 10, 20, or 30 min of LED blue light. Western blots of whole cell lysates were incubated with pTyr99 antibody for tyrosine phosphorylation and GAPDH antibody for total protein expression in triplicate. Bands*

at ~130 kDa are endogenous bands. ***(B)*** *Quantitation of normalized pTyr band intensities at the molecular weight of each construct (~115 kDa) to GAPDH (A). Intensities were measured using Fiji ImageJ and plotted using GraphPad Prism. Error bars represent standard deviation; n=3 blots.* ***(C)*** *HEK293T cells transfected with either PMa-EphA1Cry2 or PMb-EphA1Cry2 were lysed under dark conditions (-) or after 30 min of LED blue light exposure (+). Western blots of whole cell lysates were incubated with pTyr antibody for tyrosine phosphorylation and GAPDH antibody for total protein expression.* ***(D)*** *HEK293T cells transfected with either PMa-EphA1Cry2 or PMb-EphA1Cry2 were lysed under dark conditions (-) or after 30 min of LED blue light exposure (+). Western blots of whole cell lysates were incubated with pTyr antibody for tyrosine phosphorylation, GAPDH antibody for total protein expression, and mCherry for construct expression. Red boxes indicate bands at the construct molecular weight.* ***(E)*** *Quantitation of normalized pTyr band intensity to GAPDH (D), shown as the log fold change of light vs. dark condition. Error bars represent standard deviation, n=5 blots (unpaired t-test; *p < 0.05, ***p < 0.001).*

EphA1Cry2 phosphorylates ERK upon light activation

EphA2 has been characterized in independent studies as both a promoter and an inhibitor of proliferation through the Ras/Raf/MEK/MAPK signaling cascade (Miao et al., 2001; Pratt & Kinch, 2002). Studies involving EphA2 signaling have found an increase in MAPK activation upon ephrinA1-dependent EphA2 stimulation (Z. Chen et al., 2021; Pratt & Kinch, 2002). In contrast, according to Miao et al. EphA receptors function as the opposite of growth factors to inhibit the cascade that leads to an increase in proliferation (Miao et al., 2001); as such, EphA2 has been proposed as a therapeutic target for cancer to due to this cascade, and upregulation could yield a decrease in the progression of certain cancers (Miao & Wang, 2012). Although EphA1 has also been hypothesized to promote tumorigenesis and metastasis (Ieguchi & Maru, 2019), EphA1 receptor activation of signaling proteins associated with cell proliferation is less well defined. To identify downstream signaling events specific to proliferation, we investigated whether light activation of EphA1Cry2 impacts phosphorylation of extracellular-signal regulated kinase (ERK), also called mitogen-activated protein kinases (MAPK), a known signaling target for EphA receptors (**Fig. 2.5**) (Miao et al., 2001). Interestingly, we found an increase in ERK phosphorylation upon PMb-EphA1Cry2Δ light activation over time with and without serum-starvation of cells (**Fig. 2.5A,B**). To confirm this result, we also utilized an ERK kinase translocation reporter (KTR) to visualize ERK dynamics within a cell and corroborate the western blot results (**Fig. 2.6A,B**). When ERK is phosphorylated by upstream receptor signaling proteins, p-ERK translocates into the nucleus and phosphorylates nuclear ERK-KTR. Phosphorylated ERK-KTR then translocates out of the nucleus into the cytosol (**Fig. 2.6C**). The KTR translocation event can be quantified by measuring and then calculating the ratio of the fluorescent intensity within the cytosol to the nucleus (C/N ratio) of the associated mNeonGreen

fusion (**Fig. 2.5C**). As a positive control, ERK-KTR was transfected in HEK293T cells and then treated with epidermal growth factor (EGF) to stimulate endogenous EGF receptors in the cell and promote phosphorylation of ERK. The cells transfected with ERK-KTR exhibited an immediate increase in C/N ratio after EGF stimulation, peaking at about 150 sec (**Fig. 2.5A,D**). This response is consistent with previously reported C/N changes of this reporter and other similar ERK reporters (Chavez-Abiega et al., 2022; Dessauges et al., 2022). By comparison, PMb-EphA1Cry2Δ light activation resulted in a steady increase in ERK activation over time of light exposure (**Fig. 2.5B, D; Movie AII.2**), which is consistent with the ERK phosphorylation western blots (**Fig. 2.5**). Taken together, these results indicate that light-induced PMb-EphA1Cry2Δ construct activation stimulates downstream activation of ERK. Conversely, light activation of Cry2olig did not show a trend in C/N change over time (**Fig. 2.5B,D)**, also corroborating the western blot data (**Fig. 2.5**). We note that the general trend of increasing ERK activity upon light simulation mirrors that of similar optogenetic RTK proteins, such as optoFGFR (Dessauges et al., 2022).

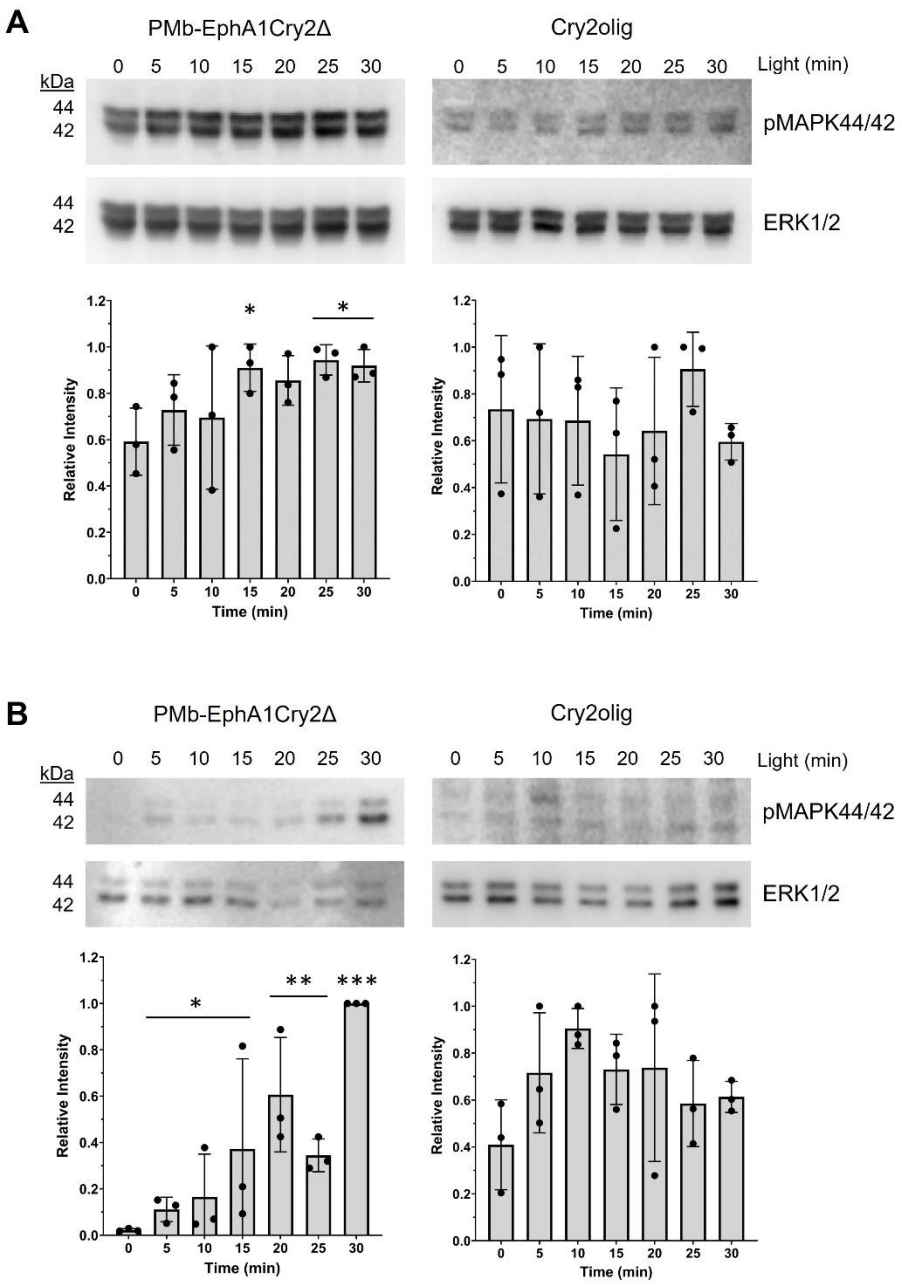

Figure 2.5. *ERK phosphorylation in response to EphA1Cry2Δ activation.* ***(A,B)*** *Western blots of PMb-EphA1Cry2Δ (left) and Cry2olig (right) transfected HEK293T cell lysates over 5 min time intervals of light stimulation, immunostained for ERK phosphorylation (pMAPK44/42) and ERK1/2 loading control. (A) Cells were not serum-starved prior to lysis. (B) Cells were serum-starved for 2 hours prior to light exposure and lysis. (A, B) Bottom graphs: Quantitation of*

*normalized pMAPK44/42 band intensity to ERK1/2. Error bars represent standard deviation, n=3 blots (unpaired t-test to 0 min time point; *p < 0.05, **p < 0.01, ***p < 0.001).*

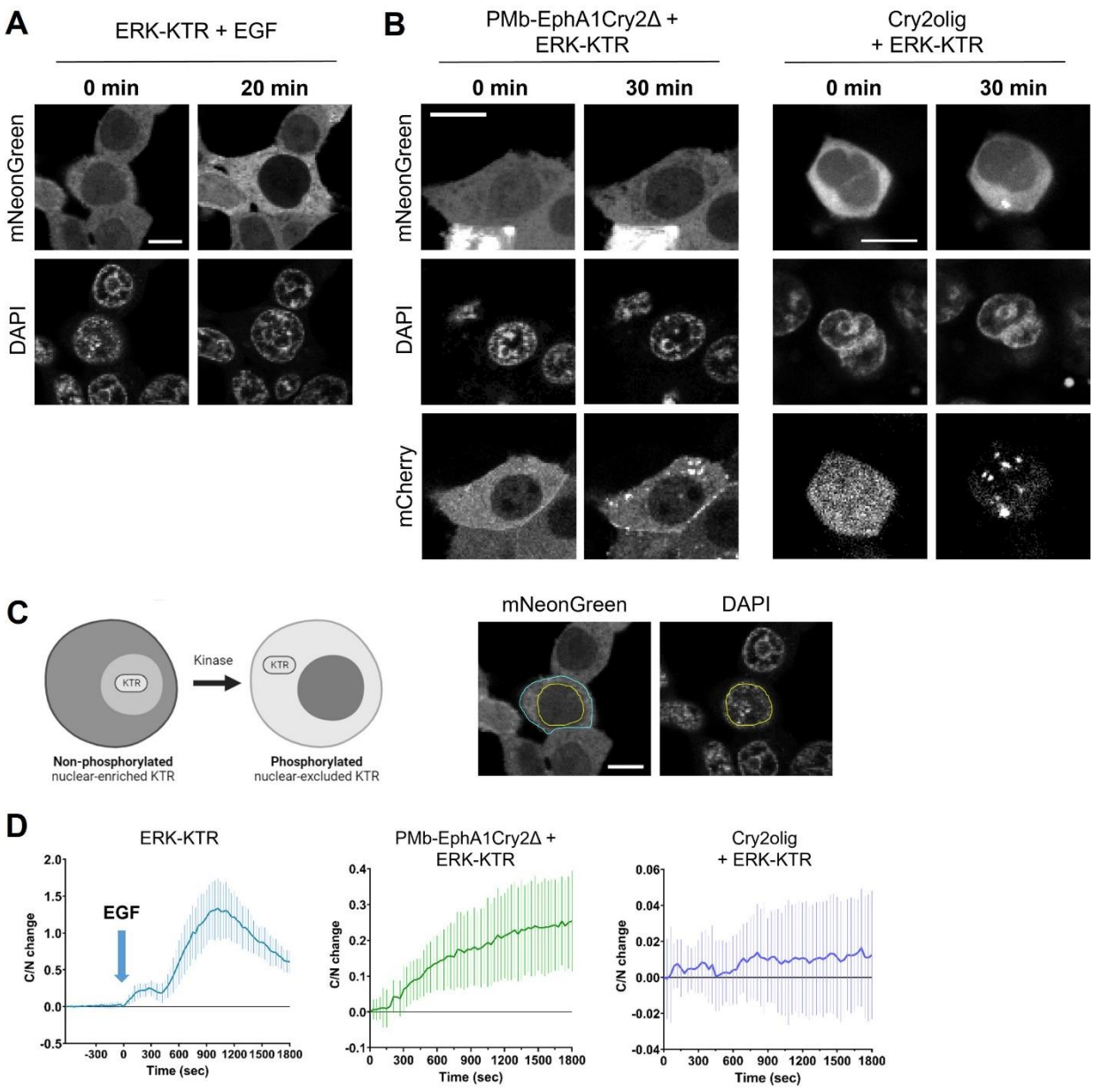

Figure 2.6. *ERK-KTR translocation in response to EphA1Cry2Δ activation.* ***(A,B)*** *Confocal images of HEK293T cells transfected with (A) only ERK-KTR with 500 ng/mL EGF stimulus, (B) ERK-KTR + PMb-EphA1Cry2Δ, and ERK-KTR + Cry2olig taken pre (0 min) and post blue light (480 nm, 30 sec intervals, over 30 min). Images collected on DAPI channel (nuclear stain), mNeonGreen channel (ERK-KTR), and for (B) mCherry channel (PMb-EphA1Cry2Δ and Cry2olig). Scale bar: 10 µm.* ***(C)*** *ERK-KTR is localized to the nucleus in its non-phosphorylated*

state. Endogenous ERK activation upon kinase activity leads to nuclear translocation, which in turn translocates ERK-KTR out of the nucleus into the cytosol. Right images: Example quantification using Fiji ImageJ to measure the fluorescent intensity of the cytosol (cyan ROI) and nucleus (yellow ROI). ***(D)*** *Quantitation of fluorescent intensity of the cytosol divided by the intensity within the nucleus (C/N) change over time. ERK-KTR (A) included 10 min pre-stimulus imaging. Error bars represent standard deviation; n=6 cells taken from three separate dishes.*

EphA1Cry2 phosphorylates Akt upon light activation

Akt, formerly protein kinase B, is a serine/threonine kinase that regulates cell proliferation and metabolism (Nitulescu et al., 2018). Activation of Akt is mediated by various receptors through the activation of phosphoinositide 3-kinase (PI3K), which phosphorylates phosphatidylinositol 4,5-bisphosphate (PIP_2) to phosphatidylinositol 4,5-trisphosphate (PIP_3). Kinases such as 3-phosphoinositide-dependent kinase 1 (PDK1) and integrin-linked kinase (ILK) then assist the phosphorylation of Akt by PIP_3. Similar to ERK, Akt activates mTORC1 (mammalian target of rapamycin complex 1) through the phosphorylation of the mTORC1 inhibitor, tuberous sclerosis complex 2 (TSC2) (Nitulescu et al., 2018). mTORC1 promotes cell growth and proliferation through the activation of protein translation and inhibition of autophagy and apoptosis (Nitulescu et al., 2018; Winter et al., 2011). A study in mTORC1 activation has found that the PI3K/Akt and Ras/ERK pathways can act concomitantly with each other and have an additive effect on mTORC1 activation compared to activation of one pathway alone (Winter et al., 2011). Conversely, under constitutively active Raf or MEK, Ras/ERK pathway has been found to inhibit the PI3K/Akt pathway leading to inhibition of cellular growth. In NIH-3T3 fibroblasts, constitutive Raf signaling upregulated EphA2 receptor expression, which was required for PI3K/Akt inhibition (Menges & McCance, 2008). In glioma and prostate cancer cells, ephrin-A1 stimulation of EphA2 receptor inhibited cell migration, while overexpression of EphA2 induced migration in the absence of ligand stimulation through the phosphorylation of residue S897. Furthermore, phosphorylation of EphA2 resulted in Akt activation and tumorigenesis in brain cancer cells (Miao et al., 2009). As we found that our EphA1Cry2 construct activated the ERK/MAPK signaling pathway, we hypothesized that ligand-independent EphA1 receptor activation would also modulate the PI3K/Akt pathway. We first immunoblotted

for Akt phosphorylation over time and found that light stimulation of our PMb-EphA1Cry2Δ resulted in an increase in phospho-Akt compared to no change in phosphorylation for Cry2olig (**Fig. 2.7**). We then utilized an Akt-KTR in the same fashion as the ERK-KTR by analyzing transfected HEK293T cells for C/N ratio (**Fig. 2.8A,B; Fig. AII.6**). Consistent with the previous KTR study from Chavez-Abiega et al., Akt-KTR showed a sharp increase in C/N ratio immediately after EGF stimulation (Chavez-Abiega et al., 2022). Compared to ERK-KTR, Akt-KTR exhibited an overall lower response and sustained phosphorylation over 30 min, as opposed to a decrease in signal at ~18 min for ERK-KTR (**Fig. AII.7A**). PMb-EphA1Cry2Δ light activation resulted in a slow increase in Akt-KTR translocation over 30 min with a lower response than ERK-KTR (**Fig. 2.8C, Fig. AII.7B**). Cry2olig showed no trend in C/N change over time (**Fig. 2.8C, Fig. AII.7C**). The slow increase in Akt over 30 min of light exposure is observed in both the analysis of western blot phosphorylation and Akt-KTR C/N ratio change. Interestingly, a dip in Akt phosphorylation was observed at 25 minutes (1500 sec) in both the western blot and the KTR C/N graph. This could be caused by Ras inhibition of Akt from sustained active Raf or through other regulatory mechanisms (Menges & McCance, 2008).

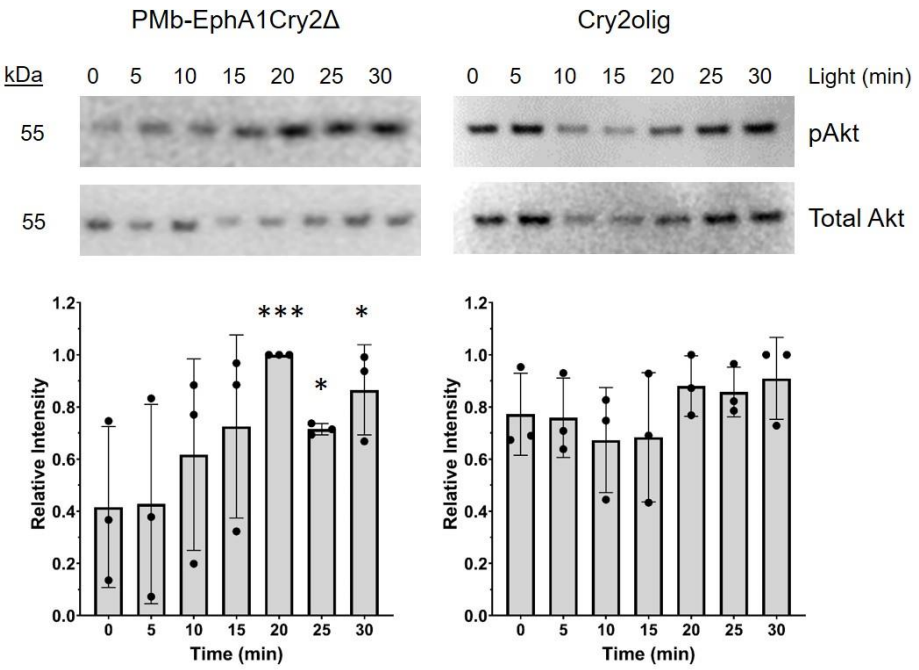

Figure 2.7. *Akt phosphorylation in response to EphA1Cry2Δ activation. Western blots of PMb-EphA1Cry2Δ (left) and Cry2olig (right) transfected HEK293T cell lysates over 5 min time intervals of light stimulation, immunoblotted for Akt phosphorylation (pAkt) and pan Akt (Total Akt) loading control. Cells were serum-starved for 2 hours prior to light exposure and lysis. Bottom graphs: Quantitation of normalized pAkt band intensity to total Akt. Error bars represent standard deviation, n=3 blots (unpaired t-test to 0 min time point; *p < 0.05, ***p < 0.001).*

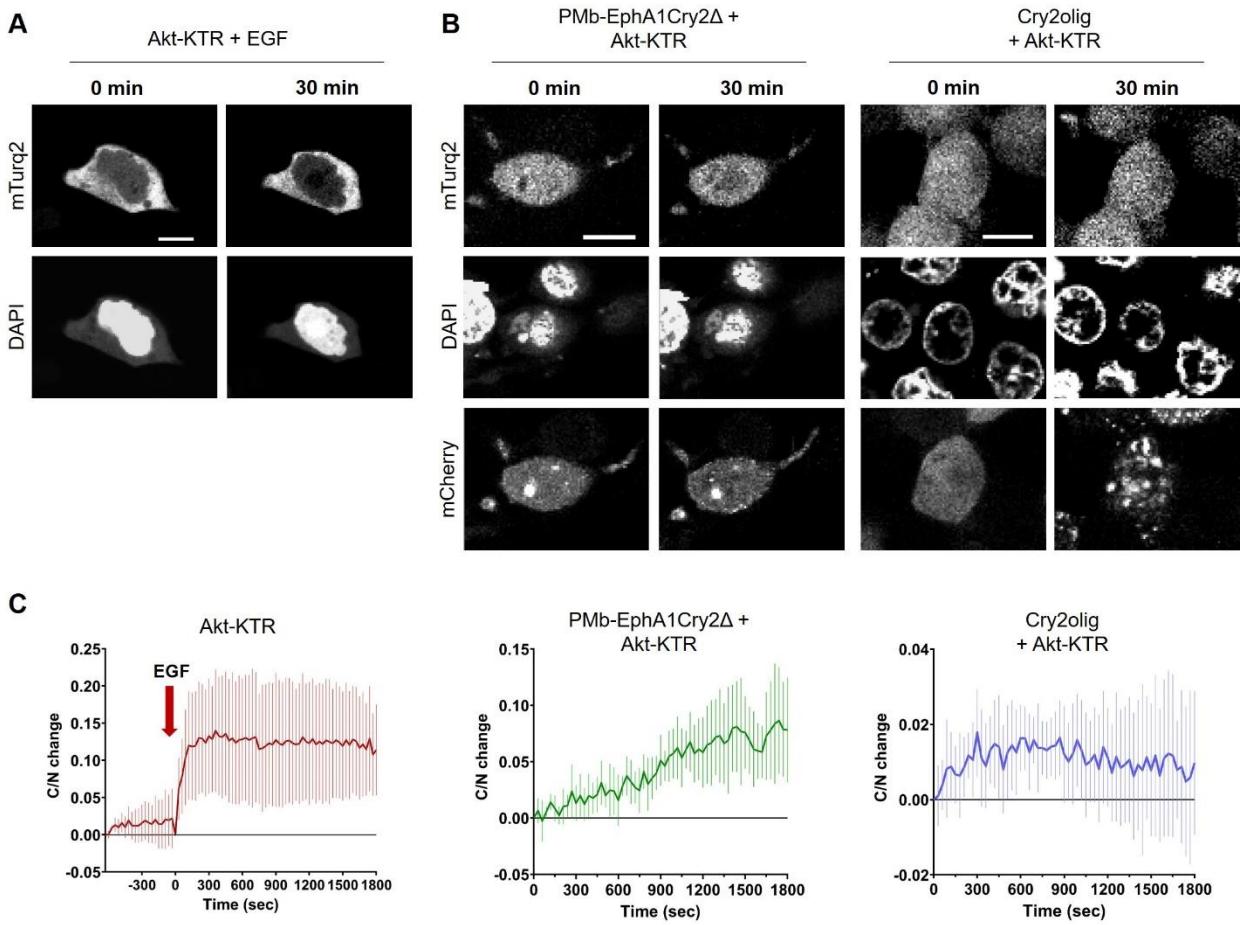

Figure 2.8. *Akt-KTR translocation in response to EphA1Cry2Δ activation.* ***(A,B)*** *Confocal images of HEK293T cells transfected with (A) only Akt-KTR with 500 ng/mL EGF stimulus, (B) Akt-KTR + PMb-EphA1Cry2Δ, and Akt-KTR + Cry2olig taken pre (0 min) and post blue light (480 nm, 30 sec intervals, over 30 min). Images collected on DAPI channel (nuclear stain), mTurquoise2 (mTurq2) channel (Akt-KTR), and for (B) mCherry channel (PMb-EphA1Cry2Δ and Cry2olig). Scale bar: 10 µm.* ***(C)*** *Quantitation of fluorescent intensity of the cytosol divided by the intensity within the nucleus (C/N) change over time. Akt-KTR (A) included 10 min pre-stimulus imaging followed by EGF stimulation (red arrow). Error bars represent standard deviation; n=6 cells taken from two separate dishes.*

RNA sequencing analysis

RNA sequencing (RNA-Seq) is a sensitive and informative method to study biological responses to a treatment through analysis of their RNA transcriptome (Koch et al., 2018). RNA-seq involves the isolation and fragmentation of RNA strands, including coding and non-coding transcripts, followed by reverse transcription of RNA into complementary DNA (cDNA). The cDNA transcripts are then ligated with an adaptor and primer-amplified via PCR for next-generation sequencing (NGS) (**Fig. 2.9A**) (Gunter et al., 2022; Koch et al., 2018). Sequenced transcripts are mapped to a known reference genome, and hit counts for each identified gene are quantified. The genes analyzed to be significantly expressed in the sample can be sorted into ontological categories for a broad interpretation of genetic data (**Fig. 2.9B**). RNA-seq can be used to catalog the transcriptome of a cell population, elucidate the structure of certain genes, or quantify the expression level of genes in a treatment sample compared to a control sample (Koch et al., 2018).

To utilize RNA-seq for the analysis of our EphA1Cry2 construct, we sent total RNA samples of transfected and non-transfected HEK293T cells to GENEWIZ Multiomics & Synthesis Solutions from Azenta Life Sciences. These samples were sequenced and analyzed per Azenta workflow (**Fig. 2.9**); gene hit counts and ontological determination, along with quality control data, were provided (**Table AII.2; Fig. AII.8-12**). Significant differentially expressed genes (DEGs) of a "treatment" group compared to a "control" group were also determined. DEGs yield information about genes that are either up-regulated or down-regulated in response to a treatment, such as EphA1Cry2 construct activation. We collected data from 7 different experimental conditions and compared gene counts of the treatment group to those of the control group (**Table 2.1**). HEK293T cells transfected with PMb-EphA1Cry2Δ or Cry2olig were either

lysed in the dark or after 30 min of blue light stimulation. HEK293T cells not transfected with construct were also lysed in the dark or after light stimulation. For an additional control condition, non-transfected cells were treated for 30 min with ephrinA1-Fc, a pre-clustered form of ephrinA1 that can bind to and activate endogenous EphA1 receptors.

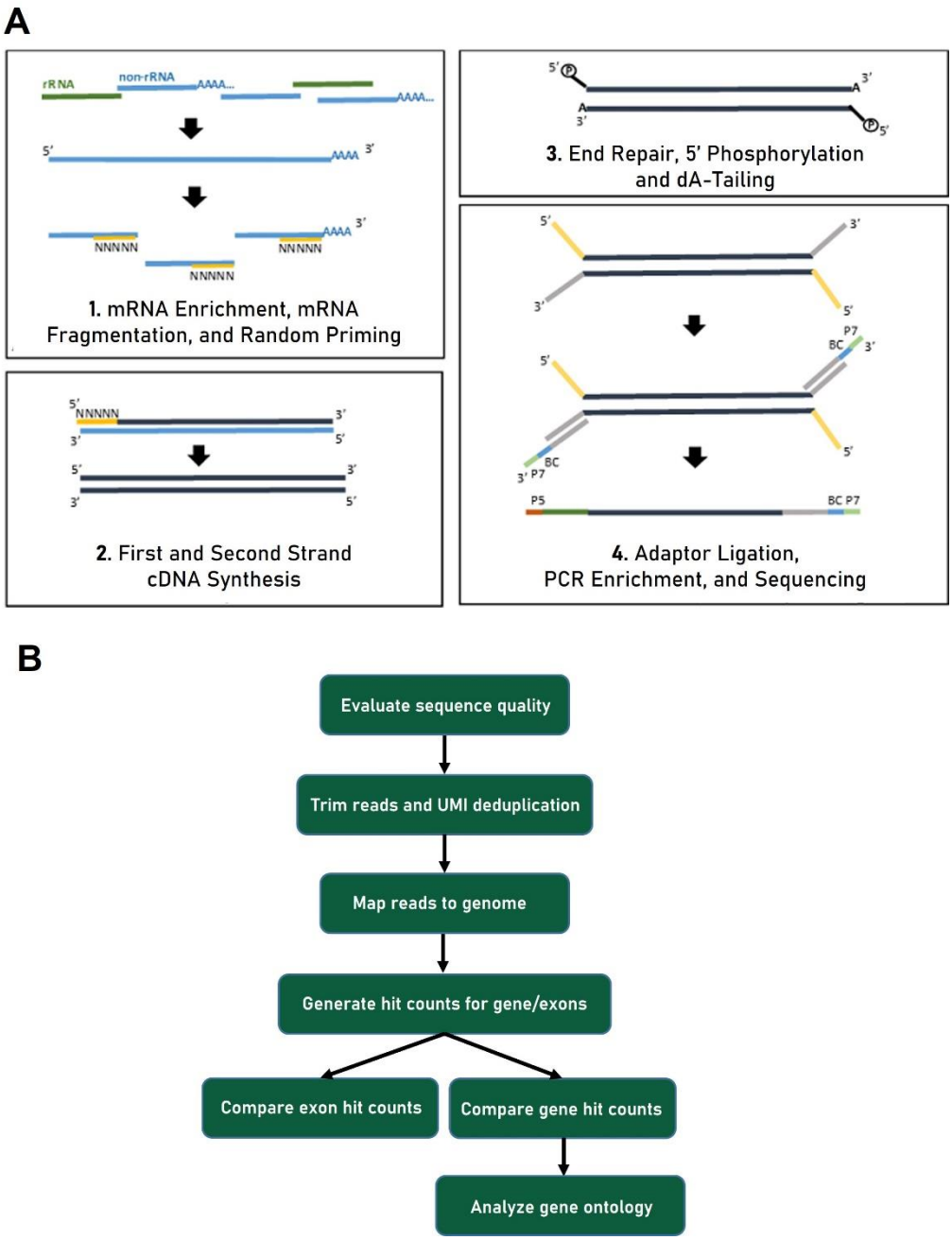

Figure 2.9. *mRNA sequencing experiment and workflow.* ***(A)*** *1. mRNA is enriched, fragmented, then undergoes random priming. 2. First and then second strand cDNA is synthesized by reverse transcriptase of mRNA transcripts. 3. Double-stranded cDNA undergoes end repair, 5'phosphorylation, and poly(A)+ tail addition. 4. Strands are ligated with UMI adapters. A library is created using UDI primer PCR amplification. DNA is sequenced.* ***(B)*** *The library*

sequences were evaluated for quality and mapped to a reference genome. Hit counts corresponding to exons were removed; only gene hit counts were reported and analyzed for gene ontology. Provided by Azenta Life Sciences.

Six condition comparisons were analyzed for DEGs: PMb-EphA1Cry2Δ light vs. dark; PMb-EphA1Cry2Δ light vs. Cry2olig light; PMb-EphA1Cry2Δ vs. ephrinA1-stimulated; Cry2olig light vs. dark; ephrinA1-stimulated vs. no transfection dark; no transfection light vs. dark (**Table 2.1**). PMb-EphA1Cry2Δ transfected cells under light condition exhibited an upregulation of 30 genes and no downregulated genes. In comparison to Cry2olig transfected cells under light, about 82% of DEGs (933 genes) within the PMb-EphA1Cry2Δ light condition were significantly upregulated, and 17% of DEGs (199 genes) were downregulated. The comparison between PMb-EphA1Cry2Δ light condition and the ephrinA1-stimulated condition yielded the most upregulated and downregulated genes amongst all comparisons, with 1732 upregulated genes and 366 downregulated genes in response to PMb-EphA1Cry2Δ light condition. Interestingly, Cry2olig light condition exhibited a downregulation of 73 genes compared to its dark condition (**Table AII.3**); we hypothesize this downregulation is contributed to sequestration of proteins such as transcription factors within the large Cry2olig clusters, preventing gene expression and other signaling pathways. Although significantly downregulated genes were identified, no significant ontological processes were reportable. EphrinA1-stimulation compared to the no transfection dark condition resulted in no significant DEGs. While HEK293 cells do not endogenously express high levels of EphA1 receptor, endogenous EphA2 receptor is expressed in Hek293 cells (Miao et al., 2001). Although ephrinA1-Fc has been shown to activate EphA2 receptor (Pratt & Kinch, 2002), no genes were significantly up- or

downregulated in response to ephrinA1-Fc stimulation of endogenous EphA2 receptor. The no transfection light condition only had three downregulated genes compared to its dark condition (**Table AII.4**); any significant DEGs as a result of light stimulation could be an endogenous response to extended blue light exposure.

Table 2.1. *Comparison of significant upregulated and downregulated genes, including the total significant differentially expressed genes (DEGs). Genes were up- or downregulated in cells under Condition 1 ("treatment" condition) compared to cells under Condition 2 ("control" condition).*

Condition 1 (treatment)	***Condition 2 (control)***	***Upregulated Genes***	***Downregulated Genes***	***Total significantly DEGs***
PMb-EphA1Cry2Δ Light	PMb-EphA1Cry2Δ Dark	30	0	30
PMb-EphA1Cry2Δ Light	Cry2olig Light	933	199	1132
PMb-EphA1Cry2Δ Light	EphrinA1-stimulated	1732	366	2098
Cry2olig Light	Cry2olig Dark	2	73	75
EphrinA1-stimulated	No Transfection Dark	0	0	0
No Transfection Light	No Transfection Dark	0	3	3

RNA-seq of total RNA transcripts yields hit counts of coding and non-coding transcripts. Of these genes reported, the log fold change of gene expression of the treatment group compared to the control group was provided along with the p-value adjusted for variations of transcript yield between samples. For the coding transcripts, gene ontology analysis categorized these transcripts by similar roles or functions of its encoded protein within a cell. The comparison between PMb-EphA1Cry2Δ light and dark conditions yielded ontological data of only significant DEGs. The 11 categories most upregulated by light stimulation of PMb-EphA1Cry2Δ-transfected cells were associated with cellular respiration and membrane potential regulation (**Fig. 2.10**). The two most upregulated processes were mitochondrial ATP synthesis and ATP biosynthesis; four of the top upregulated processes involve phosphate transport. The individual genes upregulated were also related to ATP synthesis, cellular respiration, and ion membrane transport (**Table 2.2; Table AII.5**). As activation of Eph receptors (including our EphA1Cry2 construct) requires ATP and phosphate transfer, the upregulation of these processes after construct activation is not entirely surprising. While the significant DEGs between light and dark conditions of PMb-EphA1Cry2Δ- transfected cells were not associated with cellular signaling, this could be caused by the drastic change in ATP concentration from receptor activation which masks other smaller signaling activities occurring in the background.

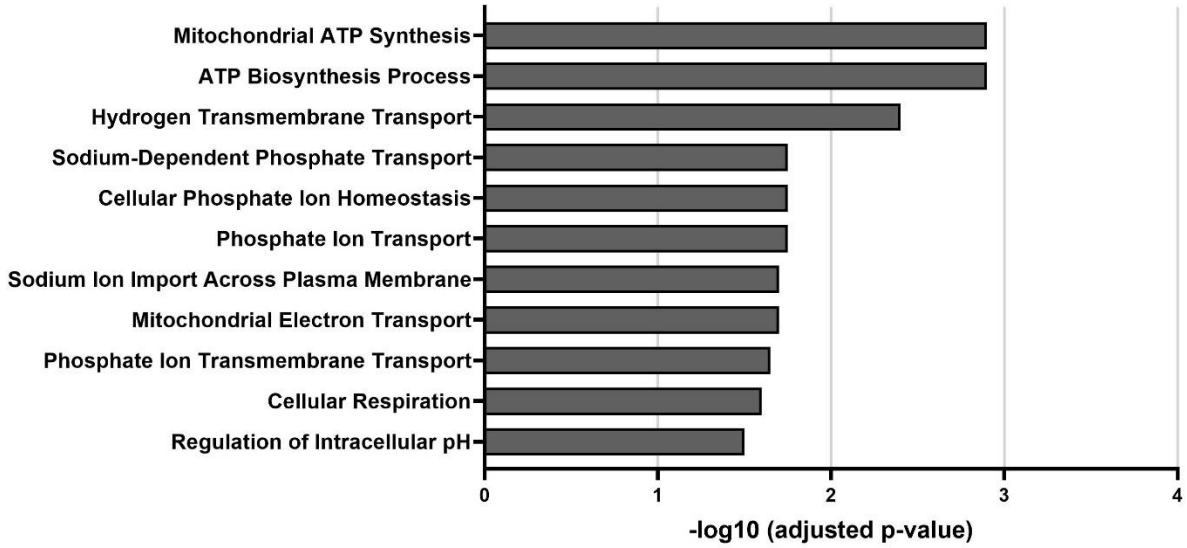

Figure 2.10. *Gene ontology analysis for PMb-EphA1Cry2Δ light vs. dark conditions. X-axis represents the -log10(adjusted p-value) of light condition compared to dark condition for statistically significant values only ($p < 0.05$).*

Table 2.2. *Significant DEGs of interest for PMb-EphA1Cry2Δ light condition compared to its dark condition. The encoded protein and its function are provided.*

Gene Name	*Log2 FoldChange*	*Adj p-value*	*Encoded Protein*	*Protein Function*	*Reference*
MT-ATP6	1.09	0.00	Mitochondrial complex V	ATP synthesis	(Ganetzky et al., 2019)
MTCO1P12	1.19	0.01	Cytochrome c oxidase subunit I	Cellular respiration	(Mani et al., 2020)
MT-CYB	1.06	0.00	Cytochrome b	Mitochondrial electron transport	(Mori et al., 2015)
MT-ND1	1.21	0.00	Mitochondrially-encoded NADH dehydrogenase 1	Cellular respiration	(Ng et al., 2020)
MT-TL1	1.38	0.00	Mitochondrial $tRNA^{leu}$	Protein synthesis	(Keilland et al., 2016)
MT-TY	1.41	0.00	Mitochondrial $tRNA^{tyr}$	Protein synthesis	(Lim et al., 2020)
SLC34A3	1.17	0.00	Sodium-dependent phosphate transporter	Na^+ and PO_4^{3-} transport	(Wagner et al., 2014)
SLC9A3	1.03	0.00	Sodium-hydrogen antiporter 3	Na^+ and K^+ transmembrane transport	(Klisic et al., 2002)

Comparisons between the PMb-EphA1Cry2Δ light condition and Cry2olig light control groups can yield information on the major differences in signaling activities. PMb-EphA1Cry2Δ-transfected cells under light stimulation exhibited a significant increase in nucleosome assembly compared to Cry2olig light condition (**Fig. 2.11**). Nucleosome assembly is tightly associated with DNA replication as newly replicated DNA is wound into nucleosome by histones (Serra-Cardona & Zhang, 2018). In fact, all 15 upregulated genes in the nucleosome assembly ontological category were genes coded for histones (**Table AII.6**). The second largest differentially regulated process is response to cAMP. Activation of adenyl cyclase by G-protein coupled receptors converts ATP to cyclic AMP (cAMP); cAMP is a messenger protein that modulates various cellular processes, such as ion channel activation and gene expression (Sassone-Corsi, 2012). An upregulation of response to cAMP could be related to the processes

upregulated in PMb-EphA1Cry2Δ light vs. dark comparison, e.g. ATP synthesis and ion membrane transport. Other processes such as response to oxidative stress and inflammatory response could be caused by the lack of ATP present as a result of the over-activation of PMb-EphA1Cry2Δ. This is also evident in the highly upregulated genes coding the proteins Interleukin 17F, which functions as an inflammatory response, and heat shock proteins A6 and A7, which are activated in response to oxidative stress (**Table 2.3**) (S. H. Chang & Dong, 2009; Guan et al., 2021). The increased expression of heat shock proteins could also be related to the reduced concentration of ATP in the cell. Increased thyroglobulin expression levels may be related to the increased response to cAMP, as cAMP activates protein kinase A, which in turn activates CREB promoting the expression of steroid genes such as thyroglobulin (Nicolaides & Chrousos, 2023). An increase in thyroglobulin is associated with increased cell metabolism and cell growth, specifically of the skin, hair, and nails (Prpić et al., 2018). The upregulation of these processes suggests that activation of PMb-EphA1Cry2Δ results in cell growth and proliferation.

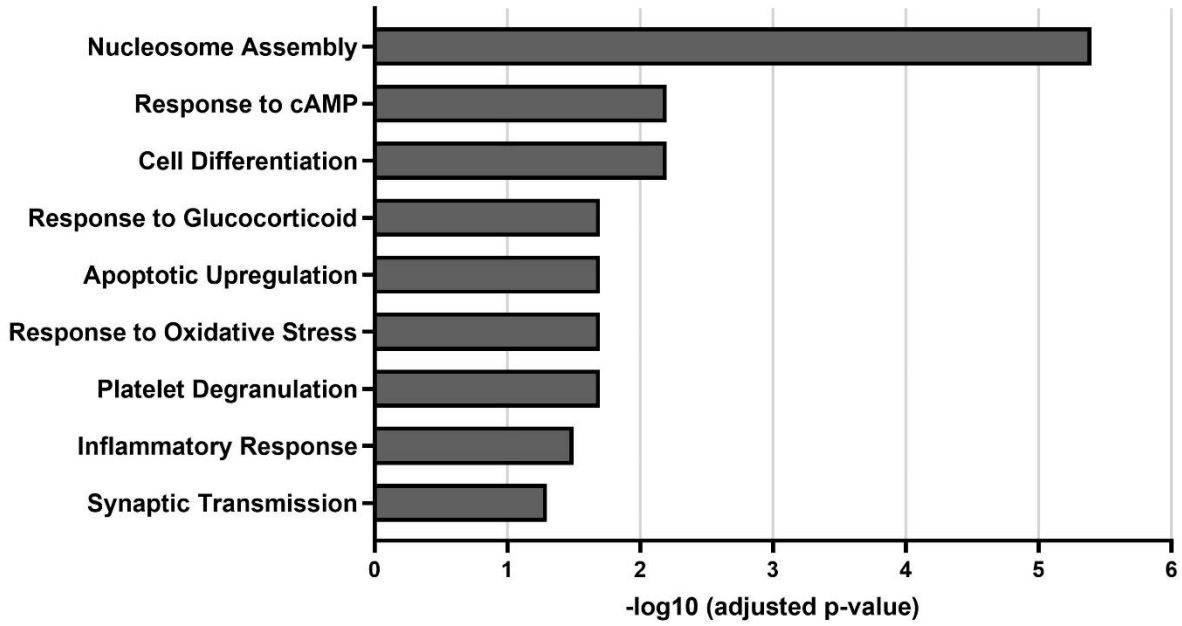

Figure 2.11. *Gene ontology analysis for PMb-EphA1Cry2Δ light vs. Cry2olig light condition. X-axis represents the -log10(adjusted p-value) of first condition compared to second condition for statistically significant values only ($p < 0.05$).*

Table 2.3. *Top up-regulated DEGs by Log2FoldChange for PMb-EphA1Cry2Δ light condition compared to Cry2olig light condition. The encoded protein and its function are provided. All genes have an adjusted p-value of 0.00.*

Gene Name	***Log2 FoldChange***	***Encoded Protein***	***Protein Function***	***Reference***
IL17F	4.09	Interleukin 17F	Inflammatory response	(S. H. Chang & Dong, 2009)
TG	3.92	Thyroglobulin	Metabolism and cell growth	(Prpić et al., 2018)
HFE	3.64	HFE	Iron absorption	(Barton et al., 2015)
HSPA6	3.6	Heat Shock Protein A6	Stress Response	(Guan et al., 2021)
HSPA7	3.52	Heat Shock Protein A7	Stress Response	(Guan et al., 2021)

The downregulation of certain genes can reveal additional information on biological effect of EphA1 receptor activation (**Table 2.4**). The highest downregulated gene was found to be *FOXE3*, a gene encoding a transcriptional regulator critical for proper epithelial differentiation (Hannenhalli & Kaestner, 2009; Reis et al., 2010). Other downregulated proteins include thioredoxin (gene: *TXNDC2*), a reactive oxygen species scavenger; sodium-glucose transporter A4 (gene: *SLC5A4*); T-cell immunoglobulin and mucin domain-3 (TIM3) (gene: *HAVCR2*); and CYFIP-related Rac Interactor (CYRI) (gene: *FAM49A*), a regulator of the WAVE-regulatory complex (Javadirad & Mokhtari, 2021; Wagner et al., 2014; Whitelaw et al., 2019; Zhai et al., 2021). Of particular interest is the downregulation of CYRI, CYRI acts as an inhibitor of the WAVE-regulatory complex (WRC) by competitive Rac1 binding, which results in inhibition of the Arp2/3 complex. As the Arp2/3 complex is critical for the branching of F-actin to produce lamellipodia, a downregulation of CYRI could result in an increase in lamellipodia formation (Whitelaw et al., 2019).

Table 2.4. *Top down-regulated DEGs by Log2FoldChange for PMb-EphA1Cry2Δ light condition compared to Cry2olig light condition. The encoded protein and its function are provided. All genes have an adjusted p-value of 0.00.*

Gene Name	***Log2 FoldChange***	***Encoded Protein***	***Protein Function***	***Reference***
FOXE3	-4.06	Forkhead box transcription factors	Cell-cycle control, differentiation	(Reis et al., 2010)
TXNDC2	-2.42	Thioredoxin	Response to oxidative stress	(Javadirad & Mokhtari, 2021)
SLC5A4	-2.16	Sodium-glucose transporter	Na^+ transmembrane transport	(Schäfer et al., 2018)
HAVCR2	-2.00	T-cell immunoglobulin and mucin domain-3	Antigen recognition, immune response	(Zhai et al., 2021)
FAM49A	-1.74	CYFIP-related Rac interactor	Rac1 inhibition	(Whitelaw et al., 2019)

Other upregulated genes of interest are *EGR1/EGR4*, *FOS*, *ETV4*, and *CREB5*, which encode the proteins early growth response factor (EGR1/EGR4), protein c-Fos (Fos), ETS translocation variant 4 (ETV4), and cAMP responsive element binding protein 5 (CREB5), respectively (**Table 2.5**). All five of these proteins are transcription factors that play a role in cell proliferation, cell migration, and angiogenesis; their expression is a result of Ras/Raf/MEK/ERK activation and itself promotes or inhibits the expression of various genes (Fraguas et al., 2014; Lavoie et al., 2020; B. Wang et al., 2021). Fos is considered a proto-oncogene for its role in cancer proliferation and metastasis (Lavoie et al., 2020). ETV4 is a part of the PEA3 subfamily of transcription factors, itself a part of the larger family of E26 transformation-specific (ETS) transcription factors, that is activated by ERK and binds to and initiates transcription through ETS DNA-binding motifs; the genes transcribed through these motifs are involved in cell proliferation and play a role as oncogenes in some types of cancer (Lavoie et al., 2020). The transcription activator CREB5 can be activated by cAMP and in turn promotes the expression of the RTK, Met (S. Wang et al., 2020). Upregulation of EGR, Fos, ETV4, and CREB5 have all been found to promote tumorigenesis within cancer cells (Fraguas et al., 2014; Lavoie et al., 2020; B. Wang et al., 2021). Growth factor receptor bound protein 7 (Grb7; *GRB7*) is an adaptor protein that interacts with RTKs and integrins for signal transduction. Phosphorylated Grb7 can activate Akt and ERK to induce proliferation, cell invasion, and cell migration. Activating transcription factor 3 (AT3) is another transcription factor that regulates gene expression of growth factors, cytokines, and CREB. Additionally, both Akt and MAPK can interact with and post-translationally modify ATF3. Its expression is typically induced under stress conditions found in tumor microenvironments (Hai et al., 2010). Interestingly, ATF3 can upregulate the expression of EphA1 receptor through CREB, which in turn stimulates angiogenesis (Masuda et

al., 2008). The upregulation of genes described here are most likely a result of signaling in response to PMb-EphA1Cry2Δ light activation. In contrast, the EphA2 receptor ligand, ephrinA4 (gene: *EFNA4*), was downregulated in response to PMb-EphA1Cry2Δ activation. This downregulation could be due to overexpression of the EphA1 receptor gene leading to negative regulation of an EphA receptor ligand (D. N. Arvanitis & Davy, 2012).

Table 2.5. *Significant DEGs of interest for PMb-EphA1Cry2Δ light condition compared to Cry2olig light condition. The encoded protein and its function are provided. All genes have an adjusted p-value of 0.00.*

Gene Name	***Log2 FoldChange***	***Encoded Protein***	***Protein Function***	***Reference***
EGR1*	2.77	Early growth response factor 1	Proliferation	(B. Wang et al., 2021)
GRB7	2.67	Growth factor receptor bound protein 7	Proliferation	(Chu et al., 2019)
EGR4*	2.41	Early growth response factor 4	Proliferation, differentiation	(Fraguas et al., 2014)
ATF3	2.09	Activating transcription factor 3	Metabolism, stress response	(Hai et al., 2010)
FOS*	2.20	Protein c-Fos	Proliferation (proto-oncogene)	(Lavoie et al., 2020)
GPR3	1.89	G protein-coupled receptor 3	Response to cAMP	(Valverde et al., 2009)
ETV4*	1.39	ETS translocation variant 4	Glycolysis, proliferation	(Lavoie et al., 2020)
CREB5*	1.29	cAMP responsive element binding protein	Proliferation	(S. Wang et al., 2020)
EFNA4	-1.5	EphrinA4	Angiogenesis	(Lin et al., 2021)

*genes associated with ERK signaling pathways

For the comparison of PMb-EphA1Cry2Δ light condition compared to ephrinA1-stimulated condition, upregulated ontological processes include regulation of transcription and gene expression, response to cAMP and inflammation, differentiation and proliferation, and nucleosome assembly (**Fig. 2.12; Table AII.7**). These processes share overlap with the processes

upregulated by PMb-EphA1Cry2Δ light condition compared to Cry2olig light condition. Ontological processes unique to the ephrinA1-stimulated comparison are cilium-dependent cell mobility and response to lipopolysaccharide. Heat shock protein A6 and A7 and interleukin 17F were three of the top upregulated proteins, similar to the Cry2olig light comparison. The other two top upregulated proteins were ADP ribosylation factor-like GTPase 14 (ARL14) (gene: *ARL14*) and transglutaminase 7 (TGM7) (gene: *TGM7*) (**Table 2.6**). ARL proteins are part of the Ras superfamily and mainly regulate membrane trafficking and development. ARL14 has been implicated in cancer progression; specifically, an upregulation of ARL14 has been found in endometrial cancer (J. Zhang et al., 2020). Transglutaminases are enzymes that crosslink proteins via a transferase reaction for the stabilization of protein assemblies, especially those in the extracellular matrix. Transglutaminases play a major role in blood clot formation and keratinization, which are integral for wound healing. They can also regulate interleukins and growth factors in addition to interacting with integrins. ARL14 and TGM7 may play regulatory roles in signaling upon PMb-EphA1Cry2Δ activation, but the link between Eph receptor signaling and their gene expression is still unclear.

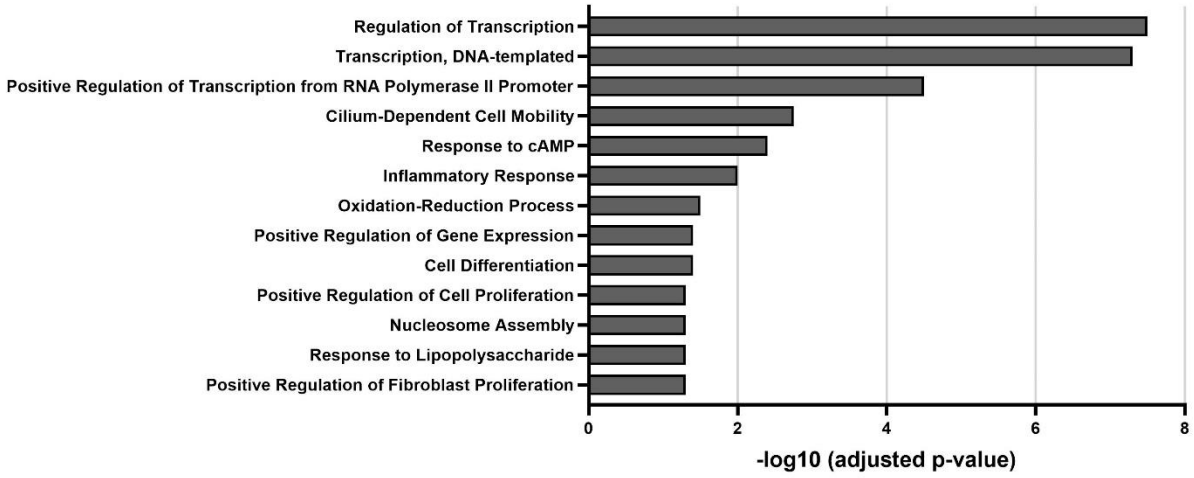

Figure 2.12. *Gene ontology analysis for PMb-EphA1Cry2Δ light vs. ephrinA1-stimulated conditions. X-axis represents the -log10(adjusted p-value) of first condition compared to second condition for statistically significant values only ($p < 0.05$).*

Table 2.6. *Top upregulated DEGs by Log2FoldChange for PMb-EphA1Cry2Δ light condition compared to ephrinA1-stimulated condition. The encoded protein and its function are provided. All genes have an adjusted p-value of 0.00.*

Gene Name	***Log2 FoldChange***	***Encoded Protein***	***Protein Function***	***Reference***
HSPA6	9.64	Heat Shock Protein A6	Stress response	(Guan et al., 2021)
ARL14	8.07	ADP ribosylation factor-like GTPase 14	Membrane trafficking	(J. Zhang et al., 2020)
TGM7	7.35	Transglutaminase 7	Cytoskeletal organization	(Grenard et al., 2001)
IL17F	7.08	Interleukin 17F	Inflammatory response	(S. H. Chang & Dong, 2009)
HSPA7	7.00	Heat Shock Protein A7	Stress Response	(Guan et al., 2021)

The top downregulated gene-encoding proteins in response to PMb-EphA1Cry2Δ light activation compared to ephrinA1-stimulated control were prostaglandin D synthase (PTGDS), tropomyosin 3 (TPM3), kinesin-related protein 12 (KIF12), cholinergic receptor nicotinic gamma subunit (CHRNG), and Rab26 (**Table 2.7**). PTGDS, a glycoprotein important in prostaglandins metabolism, has been found to regulate MAPK and STAT3 and is downregulated in some types of cancers (Hu et al., 2022). TPM3 forms strands with itself and associates with actin filaments, recruiting and activating actin-binding proteins such as troponin, Arp2/3 complex, and ADF/cofilin. Its function within the cell is to regulate actin dynamics and actin-myosin interactions, specifically during muscle contraction (Lawlor et al., 2010). KIF12 is a motor protein that moves along microtubules to transport organelles within the cell and to move chromosomes along the mitotic spindle (Veljačić Visković et al., 2023). CHRNG is a subunit of muscle nicotinic acetylcholine receptor (AChR), which regulates blood pressure and cell proliferation and differentiation during development. In bovine preadipocytes, an upregulation of CHRNG inhibited cell proliferation and differentiation (Du et al., 2023); therefore, a downregulation of CHRNG could promote proliferation and differentiation. Rab26 is a small Rab GTPase that plays a crucial role in membrane trafficking and cell mobility/adhesion through the endocytosis of membrane receptors. Its function in the degradation of active phosphorylated Src kinases through autophagy leads to an inhibition of cell migration and adhesion. Unsurprisingly, Rab26 is under-expressed in highly invasive breast cancer cells.

Table 2.7. *Top downregulated DEGs by Log2FoldChange for PMb-EphA1Cry2Δ light condition compared to ephrinA1-stimulated condition. The encoded protein and its function are provided. All genes have an adjusted p-value of 0.00.*

Gene Name	***Log2 FoldChange***	***Encoded Protein***	***Protein Function***	***Reference***
PTGDS	-3.03	Prostaglandin D synthase	Metabolism, lipid transport	(Hu et al., 2022)
TPM3P6	-2.34	Tropomyosin 3	Cytoskeletal regulation	(Lawlor et al., 2010)
KIF12	-2.18	Kinesin-related protein 12	Organelle transport	(Veljačić Visković et al., 2023)
CHRNG	-2.11	Cholinergic receptor nicotinic gamma subunit	Differentiation, cell growth	(Du et al., 2023)
RAB26	-1.85	Rab26	Autophagy, cell trafficking	(H. Liu et al., 2021)

Other significant DEGs of interest are listed in **Table 2.8**. *ATF3* (Log2FoldChange: 4.09), *TG* (5.05), *EGR1* (2.65), *EGR4* (4.67), *GRB7* (3.41), *FOS* (2.68), *CREB5* (1.95), and *ETV4* (1.48) genes are all overexpressed in response to PMb-EphA1Cry2Δ light stimulation compared to not only the Cry2olig light control condition, but also the ephrinA1-stimulated control condition. C-C chemokine ligand 5 (CCL5) (gene: *CCL5*) is a chemokine that is highly expressed in immune cells. CCL5 transcription is regulated by CREB, and its binding to the GPCR C-C chemokine receptor 5 (CCR5) activates downstream signaling pathways PI3K/Akt, Ras/Raf/MEK/ERK, NF-κB, HIF-α, and JAK-STAT. CCL5 upregulation is associated with inflammation and cancer through these signaling pathways that promote proliferation, cell invasion, inflammation, and angiogenesis (Zeng et al., 2022). Transmembrane protein 52 (TMEM52) (gene: *TMEM52*) also regulates proliferation and migration; however, unlike CCRL5, TMEM52 attenuates these processes. In cancer cells, suppression of TMEM52 expression induces the cleavage of extracellular E-cadherin, which activates EGFR and Akt/ERK

downstream signaling (Y. Lee et al., 2021). Under-expression of TMEM52 has been detected in renal cell carcinomas, the same type of cancer where overexpressed EphA1 receptor was correlated with metastasis and poor prognosis (Lee et al., 2021; Toma et al., 2014). TMEM52 was also significantly under-expressed in response to our EphA1Cry2 construct activation. Jun (gene: *JUN*), part of the same family of transcription factors as Fos, is phosphorylated by ERK and can form dimers with Fos and ATF2 to activate downstream DNA-binding motifs such as the TPA response element (TRE) or the cAMP response element (CRE). Transcription of these genes, called the immediate early genes (IEGs), result in the transition of a cell from G1 phase to S phase (Lavoie et al., 2020). Paired box 5 (PAX5) (gene: *PAX5*) is a transcription factor crucial for controlling cell proliferation, differentiation, and viability. PAX5 undergoes many alterations, such as post-translational modifications and alternative splicing, for the control of its spatiotemporal expression. Due to this, PAX5 expression and its activation or repression of other genes is extensive and complex. One role studied in breast cancer cells is the PAX5-induced expression of E-cadherin, which promotes the transition of cancer cells from a mesenchymal to epithelial phenotype. This transition yields an anti-invasive property, suppressing tumor metastasis (Nasri Nasrabadi et al., 2022). Although the biological processes triggered by upregulation of PAX5 are contradictory to the other upregulated effects described above, PAX5 could contain alterations that would result in the regulation of other processes.

Table 2.8. *Significant DEGs of interest by Log2FoldChange for PMb-EphA1Cry2Δ light condition compared to ephrinA1-stimulated condition. The encoded protein and its function are provided. All genes have an adjusted p-value of 0.00.*

Gene Name	***Log2 FoldChange***	***Encoded Protein***	***Protein Function***	***Reference***
CCL5	6.39	C–C chemokine ligand 5	Adhesion, migration	(Zeng et al., 2022)
CCR4	4.16	C-C chemokine receptor 4	Angiogenesis	(Lavoie et al., 2020)
PAX5	3.82	Paired Box 5	Proliferation, differentiation	(Nasri Nasrabadi et al., 2022)
JUN*	1.81	Transcription factor Jun	Proliferation (proto-oncogene)	(Lavoie et al., 2020)
TMEM52	-1.877	Transmembrane protein 5	Tumor suppressor	(Lee et al., 2021)

*genes associated with ERK signaling pathways

EphA1Cry2 activation in differentiated Neuro2a cells

We also investigated the effects of PMb-EphA1Cry2Δ activation in other cell types other than HEK293T cells. Neuro2a (N2a) cells were selected as the N2a cell line is a mouse neural crest-derived cell line commonly used to study neuronal differentiation and its related signaling pathways (Tremblay et al., 2010). Differentiated N2a cells transfected with PMb-EphA1Cry2Δ show reversible, localized clustering at the membrane of the neuronal-like processes (**Fig. 2.13A**). Small protrusions along these processes were identified at time 0 min of the PMb-EphA1Cry2Δ transfected cells and retract into the processes 10 min after light exposure. These protrusions returned after 10 min in the dark condition (**Fig. 2.13B; Movie AII.3**). Based on these results, the EphA1Cry2 construct could be applied for the induction of morphological changes relevant to synaptic structural plasticity.

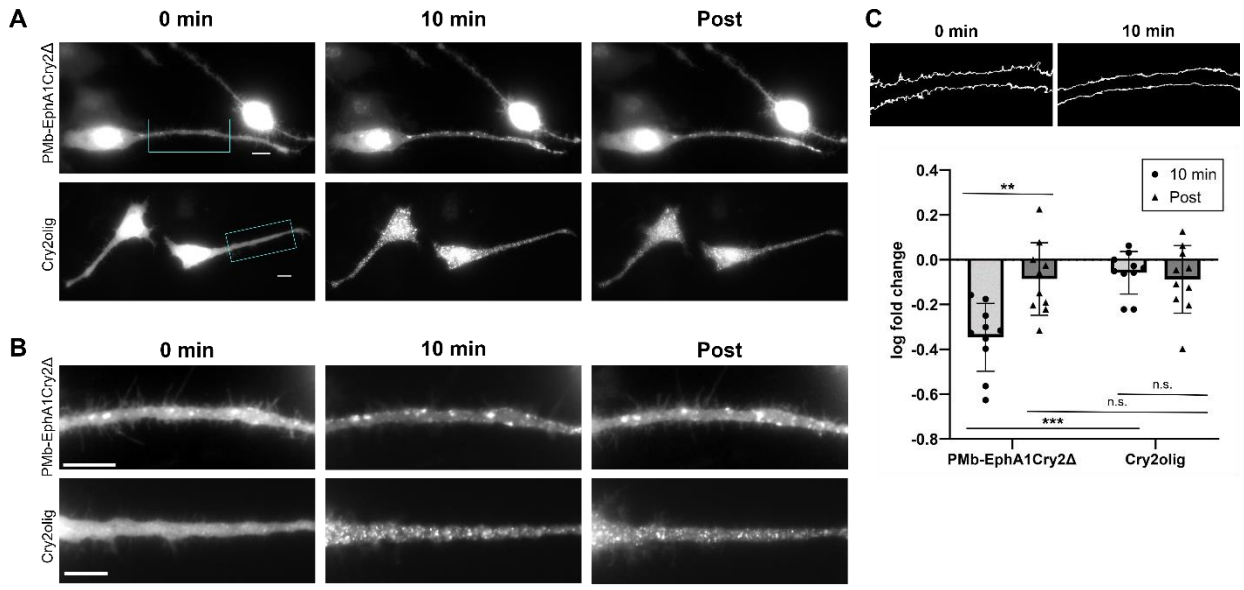

Figure 2.13. *Optogenetic clustering of transfected N2a cells.* ***(A)*** *Widefield images of differentiated N2a cells transfected with PMb-EphA1Cry2Δ and Cry2olig taken pre-light exposure (0 min), after 10 min of blue light exposure (480 nm, 50 ms exposure, 30 sec intervals), and 10 min post-light exposure (Post). Images collected on mCherry channel (200 ms exposure, 553 nm). Scale bar: 10 µm.* ***(B)*** *Zoomed region of interest (cyan box) of neuronal-like process of a cell in (A). Scale bar: 10 µm.* ***(C)*** *Top: Threshold images of PMb-EphA1Cry2Δ transfected cells (at 0 min and 10 min of light exposure) from (B) used to count protrusions along neuronal-like processes of differentiated N2a cells. Bottom: Log fold change in protrusion number on the neuronal-like processes. 10 min of light exposure and post-light exposure were quantified in respect to protrusion number at time 0 min of light exposure. Error bars represent standard deviation, n=10 cells taken from two separate dishes (unpaired t-test; ***p < 0.0001, **p < 0.01, n.s. = not significant).*

Discussion and Summary

Eph receptors are the key to many signaling pathways that regulate cell-cycle progression and cell migration (L. Y. Liang et al., 2019). In our studies, we designed constructs of an optogenetic EphA1 receptor using Cry2olig that clustered in response to blue light stimulus. We found that this light-initiated clustering resulted in activation by auto-phosphorylation of the EphA1 receptor's tyrosine kinase domain and induced downstream ERK signaling in HEK293T cells. We also found that expression of our PMb-EphA1Cry2Δ construct in N2a cells resulted in modulation of protrusive activity along the neuronal-like processes of the cells.

Previous studies on EphA1 receptor have elucidated its role in cell mobility and morphology (Ieguchi & Maru, 2019; Yamazaki et al., 2009). Specifically, ephrinA1 stimulation of EphA1 receptor resulted in activation of the RhoA/ROCK pathway, which promotes cell rounding and migration (Yamazaki et al., 2009). Rho-GTPases are associated with the integrin-linked kinase (ILK) pathways and help regulate the actin cytoskeleton through GTP binding and hydrolysis (Yamazaki et al., 2009). Of the Rho GTPases, RhoA regulates actomyosin contractility and stress-fiber formation, and Rac1 regulates lamellipodia formation by the WAVE-mediated ARP2/3 complex (Beco et al., 2018; Kunschmann et al., 2019). EphA1 has been shown to interact with ILK, a kinase that binds to integrin and promotes signaling transduction from the ECM to the cytosol. Activated EphA1 inhibits ILK activity, which inactivates Rac1, thereby inhibiting cell spreading in an ephrin-dependent manner (Yamazaki et al., 2009). Removal of the SAM domain prevented the binding of ILK and eliminated the cell spreading defect (Yamazaki et al., 2009). Conversely, studies of the SAM domain in EphA2 receptor found that a deletion of the SAM domain results in an increase in the ability of the receptor to dimerize and activate even in the absence of ephrinA1-Fc stimulation (Singh et al.,

2017). A ΔSAM mutant of EphA1 receptor specifically can still be activated through its kinase domain but associated morphological change were inhibited (Yamazaki et al., 2009). Interestingly, our results indicate that activation of receptor tyrosine kinase domains via EphA1Cry2olig clustering can induce cell rounding with and without the presence of the SAM domain. While a pathway of EphA1 signaling has been proposed (Ieguchi & Maru, 2019), further elucidation of EphA1 signaling pathways is still needed to determine the effect of EphA1 activity. The benefit of our optogenetic constructs is that the EphA1 signaling is simplified to include only forward signaling, as the extracellular regions have been removed.

Other studies in EphA receptor signaling reported ephrinA1-induced EphA receptor activation resulted in an inhibition of the Ras/Raf/MEK/MAPK pathway that regulates cell proliferation (Miao et al., 2000, 2001). These studies were also conducted in HEK293T cells; however, EphA2 receptor is the predominate endogenously expressed EphA receptor in HEK293T cells and the other cell types used (Miao et al., 2001). Juxtaposing these results, EphA2 specific signaling was reported in the same cell types as promoting the MAPK pathway and forming a complex with the adaptor proteins SHC and Grb2 (Pratt & Kinch, 2002). Our light-activated PMb-EphA1Cry2Δ construct induced ERK and Akt phosphorylation, which upregulates proliferation (Mebratu & Tesfaigzi, 2009; Nitulescu et al., 2018). This finding may not be surprising as EphA1 receptor has been found to up-regulated in certain types of cancer (Ieguchi & Maru, 2019). As EphA1 receptors are essential for angiogenesis, tumors may increase expression of EphA1 receptor to promote proliferation. Coupled with a decrease in cell adhesion and an increase in cell migration, EphA1 receptor-activated proliferation would induce metastasis of a tumor cell if EphA1 was overexpressed (Ieguchi & Maru, 2019). EphA1 expression is up-regulated by the ATF3, which has been found to be induced under stress

conditions (Masuda et al., 2008). A study of expression patterns in clear cell renal cell carcinoma (ccRCC) consistently showed that a lower EphA1 expression in tumor cells corresponded to a more positive prognosis (Toma et al., 2014). In hepatocellular carcinoma (HCC), a common liver tumor, up-regulated EphA1 promotes Akt/mTOR-activated transcription of the chemokine, stromal cell-derived factor 1 (SDF-1). SDF-1 is then secreted by the tumor cell and binds to the CXCR4 receptor on an endothelial progenitor cell, leading to chemotaxis and tumorigenesis (Y. Wang et al., 2016).

Based on our RNA-sequencing results, many proteins related to inflammatory response, proliferation, differentiation, and migration are upregulated in response to our light-activated EphA1 construct, consistent with studies on ephrinA1-stimulated EphA1 receptor signaling outcomes (Holen et al., 2010; Masuda et al., 2008; Pratt & Kinch, 2002; Y. Wang et al., 2016; Yamazaki et al., 2009). Proliferation is promoted by the upregulation of EGR1, EGR4, Grb7, Fos, Jun, ETV4, and CREB5. In fact, EGR1, EGR4, Grb7, Fos, Jun, and CREB5 have been found to be upregulated in cancer cells and associated with metastasis (Chu et al., 2019; Lavoie et al., 2020; B. Wang et al., 2021; S. Wang et al., 2020). HspA6, HspA7, IL17F, and AT3 are upregulated in response to stress factors, especially those found in tumor microenvironments (S. H. Chang & Dong, 2009; Guan et al., 2021; Masuda et al., 2008). High TG serum levels are indicative of tumor metastasis in thyroid cancer (Prpić et al., 2018). Downregulation of certain genes can also exacerbate tumorigenesis; suppression of TMEM52 in cancer cells increases invasion and survival, promoting tumorigenesis (Y. Lee et al., 2021). As a tumor suppressor, Rab26 downregulation would attenuate cancer invasion and migration (H. Liu et al., 2021). CYRI under-expression would also increase cancer cells' ability to migrate through a decrease of negative regulation of actin polymerization (Whitelaw et al., 2019). The upregulation or

downregulation of these genes in response to EphA1 expression or activation could also be modulated by *cis*-interactions with other endogenous receptor. EphA receptors have been shown to interact along the plasma membrane with FGFR, integrins, and CXCR-4 to promote the activation of downstream signaling targets of MAPK and small GTPases (D. N. Arvanitis & Davy, 2012). Interactions with these receptors endogenously could affect the level of expression of signal transducers or their signaling outcomes. Studies involving receptor knockouts, receptor mutants, or receptor-interaction inhibitors could elucidate the role these interactions play in proliferation.

Similar to EphA2 receptor, constitutive or dysregulated EphA1 receptor downstream signaling can result in tumor progression and metastasis. As anticancer drugs are becoming more selective to cancer type-specific targeting, a drug selective for EphA1 receptor could be utilized for drug delivery. An EphA2-targeting peptide has been synthesized for the inhibition of tumor growth (S. Wang et al., 2012). This short peptide (YSA) with amino acid sequence YSAYPDSVPMMS can not only inhibit ephrinA binding to EphA2 receptors, but also induce EphA2 activation and endocytosis, resulting in lower receptor levels at the plasma membrane and internalizing the peptide within the cell. A fusion of the anticancer drug paclitaxel with this peptide resulted in a novel drug delivery system that effectively reduced tumor growth and proliferation through an increase in internalized drug (S. Wang et al., 2012; Y. Wang et al., 2015). As EphA1 and EphA2 receptors can both bind ephrinA1, YSA peptide (or a modified version of YSA) may be able to selectively bind and internalize EphA1 receptor, providing a novel drug delivery system for tumors that overexpress EphA1 receptor.

Although there have been few studies on EphA receptors in neurons, the research on their ligand, ephrinA1, has suggested that stimulation of ephrinA1 results in neuron migration (Bravo-

Cordero et al., 2013). One of the major EphA receptors in neurons is EphA4, a homolog of EphA1 and EphA2, that has been shown to interact with EphA1 (Murai et al., 2003). Through binding of ephrinA3 on a neighboring astrocyte, EphA4 forward signaling on a dendritic spine can decrease its spine length and width (Murai et al., 2003). This may also be the case with PMb-EphA1Cry2Δ, as the construct's activation resulted in a decrease of protrusions along the processes of N2a cells. In primary neurons, EphA1 activation could result in a decrease in spines which would prime the neuron for deadhesion and migration (Holen et al., 2010; Murai et al., 2003). As Eph receptors are integral in cell-cell communication during neurogenesis, their dysfunction can play a role in neurological disorders and neurodegenerative diseases (Liang et al., 2019). Recently, researchers have found that Alzheimer's disease (AD) pathology could be detected via biomarkers in a patient's genome (H. F. Wang et al., 2015). In an analysis of recent genome studies, the EphA1 locus was found to be highly associated with AD (Carrasquillo et al., 2011; Naj et al., 2011; H. F. Wang et al., 2015). The A-allele of EphA1 was correlated with a decrease in hippocampal atrophy in mild cognitive impairment patients and was associated with a higher glucose cerebral metabolic rate in certain parts of the brain (H. F. Wang et al., 2015).

In vivo experiments on mice brains have also been conducted using ephrinA1. When ephrinA1-Fc was injected into the lateral ventricle, neural stem/progenitor cells proliferated and migrated to the part of the brain that contained a lesion. These cells then differentiated into astrocytes or dopaminergic cells, and an overall increase in angiogenesis occurred. Behavioral abnormalities used as a model for Parkinson's disease were alleviated after the ephrinA1 injection (Jing et al., 2012). A recent study has also identified EphA1 as an upstream activator for Connexin32 tyrosine phosphorylation, an important process for gap junction trafficking in the brain. Dysfunction of Connexin32 has been linked to Charcot-Marie-Tooth disease, a family of

disorders that cause degenerative nerve damage (Trease et al., 2019). Overall, understanding the role EphA1 plays in neurons, astrocytes, and glia could yield new insights into neurodegenerative diseases.

While ephrin signaling in the heart has been a recent highlight in research, Eph receptor signaling has not been widely studied in cardiomyocytes. Progressive research into ephrinA1's role in the heart and myocardial infarction has been conducted; in mice with simulated myocardial infarction (MI), ephrinA1-Fc intramyocardial injections improved negative factors resulting from coronary artery ligation, such as reduced infarct size and a decrease in percent necrosis of affected tissue (Dries et al., 2011; O'Neal et al., 2013). Interestingly, EphA1 receptor was found to be upregulated 10-fold after the ephrinA1-Fc injection. Although this upregulation was hypothesized to be a compensation for endocytosis of the receptor after ligand binding, studies on EphA1 in cardiomyocytes could be explored using our EphA1Cry2 construct (Dries et al., 2011; Hartmann et al., 2015; O'Neal et al., 2013). Subsequent research on this topic revealed that an EphA2 knockout in mice produced opposite effects as the ephrinA1-Fc injection, worsening factors resulting from simulated MI. A suggested explanation is that EphA2 stimulates the pro-inflammatory response of leukocyte migration to injury (O'Neal et al., 2013). EphA receptors are known to regulate immune cell migration to injury sites, and EphA1 specifically is involved in migration of T-cells (Darling & Lamb, 2019; Holen et al., 2010). Connexins play an integral role not only in the brain, but also in gap junctions in the heart. Since EphA1 receptors have been linked to connexin32 phosphorylation in the liver and brain, it would be of interest to investigate the role of EphA1 in cardiomyocytes (Trease et al., 2019). Another protein of interest, ROCK, has been shown to play a critical role in heart cells and cardiovascular disease (Hartmann et al., 2015). Increase activity of ROCK has been linked to myocardial

infarction and cardiac fibrosis and could potentially be a biomarker of various heart diseases (Dong et al., 2013; Y.-M. Zhang et al., 2006). The connection between connexin and ROCK, and its upstream activator EphA1, could lead to new insights into heart disease.

The potential future studies using optogenetic Eph receptors are vast. We have shown here that our EphA1Cry2 construct induced ERK and Akt phosphorylation in response to light activation. Locke, et. al. showed that OptoEphB2 exhibited increased filopodia in the dendritic region after light stimulation through the Arg kinase pathway of actin polymerization (Locke et al., 2017). Other optoEphA constructs could be designed and validated in HEK293 cells and transfected into specialized cell lines. EphA4 receptor could be studied in N2a cells or primary neurons to optically regulate spine retraction (Lai & Ip, 2009). To confirm the results of previous studies involving ephrin-A1 stimulation of EphA2 during MI, an optogenetic EphA2 construct based on the EphA1Cry2 design could be utilized for ephrinA1-independent EphA2 signaling investigations (Dries et al., 2011; DuSablon et al., 2014). Other EphA receptors can be applied to this optoEph design to delineate ephrin-independent activation with potential to further investigate *cis*-interactions with receptors, for example optoEphA1 to optoEphA4 dimerization or optoEphA to optoFGFR dimerization.

References

Arvanitis, D., & Davy, A. (2008). Eph/ephrin signaling: Networks. In *Genes and Development* (Vol. 22, Issue 4). https://doi.org/10.1101/gad.1630408

Arvanitis, D. N., & Davy, A. (2012). Regulation and misregulation of Eph/ephrin expression. *Cell Adhesion & Migration*, *6*(2), 131–137. https://doi.org/10.4161/cam.19690

Barquilla, A., & Pasquale, E. B. (2015). Eph receptors and ephrins: Therapeutic opportunities. In *Annual Review of Pharmacology and Toxicology* (Vol. 55). https://doi.org/10.1146/annurev-pharmtox-011112-140226

Barton, J. C., Edwards, C. Q., & Acton, R. T. (2015). HFE gene: Structure, function, mutations, and associated iron abnormalities. *Gene*, *574*(2), 179–192. https://doi.org/10.1016/j.gene.2015.10.009

Beco, S. de, Vaidžiulytė, K., Manzi, J., Dalier, F., Federico, F. di, Cornilleau, G., Dahan, M., & Coppey, M. (2018). Optogenetic dissection of Rac1 and Cdc42 gradient shaping. *Nature Communications*, *9*(1). https://doi.org/10.1038/s41467-018-07286-8

Bravo-Cordero, J. J., Magalhaes, M. A. O., Eddy, R. J., Hodgson, L., & Condeelis, J. (2013). Functions of cofilin in cell locomotion and invasion. In *Nature Reviews Molecular Cell Biology* (Vol. 14, Issue 7). https://doi.org/10.1038/nrm3609

Bugaj, L. J., Spelke, D. P., Mesuda, C. K., Varedi, M., Kane, R. S., & Schaffer, D. V. (2015). Regulation of endogenous transmembrane receptors through optogenetic Cry2 clustering. *Nature Communications*, *6*. https://doi.org/10.1038/ncomms7898

Carrasquillo, M. M., Belbin, O., Hunter, T. A., Ma, L., Bisceglio, G. D., Zou, F., Crook, J. E., Pankratz, V., Sando, S. B., Aasly, J. O., Barcikowska, M., Wszolek, Z. K., Dickson, D. W., Graff-Radford, N. R., Petersen, R. C., Passmore, P., Morgan, K., & Younkin, S. G. (2011). Replication of EPHA1 and CD33 associations with late-onset Alzheimer's disease: A multi-centre case-control study. *Molecular Neurodegeneration*, *6*(1). https://doi.org/10.1186/1750-1326-6-54

Chang, S. H., & Dong, C. (2009). IL-17F: Regulation, signaling and function in inflammation. *Cytokine*, *46*(1), 7–11. https://doi.org/10.1016/j.cyto.2008.12.024

Chavez-Abiega, S., Gönloh, M. L. B., Gadella, T. W. J., Bruggeman, F. J., & Goedhart, J. (2022). Single-cell imaging of ERK and Akt activation dynamics and heterogeneity induced by G-protein-coupled receptors. *Journal of Cell Science*, *135*(6). https://doi.org/10.1242/jcs.259685

Chen, Z., Oh, D., Biswas, K. H., Zaidel-Bar, R., & Groves, J. T. (2021). Probing the effect of clustering on EphA2 receptor signaling efficiency by subcellular control of ligand-receptor mobility. *eLife*, *10*, e67379. https://doi.org/10.7554/eLife.67379

Chu, P.-Y., Tai, Y.-L., & Shen, T.-L. (2019). Grb7, a Critical Mediator of EGFR/ErbB Signaling, in Cancer Development and as a Potential Therapeutic Target. *Cells*, *8*(5), 435. https://doi.org/10.3390/cells8050435

Darling, T. K., & Lamb, T. J. (2019). Emerging roles for Eph receptors and ephrin ligands in immunity. In *Frontiers in Immunology* (Vol. 10, Issue JULY). https://doi.org/10.3389/fimmu.2019.01473

Dessauges, C., Mikelson, J., Dobrzyński, M., Jacques, M., Frismantiene, A., Gagliardi, P. A., Khammash, M., & Pertz, O. (2022). Optogenetic actuator – ERK biosensor circuits identify MAPK network nodes that shape ERK dynamics. *Molecular Systems Biology*, *18*(6), e10670. https://doi.org/10.15252/msb.202110670

Dong, M., Liao, J. K., Yan, B., Li, R., Zhang, M., & Yu, C. M. (2013). A combination of increased Rho kinase activity and N-terminal pro-B-type natriuretic peptide predicts worse cardiovascular outcome in patients with acute coronary syndrome. *International Journal of Cardiology*, *167*(6). https://doi.org/10.1016/j.ijcard.2012.07.007

Dries, J. L., Kent, S. D., & Virag, J. A. I. (2011). Intramyocardial administration of chimeric ephrinA1-Fc promotes tissue salvage following myocardial infarction in mice. *Journal of Physiology*, *589*(7). https://doi.org/10.1113/jphysiol.2010.202366

Du, J., Zhao, H., Song, G., Pang, Y., Jiang, L., Zan, L., & Wang, H. (2023). Overexpression of cholinergic receptor nicotinic gamma subunit inhibits proliferation and differentiation of bovine preadipocytes. *Animal Bioscience*, *36*(2), 200–208. https://doi.org/10.5713/ab.22.0144

Duan, L., Hope, J., Ong, Q., Lou, H. Y., Kim, N., McCarthy, C., Acero, V., Lin, M. Z., & Cui, B. (2017). Understanding CRY2 interactions for optical control of intracellular signaling. *Nature Communications*, *8*(1). https://doi.org/10.1038/s41467-017-00648-8

DuSablon, A., Kent, S., Coburn, A., & Virag, J. (2014). EphA2-receptor deficiency exacerbates myocardial infarction and reduces survival in hyperglycemic mice. *Cardiovascular Diabetology*, *13*(1). https://doi.org/10.1186/s12933-014-0114-y

Fraguas, S., Barberán, S., Iglesias, M., Rodríguez-Esteban, G., & Cebrià, F. (2014). *Egr-4* , a target of EGFR signaling, is required for the formation of the brain primordia and head regeneration in planarians. *Development*, *141*(9), 1835–1847. https://doi.org/10.1242/dev.101345

Ganetzky, R. D., Stendel, C., McCormick, E. M., Zolkipli-Cunningham, Z., Goldstein, A. C., Klopstock, T., & Falk, M. J. (2019). MT-ATP6 mitochondrial disease variants: Phenotypic and biochemical features analysis in 218 published cases and cohort of 14 new cases. *Human Mutation*, *40*(5), 499–515. https://doi.org/10.1002/humu.23723

Grenard, P., Bates, M. K., & Aeschlimann, D. (2001). Evolution of Transglutaminase Genes: Identification of a Transglutaminase Gene Cluster on Human Chromosome 15q15.

Journal of Biological Chemistry, *276*(35), 33066–33078. https://doi.org/10.1074/jbc.M102553200

Guan, Y., Zhu, X., Liang, J., Wei, M., Huang, S., & Pan, X. (2021). Upregulation of HSPA1A/HSPA1B/HSPA7 and Downregulation of HSPA9 Were Related to Poor Survival in Colon Cancer. *Frontiers in Oncology*, *11*, 749673. https://doi.org/10.3389/fonc.2021.749673

Gucciardo, E., Sugiyama, N., & Lehti, K. (2014). Eph- and ephrin-dependent mechanisms in tumor and stem cell dynamics. In *Cellular and molecular life sciences: CMLS* (Vol. 71, Issue 19). https://doi.org/10.1007/s00018-014-1633-0

Gunter, H. M., Youlten, S. E., Madala, B. S., Reis, A. L. M., Stevanovski, I., Wong, T., Kummerfield, S. K., Deveson, I. W., Santini, N. S., Marcellin, E., & Mercer, T. R. (2022). Library adaptors with integrated reference controls improve the accuracy and reliability of nanopore sequencing. *Nature Communications*, *13*(1), 6437. https://doi.org/10.1038/s41467-022-34028-8

Hai, T., Wolford, C. C., & Chang, Y.-S. (2010). ATF3, a hub of the cellular adaptive-response network, in the pathogenesis of diseases: Is modulation of inflammation a unifying component? *Gene Expression*, *15*(1), 1–11. https://doi.org/10.3727/105221610x12819686555015

Hannenhalli, S., & Kaestner, K. H. (2009). The evolution of Fox genes and their role in development and disease. *Nature Reviews. Genetics*, *10*(4), 233–240. https://doi.org/10.1038/nrg2523

Hartmann, S., Ridley, A. J., & Lutz, S. (2015). The function of rho-associated kinases ROCK1 and ROCK2 in the pathogenesis of cardiovascular disease. In *Frontiers in Pharmacology* (Vol. 6, Issue NOV). https://doi.org/10.3389/fphar.2015.00276

Hernández-Candia, C. N., Pearce, S., & Tucker, C. L. (2021). A modular tool to query and inducibly disrupt biomolecular condensates. *Nature Communications*, *12*(1). https://doi.org/10.1038/s41467-021-22096-1

Hirai, H., Maru, Y., Hagiwara, K., Nishida, J., & Takaku, F. (1987). A novel putative tyrosine kinase receptor encoded by the eph gene. *Science*, *238*(4834). https://doi.org/10.1126/science.2825356

Holen, H. L., Nustad, K., & Aasheim, H. C. (2010). Activation of EphA receptors on CD4+CD45RO+ memory cells stimulates migration. *Journal of Leukocyte Biology*, *87*(6). https://doi.org/10.1189/jlb.0709497

Hu, S., Ren, S., Cai, Y., Liu, J., Han, Y., Zhao, Y., Yang, J., Zhou, X., & Wang, X. (2022). Glycoprotein PTGDS promotes tumorigenesis of diffuse large B-cell lymphoma by MYH9-mediated regulation of Wnt-β-catenin-STAT3 signaling. *Cell Death and Differentiation*, *29*(3), 642–656. https://doi.org/10.1038/s41418-021-00880-2

Hughes, R. M. (2018). A compendium of chemical and genetic approaches to light-regulated gene transcription. In *Critical Reviews in Biochemistry and Molecular Biology* (Vol. 53, Issue 5). https://doi.org/10.1080/10409238.2018.1487382

Hughes, R. M., & Virag, J. A. I. (2020). Harnessing the power of eph/ephrin biosemiotics for theranostic applications. In *Pharmaceuticals* (Vol. 13, Issue 6). https://doi.org/10.3390/ph13060112

Ieguchi, K., & Maru, Y. (2019). Roles of EphA1/A2 and ephrin-A1 in cancer. In *Cancer Science* (Vol. 110, Issue 3). https://doi.org/10.1111/cas.13942

Javadirad, S.-M., & Mokhtari, M. (2021). TXNDC2 joint molecular marker is associated with testis pathology and is an accurate predictor of sperm retrieval. *Scientific Reports*, *11*(1), 13064. https://doi.org/10.1038/s41598-021-92603-3

Jing, X., Miwa, H., Sawada, T., Nakanishi, I., Kondo, T., Miyajima, M., & Sakaguchi, K. (2012). Ephrin-A1-mediated dopaminergic neurogenesis and angiogenesis in a rat model of Parkinson's disease. *PLoS ONE*, *7*(2). https://doi.org/10.1371/journal.pone.0032019

Keilland, E., Rupar, C. A., Prasad, A. N., Tay, K. Y., Downie, A., & Prasad, C. (2016). The expanding phenotype of MELAS caused by the m.3291T > C mutation in the MT-TL1 gene. *Molecular Genetics and Metabolism Reports*, *6*, 64–69. https://doi.org/10.1016/j.ymgmr.2016.02.003

Kennedy, M. J., Hughes, R. M., Peteya, L. A., Schwartz, J. W., Ehlers, M. D., & Tucker, C. L. (2010). Rapid blue-light-mediated induction of protein interactions in living cells. *Nature Methods*, *7*(12). https://doi.org/10.1038/nmeth.1524

Klisic, J., Hu, M. C., Nief, V., Reyes, L., Fuster, D., Moe, O. W., & Ambühl, P. M. (2002). Insulin activates Na^+/H^+ exchanger 3: Biphasic response and glucocorticoid dependence. *American Journal of Physiology-Renal Physiology*, *283*(3), F532–F539. https://doi.org/10.1152/ajprenal.00365.2001

Koch, C. M., Chiu, S. F., Akbarpour, M., Bharat, A., Ridge, K. M., Bartom, E. T., & Winter, D. R. (2018). A Beginner's Guide to Analysis of RNA Sequencing Data. *American Journal of Respiratory Cell and Molecular Biology*, *59*(2), 145–157. https://doi.org/10.1165/rcmb.2017-0430TR

Kunschmann, T., Puder, S., Fischer, T., Steffen, A., Rottner, K., & Mierke, C. T. (2019). The Small GTPase Rac1 Increases Cell Surface Stiffness and Enhances 3D Migration Into Extracellular Matrices. *Scientific Reports*, *9*(1). https://doi.org/10.1038/s41598-019-43975-0

Lai, K.-O., & Ip, N. Y. (2009). Synapse development and plasticity: Roles of ephrin/Eph receptor signaling. *Current Opinion in Neurobiology*, *19*(3), 275–283. https://doi.org/10.1016/j.conb.2009.04.009

Lavoie, H., Gagnon, J., & Therrien, M. (2020). ERK signalling: A master regulator of cell behaviour, life and fate. *Nature Reviews Molecular Cell Biology*, *21*(10), 607–632. https://doi.org/10.1038/s41580-020-0255-7

Lawlor, M. W., Dechene, E. T., Roumm, E., Geggel, A. S., Moghadaszadeh, B., & Beggs, A. H. (2010). Mutations of tropomyosin 3 (TPM3) are common and associated with type 1 myofiber hypotrophy in congenital fiber type disproportion. *Human Mutation*, *31*(2), 176–183. https://doi.org/10.1002/humu.21157

Lee, Y., Ko, D., Yoon, J., Lee, Y., & Kim, S. (2021). TMEM52B suppression promotes cancer cell survival and invasion through modulating E-cadherin stability and EGFR activity. *Journal of Experimental & Clinical Cancer Research*, *40*(1), 58. https://doi.org/10.1186/s13046-021-01828-7

Liang, L. Y., Patel, O., Janes, P. W., Murphy, J. M., & Lucet, I. S. (2019). Eph receptor signalling: From catalytic to non-catalytic functions. In *Oncogene* (Vol. 38, Issue 39). https://doi.org/10.1038/s41388-019-0931-2

Lim, A. Z., McMacken, G., Rastelli, F., Oláhová, M., Baty, K., Hopton, S., Falkous, G., Töpf, A., Lochmüller, H., Marini-Bettolo, C., McFarland, R., & Taylor, R. W. (2020). A novel, pathogenic dinucleotide deletion in the mitochondrial MT-TY gene causing myasthenia-like features. *Neuromuscular Disorders: NMD*, *30*(8), 661–668. https://doi.org/10.1016/j.nmd.2020.06.008

Lin, J., Zeng, C., Zhang, J., Song, Z., Qi, N., Liu, X., Zhang, Z., Li, A., & Chen, F. (2021). EFNA4 promotes cell proliferation and tumor metastasis in hepatocellular carcinoma through a PIK3R2/GSK3β/β-catenin positive feedback loop. *Molecular Therapy. Nucleic Acids*, *25*, 328–341. https://doi.org/10.1016/j.omtn.2021.06.002

Lisabeth, E. M., Falivelli, G., & Pasquale, E. B. (2013). Eph receptor signaling and ephrins. *Cold Spring Harbor Perspectives in Biology*, *5*(9). https://doi.org/10.1101/cshperspect.a009159

Liu, H., Zhou, Y., Qiu, H., Zhuang, R., Han, Y., Liu, X., Qiu, X., Wang, Z., Xu, L., Tan, R., Hong, W., & Wang, T. (2021). Rab26 suppresses migration and invasion of breast cancer cells through mediating autophagic degradation of phosphorylated Src. *Cell Death & Disease*, *12*(4), 284. https://doi.org/10.1038/s41419-021-03561-7

Locke, C., Machida, K., Wu, Y., & Yu, J. (2017). Optogenetic activation of EphB2 receptor in dendrites induced actin polymerization by activating Arg kinase. *Biology Open*, *6*(12). https://doi.org/10.1242/bio.029900

Mani, S., Rao, S. N., & Kumar, M. V. K. (2020). G6036A substitution in mitochondrial COX I gene compromises cytochrome c oxidase activity in thiamine responsive Leigh syndrome patients. *Journal of the Neurological Sciences*, *415*, 116870. https://doi.org/10.1016/j.jns.2020.116870

Masuda, J., Usui, R., & Maru, Y. (2008). Fibronectin type I repeat is a nonactivating ligand for EphA1 and inhibits ATF3-dependent angiogenesis. *The Journal of Biological Chemistry*, *283*(19), 13148–13155. https://doi.org/10.1074/jbc.M702164200

Mebratu, Y., & Tesfaigzi, Y. (2009). How ERK1/2 activation controls cell proliferation and cell death: Is subcellular localization the answer? *Cell Cycle (Georgetown, Tex.)*, *8*(8), 1168–1175. https://doi.org/10.4161/cc.8.8.8147

Menges, C. W., & McCance, D. J. (2008). Constitutive activation of the Raf-MAPK pathway causes negative feedback inhibition of Ras-PI3K-AKT and cellular arrest through the EphA2 receptor. *Oncogene*, *27*(20), 2934–2940. https://doi.org/10.1038/sj.onc.1210957

Miao, H., Burnett, E., Kinch, M., Simon, E., & Wang, B. (2000). Activation of EphA2 kinase suppresses integrin function and causes focal-adhesion-kinase dephosphorylation. *Nature Cell Biology*, *2*(2), 62–69. https://doi.org/10.1038/35000008

Miao, H., Li, D.-Q., Mukherjee, A., Guo, H., Petty, A., Cutter, J., Basilion, J. P., Sedor, J., Wu, J., Danielpour, D., Sloan, A. E., Cohen, M. L., & Wang, B. (2009). EphA2 mediates ligand-dependent inhibition and ligand-independent promotion of cell migration and invasion via a reciprocal regulatory loop with Akt. *Cancer Cell*, *16*(1), 9–20. https://doi.org/10.1016/j.ccr.2009.04.009

Miao, H., & Wang, B. (2012). EphA receptor signaling—Complexity and emerging themes. *Seminars in Cell & Developmental Biology*, *23*(1), 16–25. https://doi.org/10.1016/j.semcdb.2011.10.013

Miao, H., Wei, B.-R., Peehl, D. M., Li, Q., Alexandrou, T., Schelling, J. R., Rhim, J. S., Sedor, J. R., Burnett, E., & Wang, B. (2001). Activation of EphA receptor tyrosine kinase inhibits the Ras/MAPK pathway. *Nature Cell Biology*, *3*(5), 527–530. https://doi.org/10.1038/35074604

Mori, M., Goldstein, J., Young, S. P., Bossen, E. H., Shoffner, J., & Koeberl, D. D. (2015). Complex III deficiency due to an in-frame MT-CYB deletion presenting as ketotic hypoglycemia and lactic acidosis. *Molecular Genetics and Metabolism Reports*, *4*, 39–41. https://doi.org/10.1016/j.ymgmr.2015.06.001

Murai, K. K., Nguyen, L. N., Irie, F., Yu, Y., & Pasquale, E. B. (2003). Control of hippocampal dendritic spine morphology through ephrin-A3/EphA4 signaling. *Nature Neuroscience*, *6*(2). https://doi.org/10.1038/nn994

Naj, A. C., Jun, G., Beecham, G. W., Wang, L. S., Vardarajan, B. N., Buros, J., Gallins, P. J., Buxbaum, J. D., Jarvik, G. P., Crane, P. K., Larson, E. B., Bird, T. D., Boeve, B. F., Graff-Radford, N. R., Jager, P. L. D., Evans, D., Schneider, J. A., Carrasquillo, M. M., Ertekin-Taner, N., … Schellenberg, G. D. (2011). Common variants at MS4A4/MS4A6E, CD2AP, CD33 and EPHA1 are associated with late-onset Alzheimer's disease. *Nature Genetics*, *43*(5). https://doi.org/10.1038/ng.801

Nasri Nasrabadi, P., Martin, D., Gharib, E., & Robichaud, G. A. (2022). The Pleiotropy of PAX5 Gene Products and Function. *International Journal of Molecular Sciences*, *23*(17), 10095. https://doi.org/10.3390/ijms231710095

Ng, Y. S., Thompson, K., Loher, D., Hopton, S., Falkous, G., Hardy, S. A., Schaefer, A. M., Shaunak, S., Roberts, M. E., Lilleker, J. B., & Taylor, R. W. (2020). Novel MT-ND Gene Variants Causing Adult-Onset Mitochondrial Disease and Isolated Complex I Deficiency. *Frontiers in Genetics*, *11*, 24. https://doi.org/10.3389/fgene.2020.00024

Nicolaides, N. C., & Chrousos, G. P. (2023). Glucocorticoid Signaling Pathway: From Bench to Bedside. *International Journal of Molecular Sciences*, *24*(13), 11030. https://doi.org/10.3390/ijms241311030

Nitulescu, G., Van De Venter, M., Nitulescu, G., Ungurianu, A., Juzenas, P., Peng, Q., Olaru, O., Grădinaru, D., Tsatsakis, A., Tsoukalas, D., Spandidos, D., & Margina, D. (2018). The Akt pathway in oncology therapy and beyond (Review). *International Journal of Oncology*. https://doi.org/10.3892/ijo.2018.4597

O'Neal, W. T., Griffin, W. F., Dries-Devlin, J. L., Kent, S. D., Chen, J., Willis, M. S., & Virag, J. A. I. (2013). Ephrin-Eph signaling as a potential therapeutic target for the treatment of myocardial infarction. *Medical Hypotheses*, *80*(6). https://doi.org/10.1016/j.mehy.2013.02.024

Pratt, R. L., & Kinch, M. S. (2002). Activation of the EphA2 tyrosine kinase stimulates the MAP/ERK kinase signaling cascade. *Oncogene*, *21*(50), 7690–7699. https://doi.org/10.1038/sj.onc.1205758

Prpić, M., Franceschi, M., Romić, M., Jukić, T., & Kusić, Z. (2018). THYROGLOBULIN AS A TUMOR MARKER IN DIFFERENTIATED THYROID CANCER - CLINICAL CONSIDERATIONS. *Acta Clinica Croatica*, *57*(3), 518–527. https://doi.org/10.20471/acc.2018.57.03.16

Reis, L. M., Tyler, R. C., Schneider, A., Bardakjian, T., Stoler, J. M., Melancon, S. B., & Semina, E. V. (2010). FOXE3 plays a significant role in autosomal recessive microphthalmia. *American Journal of Medical Genetics. Part A*, *152A*(3), 582–590. https://doi.org/10.1002/ajmg.a.33257

Resh, M. D. (1999). Fatty acylation of proteins: New insights into membrane targeting of myristoylated and palmitoylated proteins. *Biochimica Et Biophysica Acta*, *1451*(1), 1–16. https://doi.org/10.1016/s0167-4889(99)00075-0

Sassone-Corsi, P. (2012). The cyclic AMP pathway. *Cold Spring Harbor Perspectives in Biology*, *4*(12), a011148. https://doi.org/10.1101/cshperspect.a011148

Schäfer, N., Friedrich, M., Jørgensen, M. E., Kollert, S., Koepsell, H., Wischmeyer, E., Lesch, K.-P., Geiger, D., & Döring, F. (2018). Functional analysis of a triplet deletion in the gene encoding the sodium glucose transporter 3, a potential risk factor for ADHD. *PloS One*, *13*(10), e0205109. https://doi.org/10.1371/journal.pone.0205109

Schindelin, J., Arganda-Carreras, I., Frise, E., Kaynig, V., Longair, M., Pietzsch, T., Preibisch, S., Rueden, C., Saalfeld, S., Schmid, B., Tinevez, J.-Y., White, D. J., Hartenstein, V., Eliceiri, K., Tomancak, P., & Cardona, A. (2012). Fiji: An open-source platform for biological-image analysis. *Nature Methods*, *9*(7), 676–682. https://doi.org/10.1038/nmeth.2019

Serra-Cardona, A., & Zhang, Z. (2018). Replication-Coupled Nucleosome Assembly in the Passage of Epigenetic Information and Cell Identity. *Trends in Biochemical Sciences*, *43*(2), 136–148. https://doi.org/10.1016/j.tibs.2017.12.003

Singh, D. R., Ahmed, F., Paul, M. D., Gedam, M., Pasquale, E. B., & Hristova, K. (2017). The SAM domain inhibits EphA2 interactions in the plasma membrane. *Biochimica et Biophysica Acta - Molecular Cell Research*, *1864*(1). https://doi.org/10.1016/j.bbamcr.2016.10.011

Taslimi, A., Vrana, J. D., Chen, D., Borinskaya, S., Mayer, B. J., Kennedy, M. J., & Tucker, C. L. (2014). An optimized optogenetic clustering tool for probing protein interaction and function. *Nature Communications*, *5*. https://doi.org/10.1038/ncomms5925

Thaa, B., Biasiotto, R., Eng, K., Neuvonen, M., Götte, B., Rheinemann, L., Mutso, M., Utt, A., Varghese, F., Balistreri, G., Merits, A., Ahola, T., & McInerney, G. M. (2015). Differential Phosphatidylinositol-3-Kinase-Akt-mTOR Activation by Semliki Forest and Chikungunya Viruses Is Dependent on nsP3 and Connected to Replication Complex Internalization. *Journal of Virology*, *89*(22), 11420–11437. https://doi.org/10.1128/JVI.01579-15

Toma, M. I., Erdmann, K., Diezel, M., Meinhardt, M., Zastrow, S., Fuessel, S., Wirth, M. P., & Baretton, G. B. (2014a). Lack of ephrin receptor A1 is a favorable independent prognostic factor in clear cell renal cell carcinoma. *PloS One*, *9*(7), e102262. https://doi.org/10.1371/journal.pone.0102262

Toma, M. I., Erdmann, K., Diezel, M., Meinhardt, M., Zastrow, S., Fuessel, S., Wirth, M. P., & Baretton, G. B. (2014b). Lack of ephrin receptor A1 is a favorable independent prognostic factor in clear cell renal cell carcinoma. *PLoS ONE*, *9*(7). https://doi.org/10.1371/journal.pone.0102262

Trease, A. J., Li, H., Spagnol, G., Zheng, L., Stauch, K. L., & Sorgen, P. L. (2019). Regulation of Connexin32 by ephrin receptors and T-cell protein-tyrosine phosphatase. *Journal of Biological Chemistry*, *294*(1). https://doi.org/10.1074/jbc.RA118.003883

Tremblay, R. G., Sikorska, M., Sandhu, J. K., Lanthier, P., Ribecco-Lutkiewicz, M., & Bani-Yaghoub, M. (2010). Differentiation of mouse Neuro 2A cells into dopamine neurons. *Journal of Neuroscience Methods*, *186*(1). https://doi.org/10.1016/j.jneumeth.2009.11.004

Valverde, O., Célérier, E., Baranyi, M., Vanderhaeghen, P., Maldonado, R., Sperlagh, B., Vassart, G., & Ledent, C. (2009). GPR3 receptor, a novel actor in the emotional-like responses. *PloS One*, *4*(3), e4704. https://doi.org/10.1371/journal.pone.0004704

Veljačić Visković, D., Lozić, M., Vukoja, M., Šoljić, V., Vukojević, K., Glavina Durdov, M., Filipović, N., & Lozić, B. (2023). Spatio-Temporal Expression Pattern of CAKUT Candidate Genes DLG1 and KIF12 during Human Kidney Development. *Biomolecules*, *13*(2), 340. https://doi.org/10.3390/biom13020340

Wagner, C. A., Hernando, N., Forster, I. C., & Biber, J. (2014). The SLC34 family of sodium-dependent phosphate transporters. *Pflugers Archiv: European Journal of Physiology*, *466*(1), 139–153. https://doi.org/10.1007/s00424-013-1418-6

Wang, B., Guo, H., Yu, H., Chen, Y., Xu, H., & Zhao, G. (2021). The Role of the Transcription Factor EGR1 in Cancer. *Frontiers in Oncology*, *11*, 642547. https://doi.org/10.3389/fonc.2021.642547

Wang, H. F., Tan, L., Hao, X. K., Jiang, T., Tan, M. S., Liu, Y., Zhang, D. Q., & Yu, J. T. (2015). Effect of EPHA1 genetic variation on cerebrospinal fluid and neuroimaging biomarkers in healthy, mild cognitive impairment and Alzheimer's disease cohorts. *Journal of Alzheimer's Disease*, *44*(1). https://doi.org/10.3233/JAD-141488

Wang, S., Placzek, W. J., Stebbins, J. L., Mitra, S., Noberini, R., Koolpe, M., Zhang, Z., Dahl, R., Pasquale, E. B., & Pellecchia, M. (2012). Novel Targeted System To Deliver Chemotherapeutic Drugs to EphA2-Expressing Cancer Cells. *Journal of Medicinal Chemistry*, *55*(5), 2427–2436. https://doi.org/10.1021/jm201743s

Wang, S., Qiu, J., Liu, L., Su, C., Qi, L., Huang, C., Chen, X., Zhang, Y., Ye, Y., Ding, Y., Liang, L., & Liao, W. (2020). CREB5 promotes invasiveness and metastasis in colorectal cancer by directly activating MET. *Journal of Experimental & Clinical Cancer Research*, *39*(1), 168. https://doi.org/10.1186/s13046-020-01673-0

Wang, Y., Liu, Y., Li, G., Su, Z., Ren, S., Tan, P., Zhang, X., Qiu, Y., & Tian, Y. (2015). Ephrin type-A receptor 2 regulates sensitivity to paclitaxel in nasopharyngeal carcinoma via the phosphoinositide 3-kinase/Akt signalling pathway. *Molecular Medicine Reports*, *11*(2), 924–930. https://doi.org/10.3892/mmr.2014.2799

Wang, Y., Yu, H., Shan, Y., Tao, C., Wu, F., Yu, Z., Guo, P., Huang, J., Li, J., Zhu, Q., Yu, F., Song, Q., Shi, H., Zhou, M., & Chen, G. (2016). EphA1 activation promotes the homing of endothelial progenitor cells to hepatocellular carcinoma for tumor neovascularization through the SDF-1/CXCR4 signaling pathway. *Journal of Experimental and Clinical Cancer Research*, *35*(1). https://doi.org/10.1186/s13046-016-0339-6

Whitelaw, J. A., Lilla, S., Paul, N. R., Fort, L., Zanivan, S., & Machesky, L. M. (2019). CYRI/Fam49 Proteins Represent a New Class of Rac1 Interactors. *Communicative & Integrative Biology*, *12*(1), 112–118. https://doi.org/10.1080/19420889.2019.1643665

Winter, J. N., Jefferson, L. S., & Kimball, S. R. (2011). ERK and Akt signaling pathways function through parallel mechanisms to promote mTORC1 signaling. *American Journal of Physiology. Cell Physiology*, *300*(5), C1172-1180. https://doi.org/10.1152/ajpcell.00504.2010

Yamazaki, T., Masuda, J., Omori, T., Usui, R., Akiyama, H., & Maru, Y. (2009). EphA1 interacts with integrin-linked kinase and regulates cell morphology and motility. *Journal of Cell Science*, *122*(2). https://doi.org/10.1242/jcs.036467

Yang, J. S., Wei, H. X., Chen, P. P., & Wu, G. (2018). Roles of Eph/ephrin bidirectional signaling in central nervous system injury and recovery (Review). In *Experimental and Therapeutic Medicine* (Vol. 15, Issue 3). https://doi.org/10.3892/etm.2018.5702

Zeng, Z., Lan, T., Wei, Y., & Wei, X. (2022). CCL5/CCR5 axis in human diseases and related treatments. *Genes & Diseases*, *9*(1), 12–27. https://doi.org/10.1016/j.gendis.2021.08.004

Zhai, Y., Celis-Gutierrez, J., Voisinne, G., Mori, D., Girard, L., Burlet-Schiltz, O., De Peredo, A. G., Roncagalli, R., & Malissen, B. (2021). Opposing regulatory functions of the TIM3 (HAVCR2) signalosome in primary effector T cells as revealed by quantitative interactomics. *Cellular & Molecular Immunology*, *18*(6), 1581–1583. https://doi.org/10.1038/s41423-020-00575-7

Zhang, J., Zhang, Q., Sun, C., Huang, Y., Zhang, J., & Wang, Q. (2020). Clinical relevance of ARF/ARL family genes and oncogenic function of ARL4C in endometrial cancer. *Biomedicine & Pharmacotherapy*, *125*, 110000. https://doi.org/10.1016/j.biopha.2020.110000

Zhang, X., Young, C., Morishita, Y., Kim, K., Kabil, O. O., Clarke, O. B., Di Jeso, B., & Arvan, P. (2022). Defective Thyroglobulin: Cell Biology of Disease. *International Journal of Molecular Sciences*, *23*(21), 13605. https://doi.org/10.3390/ijms232113605

Zhang, Y.-M., Bo, J., Taffet, G. E., Chang, J., Shi, J., Reddy, A. K., Michael, L. H., Schneider, M. D., Entman, M. L., Schwartz, R. J., & Wei, L. (2006). Targeted deletion of ROCK1 protects the heart against pressure overload by inhibiting reactive fibrosis. *The FASEB Journal*, *20*(7). https://doi.org/10.1096/fj.05-5129com

Zheng, Y., Pei, Y., Yang, L., Zeng, Z., Wang, J., Xie, G., Wang, L., & Yuan, J. (2020). Upregulated GRB7 promotes proliferation and tumorigenesis of Bladder Cancer via Phospho-AKT Pathway. *International Journal of Biological Sciences*, *16*(16), 3221–3230. https://doi.org/10.7150/ijbs.49410

CHAPTER 3

CRY-BARs: Versatile light-gated tools for the remodeling of membrane architectures

(Reproduced in part with permission from Wurz, A.I., Bunner, W.P., Szatmari, S.Z., Hughes, R.M. (2022). *JBC*. 298(10), 102388.)

Introduction

Membrane-bound architectures, including filopodia, lamellipodia, and dendritic spines in neurons, are critical for a cell's ability to transmit and respond to extracellular cues. As such, chemists and biologists have developed numerous optogenetic and chemo-optogenetic tools to control cellular architectures via manipulation of plasma membrane dynamics (Kichuk et al., 2021; Klewer & Wu, 2019; Ueda & Sato, 2018). However, these tools have to date incorporated a relatively small fraction of the numerous proteins involved in the building and dismantling of these architectural features. In particular, nonenzymatic proteins have been overlooked: while numerous optogenetic strategies exist for enzyme-mediated control of membrane dynamics (Khamo et al., 2019b; O'Banion et al., 2018, 2019; Shaaya et al., 2020; Wu et al., 2009, 2011), far fewer have incorporated nonenzymatic proteins as the basis of optogenetic switch action (Redchuk et al., 2020). As mechanical control of membrane architecture by nonenzymatic proteins is a critical component of cellular signaling (Hughes & Kumar, 2016), addressing this oversight will be a bridge to a more comprehensive understanding of cellular dynamics and function.

In recent years, the critical role of proteins involved in membrane curvature inducing and sensing has come to light (Antonny, 2011). In particular, BAR (Bin, Amphiphysin, and Rvs) domain–containing proteins possess diverse activities at the plasma membrane (Linkner et al.,

2014; Prévost et al., 2015; Pykäläinen et al., 2011; Saarikangas et al., 2011, 2015; D. Yu et al., 2011; Zhao et al., 2011); as such, a heightened understanding of these roles has invited recent investigations of their suitability for control with optogenetic tools. In a recent work, Jones et al. (Jones et al., 2020) used a two-component approach (iLID/SspB) to design a light-activated switch enabling recruitment of the extended Fes–CIP4 homology BAR domain from FBP17 to the plasma membrane and a hybrid two-component approach (iLID/SspB/pdDronpa1) enabling recruitment of the inverse BAR (I-BAR) domain from IRSp53 to the plasma membrane. These switches, designed to have minimal interaction with the cell membrane in the absence of light, promoted either positive (Fes–CIP4 homology BAR; FBP17) or negative (I-BAR; IRSp53) membrane curvature in response to light activation.

The MTSS1 (Missing in Metastasis 1) protein is considered the prototype of I-BAR proteins (Li et al., 2016), but, to the best of our knowledge, has not previously been applied in an optogenetic context. In this work, we investigated the potential of the MTSS1 I-BAR domain to serve as an actuator of membrane architecture and plasma membrane dynamics. We demonstrate that the I-BAR domain from MTSS1, in conjunction with the Cry2 photoreceptor protein (Che et al., 2015; Kennedy et al., 2010a; Park et al., 2017; Taslimi et al., 2014), forms the basis of a versatile optogenetic approach ("CRY–BAR") for controlling membrane dynamics and cellular architecture. In contrast to previous approaches, we have not sought to minimize the interaction between our constructs and the plasma membrane. Instead, CRY–BAR combines the intrinsic membrane-binding affinity of the I-BAR domain (Saarikangas et al., 2009) with the homo-oligomerizing capability of Cry2 (Che et al., 2015), resulting in a membrane-localized switch that induces membrane remodeling in response to blue light. We also provide insight into the mode of action of CRY–BAR by showing that ezrin, a membrane- and cytoskeletal-relay

protein, is linked to the ability of CRY–BAR to induce light-activated membrane remodeling and restriction of cellular dynamics by acting as a relay between CRY–BAR activation and the actin cytoskeleton.

Material and Methods

Plasmids and cloning

Cloning of I-BAR–Cry2–mCh, Cry2–mCh–I-BAR, I-BAR–Cry2–mCh–WH2, and Cry2–mCh–MTSS1 constructs was conducted using a previously described cloning scheme (Salem et al., 2020). Briefly, the I-BAR domain from MTSS1, the WH2 domain from MTSS1, and MTSS1 were PCR amplified from human MTSS1 complementary DNA obtained from the Arizona State University DNA repository (DNASU ID: HsCD00746054). N-terminal I-BAR genes were cloned into Cry2PHR–mCherry (Addgene; #26866) using NheI and XhoI restriction sites (Kennedy et al., 2010a). C-terminal I-BAR, WH2, and MTSS1 genes were cloned into Cry2PHR–mCherry using BsrgI and NotI restriction sites. The ezrin–GFP expression construct was a gift from Stephen Shaw (plasmid pHJ421; Addgene; #20680 (Hao et al., 2009)). The actin expression construct (pCAG-mGFPactin; Addgene; #21948) was a gift from Ryohei Yasuda. CIBN–GFP–CAAX (pCIBN(deltaNLS)-pmGFP; Addgene; #26867) was a gift from Chandra Tucker. Midi prep quantities of DNA of each construct were created from *Escherichia coli* and collected for cell transfection.

Cell lines and transfection

HEK293T cells (passage 8) used for these experiments were purchased from American Type Culture Collection and were cultured in Dulbecco's modified Eagle's medium (DMEM) containing 10% fetal bovine serum (FBS) and 1% penicillin–streptomycin. Cultures were transfected at 70% confluency with the Lipofectamine 3000 reagent (Invitrogen) following the manufacturer's suggested protocols. Briefly, for dual transfections in 35 mm glass bottom dishes for cell imaging or 6-well culture plates for lysis, plasmid DNA was combined in a 1:1 ratio

(1250 ng per plasmid) in 125 µl of Opti-MEM, followed by the addition of 5 µl of P3000 reagent. For single transfections, 2500 ng of plasmid DNA was used per transfection. In a separate vial, 3.75 µl of Lipofectamine 3000 were added to 125 µl of Opti-MEM. The two 125 µl solutions were combined and allowed to incubate at room temperature for 10 min, followed by dropwise addition to cell culture. For ezrin–GFP and actin–GFP cotransfection with CRY–BAR, 2000 ng of CRY–BAR DNA and 1000 ng of GFP DNA were added to 100 µl of DMEM along with subsequent addition of 3 µl of CalFectin (SignaGen Laboratories). After 10 min of incubation at room temperature, the solution was added dropwise to cell cultures. Each transfection solution remained on cells overnight. Transfected cells were maintained at 37 °C and 5% CO2 in a humidified tissue culture incubator, in culture medium consisting of DMEM supplemented with 10% FBS and 1% penicillin–streptomycin.

Neuron cultures and transfection

Postnatal-dissociated cortical neuron cultures were prepared as previously described (Bunner et al., 2021; J.-Y. Chang et al., 2017), from newborn B6 mice. Neurons were plated into 35 mm glass bottom Petri dishes at a 1 million/ml density in culture medium consisting of Basal Medium Eagle supplemented with 10% bovine calf serum and 1% penicillin–streptomycin. On day in vitro 2 (DIV2), culture medium was changed to Neurobasal A medium, supplemented with B27-plus reagent (Invitrogen), Glutamax, and 1% penicillin–streptomycin. Neurons were transfected with the CryBAR optogenetic system (6 µg plasmid/plate) on DIV5 using Lipofectamine LTX reagent. On DIV7, culture medium was removed and neurons were placed in imaging solution (Mg-free HEPES-buffered artificial cerebrospinal fluid (Sun et al., 2021)). Live-cell imaging was performed before and after illumination using a Leica DMi8 Live Cell

Imaging System. Animal use protocols were approved by East Carolina University Institutional Animal Care and Use Committee.

Fixed and live-cell imaging preparation

Fixed cell experiments: Immediately prior to fixation, transfected HEK293T cells were either kept in dark conditions or continually illuminated with LED blue light (Sunlite LED Par30 Reflector, item #80021, 4 W, 120 V, 66.21 μmol/s/m^2; placed 10 cm from cell culture dishes) for 5 min. Cells were washed with Dulbecco's PBS (DPBS) (with calcium and magnesium; 1× 1 ml), then fixed for 10 min at room temperature with prewarmed 4% paraformaldehyde solution in DPBS (37 °C; prepared from 16% paraformaldehyde [Electron Microscopy Sciences]). Following fixation, cells were washed with DPBS and then stored in DPBS at 4 °C.

Live-cell experiments: Transfected HEK293T cell media were replaced with 10% FBS in Leibovitz's L-15 medium. Cells were allowed to equilibrate in the live-cell incubation system (OKOLab) for 10 min prior to beginning the illumination sequence.

Imaging

Confocal microscopy: Confocal images of fixed cells were collected with a Zeiss LSM 700 laser scanning microscope using ZEN Black 2012 software. Ezrin–GFP and actin–GFP live-cell images were collected with a Zeiss LSM 700 laser scanning microscope equipped with a stage-top incubator and ZEN Black 2012 software. Fluorescence images were colorized and overlaid using FIJI software (Schindelin et al., 2012) equipped with Bio Formats (Linkert et al., 2010).

Widefield microscopy: A Leica DMi8 Live Cell Imaging System, equipped with an OKOLab stage-top live cell incubation system, LASX software, Leica HCX PL APO 63×/1.40 to 0.60

numerical objective oil objective, Lumencor LED light engine, CTRadvanced+ power supply, and a Leica DFC900 GT camera, was used to acquire images. Exposure times were set at 200 ms (mCherry, 553 nm) and 50 ms (GFP, 480 nm), with LED light sources at 50% power, and images were acquired every 30 s over specified time course.

Western blotting

Transfected HEK293T cells were lysed with 200 µl of M-PER lysis buffer (Thermo Fisher Scientific) containing 1× Halt protease–phosphatase inhibitor cocktail (Thermo Fisher Scientific). After 10 min on ice, lysates were collected and centrifuged for 15 min (94 rcf; 4 C). The supernatants were combined with Laemmli SDS sample buffer (Alfa Aesar) and incubated at 65 °C for 10 min. The resulting lysates were subjected to electrophoresis on a 10% SDS-PAGE gel and then transferred onto polyvinylidene fluoride membranes (20 V, 800 min). Membranes were then blocked for 1 h with 5% bovine serum albumin (BSA) in 1× Tris-buffered saline (TBS) with 1% Tween (TBST), followed by incubation with primary antibody (anti-mCherry antibody [Cell Signaling] 1:1000 dilution in 5% BSA–TBST; anti-GAPDH antibody [Invitrogen] 1:1000 dilution in 5% BSA–TBST) overnight at 4 °C on a platform rocker. The membranes were then washed 3× for 5 min each with TBST and incubated with the appropriate secondary antibody in 5% BSA–TBST (1 h; room temperature). After washing 3× for 5 min with TBST, the membranes were exposed to a chemiluminescent substrate for 5 min and imaged with an Azure cSeries imaging station.

Statistical analyses

Statistical significance (p values; Figs. 4–8, 10, and 11) was determined using a one-way ANOVA (Holm–Sidak method) in SigmaPlot v. 13.0 (Systat Software, Inc). Mean ± S.D. plots were constructed using GraphPad Prism version 8.2.1 for Windows, GraphPad Software, San Diego, California, USA (www.graphpad.com).

Results and Discussion

Increased MTSS1 activity has been associated with exercise-induced enhancement of synaptic function (Chatzi et al., 2019). This prosynaptic plasticity effect of MTSS1 is attributed to the presence of an I-BAR domain within its structure. Moreover, I-BAR domains have also been shown to promote formation and stabilization of dendritic spines (**Fig. 3.1A**), leading to improved synaptic function and resilience against neurodegeneration (Saarikangas et al., 2015). To gain insights into the molecular mechanisms that control membrane expansion associated with cell morphology changes, we fused the I-BAR domain of MTSS1 with a blue light–sensing domain (Cry2PHR; **Fig. 3.1, B & C**), creating a light-activatable I-BAR protein (CRY–BAR). For this investigation, we engineered four permutations of the CRY–BAR switch: I-BAR–Cry2–mCh, I-BAR–Cry2–mCh–WH2, Cry2–mCh–I-BAR, and Cry2–mCh–MTSS1 (**Fig. 3.1C**), where I-BAR = residues 1 to 250 of MTSS1, WH2 = residues 601 to 759 of MTSS1, and MTSS1 = the intact 759 residue protein. Each construct was confirmed by Sanger and NextGen sequencing and expressed predominantly at the expected molecular weight (**Fig. AIII.1**).

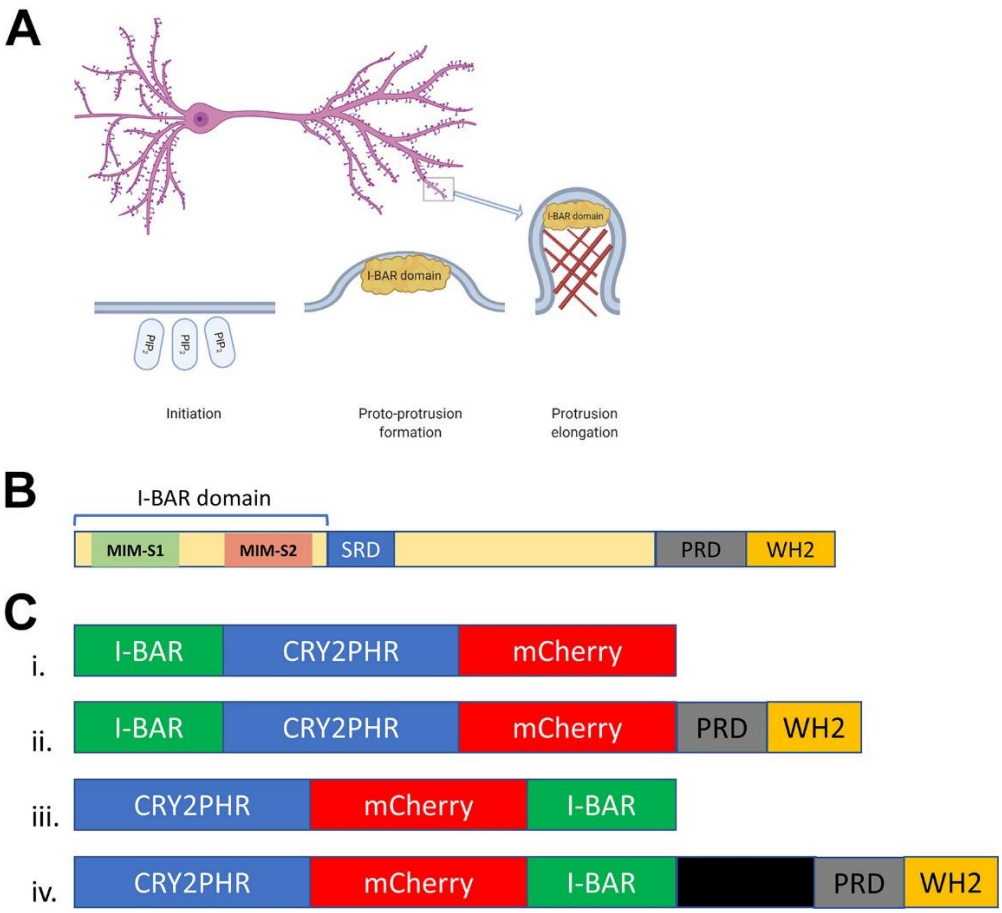

Figure 3.1. ***(A)*** *I-BAR-mediated initiation of dendritic spine generation in neurons. Phosphoinositide (PIP2) signaling recruits I-BAR domain proteins to the plasma membrane, inducing a proto-protrusion. Subsequent recruitment of actin (brown crosshatches) and actin-binding and remodeling proteins promotes protrusion elongation. Mature dendritic spines (purple nodules on dendrite) are mushroom-shaped bulbous protrusions and major sites of excitatory synaptic transmission in the mammalian brain.* ***(B)*** *Diagram of MTSS1, an I-BAR domain–containing protein. The N-terminal I-BAR domain (250 amino acids) is comprised of three alpha helices. MIM-S1 and MIM-S2 represent the I-BAR domain dimerization interface as determined from X-ray crystallography (40). C, schematic of CRY–BAR optogenetic switches: (i) The N-terminal I-BAR domain (250 amino acids) is fused to photoreceptor protein CRY2, which is fused to the red fluorescent mCherry protein for visualization purposes. (ii) At the C terminus,*

proline-rich and WH2 domains can be included for actin recruitment. (iii) The N-terminal I-BAR domain is fused to the C terminus of mCherry. (iv) The intact MTSS1 protein (green, I-BAR; black, internal domains as shown in panel B; and yellow, WH2) is fused to the C terminus of mCherry. Graphic (A) generated with BioRender (https://biorender.com/). BAR, Bin, Amphiphysin, and Rvs; I-BAR, inverse BAR; MTSS1, Missing in Metastasis 1; PIP2, phosphatidylinositol 4,5-bisphosphate; PRD, proline-rich domain; SRD, serine-rich domain; WH2, Wiskott–Aldrich syndrome homology region.

CRY–BAR constructs were initially probed for their response to blue light in the presence of CIBN–CAAX, a membrane-localized binding partner to Cry2, in human embryonic kidney 293T (HEK293T) cells. As anticipated, light activation of the Cry2–mCh control resulted in rapid recruitment to the plasma membrane (**Figs. 3.2A and 3.3A**). Light-activated recruitment to CIBN–CAAX was also observed for all the I-BAR-containing constructs (**Figs. 3.2 and 3.3, B and C**). Interestingly, the I-BAR domain–containing constructs I-BAR–Cry2–mCh and Cry2–mCh–I-BAR, while exhibiting light-activated recruitment to the plasma membrane (**Fig. 3.2, A and C**), had significant prelocalization to the plasma membrane in the dark. We attributed this to the phosphatidylinositol 4,5-bisphosphate (PIP2)–binding propensity of the I-BAR domain (readily observed in the preillumination images in **Fig. 3.2, A and C**). Because of the significant prelocalization of these constructs to the plasma membrane, we then investigated whether they might exhibit light-activated recruitment, via Cry2 homo-oligomerization, in the absence of CIBN–CAAX. These experiments revealed significant light-activated clustering/membrane recruitment (**Fig. 3.2, B and D**) in the absence of CIBN–CAAX. By contrast, Cry2–mCh–MTSS1, which also accumulated in nonlight responsive clusters, did not exhibit light-activated membrane recruitment in the absence of CIBN–CAAX (50 of 50 cells pooled from six replicates; **Fig. 3.2D**). As a result, this construct was not pursued further.

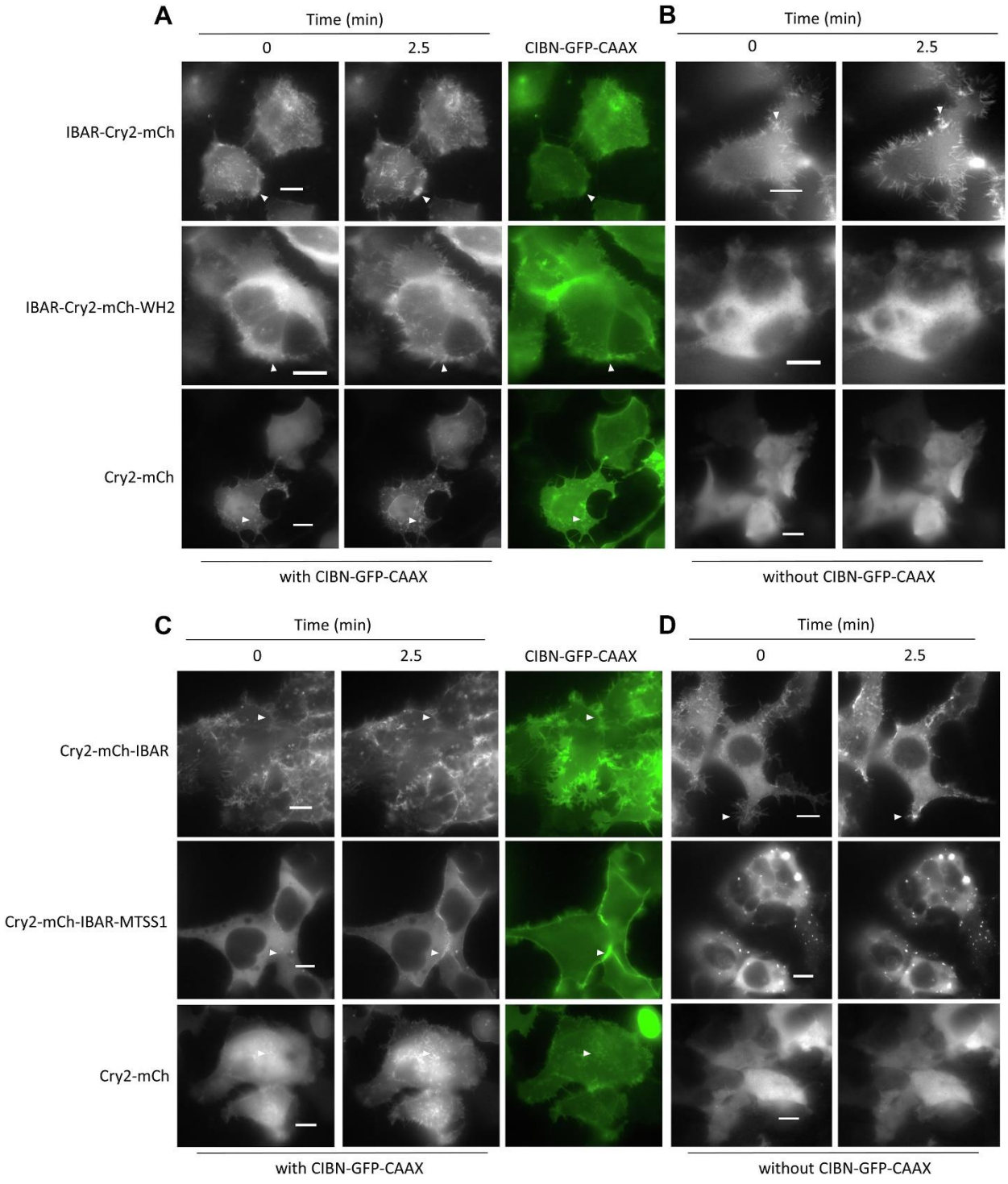

Figure 3.2*. Light-activated responses of CRY–BAR constructs.* ***(A)*** *HEK293T cells were cotransfected with CIBN–GFP–CAAX and CRY–BAR fusions I-BAR–Cry2–mCh or I-BAR–Cry2–mCh–WH2 or Cry2–mCh and imaged on a widefield fluorescent microscope. I-BAR*

labeled as IBAR in figure. ***(B)*** *HEK293T cells were transfected with CRY–BAR fusions I-BAR–Cry2–mCh and I-BAR–Cry2–mCh–WH2 or Cry2–mCh and imaged on a widefield fluorescent microscope.* ***(C)*** *HEK293T cells were cotransfected with CIBN–GFP–CAAX and CRY–BAR fusions Cry2–mCh–I-BAR and Cry2–mCh–MTSS1 or Cry2–mCh and imaged on a widefield fluorescent microscope.* ***(D)*** *HEK293T cells were transfected with CRY–BAR fusions Cry2–mCh–I-BAR and Cry2–mCh–MTSS1 or Cry2–mCh and imaged on a widefield fluorescent microscope. Images acquired every 30 s (50 ms exposure of 480 nm light and 200 ms exposure of 553 nm light every 30 s). White arrows indicate example areas of light-activated recruitment. The scale bars represent 10 microns.*

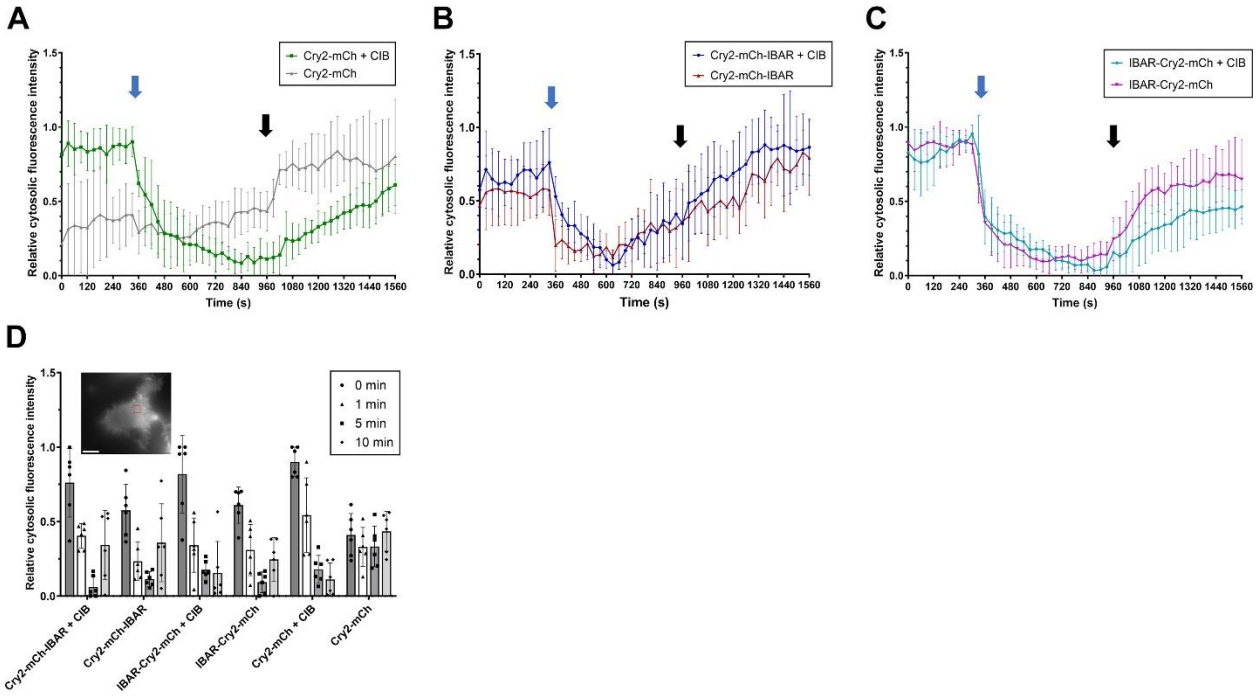

Figure 3.3. *Analysis of light-activated responses of CRY–BAR constructs.* ***(A)*** *Cry2–mCh construct shows large decrease in cytosolic fluorescence intensity in the presence of plasma membrane–anchored CIBN–GFP–CAAX (CIB) but not in its absence.* ***(B)*** *Cry2–mCh–I-BAR construct shows a decrease in cytosolic fluorescence intensity in both the presence and absence of plasma membrane–anchored CIB, indicative of significant homo-oligomerization at the plasma membrane.* ***(C)*** *I-BAR–Cry2–mCh construct shows a decrease in cytosolic fluorescence intensity in both the presence and absence of plasma membrane–anchored CIBN, indicative of significant homo-oligomerization at the plasma membrane. Blue arrows indicate beginning of blue light illumination (50 ms exposure of 480 nm light every 30 s); black arrows indicate end of blue light illumination. Graphs show changes in normalized cytosolic mCherry fluorescence in HEK293T cells. Cells were initially imaged on mCherry channel (0–300 s), illuminated with 470 nm light for 10 min (330–930 s), then imaged on mCherry channel again for 10 min (960–1560 s).* ***(D)*** *quantitation of the fluorescence of ROIs (n = 6 cells) at the time points: immediately before light exposure (0 min), then 1 min, 5 min, and 10 min of light exposure. Inset cell image:*

representative ROI inside the cytosol of HEK293T cell transfected with I-BAR–Cry2–mCh; this image is duplicated from Figure 2A to demonstrate measurement methodology. The scale bar represents 10 microns; ROI dimensions: 4.02 × 4.02 microns.

Homo-oligomerization of the CRY–BAR constructs I-BAR–Cry2–mCh and Cry2–mCh–I-BAR results in membrane deformation and restriction of cellular dynamics through membrane rretraction (**Movie AIII.1, A and B**). These effects are reversible in the dark. To demonstrate this using Cry2–mCh–I-BAR, we conducted a 10 min light activation sequence, followed by a 30 min observation period in the absence of blue light. Rapid restriction of membrane dynamics was observed during the 10 min blue light activation period, with full reversibility of membrane rounding achieved after 30 min in the absence of blue light (**Fig. 3.4 and Movie AIII.2**). We subsequently demonstrated that this effect can be selectively induced using localized illumination of the cell on a confocal microscope (**Fig. 3.5 and Movie AIII.3**). We also investigated whether the presence of a WH2 domain (present in I-BAR–Cry2–mCh–WH2 but not in I-BAR–Cry2–mCh and Cry2–mCh–I-BAR) impacted the membrane remodeling capabilities of the optogenetic switch. Light activation of an N-terminal I-BAR domain without a C-terminal WH2 domain (I-BAR–Cry2–mCh) promoted its accumulation in numerous filopodia-like protrusions that rapidly coalesced with continued light exposure (**Fig. 3.6A**). By contrast, a construct that paired an N-terminal I-BAR domain with a Cterminal WH2-containing domain (I-BAR–Cry2–mCh–WH2) did not accumulate in filopodia-like protrusions (**Fig. 3.6**). The interaction between WH2 and monomeric actin and associated complexes (Paunola et al., 2002), which would disfavor the preassociation of I-BAR and PIP2 required for CRY–BAR function, is likely responsible for the observed failure to accumulate at the plasma membrane. Analogously, a recent investigation of the I-BAR protein IRSp53 revealed that the I-BAR domain of IRSp53, expressed as a fusion to GFP, localized to filopodia, whereas the C terminus of IRSp53 was entirely cytosolic (Pipathsouk et al., 2021). Taken together, these results illustrate the modular nature of I-BAR proteins, where the N-terminal I-BAR-containing domain is required for

membrane binding and localization, and the WH2 domain is required for recruitment of actin polymerizing components that promote protrusion formation and elongation (Saarikangas et al., 2011). Only upon expression as isolated entities are the competing contributions of these domains to subcellular localization apparent. Finally, a side-by-side comparison of light activation of I-BAR–Cry2–mCh, I-BAR–Cry2–mCh–WH2, and Cry2–mCh–I-BAR demonstrated that while robust membrane recruitment is associated with light activation of Cry2–mCh–I-BAR and I-BAR–Cry2–mCh (**Movie AIII.4**), Cry2–mCh–I-BAR induces a more robust effect on cell membranes, as evidenced by impact on total cell area (**Fig. 3.4B**). We attribute this to enhanced PIP2 binding and clustering capability of the I-BAR domain when in the C-terminal position of the optogenetic fusion protein.

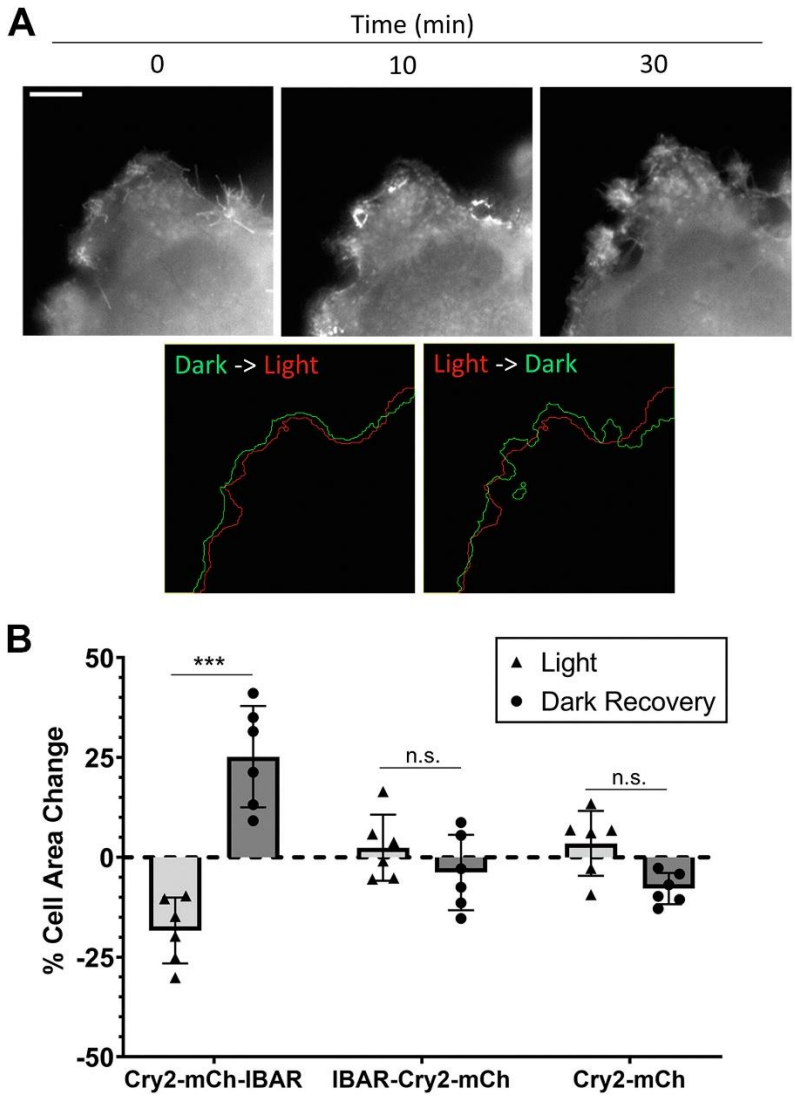

Figure 3.4. *Reversible light-activated membrane remodeling with CRY–BAR.* ***(A)*** *HEK293T cells transfected with Cry2–mCh–I-BAR were subjected to blue light illumination for 10 min (activation), followed by 30 min without blue light (dark recovery). Membrane retraction and reshaping is observed during blue light illumination, followed by recovery in the absence of blue light. The scale bar represents 10 microns.* ***(B)*** *quantification of changes in percent cell area during alternating cycles of light activation (10 min) and dark recovery (30 min) from n = 6 cells per construct pooled from three replicate measurements. Statistical analysis conducted with one-way ANOVA (∗∗∗p < 0.001; n.s., not significant [p > 0.05]).*

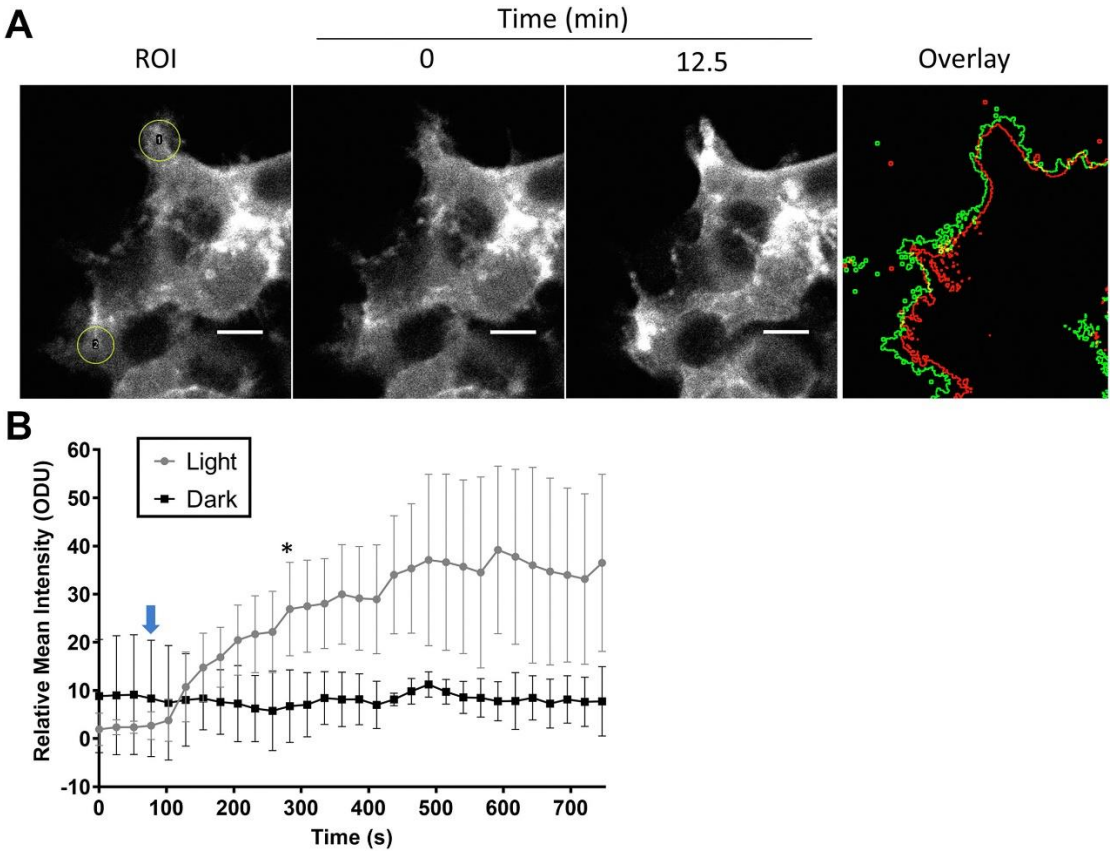

Figure 3.5. *Localized light activation of membrane remodeling with CRY–BAR.* ***(A)*** *HEK293T cells transfected with Cry2–mCh–I-BAR were subjected to restricted blue light illumination (yellow circles) using a confocal microscope. Clustering of Cry–BAR is apparent in the areas illuminated 25 frames post–blue light stimulation. An overlay of the cell outline is shown before (green) and after (red) blue light illumination. The scale bar represents 10 microns.* ***(B)*** *Quantification of fluorescence intensity changes in illuminated versus nonilluminated cell areas for n = 3 circular ROIs (area = 61.4 microns2) per condition. Blue arrow indicates time of applied restricted blue light illumination (488 nm laser at 5% power). Error bars represent standard deviations. Differences are statistically significant (one-way ANOVA, $p < 0.05$) beginning at the 283 s time point (∗) and beyond.*

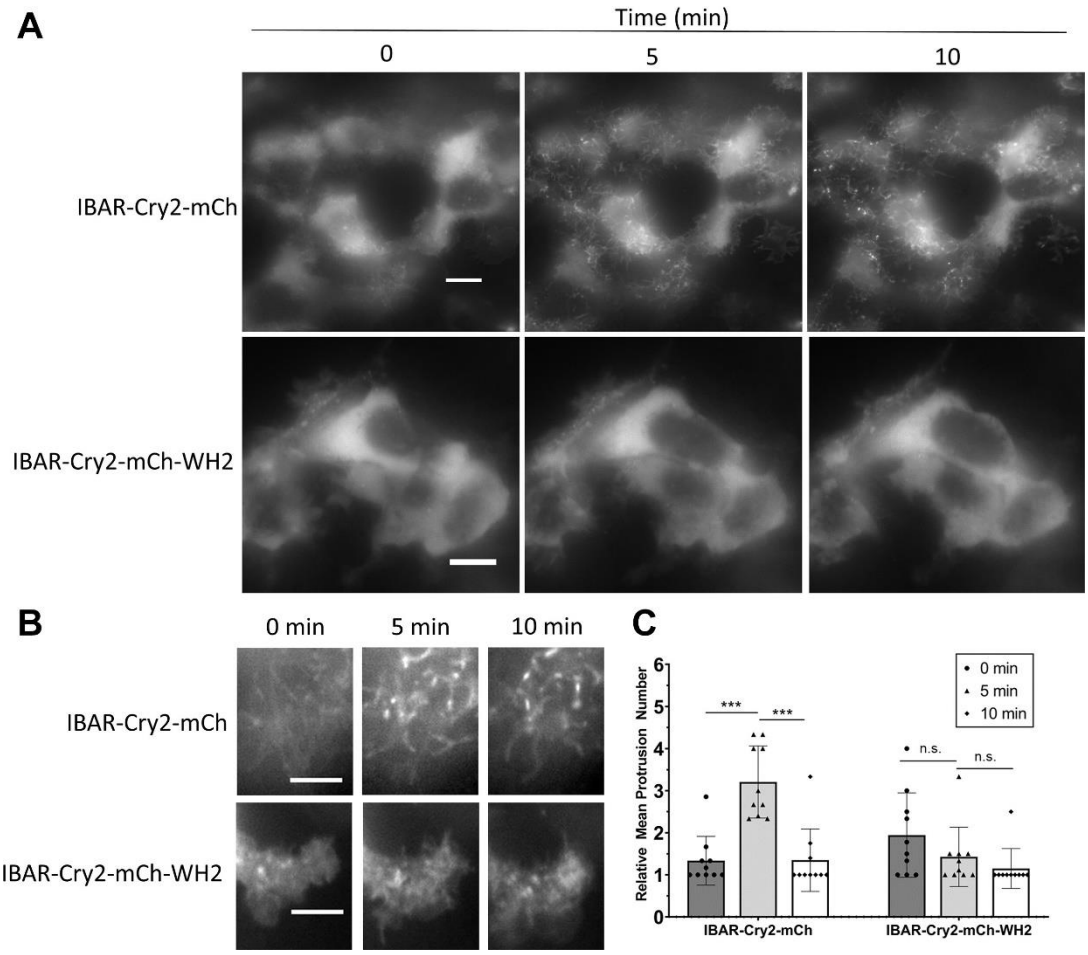

Figure 3.6*. Light activation of N-terminal I-BAR–Cry2 fusions with and without a C-terminal WH2 domain.* ***(A)*** *HEK293T cells transfected with I-BAR–Cry2–mCh or I-BAR–Cry2–mCh–WH2 were subjected to blue light illumination (50 ms pulse every 30 s) using a widefield microscope. I-BAR–Cry2–mCh rapidly coalesces into dynamic filopodial structures. The scale bars represent 10 microns.* ***(B)*** *The presence of a C-terminal WH2 domain results in a cytosolic distribution, reducing impact on filopodial dynamics. The scale bars represent 5 microns.* ***(C)*** *Average number of protrusions at time 0, 5, or 10 min of light exposure from n = 10 cells pooled from three replicate measurements. Statistical analysis conducted with one-way ANOVA (***p < 0.001; *p = 0.002; n.s., not significant [p > 0.05]).*

We postulated that the dynamic membrane-remodeling activity observed with CRY–BARs might be due to its interaction with proteins that link the plasma membrane with the cytoskeleton. Ezrin is one such protein that has both lipid-binding and cytoskeleton-binding domains (Tsai et al., 2018). We hypothesized that clustering of the PIP2-bound CRY–BARs might impact dynamics by also clustering ezrin, resulting in restriction of cytoskeletal-associated phenomenon such as membrane ruffling. To investigate this, we cotransfected Cry2–mCh–I-BAR with an ezrin–GFP fusion. In the presence of light, we observed colocalization of ezrin–GFP with Cry2–mCh–I-BAR clusters at the plasma membrane (**Fig. 3.7**). This effect was pronounced in the light, and absent in the dark, indicating that CRY–BAR activation actively restricts ezrin dynamics. CRY–BAR activation accompanied by ezrin sequestration also resulted in increased cell thickness (**Fig. 3.8**), with no such effect being observed in cells expressing the Cry2–mCh control. Accompanying live-cell experiments demonstrate that, while not exclusively so, the accumulation of ezrin near the cell membrane largely followed that of CRY–BAR during light activation and exhibits a close temporal relationship with CRY–BAR activation (**Fig. AIII.2**). The CRY–BAR–ezrin link implies that CRY–BAR impacts actin dynamics as well. To explore this, we performed live-cell imaging of CRY–BAR light activation in the presence of a GFP-labeled actin (**Fig. 3.9**). Actin-rich protrusions were observed to coalesce upon CRY–BAR activation (**Fig. 3.9A**) but were not generally colocalized with CRY–BAR. Interestingly, in the dark, CRY–BAR is present in filopodia tips and at lamellipodial edges and interspersed with actin (**Fig. 3.9A**). However, upon light activation, their spatial relationship changes, as rounded CRY–BAR clusters and actin-rich regions at the cell membrane become distinct (**Fig. 3.9A, inset and Movie AIII.5**).

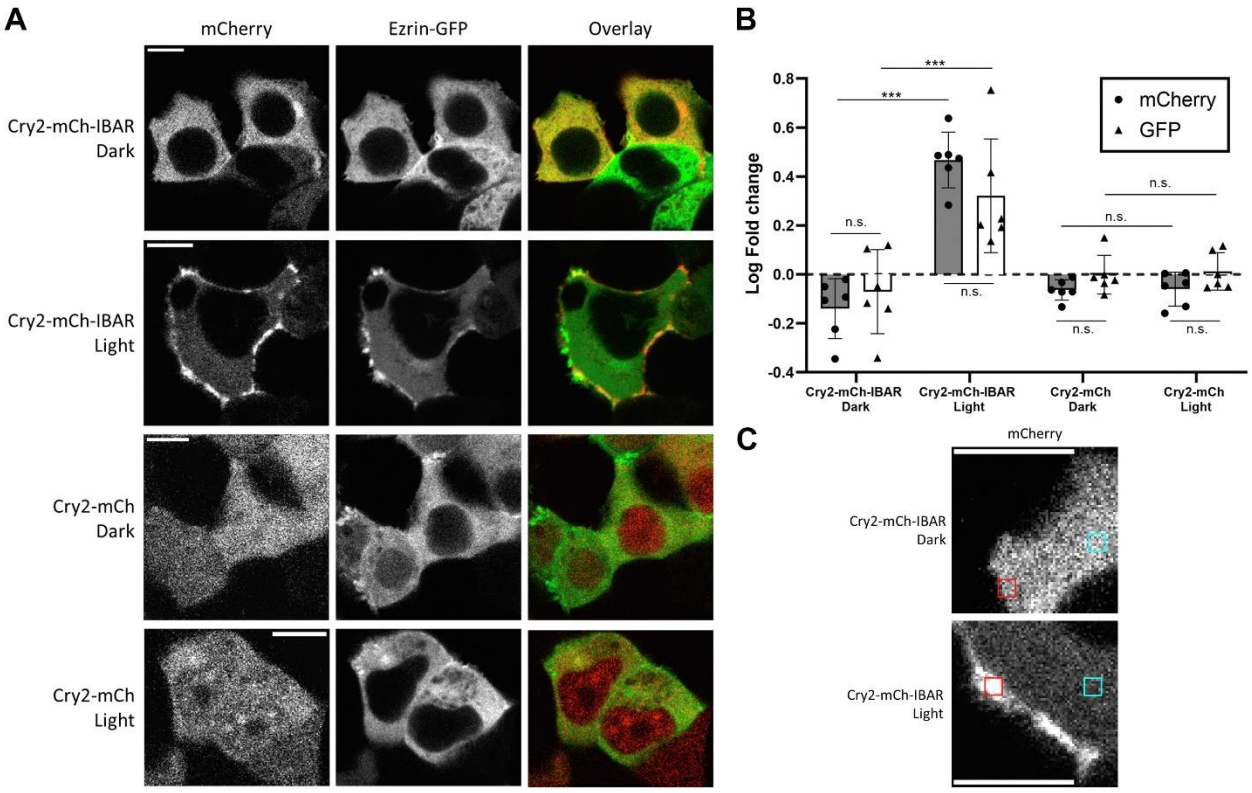

Figure 3.7*. CRY–BAR activation linked to ezrin.* ***(A)*** *HEK293T cells cotransfected with Cry2–mCh–I-BAR and ezrin–GFP were subjected to blue light illumination or dark followed by fixation. Confocal microscopy reveals colocalization of CRY–BAR and ezrin–GFP as a result of CRY–BAR activation. The scale bar represents 10 microns.* ***(B)*** *Plot of the log ratio of membrane ROI versus cytosol ROI intensity (n = 6 cells per construct), normalized intensity for each channel. ROI dimensions: 1.4 × 1.4 microns. Statistical analysis conducted with one-way ANOVA (∗∗∗p < 0.001; n.s., not significant [p > 0.05]).* ***(C)*** *Representative images of ROIs positioned in the cytosol (cyan) and at the membrane (red). The scale bar represents 10 microns.*

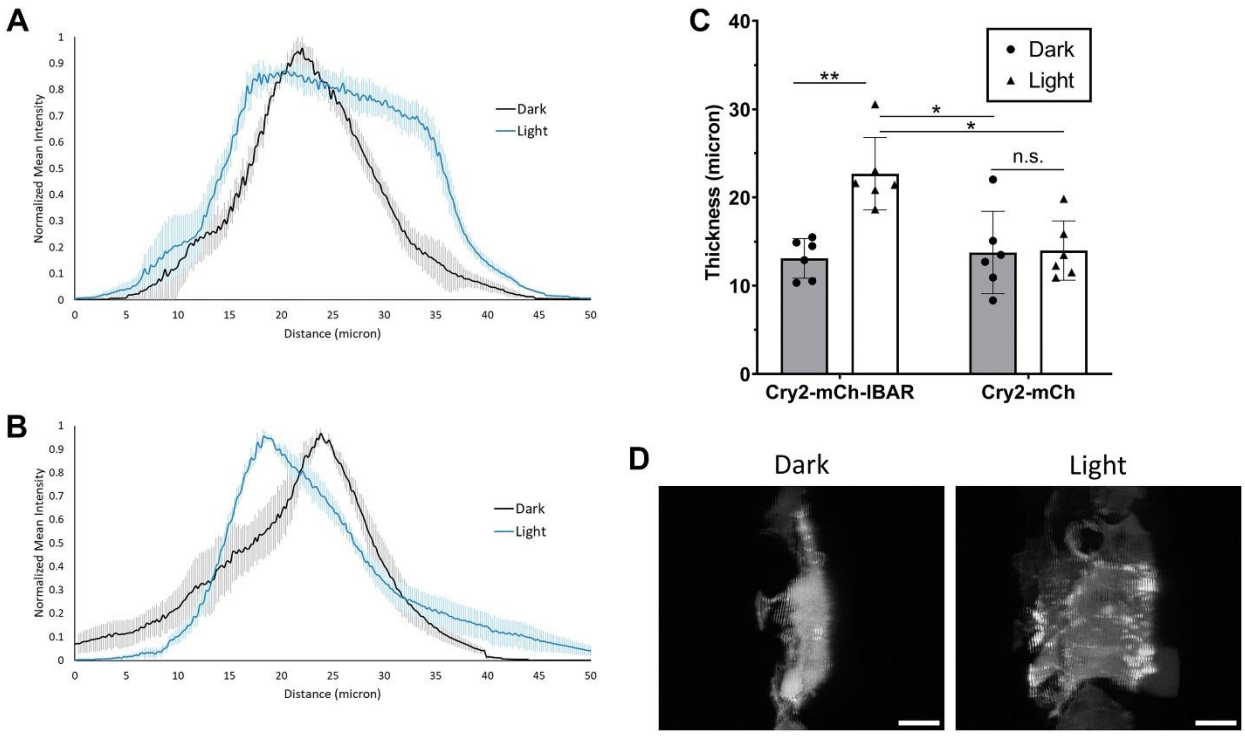

Figure 3.8*. CRY–BAR activation and cell thickness. HEK293T cells cotransfected with Cry2–mCh–I-BAR and ezrin–GFP were subjected to blue light illumination or dark followed by fixation. Cellular thickness was analyzed for n = 6 cells per experimental condition.* ***(A)*** *Average cellular thickness of Cry2–mCherry–I-BAR–transfected HEK293T cells before and after illumination.* ***(B)*** *Average cellular thickness of Cry2–mCh–transfected HEK293T cells before and after illumination.* ***(C)*** *Analysis of average cellular thickness at half height (one-way ANOVA: ∗∗p = 0.001; ∗p = 0.002, n.s., not significant [p > 0.05]).* ***(D)*** *Representative images of Z-projections of ezrin–GFP distribution in Cry2–mCherry–I-BAR transfected cells before and after illumination and fixation. The scale bars represent 10 microns.*

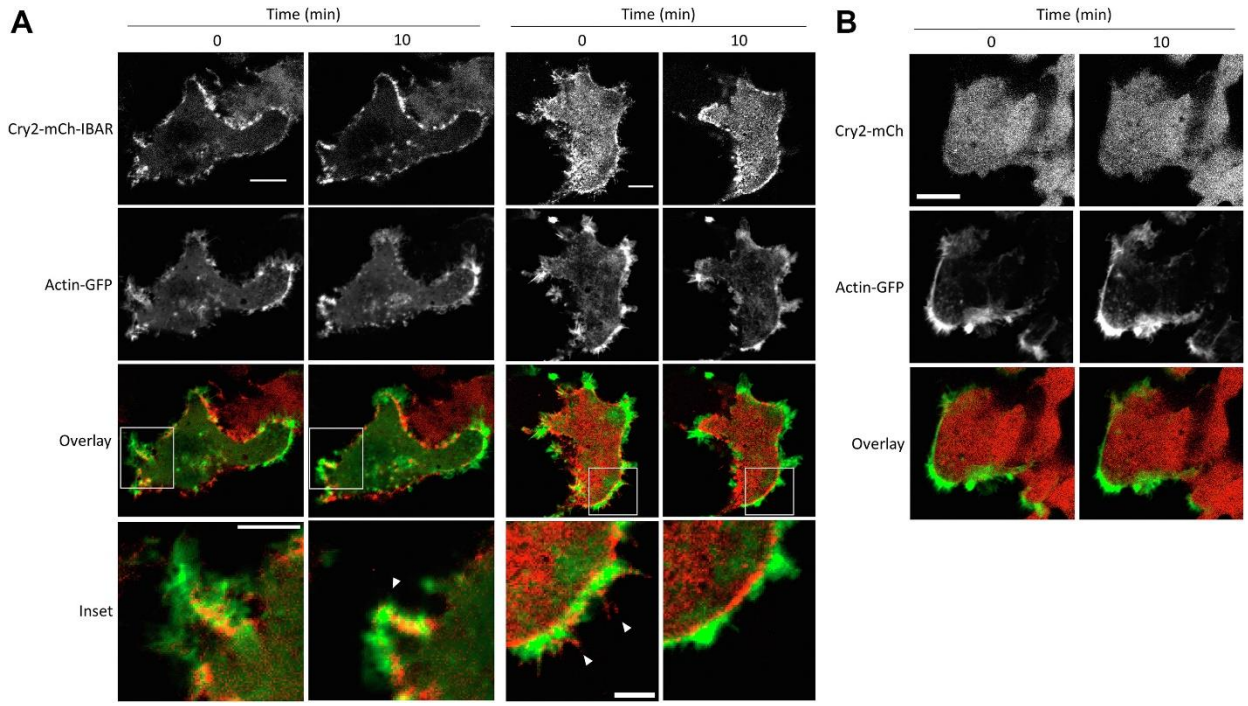

Figure 3.9*. Coalescence of actin-rich protrusions in response to CRY–BAR activation.* ***(A)*** *HEK293T cells cotransfected with Cry2–mCh–I-BAR and actin–GFP were illuminated with 488 nm light (5% power) for 10 min on a confocal microscope. Individual images of channels for mCherry (top row) and GFP (second row) in addition to an overlay (mCherry in red; GFP in green; inset in white box) showed a coalescence of actin-enriched protrusions in conjunction with CRY–BAR-induced membrane rounding after 10 min light exposure (arrow in left cell inset). Cry2–mCh–I-BAR is also enriched at the tips of actin-enriched protrusions in images before light illumination (arrows in right cell inset). After 10 min of light exposure, Cry2–mCh–I-BAR is retracted into the cell and no longer observed in protrusions (right cell inset, fourth column). Full cell image scale bar represents 10 microns. Inset image scale bar represents 5 microns.* ***(B)*** *HEK293T cells cotransfected with Cry2–mCh and actin–GFP were illuminated with 488 nm light (5% power) for 10 min on a confocal microscope. Individual images of channels for mCherry (top row) and GFP (second row) in addition to an overlay (mCherry in*

red; GFP in green). Cry2–mCh and actin–GFP exhibit no change after 10 min light exposure. The scale bar represents 10 microns.

Having investigated the CRY–BAR response in immortalized cell culture, we next evaluated the capability of the sensor to report membrane expansion dynamics in neurons. For this, dissociated postnatal cortical neuron cultures prepared from newborn mice were transfected with Cry2–mCh–I-BAR, or cotransfected with CIBN–GFP–CAAX, according to protocol we developed for expressing optogenetic sensors in primary cultures (Bunner et al., 2021). Light activation of Cry2–mCh–I-BAR, but not Cry2–mCh, resulted in elongation of neuronal processes that might indicate early stage spinogenesis (**Fig. 3.10, Movies AIII.6 and AIII.7**). There was no apparent benefit to activation of Cry2–mCh–I-BAR in the presence of CIBN–GFP–CAAX, providing additional evidence that activation of Cry2–mCh–I-BAR alone is sufficient for effecting membrane dynamics (**Fig. 3.10C**). Accordingly, whole-cell illumination of neurons transfected with only Cry2–mCh–I-BAR results in abundant membranous cluster formation throughout neuronal processes (**Fig. AIII.3A**). Notably, oligomerization of I-BAR domain proteins is essential for their membrane-remodeling activities (Nepal et al., 2021). In the context of CRY–BAR, optimal membrane remodeling is achieved via the homo-oligomerization of Cry2. By contrast, recruitment of CRY–BAR to CIBN–GFP–CAAX, while not completely detrimental to CRY–BAR activity, results in less membrane activity than activation of CRY–BAR alone (**Fig. 3.10C**). This is presumably because of a combination of reduced CRY2 homooligomerization in the presence of CIB, a phenomenon that has been previously described (Che et al., 2015), and possible orientation effects of the Cry2–CIB interaction on the I-BAR domain. CIBN–GFP–CAAX has a similar membrane distribution to CRY–BAR and could interfere with CRY–BAR activity at the cell membrane (**Fig. AIII.4**).

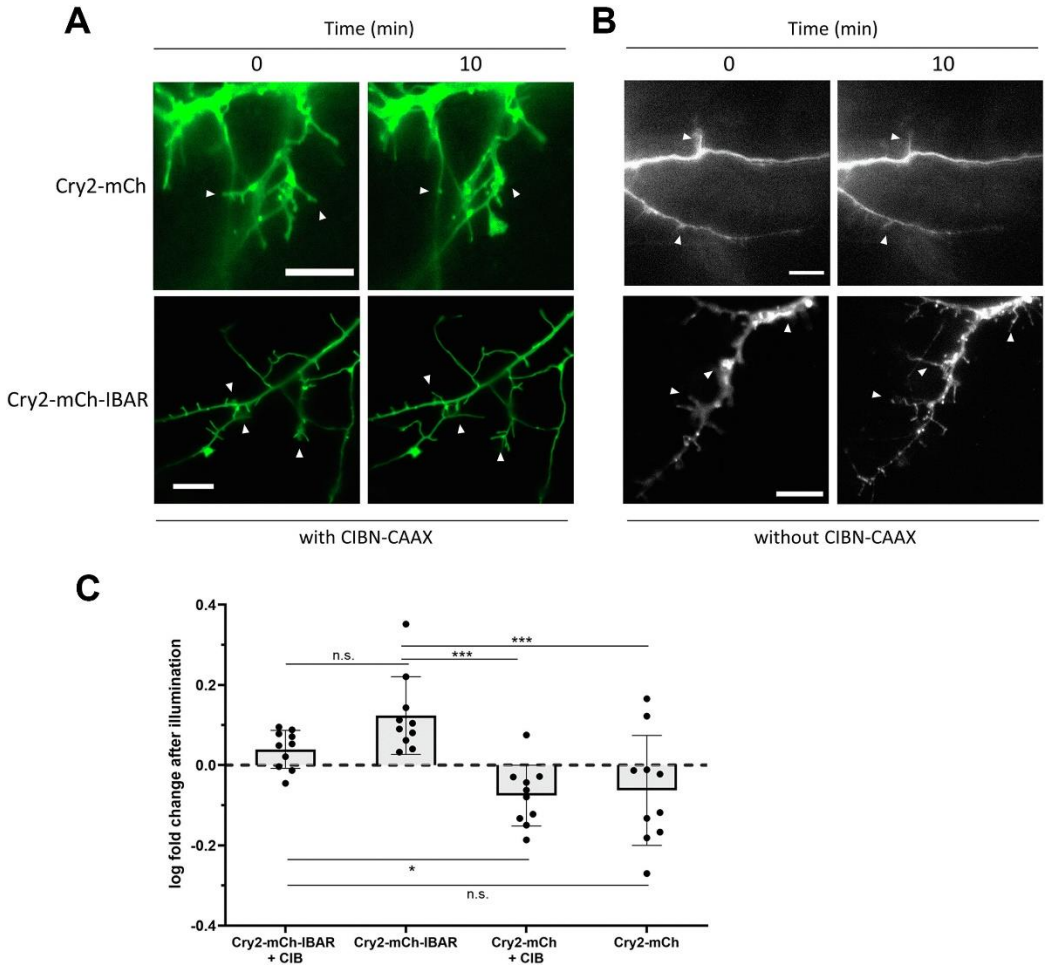

Figure 3.10. *CRY–BAR plasma membrane recruitment in neurons. Pre- and 10 min-post 480 nm light illumination of processes in dissociated hippocampal neuron cultures.* ***(A)*** *Neurons cotransfected with Cry2–mCh–I-BAR or Cry2–mCh and CIBN–GFP–CAAX (GFP channel shown).* ***(B)*** *Neurons transfected with Cry2–mCh–I-BAR or Cry2–mCh. White arrows indicate example protrusions. The scale bars represent 10 microns.* ***(C)*** *Log fold increase in length of protrusions of Cry2–mCh–I-BAR and Cry2–mCh expressing neurons with or without CIBN–GFP–CAAX (CIB) after 10 min of 480 nm light illumination (n = 10 neurons per construct; neurons from three separate cultures; number of protrusions per neuron analyzed: Cry2–mCh–I-BAR + CIB: range 24–141, average 65; Cry2–mCh–I-BAR: range 35–75, average 50; Cry2–mCh + CIB: range 34–116, average 61; Cry2–mCh: range 4–17; average 10. Statistical*

analysis conducted with one-way ANOVA: ∗∗∗p < 0.001; ∗p = 0.04; n.s.: p > 0.05). Error bars represent standard deviations.

Finally, using localized illumination conditions, we demonstrated that Cry2–mCh–I-BAR can be selectively activated in neuronal processes (**Fig. 3.11 and Movie AIII.8**). Taken together, this work provides evidence that the Cry2–mCh–I-BAR molecular optogenetic tool is suitable for the targeted manipulation of cytoskeletal structures and dynamics at the plasma membrane. To our knowledge, this switch represents the first application of the I-BAR domain from MTSS1 in an optogenetic switch. In comparison to prior work in this area, CRY–BAR has the advantage of being a single-component switch, which can reduce experimental complexity and facilitate its implementation into transgenic model organisms. We note that the mechanisms of I-BAR domain proteins are not completely understood, and there are structural and mechanistic differences in the I-BAR domains across different proteins (Saarikangas et al., 2009). As a result, one can reasonably anticipate that the incorporation of I-BAR domains from different I-BAR-containing proteins and their orthologs could produce different experimental phenotypes within the same optogenetic background. This intriguing possibility illustrates the value of pursuing multiple optogenetic variations of BAR domain proteins. Potential applications of CRY–BARs include site-directed mutagenesis of the I-BAR domain, which could provide valuable structure-function information regarding the mechanism of the I-BAR–plasma membrane interaction, and investigation of membrane deformation–dependent cell signaling pathways, such as calcium signaling (Tu et al., 2016).

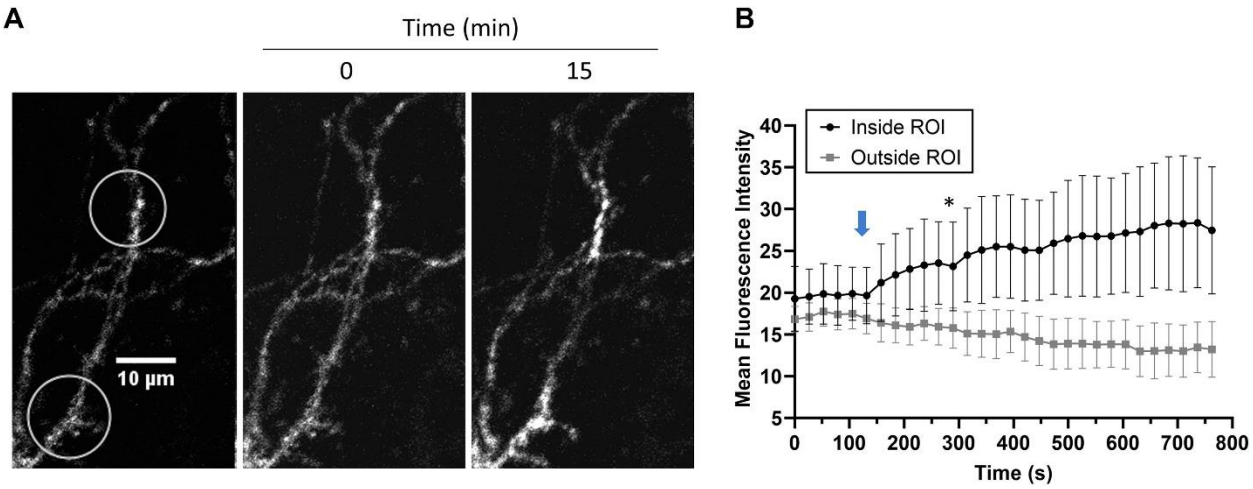

Figure 3.11. *Localized light activation of CRY–BAR in neurons. (A) Neurons transfected with Cry2–mCh–I-BAR were subjected to restricted blue light illumination (white circles) using a confocal microscope. Clustering of CRY–BAR is apparent in the areas illuminated 15 min post–blue light stimulation (irradiation with 488 nm laser at 5% power at the 120 s mark). The scale bar represents 10 microns. (B) A plot of fluorescence intensity from four illuminated ROIs versus four nonilluminated regions is shown at right (error bars = standard deviation; differences are statistically significant [one-way ANOVA, $p < 0.05$] beginning at the 263 s time point [$*$] and beyond). Blue arrow indicates time of blue light illumination.*

Overall, we describe the development of a family of optogenetic switches, collectively named CRY–BAR, that comprise a versatile platform for controlling membrane dynamics in live cells with high spatial and temporal resolution. These switches combine homo- and hetero-oligomerization of the Cry2–CIB photoreceptor system with the innate PIP2-binding affinity of the I-BAR domain. As their function varies depending on the presence of various functional elements, such as WH2-binding domains, we anticipate that a modular approach can be undertaken to adapt these optogenetic switches for other applications, including the recruitment of enzyme and receptor-activating and -inhibitory domains. Finally, CRY–BARs are suitable tools to study membrane dynamics not only in immortalized cells but also in sensitive and difficult to transfect primary cultures, such as neurons. Therefore, the CRY–BAR optogenetic switches we report here are expected to have wide applicability for investigating cellular processes associated with membrane dynamics in a variety of experimental paradigms.

References

Antonny, B. (2011). Mechanisms of membrane curvature sensing. *Annual Review of Biochemistry*, *80*, 101–123. https://doi.org/10.1146/annurev-biochem-052809-155121

Bunner, W. P., Dodson, R., Hughes, R. M., & Szatmari, E. M. (2021). Transfection and Activation of CofActor, a Light and Stress Gated Optogenetic Tool, in Primary Hippocampal Neuron Cultures. *Bio-Protocol*, *11*(8), e3990. https://doi.org/10.21769/BioProtoc.3990

Chang, J.-Y., Parra-Bueno, P., Laviv, T., Szatmari, E. M., Lee, S.-J. R., & Yasuda, R. (2017). CaMKII Autophosphorylation Is Necessary for Optimal Integration of Ca2+ Signals during LTP Induction, but Not Maintenance. *Neuron*, *94*(4), 800-808.e4. https://doi.org/10.1016/j.neuron.2017.04.041

Chatzi, C., Zhang, Y., Hendricks, W. D., Chen, Y., Schnell, E., Goodman, R. H., & Westbrook, G. L. (2019). Exercise-induced enhancement of synaptic function triggered by the inverse BAR protein, Mtss1L. *eLife*, *8*, e45920. https://doi.org/10.7554/eLife.45920

Che, D. L., Duan, L., Zhang, K., & Cui, B. (2015). The Dual Characteristics of Light-Induced Cryptochrome 2, Homo-oligomerization and Heterodimerization, for Optogenetic Manipulation in Mammalian Cells. *ACS Synthetic Biology*, *4*(10). https://doi.org/10.1021/acssynbio.5b00048

Hao, J.-J., Liu, Y., Kruhlak, M., Debell, K. E., Rellahan, B. L., & Shaw, S. (2009). Phospholipase C-mediated hydrolysis of PIP2 releases ERM proteins from lymphocyte membrane. *The Journal of Cell Biology*, *184*(3), 451–462. https://doi.org/10.1083/jcb.200807047

Jones, T., Liu, A., & Cui, B. (2020). Light-Inducible Generation of Membrane Curvature in Live Cells with Engineered BAR Domain Proteins. *ACS Synthetic Biology*, *9*(4), 893–901. https://doi.org/10.1021/acssynbio.9b00516

Kennedy, M. J., Hughes, R. M., Peteya, L. A., Schwartz, J. W., Ehlers, M. D., & Tucker, C. L. (2010). Rapid blue-light-mediated induction of protein interactions in living cells. *Nature Methods*, *7*(12). https://doi.org/10.1038/nmeth.1524

Khamo, J. S., Krishnamurthy, V. V., Chen, Q., Diao, J., & Zhang, K. (2019). Optogenetic Delineation of Receptor Tyrosine Kinase Subcircuits in PC12 Cell Differentiation. *Cell Chemical Biology*, *26*(3), 400-410.e3. https://doi.org/10.1016/j.chembiol.2018.11.004

Kichuk, T. C., Carrasco-López, C., & Avalos, J. L. (2021). Lights up on organelles: Optogenetic tools to control subcellular structure and organization. *WIREs Mechanisms of Disease*, *13*(1), e1500. https://doi.org/10.1002/wsbm.1500

Klewer, L., & Wu, Y.-W. (2019). Light-Induced Dimerization Approaches to Control Cellular Processes. *Chemistry (Weinheim an Der Bergstrasse, Germany)*, *25*(54), 12452–12463. https://doi.org/10.1002/chem.201900562

Li, L., Liu, H., Baxter, S. S., Gu, N., Ji, M., & Zhan, X. (2016). The SH3 domain distinguishes the role of I-BAR proteins IRTKS and MIM in chemotactic response to serum. *Biochemical and Biophysical Research Communications*, *479*(4), 787–792. https://doi.org/10.1016/j.bbrc.2016.09.131

Linkert, M., Rueden, C. T., Allan, C., Burel, J.-M., Moore, W., Patterson, A., Loranger, B., Moore, J., Neves, C., Macdonald, D., Tarkowska, A., Sticco, C., Hill, E., Rossner, M., Eliceiri, K. W., & Swedlow, J. R. (2010). Metadata matters: Access to image data in the real world. *The Journal of Cell Biology*, *189*(5), 777–782. https://doi.org/10.1083/jcb.201004104

Linkner, J., Witte, G., Zhao, H., Junemann, A., Nordholz, B., Runge-Wollmann, P., Lappalainen, P., & Faix, J. (2014). The inverse BAR domain protein IBARa drives membrane remodeling to control osmoregulation, phagocytosis and cytokinesis. *Journal of Cell Science*, *127*(Pt 6), 1279–1292. https://doi.org/10.1242/jcs.140756

Nepal, B., Sepehri, A., & Lazaridis, T. (2021). Mechanism of negative membrane curvature generation by I-BAR domains. *Structure (London, England: 1993)*, *29*(12), 1440-1452.e4. https://doi.org/10.1016/j.str.2021.07.010

O'Banion, C. P., Priestman, M. A., Hughes, R. M., Herring, L. E., Capuzzi, S. J., & Lawrence, D. S. (2018). Design and Profiling of a Subcellular Targeted Optogenetic cAMP-Dependent Protein Kinase. *Cell Chemical Biology*, *25*(1), 100-109.e8. https://doi.org/10.1016/j.chembiol.2017.09.011

O'Banion, C. P., Vickerman, B. M., Haar, L., & Lawrence, D. S. (2019). Compartmentalized cAMP Generation by Engineered Photoactivated Adenylyl Cyclases. *Cell Chemical Biology*, *26*(10), 1393-1406.e7. https://doi.org/10.1016/j.chembiol.2019.07.004

Park, H., Kim, N. Y., Lee, S., Kim, N., Kim, J., & Heo, W. D. (2017). Optogenetic protein clustering through fluorescent protein tagging and extension of CRY2. *Nature Communications*, *8*(1), 30. https://doi.org/10.1038/s41467-017-00060-2

Paunola, E., Mattila, P. K., & Lappalainen, P. (2002). WH2 domain: A small, versatile adapter for actin monomers. *FEBS Letters*, *513*(1), 92–97. https://doi.org/10.1016/s0014-5793(01)03242-2

Pipathsouk, A., Brunetti, R. M., Town, J. P., Graziano, B. R., Breuer, A., Pellett, P. A., Marchuk, K., Tran, N.-H. T., Krummel, M. F., Stamou, D., & Weiner, O. D. (2021). The WAVE complex associates with sites of saddle membrane curvature. *The Journal of Cell Biology*, *220*(8), e202003086. https://doi.org/10.1083/jcb.202003086

Prévost, C., Zhao, H., Manzi, J., Lemichez, E., Lappalainen, P., Callan-Jones, A., & Bassereau, P. (2015). IRSp53 senses negative membrane curvature and phase separates along membrane tubules. *Nature Communications*, *6*, 8529. https://doi.org/10.1038/ncomms9529

Pykäläinen, A., Boczkowska, M., Zhao, H., Saarikangas, J., Rebowski, G., Jansen, M., Hakanen, J., Koskela, E. V., Peränen, J., Vihinen, H., Jokitalo, E., Salminen, M., Ikonen, E., Dominguez, R., & Lappalainen, P. (2011). Pinkbar is an epithelial-specific BAR domain protein that generates planar membrane structures. *Nature Structural & Molecular Biology*, *18*(8), 902–907. https://doi.org/10.1038/nsmb.2079

Redchuk, T. A., Karasev, M. M., Verkhusha, P. V., Donnelly, S. K., Hülsemann, M., Virtanen, J., Moore, H. M., Vartiainen, M. K., Hodgson, L., & Verkhusha, V. V. (2020). Optogenetic regulation of endogenous proteins. *Nature Communications*, *11*(1), 605. https://doi.org/10.1038/s41467-020-14460-4

Saarikangas, J., Kourdougli, N., Senju, Y., Chazal, G., Segerstråle, M., Minkeviciene, R., Kuurne, J., Mattila, P. K., Garrett, L., Hölter, S. M., Becker, L., Racz, I., Hans, W., Klopstock, T., Wurst, W., Zimmer, A., Fuchs, H., Gailus-Durner, V., Hrabě de Angelis, M., … Hotulainen, P. (2015). MIM-Induced Membrane Bending Promotes Dendritic Spine Initiation. *Developmental Cell*, *33*(6), 644–659. https://doi.org/10.1016/j.devcel.2015.04.014

Saarikangas, J., Mattila, P. K., Varjosalo, M., Bovellan, M., Hakanen, J., Calzada-Wack, J., Tost, M., Jennen, L., Rathkolb, B., Hans, W., Horsch, M., Hyvönen, M. E., Perälä, N., Fuchs, H., Gailus-Durner, V., Esposito, I., Wolf, E., de Angelis, M. H., Frilander, M. J., … Lappalainen, P. (2011). Missing-in-metastasis MIM/MTSS1 promotes actin assembly at intercellular junctions and is required for integrity of kidney epithelia. *Journal of Cell Science*, *124*(Pt 8), 1245–1255. https://doi.org/10.1242/jcs.082610

Saarikangas, J., Zhao, H., Pykäläinen, A., Laurinmäki, P., Mattila, P. K., Kinnunen, P. K. J., Butcher, S. J., & Lappalainen, P. (2009). Molecular mechanisms of membrane deformation by I-BAR domain proteins. *Current Biology: CB*, *19*(2), 95–107. https://doi.org/10.1016/j.cub.2008.12.029

Salem, F. B., Bunner, W. P., Prabhu, V. V., Kuyateh, A.-B., O'Bryant, C. T., Murashov, A. K., Szatmari, E. M., & Hughes, R. M. (2020). CofActor: A light- and stress-gated optogenetic clustering tool to study disease-associated cytoskeletal dynamics in living cells. *The Journal of Biological Chemistry*, *295*(32), 11231–11245. https://doi.org/10.1074/jbc.RA119.012427

Schindelin, J., Arganda-Carreras, I., Frise, E., Kaynig, V., Longair, M., Pietzsch, T., Preibisch, S., Rueden, C., Saalfeld, S., Schmid, B., Tinevez, J.-Y., White, D. J., Hartenstein, V., Eliceiri, K., Tomancak, P., & Cardona, A. (2012). Fiji: An open-source platform for biological-image analysis. *Nature Methods*, *9*(7), 676–682. https://doi.org/10.1038/nmeth.2019

Shaaya, M., Fauser, J., Zhurikhina, A., Conage-Pough, J. E., Huyot, V., Brennan, M., Flower, C. T., Matsche, J., Khan, S., Natarajan, V., Rehman, J., Kota, P., White, F. M., Tsygankov, D., & Karginov, A. V. (2020). Light-regulated allosteric switch enables temporal and subcellular control of enzyme activity. *eLife*, *9*, e60647. https://doi.org/10.7554/eLife.60647

Sun, Y., Smirnov, M., Kamasawa, N., & Yasuda, R. (2021). Rapid Ultrastructural Changes in the PSD and Surrounding Membrane after Induction of Structural LTP in Single Dendritic Spines. *The Journal of Neuroscience: The Official Journal of the Society for Neuroscience*, *41*(33), 7003–7014. https://doi.org/10.1523/JNEUROSCI.1964-20.2021

Taslimi, A., Vrana, J. D., Chen, D., Borinskaya, S., Mayer, B. J., Kennedy, M. J., & Tucker, C. L. (2014). An optimized optogenetic clustering tool for probing protein interaction and function. *Nature Communications*, *5*. https://doi.org/10.1038/ncomms5925

Tsai, F.-C., Bertin, A., Bousquet, H., Manzi, J., Senju, Y., Tsai, M.-C., Picas, L., Miserey-Lenkei, S., Lappalainen, P., Lemichez, E., Coudrier, E., & Bassereau, P. (2018). Ezrin enrichment on curved membranes requires a specific conformation or interaction with a curvature-sensitive partner. *eLife*, *7*, e37262. https://doi.org/10.7554/eLife.37262

Tu, M. K., Levin, J. B., Hamilton, A. M., & Borodinsky, L. N. (2016). Calcium signaling in skeletal muscle development, maintenance and regeneration. *Cell Calcium*, *59*(2–3), 91–97. https://doi.org/10.1016/j.ceca.2016.02.005

Ueda, Y., & Sato, M. (2018). Cell membrane dynamics induction using optogenetic tools. *Biochemical and Biophysical Research Communications*, *506*(2), 387–393. https://doi.org/10.1016/j.bbrc.2017.11.091

Wu, Y. I., Frey, D., Lungu, O. I., Jaehrig, A., Schlichting, I., Kuhlman, B., & Hahn, K. M. (2009). A genetically encoded photoactivatable Rac controls the motility of living cells. *Nature*, *461*(7260), 104–108. https://doi.org/10.1038/nature08241

Wu, Y. I., Wang, X., He, L., Montell, D., & Hahn, K. M. (2011). Spatiotemporal control of small GTPases with light using the LOV domain. *Methods in Enzymology*, *497*, 393–407. https://doi.org/10.1016/B978-0-12-385075-1.00016-0

Yu, D., Zhan, X. H., Niu, S., Mikhailenko, I., Strickland, D. K., Zhu, J., Cao, M., & Zhan, X. (2011). Murine missing in metastasis (MIM) mediates cell polarity and regulates the motility response to growth factors. *PloS One*, *6*(6), e20845. https://doi.org/10.1371/journal.pone.0020845

Zhao, H., Pykäläinen, A., & Lappalainen, P. (2011). I-BAR domain proteins: Linking actin and plasma membrane dynamics. *Current Opinion in Cell Biology*, *23*(1), 14–21. https://doi.org/10.1016/j.ceb.2010.10.005

CHAPTER 4

Conclusion

Optogenetics has emerged as a powerful tool in the field of cellular and molecular biology, offering precise spatiotemporal control over cellular processes through the use of light-sensitive proteins (Deisseroth, 2015; Joshi et al., 2019; Redchuk et al., 2020; Rost et al., 2017). The development and application of various optogenetic tools have significantly advanced our understanding of complex cellular processes, particularly in the fields of cell signaling and membrane dynamics (Bugaj et al., 2015; Jones et al., 2020; Locke et al., 2017). Both optogenetic Eph receptor (EphA1Cry2) and I-BAR domain (CRY-BAR) highlight the versatility and potential of optogenetics in controlling specific cellular functions with high spatial and temporal precision. A benefit of optogenetic regulation of certain proteins is the lack of requirement for exogenous stimulation with chemicals or ligands.

In the case of EphA receptor activation, selectively activating EphA1 receptors can be a challenging task due to the simultaneous binding and activation of EphA1 and EphA2 receptors by their ligand, ephrinA1. To overcome this limitation, an optogenetic EphA1 receptor was successfully engineered through a Cry2 fusion, enabling selective activation of EphA1 receptors in response to light stimulation. This approach not only provides a new way to study overall EphA1 receptor signal transduction but also delineate signaling outcomes resulting from ephrin-independent activation. The EphA1Cry2 construct dimerizes and phosphorylates upon light stimulation, promoting the phosphorylation of the downstream signaling proteins MAPK and Akt. Juxtaposing studies have indicated that EphA receptor activation either promotes or inhibits proliferation through the Ras/Raf/MEK/MAPK pathway (Miao et al., 2001; Pratt & Kinch, 2002). Our studies found that in the absence of ephrin ligand, EphA1 receptor *cis*-activation

induces ERK phosphorylation, in addition to Akt phosphorylation. ERK and Akt have been shown to participate in signaling crosstalk; therefore, investigations into their crosstalk regulation and feedback loops, if any, could shed light on a cell's ability to modulate proliferation. RNA sequencing of our EphA1Cry2 construct and control conditions also elucidated up- and down-regulated genes associated with EphA1 receptor activation. Differentially expressed genes induced by construct light-activation are those that promote proliferation, differentiation, and cell migration. The EphA1Cry2 construct was also expressed in Neuro2a, neuronal precursor cells; under light stimulation, EphA1Cry2 reduced the number of protrusions along neuronal-like processes. Further investigations into EphA1 receptor signaling include transfecting EphA1Cry2 constructs in other cell lines, such as various types of carcinomas, primary neurons, or cardiomyocytes. By uncoupling receptor activation from ligand binding, this approach provides a valuable tool for dissecting the specific functions of Eph receptors and identifying novel Eph-dependent signaling outcomes.

Our other optogenetic study focused on the design and implementation of light-gated I-BAR domain-containing tools, called CRY-BARs, derived from the fusion of Cry2 and I-BAR domains. As BAR domains can sense and generate membrane curvature, CRY-BARs allow for the spatial and temporal control of membrane dynamics with light through a one-construct system. Other optogenetic BAR domains required a two-part system for the recruitment of BAR domains to the plasma membrane (Jones et al., 2020); however, after initial studies, it was discovered that the utilization of Cry2-CIB hetero-oligomerization was not needed for this optogenetic switch. These CRY-BARs utilize the innate ability of I-BAR domains to bind to PIP_2 on the plasma membrane in response to clustering, resulting in robust membrane recruitment and perturbations of membrane dynamics. Using this as an advantage, membrane

remodeling and retraction were induced in HEK293T cells by CRY-BAR without the need for CIB. In primary neurons, light-activated CRY-BAR increase protrusion length along processes. Actin was also found to be colocalized with CRY-BAR and additionally identified ezrin as an important mediator of CRY-BARs' interaction between the plasma membrane and actin cytoskeleton. Further research aims to continue utilizing CRY-BARs to investigate neuronal processes involving cytoskeletal dynamics.

Taken together, these studies illustrate the power of optogenetics for elucidating complex cellular processes with high spatiotemporal precision. By enabling the manipulation of specific cellular activities with light, optogenetic tools offer opportunities to unravel the intricacies of cell signaling and membrane dynamics. As researchers continue to refine and expand the optogenetic toolkit, these tools hold great promise for further advancing our understanding of fundamental biological processes and developing novel therapeutic strategies for a wide range of diseases.

References

Bugaj, L. J., Spelke, D. P., Mesuda, C. K., Varedi, M., Kane, R. S., & Schaffer, D. V. (2015). Regulation of endogenous transmembrane receptors through optogenetic Cry2 clustering. *Nature Communications*, *6*. https://doi.org/10.1038/ncomms7898

Deisseroth, K. (2015). Optogenetics: 10 years of microbial opsins in neuroscience. *Nature Neuroscience*, *18*(9), 1213–1225. https://doi.org/10.1038/nn.4091

Jones, T., Liu, A., & Cui, B. (2020). Light-Inducible Generation of Membrane Curvature in Live Cells with Engineered BAR Domain Proteins. *ACS Synthetic Biology*, *9*(4), 893–901. https://doi.org/10.1021/acssynbio.9b00516

Joshi, J., Rubart, M., & Zhu, W. (2019). Optogenetics: Background, Methodological Advances and Potential Applications for Cardiovascular Research and Medicine. *Frontiers in Bioengineering and Biotechnology*, *7*, 466. https://doi.org/10.3389/fbioe.2019.00466

Locke, C., Machida, K., Wu, Y., & Yu, J. (2017). Optogenetic activation of EphB2 receptor in dendrites induced actin polymerization by activating Arg kinase. *Biology Open*, *6*(12). https://doi.org/10.1242/bio.029900

Miao, H., Wei, B.-R., Peehl, D. M., Li, Q., Alexandrou, T., Schelling, J. R., Rhim, J. S., Sedor, J. R., Burnett, E., & Wang, B. (2001). Activation of EphA receptor tyrosine kinase inhibits the Ras/MAPK pathway. *Nature Cell Biology*, *3*(5), 527–530. https://doi.org/10.1038/35074604

Pratt, R. L., & Kinch, M. S. (2002). Activation of the EphA2 tyrosine kinase stimulates the MAP/ERK kinase signaling cascade. *Oncogene*, *21*(50), 7690–7699. https://doi.org/10.1038/sj.onc.1205758

Redchuk, T. A., Karasev, M. M., Verkhusha, P. V., Donnelly, S. K., Hülsemann, M., Virtanen, J., Moore, H. M., Vartiainen, M. K., Hodgson, L., & Verkhusha, V. V. (2020). Optogenetic regulation of endogenous proteins. *Nature Communications*, *11*(1), 605. https://doi.org/10.1038/s41467-020-14460-4

Rost, B. R., Schneider-Warme, F., Schmitz, D., & Hegemann, P. (2017). Optogenetic Tools for Subcellular Applications in Neuroscience. In *Neuron* (Vol. 96, Issue 3). https://doi.org/10.1016/j.neuron.2017.09.047

Appendix I: IACUC Approval Letter for Chapter 3: CRY-BARs: Versatile light-gated molecular tools for the remodeling of membrane architectures

ECU

Animal Care and Use Committee
003 Ed Warren Life Sciences Building | East Carolina University | Greenville NC 27834 - 4354
252-744-2436 office | 252-744-2355 fax

October 12, 2021

Erzsebet Szatmari, Ph.D.
Department of Physical Therapy, ECU

Subject: Protocol P105, original approval date 07/11/2019

Dear Dr. Szatmari:

The amendment#3 to your Animal Use Protocol entitled, "Identifying new signaling pathways involved in Alzheimer's disease" (AUP#P105) was reviewed by this institution's Animal Care and Use Committee on 10/12/2021. The following action was taken by the Committee:

"Approved as submitted"

Please contact Aaron Hinkle prior to any hazard use

A copy of the protocols is enclosed for your laboratory files. Please be reminded that all animal procedures must be conducted as described in the approved Animal Use Protocol. Modifications of these procedures cannot be performed without prior approval of the ACUC. The Animal Welfare Act and Public Health Service Guidelines require the ACUC to suspend activities not in accordance with approved procedures and report such activities to the responsible University Official (Vice Chancellor for Health Sciences or Vice Chancellor for Academic Affairs) and appropriate federal Agencies. Please ensure that all personnel associated with this protocol have access to this approved copy of the AUP/Amendment and are familiar with its contents.

Sincerely yours,

Susan McRae, Ph.D.
Chair, Animal Care and Use Committee

JD/GD

enclosure

Appendix II: Supporting Information for Chapter 2: Optogenetic Regulation of EphA1 RTK Activation and Signaling

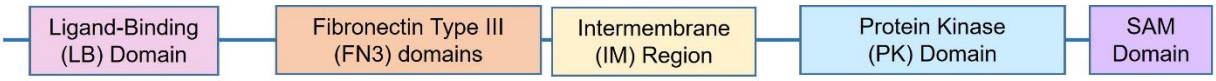

MERRWPLGLGLVLLLCAPLPPGARAKEVTLMDTSKAQGELGWLLDPPKDGWS
EQQQILNGTPLYMYQDCPMQGRRDTDHWLRSNWIYRGEEASRVHVELQFTV
RDCKSFPGGAGPLGCKETFNLLYMESDQDVGIQLRRPLFQKVTTVAADQSFTI
RDLVSGSVKLNVERCSLGRLTRRGLYLAFHNPGACVALVSVRVFYQRCPETLN
GLAQFPDTLPGPAGLVEVAGTCLPHARASPRPSGAPRMHCSPDGEWLVPVGR
CHCEPGYEEGGSGEACVACPSGSYRMDMDTPHCLTCPQQSTAESEGATICTC
ESGHYRAPGEGPQVACTGPPSAPRNLSFSASGTQLSLRWEPPADTGGRQDV
RYSVRCSQCQGTAQDGGPCQPCGVGVHFSPGARGLTTPAVHVNGLEPYANY
TFNVEAQNGVSGLGSSGHASTSVSISMGHAESLSGLSLRLVKKEPRQLELTWA
GSRPRSPGANLTYELHVLNQDEERYQMVLEPRVLLTELQPDTTYIVRVRMLTPL
GPGPFSPDHEFRTSPPVSRGLTGGEIVAVIFGLLLGAALLLGILVFRSRRAQRQR
QQRQRDRATDVDREDKLWLKPYVDLQAYEDPAQGALDFTRELDPAWLMVDTV
IGEGEFGEVYRGTLRLPSQDCKTVAIKTLKDTSPGGQWWNFLREATIMGQFSH
PHILHLEGVVTKRKPIMIITEFMENGALDAFLREREDQLVPGQLVAMLQGIASGM
NYLSNHNYV***HRDLAARN***ILVNQNLCCKVS**DFGLTRLLDDFDGTYETQGGKIPI**
RWTAPEAIAHRIFTTASDVWSFGIVMWEVLSFGDKPYGEMSNQEVMKSIEDGY
RLPPPVDCPAPLYELMKNCWAYDRARRPHFQKLQAHLEQLLANPHSLRTIANF
DPRMTLRLPSLSGSDGIPYRTVSEWLESIRMKRYILHFHSAGLDTMECVLELTA
EDLTQMGITLPGHQKRILCSIQGFKD

Figure AII.1. *Amino acid sequence of human EphA1 receptor (schematic at top) with the domains of the receptor color-coded in the sequence. Within the protein kinase domain (blue), the bold italicized sequence is the catalytic loop, and the bold underlined sequence is the activation loop.*

Table AII.1. *Primer sequences used for construct design. Nucleotide sequences of the restriction sites, linker, plasma membrane (PM) sequence, and the primers used for EphA1Cry2 constructs and Erk-KTR and Akt-KTR are labeled and color-coded.*

Description	***Nucleotide sequence***
Restriction sites	
NheI sequence	**gctagc**
Bmt1 sequence	**gctagc**
BsrgI sequence	**tgtaca**
NotI sequence	**gcggccgc**
Linker	**ggcggcagcggcggcagcggcggcagc**
PMa sequence	**atgggctgcattaaaagcaaacgcaaagataacctgaacgatgatgaa**
PMb sequence	**atgggcagcagcaaaagcaaaccgaaa**
PMa-EphA1Cry2*	
Forward Primer	tacga**gctagcatgggctgcattaaaagcaaacgcaaagataacctgaacgatgatgaaatggtgtccaggggcctgactgga**
Reverse Primer	tcgta**gctagcgctgccgccgctgccgccgctgccgcccaagtccttgaatccctgaatac**
PMa-EphA1Cry2Δ*	
Forward Primer	tacga**gctagcatgggctgcattaaaagcaaacgcaaagataacctgaacgatgatgaaatggaccctgcacagggagccttg**
Reverse Primer	tcgta**gctagcgctgccgccgctgccgccgctgccgcccccatctgagccactcaggct**
PMb-EphA1Cry2*	
Forward Primer	tacga**gctagcatgggcagcagcaaaagcaaaccgaaaatggtgtccaggggcctgactgga**
Reverse Primer	tcgta**gctagcgctgccgccgctgccgccgctgccgcccaagtccttgaatccctgaatac**
PMb-EphA1Cry2Δ*	
Forward Primer	tacga**gctagcatgggcagcagcaaaagcaaaccgaaaatggaccctgcacagggagccttg**
Reverse Primer	tcgta**gctagcgctgccgccgctgccgccgctgccgcccccatctgagccactcaggct**
IM-EphA1Cry2Δ*	
Forward Primer	tacga**gctagcatgccccctcggcccccgaaac**
Reverse Primer	tcgta**gctagcgctgccgccgctgccgccgctgccgcccaagtccttgaatccctgaatact**
IM-EphA1Cry2*	
Forward Primer (extracellular)	tacga**gctagcatggagcggcgctggcccctg**
Reverse Primer (extracellular)	tcgta**gctagcgctgccgccgctgccgccgctgccgccgcggtcacgctgcctctgctg**
Forward Primer (intracellular)	tacga**tgtacaggcggcagcggcggcagcggcggcagcgccaccgatgtggatcgagag**
Reverse Primer (intracellular)	tcgta**gcggccgcaagtccttgaatccctgaat**
	*bold black text is the sequence for EphA1 receptor
Akt-KTR-mTurq2	
Forward Primer	cgtcgacttaacagatctcgagatggcagaggcaccggc
Reverse Primer	ctagccatgaattcgaagcttctcattacccgctccccatggtttggtacag
ERK-KTR-mNeonGreen	
Forward Primer	cgtcgacttaacagatctcgagatgaaaggccgcaag
Reverse Primer	ctagccatgaattcgaagcttctcattacttgtacagctcgtccatg

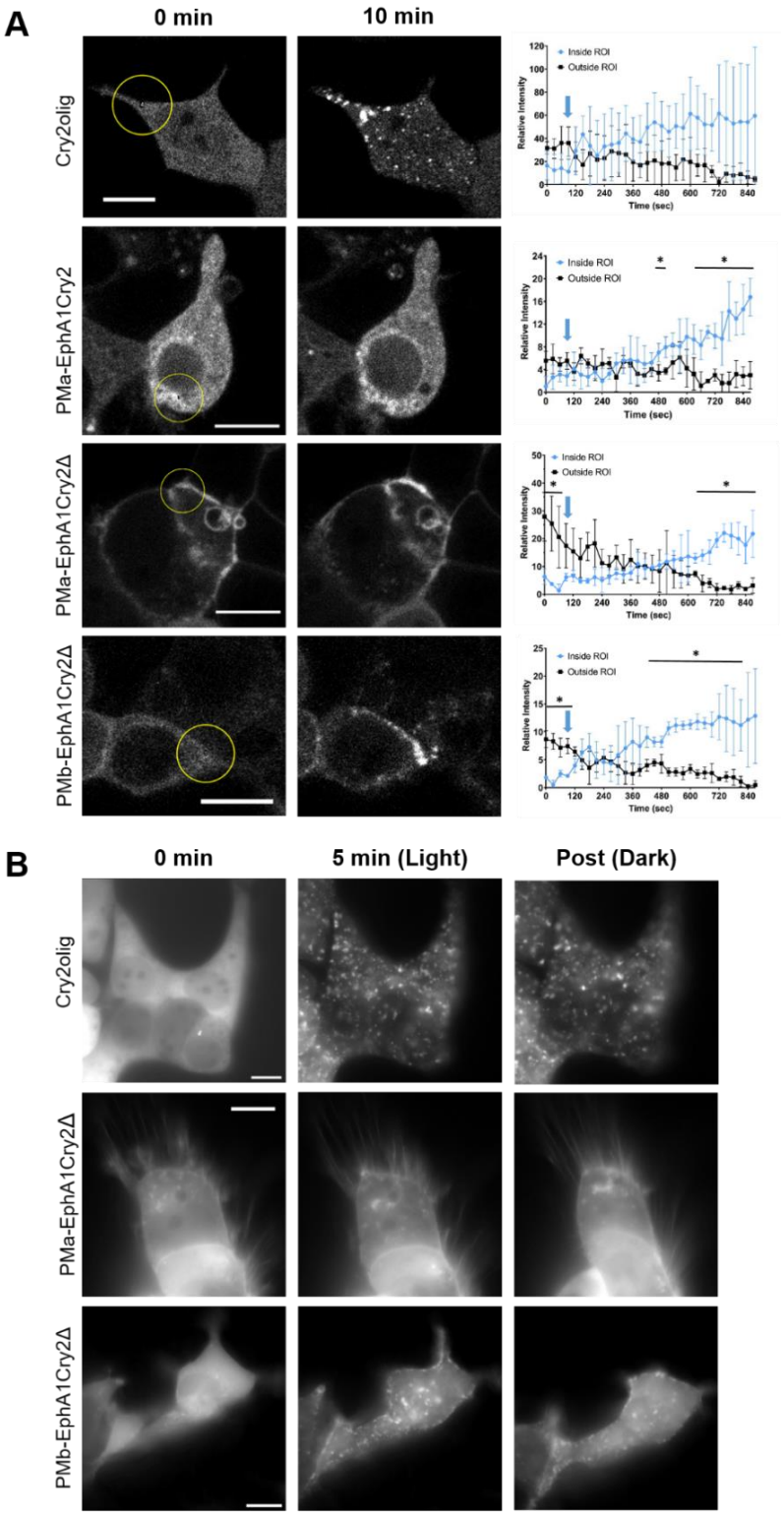

Figure AII.2. *Spatiotemporal light activation of EphA1Cry2 constructs.* ***(A)*** *Confocal images of HEK293T cells transfected with Cry2olig, PMa-EphA1Cry2, PMa-EphA1Cry2Δ, or PMb-*

*EphA1Cry2Δ taken pre-illumination (0 min) and after blue light exposure (480 nm, 30 sec intervals for 10 min) only inside circular region (yellow). Images collected on mCherry channel (200 ms exposure, 553 nm). Scale bar: 10 µm. Right column: Quantitation of the relative intensity of inside and outside the region of interest (ROI) over blue light exposure starting at 90 sec (blue arrow). Error bars represent standard deviation; n=3 regions (unpaired t-test, *p < 0.05).* ***(B)*** *Widefield images of HEK293T cells transfected with Cry2olig, PMa-EphA1Cry2Δ, or PMb-EphA1Cry2Δ before light exposure (0 min), after 5 min of light exposure (480 nm, 50 ms exposure, 30 sec intervals), and 10 min post-light exposure (Post). Images collected on mCherry channel (200 ms exposure, 553 nm). Scale bar: 10 µm.*

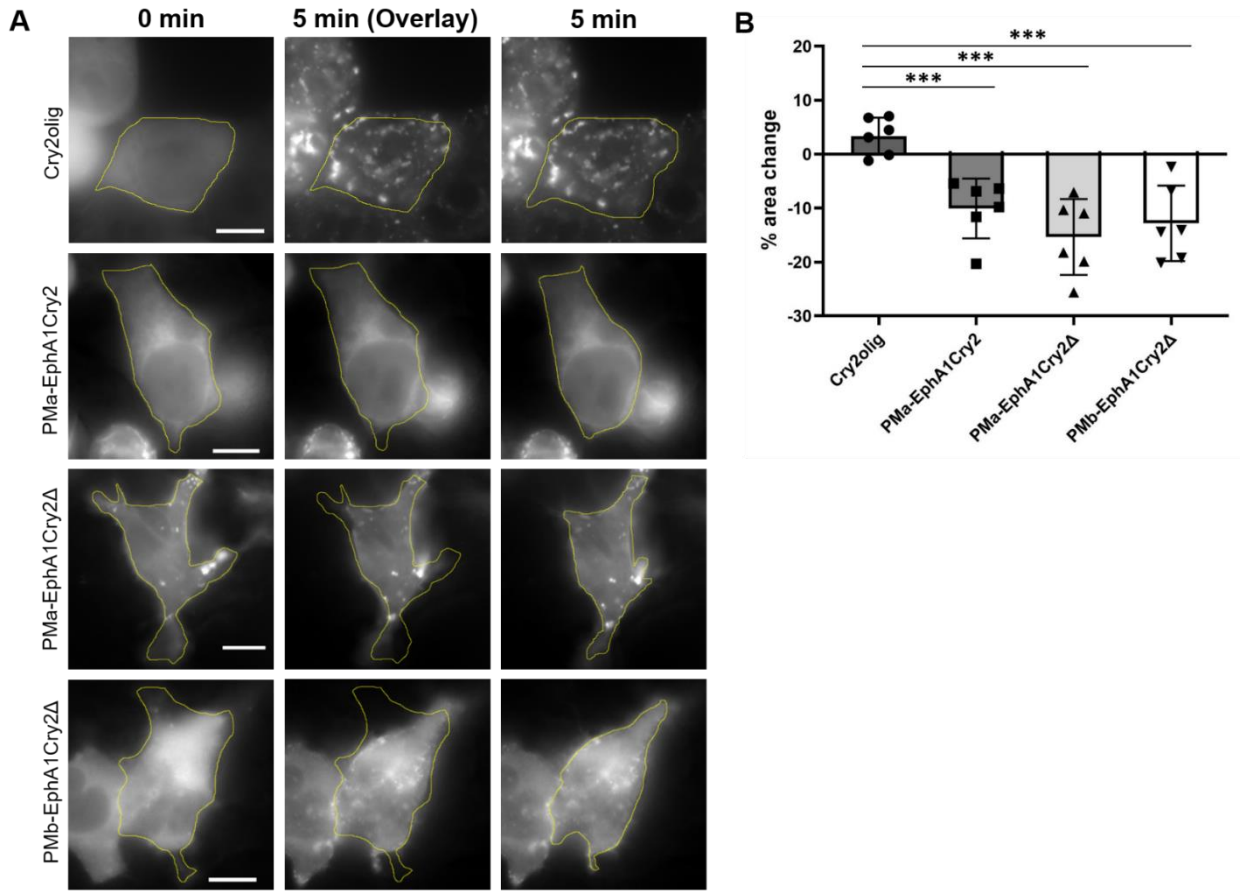

Figure AII.3. *Cell rounding assay in response to EphA1Cry2 light activation.* ***(A)*** *Widefield images of HEK293T cells transfected with Cry2olig, PMa-EphA1Cry2, PMa-EphA1Cry2Δ, or PMb-EphA1Cry2Δ before light exposure (0 min) and after 5 min of light exposure (480 nm, 50 ms exposure, 30 sec intervals). Images collected on mCherry channel (553 nm, 200 ms exposure). Cell areas were measured by tracing the cell around the membrane (yellow) using Fiji ImageJ. Middle column shows the trace of the cell area (yellow) at time 0 min overlaid with the cell at time 5 min. Scale bar: 10 µm.* ***(B)*** *Quantitation of the percent area change (% change in the cell area at 10 min over cell area at 0 min) of transfect HEK293T cells in (A). Error bars represent standard deviation, n=6 cells (unpaired t-test; ***p < 0.001).*

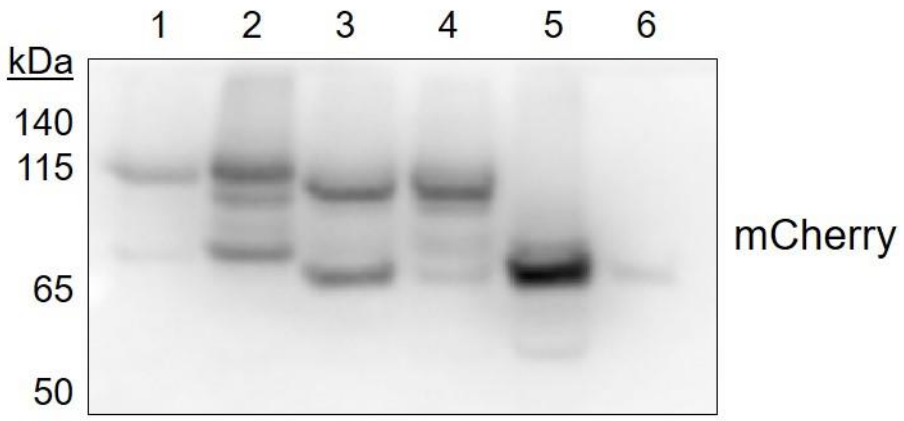

Figure AII.4*. mCherry expression of EphA1Cry2 constructs. HEK293T cells were transfected with either PMb-EphA1Cry2 (Lane 1), PMa-EphA1Cry2 (Lane 2), PMb-EphA1Cry2Δ (Lane 3), PMa-EphA1Cry2Δ (Lane 4), Cry2olig (Lane 5), or no transfection (Lane 6). Western blots of whole cell lysates were incubated with mCherry antibody. Bands at 110-115 kDa (lanes 1-4) are EphA1Cry2 construct, and 65 kDa band (lane 5) is Cry2olig.*

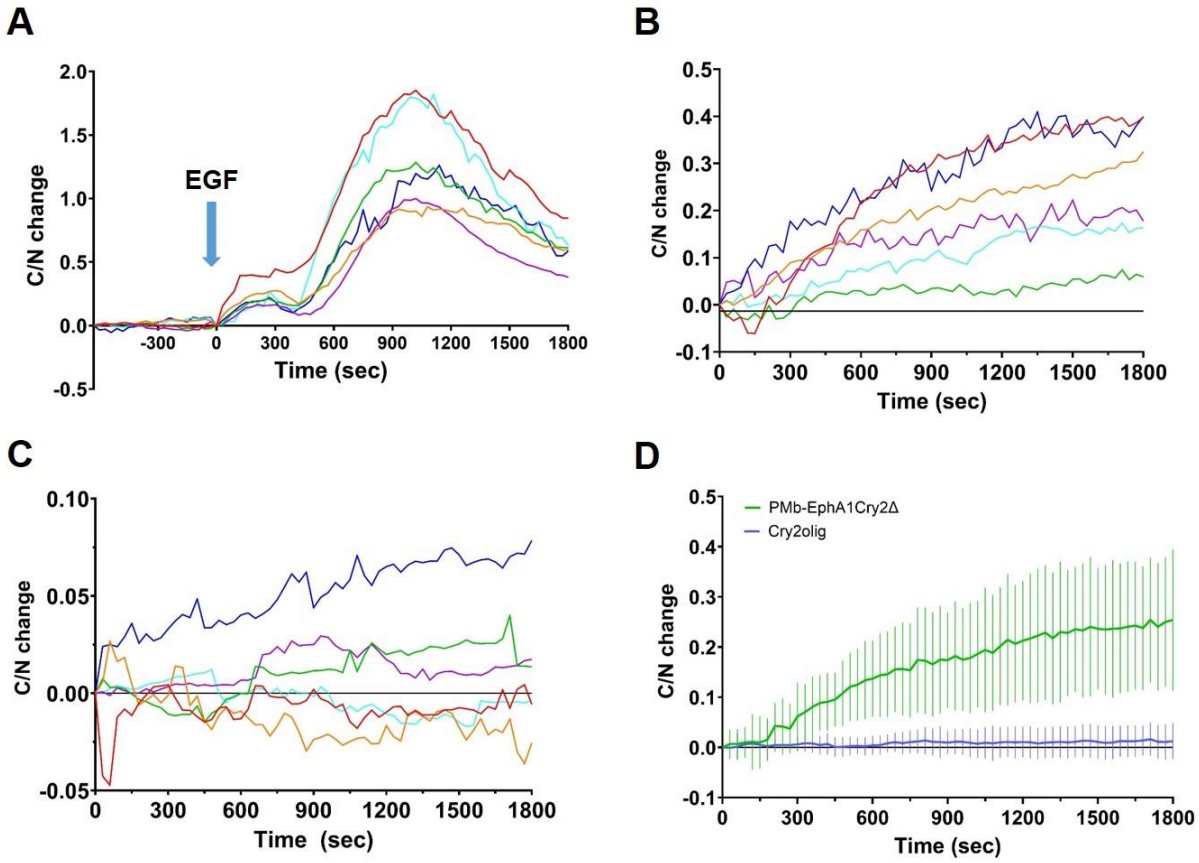

Figure AII.5. *Additional graphs for ERK-KTR C/N change analysis.* ***(A-C)*** *Quantitation of the C/N change over time for individual HEK293T cells transfected with (A) ERK-KTR, (B) PMb-EphA1Cry2Δ and ERK-KTR, or (C) Cry2olig and ERK-KTR. (A) ERK-KTR included 10 min pre-stimulus imaging followed by EGF stimulation (blue arrow).* ***(D)*** *Comparison of the average C/N change of PMb-EphA1Cry2Δ with ERK-KTR (green) and Cry2olig with ERK-KTR (purple). Error bars represent standard deviation; n=6 cells.*

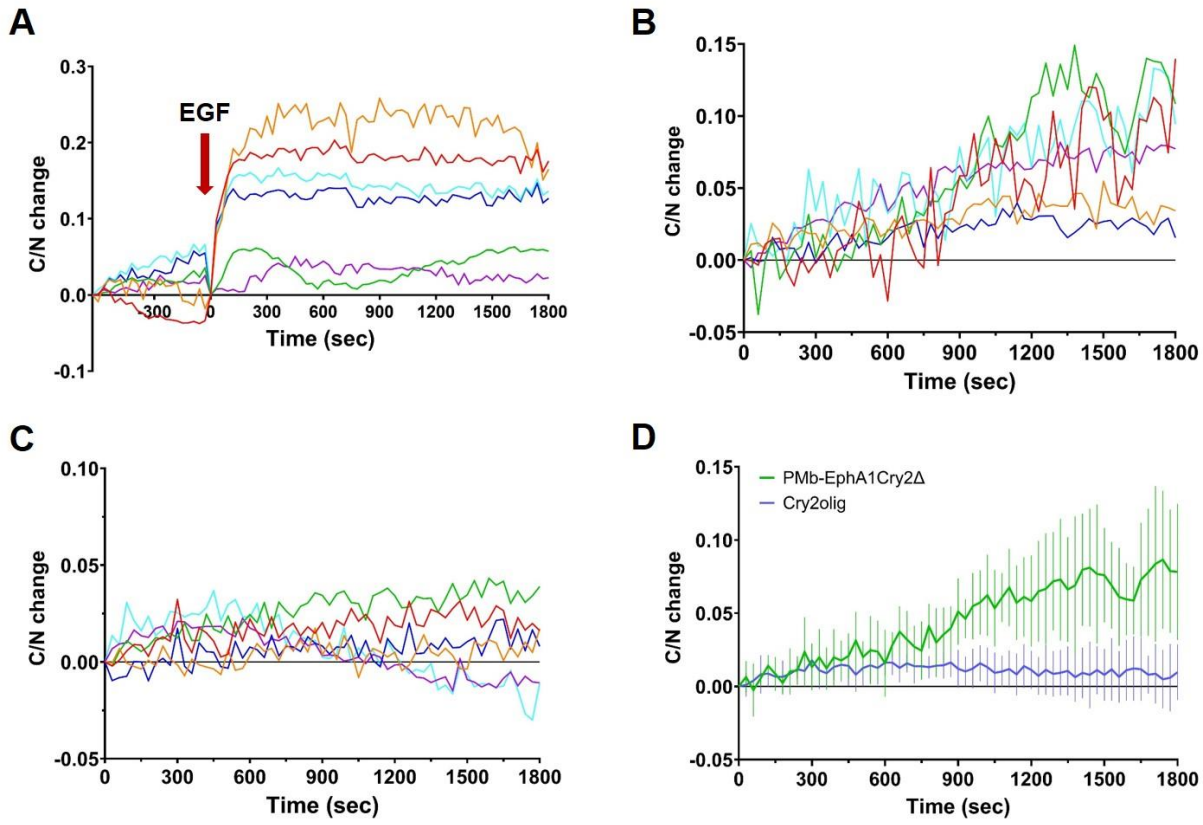

Figure AII.6. *Additional graphs for Akt-KTR C/N change analysis.* ***(A-C)*** *Quantitation of the C/N change over time for individual HEK293T cells with (A) Akt-KTR, (B) PMb-EphA1Cry2Δ and Akt-KTR, or (C) Cry2olig and Akt-KTR. (A) Akt-KTR included 10 min pre-stimulus imaging followed by EGF stimulation (red arrow).* ***(D)*** *Comparison of the average C/N change of PMb-EphA1Cry2Δ with Akt-KTR (green) and Cry2olig with Akt-KTR (purple). Error bars represent standard deviation; n=6 cells.*

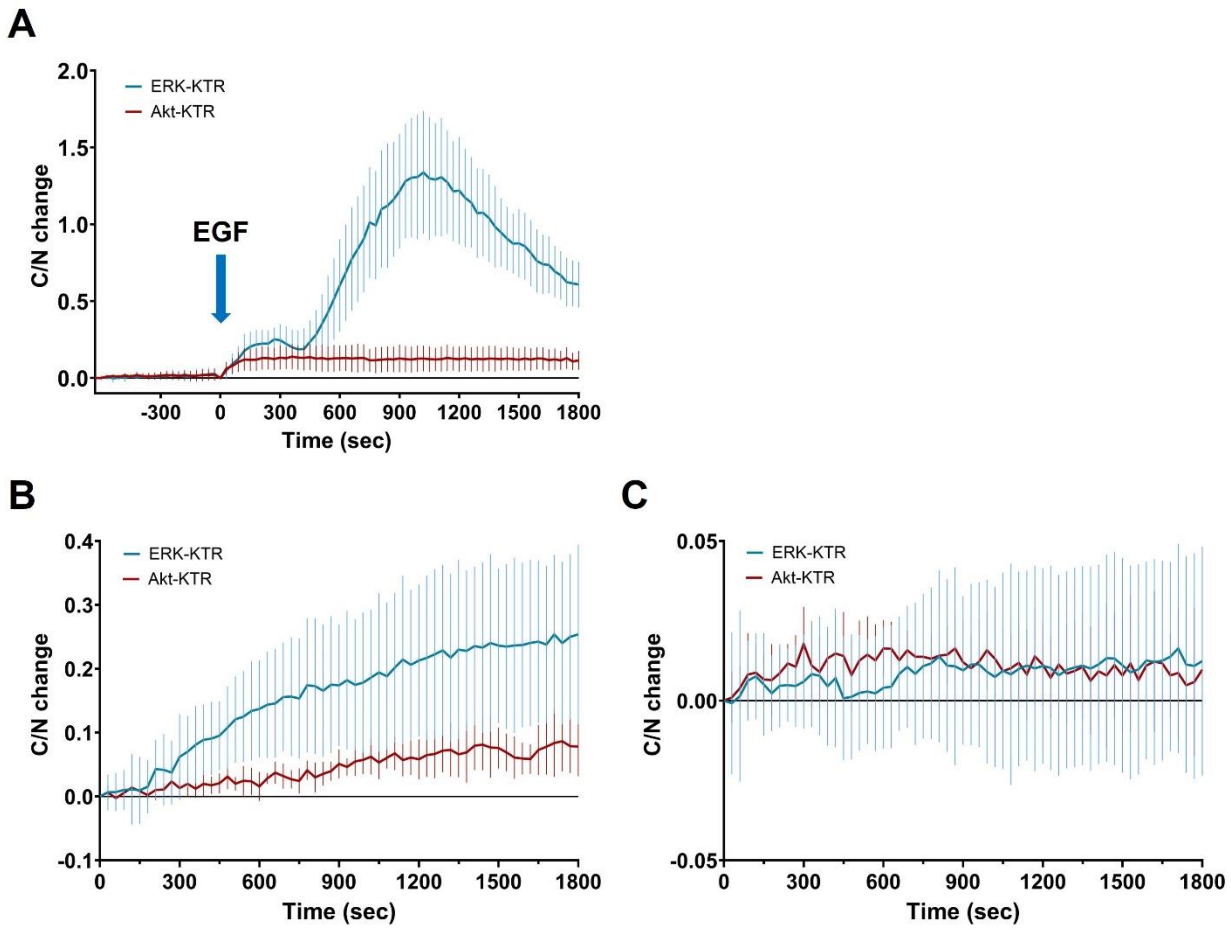

Figure AII.7. *Comparison of ERK-KTR and Akt-KTR C/N change.* ***(A-C)*** *Comparison of the average C/N change of transfected HEK293T cells with (A) ERK-KTR or Akt-KTR, (B) PMb-EphA1Cry2Δ and ERK-KTR or Akt-KTR, or (C) Cry2olig and ERK-KTR or Akt-KTR. (A) ERK-KTR and Akt-KTR included 10 min pre-stimulus imaging followed by EGF stimulation (blue arrow).) Error bars represent standard deviation; n=6 cells.*

Table AII.2. *Sample sequencing statistics and mapping sequence reads to reference human genome. Sample ID abbreviations: PMb-EphA1Cry2Δ (EphCry), No transfection (NTfect), EphrinA1-stimulated (NTfect EfnA1).*

Sample ID	*Total raw reads*	*Total base pairs (Mb)*	*Read pairs after quality control*	*Total Mapped Reads*	*Unique Mapped Reads*
EphCry *Dark-1*	77,370,938	23,211	63,040,968 (17.00%)	54,756,889 (86.85%)	53,356,775 (84.63%)
EphCry Dark-2	73,311,077	21,993	60,611,942 (15.58%)	52,843,089 (87/18%)	51,435,052 (84.85%)
EphCry Dark-3	75,799,837	22,740	61,819,119 (17.00%)	54,116,989 (87.54%)	52,720,176 (85.28%)
EphCry Light-1	61,926,810	18,578	51,228,279 (15.75%)	44,316,608 (86.50%)	43,225,952 (84.37%)
EphCry Light-2	114,192,841	34,258	92,078,622 (17.69%)	79,645,761 (86.49%)	77,682,269 (84.36%)
EphCry Light-3	55,245,898	16,574	45,335,964 (16.21%)	39,359,244 (86.81%)	38,348,956 (85.58%)
Cry2olig Dark-1	68,636,382	20,591	56,395,995 (16.12%)	52,223,530 (92.60%)	50,853,819 (90.17%)
Cry2olig Dark-2	72,924,627	21,877	59,666,822 (16.58%)	55,485,992 (92.99%)	53,982,994 (90.47%)
Cry2olig Dark-3	79,942,094	23,983	65,424,661 (16.53%)	60,787,351 (92.91%)	59,137,740 (90.39%)
Cry2olig Light-1	68,155,317	20,447	56,449,777 (15.48%)	52,187,093 (92.44%)	50,789,043 (89.97%)
Cry2olig Light-2	73,716,511	22,115	60,199,209 (16.74%)	55,689,885 (92.5%)	54,246,361 (90.11%)
Cry2olig Light-3	58,135,757	17,441	48,064,350 (15.65%)	44,337,006 (92.24%)	43,134,435 (89.74%)
NTfect Dark-1	76,443,824	22,933	63,599,318 (15.21%)	60,565,044 (95.229%)	58,923,204 (92.64%)
NTfect Dark-2	74,748,887	22,425	60,647,583 (17.29%)	57,871,139 (95.42%)	56,397,973 (92.99%)
NTfect Dark-3	69,151,722	20,746	56,226,744 (16.93%)	53,619,526 (95.36%)	52,059,334 (92.58%)
NTfect Light-1	68,610,548	20,583	57,193,159 (14.94%)	54,561,110 (95.39%)	53,003,674 (92.67%)
NTfect Light-2	57,142,002	17,143	46,599,450 (16.65%)	44,435,284 (95.35%)	43,334,086 (92.99%)
NTfect Light-3	66,989,771	20,097	54,542,038 (16.71%)	52,014,526 (95.36%)	50,631,169 (92.82%)
NTfect EfnA1-1	64,266,144	19,280	52,972,255 (15.75%)	50,504,148 (95.34%)	49,162,471 (92.80%)
NTfect EfnA1-2	70,477,357	21,143	59,103,993 (14.39%)	56,290,563 (95.23%)	54,843,489 (92.79%)
NTfect EfnA1-3	78,381,265	23,514	63,909,405 (16.73%)	60,977,478 (95.41%)	59,353,310 (92.87%)

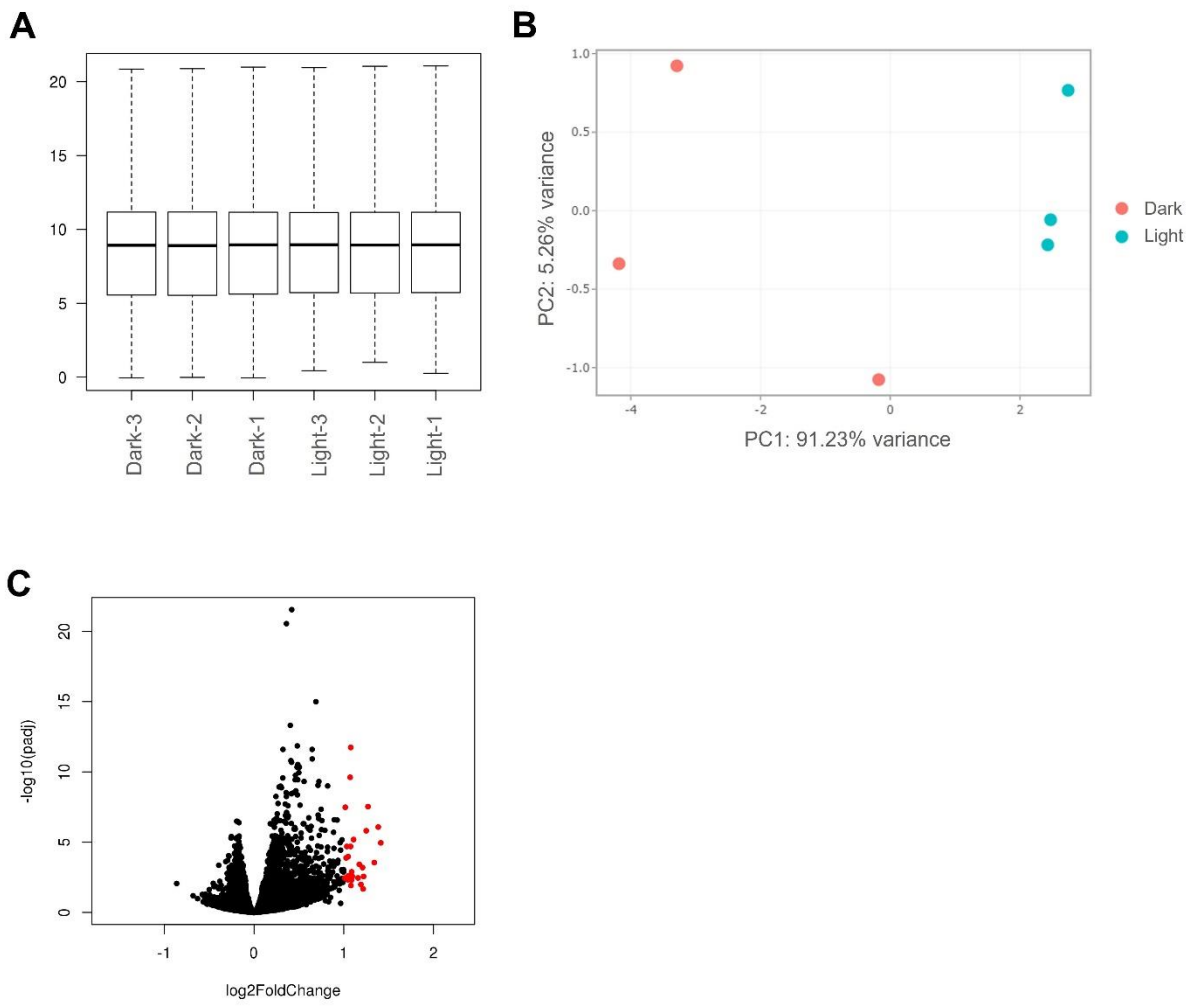

Figure AII.8. *RNA sequencing data for PMb-EphA1Cry2Δ dark vs. light control condition.* ***(A)*** *Distribution of read counts in libraries for dark and light condition were examined after normalization. The original read counts were normalized to adjust for various factors such as variations of sequencing yield between samples. These normalized read counts were used to accurately determine differentially expressed genes.* ***(B)*** *Principal component (PC) analysis between dark and light conditions shows differences between samples based on the distance matrix. Samples were projected to a 2D plane spanned by their first two principal components. The x-axis is the direction that explains the most variance, and the y-axis is the second most; the percentage of the total variance per direction is shown in the label.* ***(C)*** *The global*

transcriptional change across the groups compared was visualized by a volcano plot. Each data point in the scatter plot represents a gene. The log2 fold change of each gene is represented on the x-axis and the log10 of its adjusted p-value is on the y-axis. Un-regulated genes have an adjusted p-value less than 0.05 and a log2 fold change greater than 1, indicated by red dots. Down-regulated genes with an adjusted p-value less than 0.05 and a log2 fold change less than -1 are indicated by blue dots.

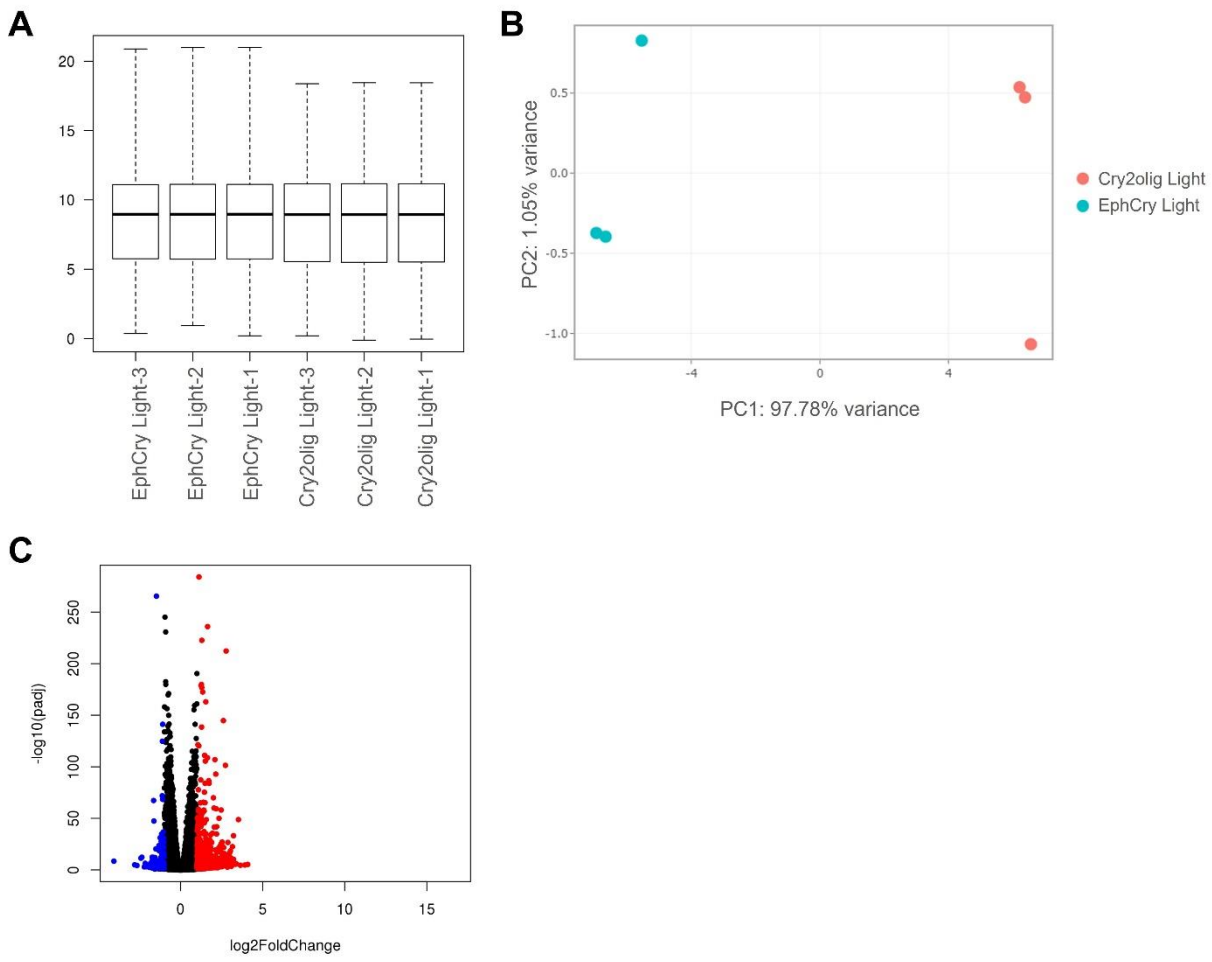

Figure AII.9. *RNA sequencing data for transfected PMb-EphA1Cry2Δ light vs. Cry2olig light condition.* ***(A)*** *Distribution of read counts in libraries for PMb-EphA1Cry2Δ (labeled EphCry) light and Cry2olig light condition was examined after normalization. The original read counts were normalized to adjust for various factors such as variations of sequencing yield between samples. These normalized read counts were used to accurately determine differentially expressed genes.* ***(B)*** *Principal component (PC) analysis between PMb-EphA1Cry2Δ light Cry2olig light conditions shows differences between samples based on the distance matrix. Samples were projected to a 2D plane spanned by their first two principal components. The x-axis is the direction that explains the most variance, and the y-axis is the second most; the percentage of the total variance per direction is shown in the label.* ***(C)*** *The global*

transcriptional change across the groups compared was visualized by a volcano plot. Each data point in the scatter plot represents a gene. The log2 fold change of each gene is represented on the x-axis and the log10 of its adjusted p-value is on the y-axis. Un-regulated genes have an adjusted p-value less than 0.05 and a log2 fold change greater than 1, indicated by red dots. Down-regulated genes with an adjusted p-value less than 0.05 and a log2 fold change less than -1 are indicated by blue dots.

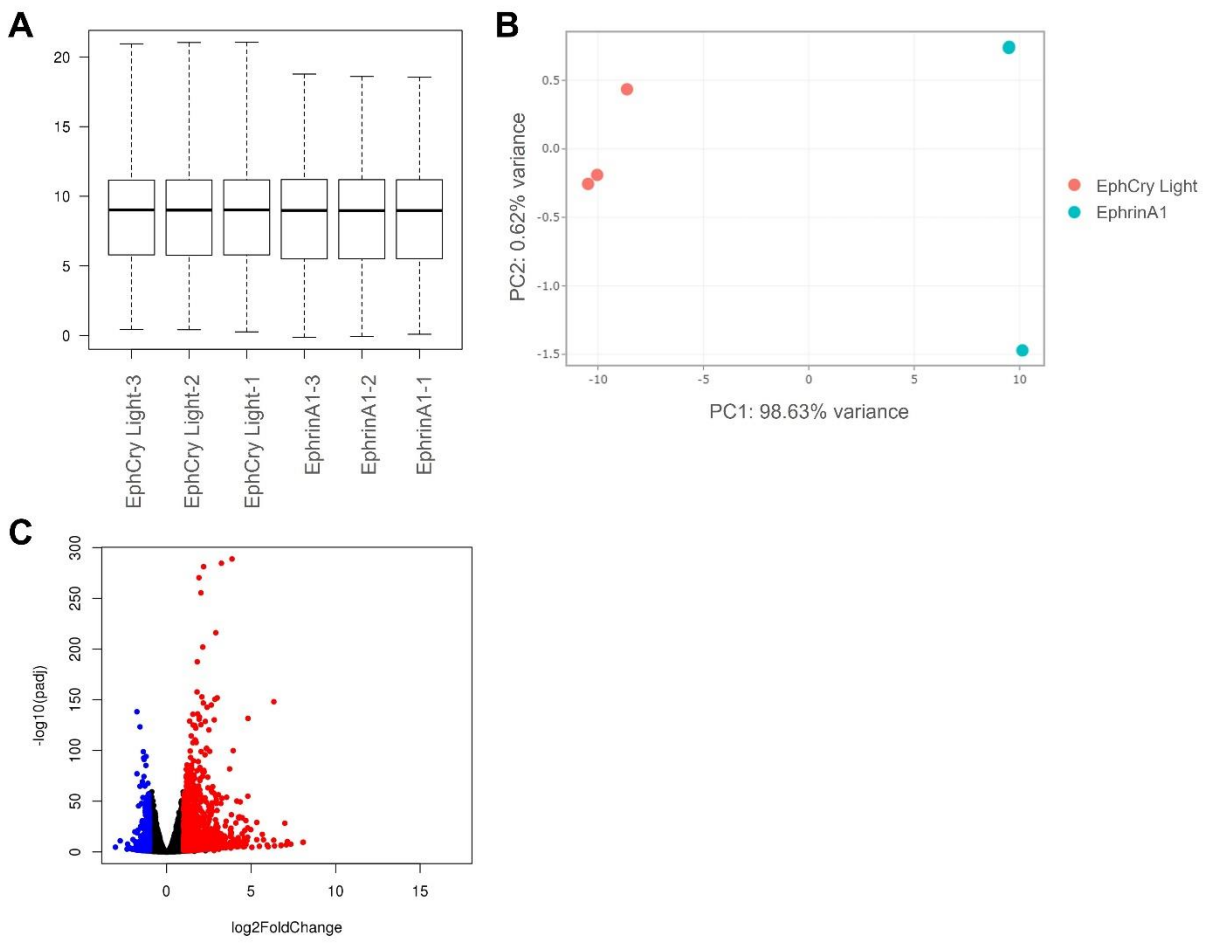

Figure AII.10. *RNA sequencing data for transfected PMb-EphA1Cry2Δ light vs. no transfection with ephrinA1-stimulated control condition.* ***(A)*** *Distribution of read counts in libraries for PMb-EphA1Cry2Δ (labeled EphCry) and ephrinA1-stimulated (labeled ephrinA1) condition were examined after normalization. The original read counts were normalized to adjust for various factors such as variations of sequencing yield between samples. These normalized read counts were used to accurately determine differentially expressed genes.* ***(B)*** *Principal component (PC) analysis between PMb-EphA1Cry2Δ and ephrinA1-stimulated conditions shows differences between samples based on the distance matrix. Samples were projected to a 2D plane spanned by their first two principal components. The x-axis is the direction that explains the most variance, and the y-axis is the second most; the percentage of the total variance per direction is*

shown in the label. ***(C)*** *The global transcriptional change across the groups compared was visualized by a volcano plot. Each data point in the scatter plot represents a gene. The log2 fold change of each gene is represented on the x-axis and the log10 of its adjusted p-value is on the y-axis. Un-regulated genes have an adjusted p-value less than 0.05 and a log2 fold change greater than 1, indicated by red dots. Down-regulated genes with an adjusted p-value less than 0.05 and a log2 fold change less than -1 are indicated by blue dots.*

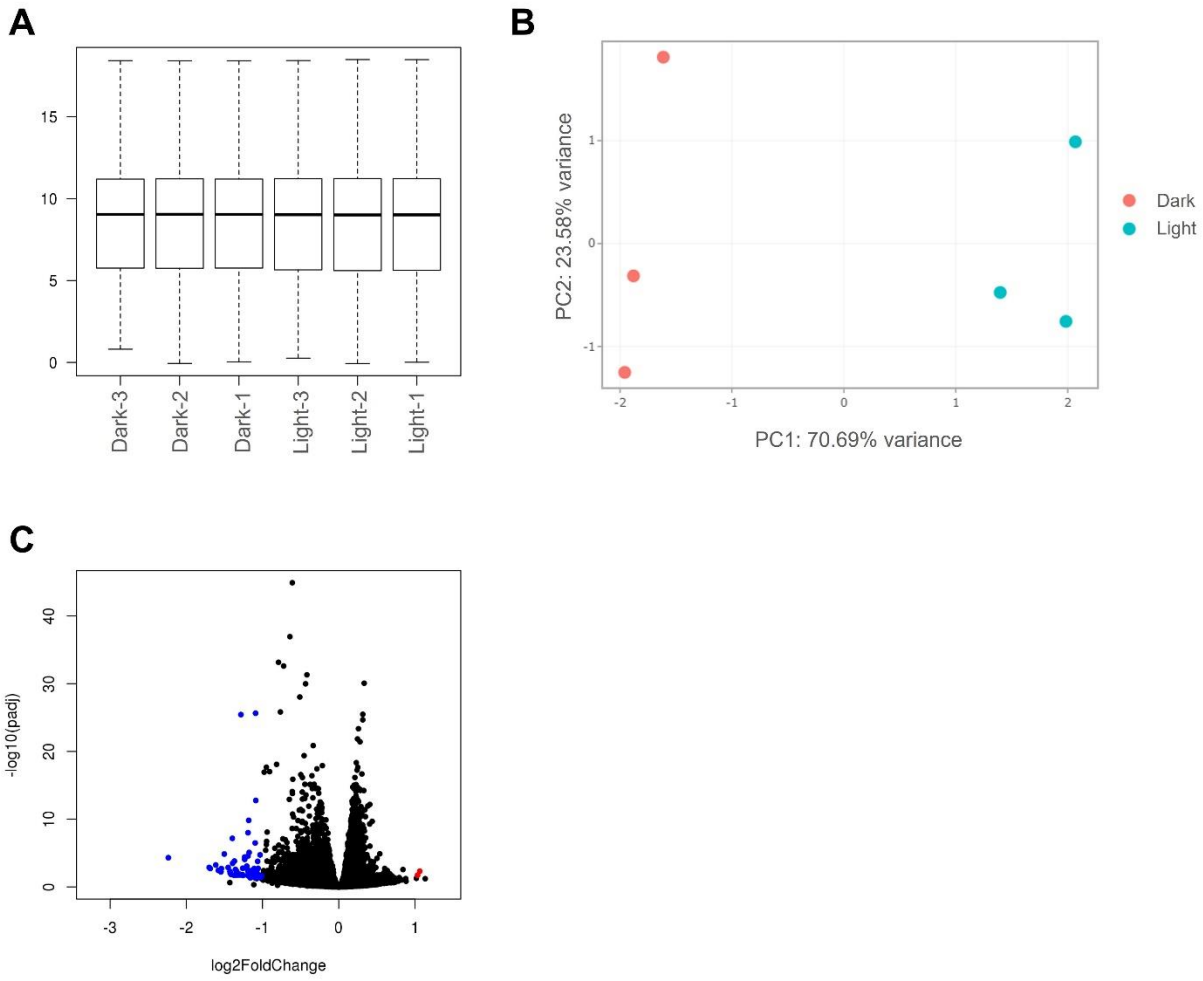

Figure AII.11. *RNA sequencing data for transfected Cry2olig dark vs. light control condition.* ***(A)*** *Distribution of read counts in libraries for dark and light condition were examined after normalization. The original read counts were normalized to adjust for various factors such as variations of sequencing yield between samples. These normalized read counts were used to accurately determine differentially expressed genes.* ***(B)*** *Principal component (PC) analysis between dark and light conditions shows differences between samples based on the distance matrix. Samples were projected to a 2D plane spanned by their first two principal components. The x-axis is the direction that explains the most variance, and the y-axis is the second most; the percentage of the total variance per direction is shown in the label.* ***(C)*** *The global*

transcriptional change across the groups compared was visualized by a volcano plot. Each data point in the scatter plot represents a gene. The log2 fold change of each gene is represented on the x-axis and the log10 of its adjusted p-value is on the y-axis. Un-regulated genes have an adjusted p-value less than 0.05 and a log2 fold change greater than 1, indicated by red dots. Down-regulated genes with an adjusted p-value less than 0.05 and a log2 fold change less than -1 are indicated by blue dots.

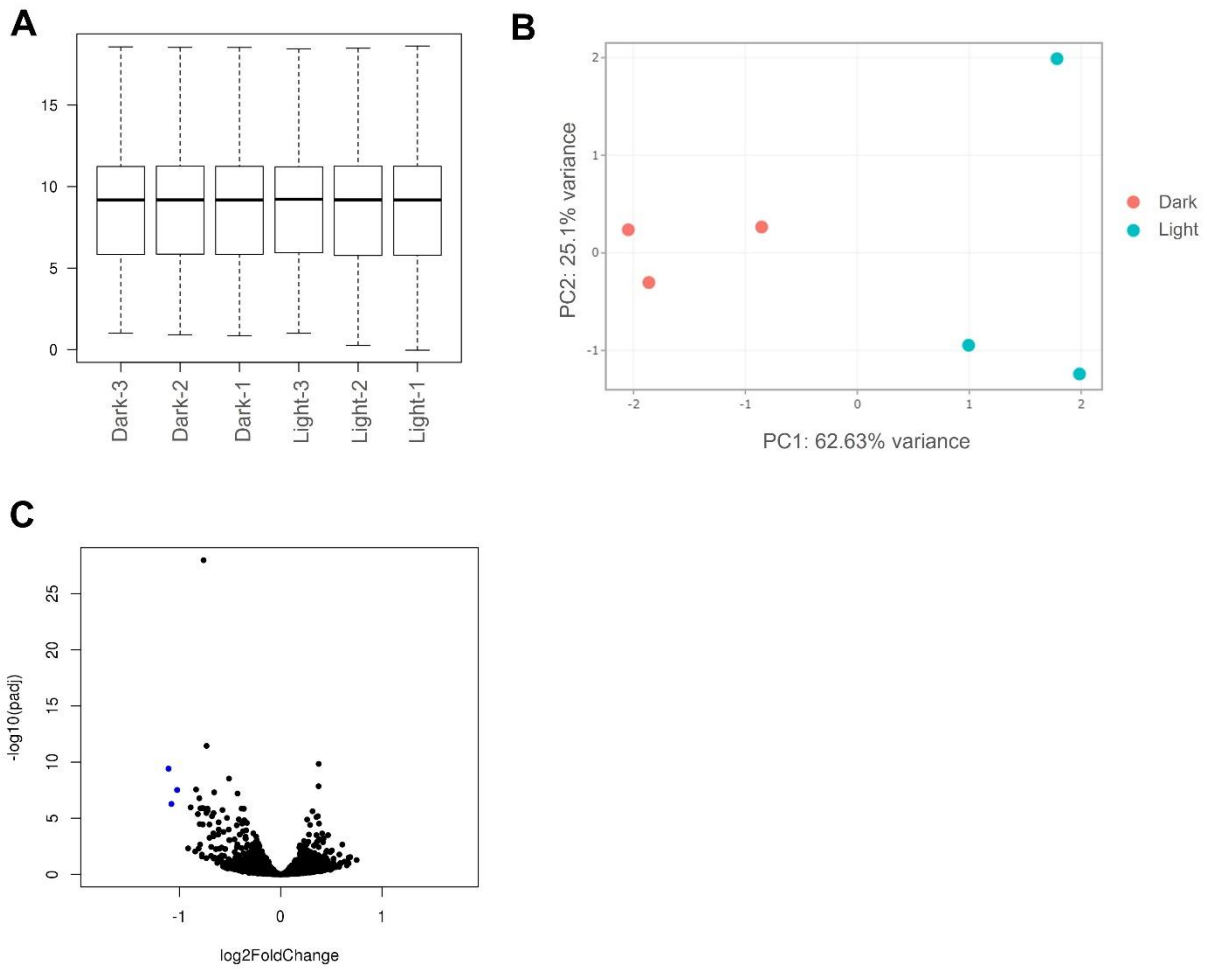

Figure AII.12. *RNA sequencing data for 'No Transfection' dark vs. light control condition.* ***(A)*** *Distribution of read counts in libraries for dark and light condition were examined after normalization. The original read counts were normalized to adjust for various factors such as variations of sequencing yield between samples. These normalized read counts were used to accurately determine differentially expressed genes.* ***(B)*** *Principal component (PC) analysis between dark and light conditions shows differences between samples based on the distance matrix. Samples were projected to a 2D plane spanned by their first two principal components. The x-axis is the direction that explains the most variance, and the y-axis is the second most; the percentage of the total variance per direction is shown in the label.* ***(C)*** *The global*

transcriptional change across the groups compared was visualized by a volcano plot. Each data point in the scatter plot represents a gene. The log2 fold change of each gene is represented on the x-axis and the log10 of its adjusted p-value is on the y-axis. Un-regulated genes have an adjusted p-value less than 0.05 and a log2 fold change greater than 1, indicated by red dots. Down-regulated genes with an adjusted p-value less than 0.05 and a log2 fold change less than -1 are indicated by blue dots.

Table AII.3. *The top downregulated and the two upregulated significant DEGs for Cry2olig light condition compared to its dark condition.*

Gene Name	*Log2FoldChange*	*Adj p-value*
MUC6	-1.55	0.01
TAS2R6P	-1.54	0.00
FAM215B	-1.45	0.00
ESRP2	-1.43	0.01
ERCC-00039	-1.42	0.01
TGFBR3L	1.03	0.02
KIAA0825	1.06	0.00

Table AII.4. *Significant DEGs for no transfection light condition compared to its dark condition.*

Gene Name	*Log2FoldChange*	*Adj p-value*
CNIH3	-1.11	0.00
MT-TY	-1.02	0.00
MTCO2P12	-1.08	0.00

Table AII.5. *Ontological process names, the genes associated with each process, and the adjusted p-values (adj p-value) for each process ($p < 0.05$) of PMb-EphA1Cry2Δ dark vs. light condition. Each process is up-regulated in PMb-EphA1Cry2Δ light condition compared to its dark condition.*

Ontological Process	***Genes***	***Adj p-value***
ATP biosynthetic process	MT-ATP6, MT-ATP8	0.00
Mitochondrial ATP synthesis coupled proton transport	MT-ATP6, MT-ATP8	0.00
Hydrogen ion transmembrane transport	MT-CYB, SLC9A3	0.00
Phosphate ion transport	SLC34A3	0.02
Cellular phosphate ion homeostasis	SLC34A3	0.02
Sodium-dependent phosphate transport	SLC34A3	0.02
Mitochondrial electron transport, ubiquinol to cytochrome c	MT-CYB	0.02
Sodium ion import across plasma membrane	SLC9A3	0.02
Phosphate ion transmembrane transport	SLC34A3	0.02
Cellular respiration	MT-ND1	0.02
Cellular phosphate ion homeostasis	SLC9A3	0.03
Mitochondrial electron transport, NADH to ubiquinone	MT-ND1	0.04

Table AII.6. *Ontological process names, the number of genes associated with each process, and the adjusted p-values (adj p-value) for each process ($p < 0.05$) of PMb-EphA1Cry2Δ light vs. Cry2olig light conditions. Each process is up-regulated in PMb-EphA1Cry2Δ light condition compared to the Cry2olig light condition.*

Ontological Process	***Gene Count***	***Adj p-value***
Nucleosome assembly	15	0.00
Response to cAMP	8	0.01
Cell differentiation	25	0.01
Platelet degranulation	10	0.02
Response to hydrogen peroxide	7	0.02
Positive regulation of apoptotic process	18	0.02
Response to glucocorticoid	8	0.02
Inflammatory response	20	0.03
Synaptic transmission, cholinergic	6	0.04

Table AII.7. *Ontological process names, the number of genes associated with each process, and the adjusted p-values (adj p-value) for each process ($p < 0.05$) of PMb-EphA1Cry2Δ light vs. ephrinA1-stimulated conditions. Each process is up-regulated in PMb-EphA1Cry2Δ light condition compared to the ephrinA1-stimulated condition.*

Ontological Process	***Gene Count***	***Adj p-value***
Regulation of transcription, DNA-templated	129	0.00
Transcription, DNA-templated	164	0.00
Positive regulation of transcription from RNA polymerase II promoter	74	0.00
Cilium-dependent cell motility	7	0.00
Response to cAMP	11	0.00
Response to drug	29	0.00
Response to virus	16	0.01
Transcription from RNA polymerase II promoter	41	0.01
Negative regulation of transcription from RNA polymerase II promoter	51	0.01
Cilium movement	8	0.01
Inflammatory response	32	0.01
Positive regulation of apoptotic process	26	0.02
Oxidation-reduction process	43	0.02
Response to hydrogen peroxide	9	0.03
Positive regulation of gene expression	23	0.04
Cell differentiation	34	0.04
Nucleosome assembly	12	0.04
Positive regulation of cell proliferation	34	0.04

Movie AII.1. *Fluorescence widefield microscopy of PMb-EphA1Cry2Δ light activation in HEK293T cells. Whole cell activation of PMb-EphA1Cry2Δ results in construct clustering at the membrane in response to blue light, which is reversible after removal of blue light. Images acquired every 30 s (553 nm; 200 ms exposure). Blue light activation (480 nm, 50 ms pulse) protocol: 0:00 to 5:30 min:s (blue light pulse every 30 s); 6:00 to 16:00 min:s (no blue light). Scale bar: 10 µm.*

Movie AII.2. *Confocal microscopy of PMb-EphA1Cry2Δ light activation with ERK-KTR and DAPI nuclear stain in HEK293T cells. Simultaneous PMb-EphA1Cry2Δ activation and imaging of ERK-KTR with 488 nm laser (5% power) occurs every 30 s over 30 min. Left panel: mCherry channel showing PMb-EphA1Cry2Δ activation. Middle panel: DAPI channel showing stain of nucleus. Right panel: mNeonGreen channel showing ERK-KTR translocation. Images acquired every 30 s (553 nm; 5% power). Scale bar: 10 µm.*

Movie AII.3. *Fluorescence widefield microscopy of PMb-EphA1Cry2Δ light activation in the neuronal-like processes of Neuro2A cells. Images acquired every 30 s (553 nm; 200 ms exposure). Blue light activation (480 nm, 50 ms pulse) protocol: 0:00 to 5:00 min:s (no blue light); 5:30 – 15:30 min:s (blue light pulse every 30 s); 16:00 – end min:s (no blue light). Scale bar: 10 µm.*

Appendix III: Supporting Information for Chapter 3: CRY-BARs: Versatile light-gated molecular tools for the remodeling of membrane architectures

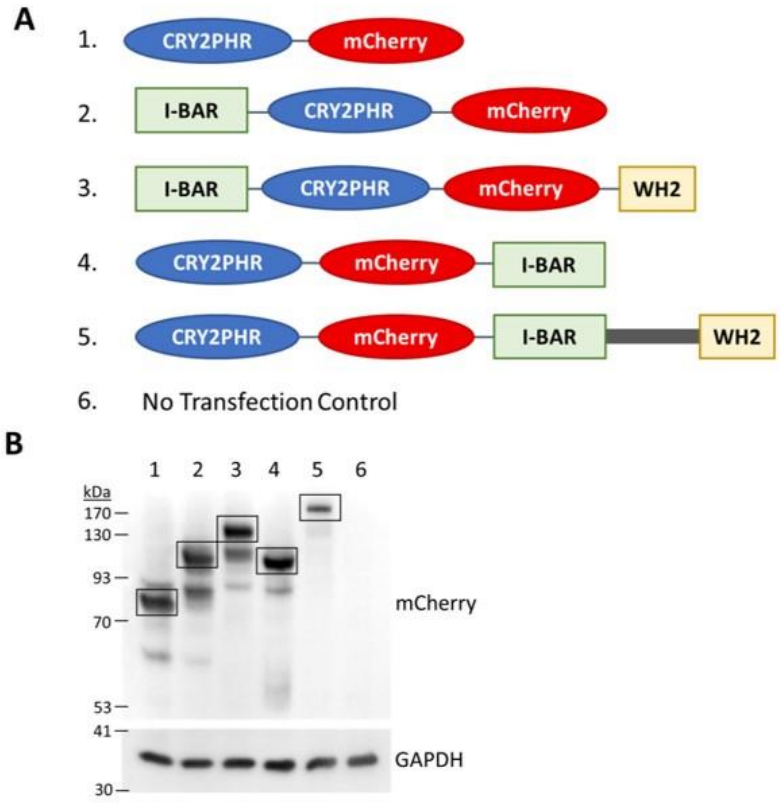

Figure AIII.1. *CRY-BAR construct design and expression.* ***(A)*** *diagrams of the CRY-BAR protein fusions; Constructs 2, 3, and 4 contain portions of the MTSS-1 protein (I-BAR, WH2, or both); Construct 5 contains the full length MTSS-1 protein.* ***(B)*** *lysates of HEK293T cells transfected with CRY-BAR constructs and controls (Lanes 1–6, numbers correspond to panel A) were Western blotted with anti-mCherry antibody. Boxes indicate the apparent molecular weights: 1. 85 kDa; 2. 111 kDa; 3. 130 kDa; 4. 111 kDa; 5. 168 kDa; 6. No transfect control. The Western blot is representative of four independent trials.*

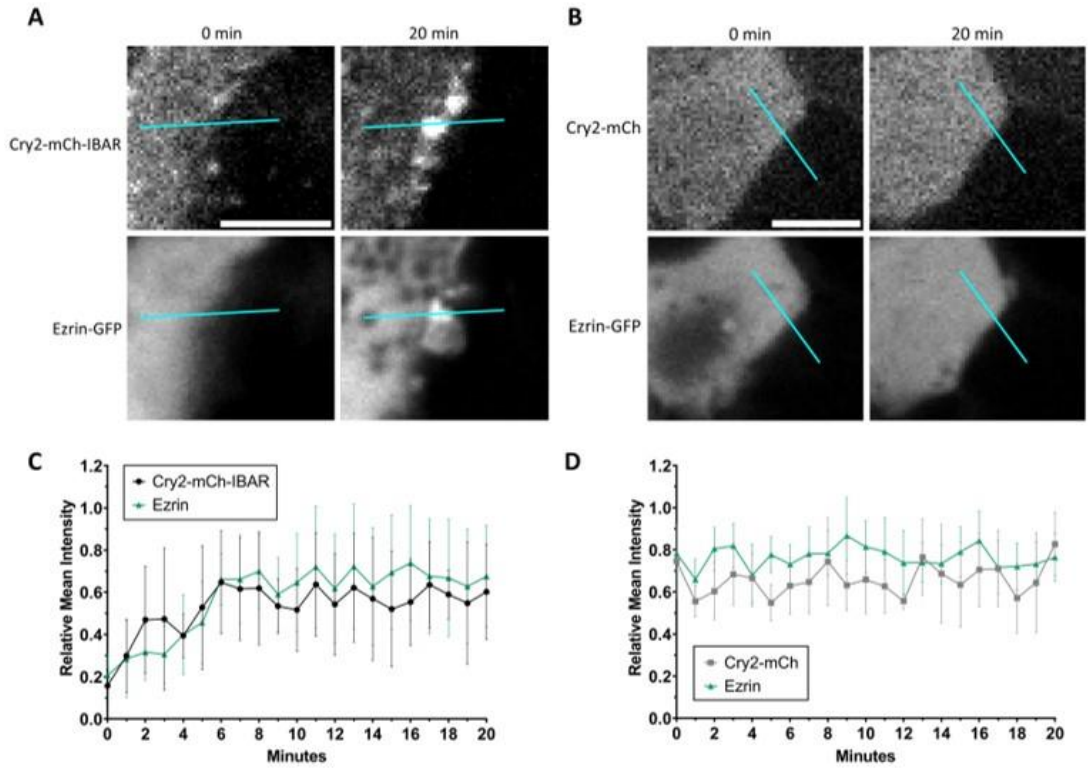

Figure AIII.2*. Temporal relationship of Cry2-mCh-IBAR and Ezrin-GFP localization.* ***(A)*** *HEK293T cells transfected with Cry2-mCh-IBAR and Ezrin-GFP were illuminated every 30 s with 488 nm light (5% power) on a confocal microscope over 20 min to assess their localization patterns in response to light activation of Cry2. Areas at the membrane exhibiting colocalization of Cry2-mCh-IBAR and Ezrin-GFP were analyzed for intensity over time by conducting a 6 micron line scan (cyan) ranging from the cytosol, through the membrane, to outside of the cell. Scale bar = 5 microns.* ***(B)*** *HEK293T cells transfected with Cry2-mCh and Ezrin-GFP were imaged similarly to (A). Co-expressing cells were analyzed for intensity over time using a line scan (cyan) as described in (A). Line length: 6 microns. Scale bar = 5 microns.* ***(C)*** *Plot of intensity at the membrane (around 3 micron point of line) over the intensity in the cytosol (at the cytosolic end of line) from line analysis shown in (A).* ***(D)*** *Plot of intensity at the membrane (around 3 micron point of line) over the intensity in the cytosol (at the cytosolic end of line) from*

line analysis shown in (B). For (C) and (D), each point of intensity was taken at time 0 min of light exposure and then in 1 min increments for a total of 20 min (n = 6 cells). Membrane to cytosol ratios were normalized for intensity for each time point before averaging (error bars = standard deviation)

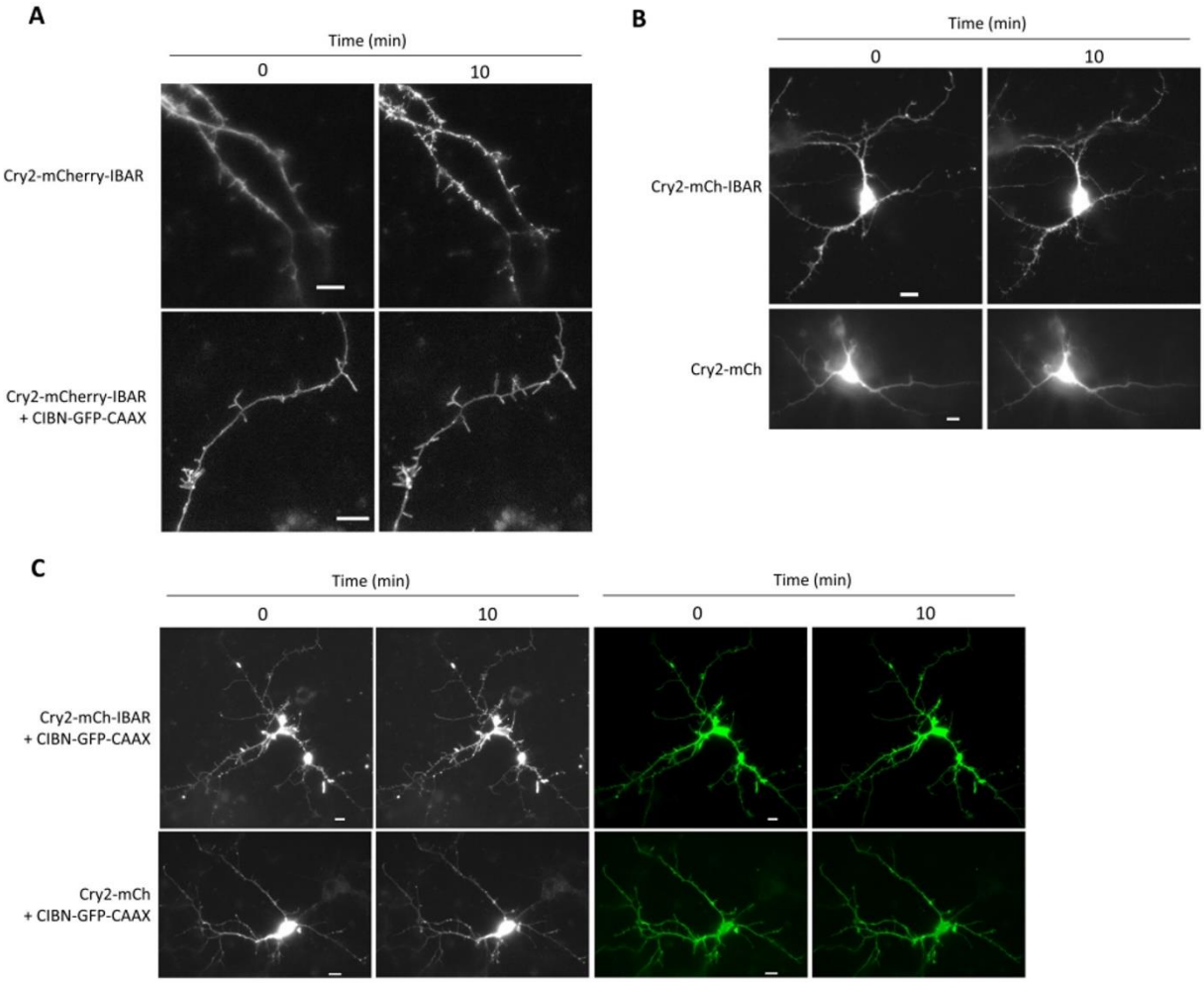

Figure AIII.3. *Global activation of CRY-BAR in hippocampal neurons.* ***(A)*** *Neurons transfected with Cry2-mCh-IBAR; and co-transfected with Cry2-mCh-IBAR and CIBN-GFP-CAAX were illuminated every 30 s with 470 nm light on a widefield microscope. After 10 min, Cry2-mCh-IBAR forms numerous clusters throughout the neuronal processes, whereas in the presence of CIB, no such clusters are formed. Scale bar = 10 microns.* ***(B)*** *Full view of neurons transfected with Cry2-mCh-IBAR or Cry2-mCh. Neurons were illuminated every 30 s with 470 nm light on a widefield microscope. Scale bar = 10 microns.* ***(C)*** *Full view of neurons co-transfected with CIBN-GFP-CAAX (right; green) and Cry2-mCh-IBAR or Cry2-mCh (left; grey). Neurons were illuminated every 30 s with 470 nm light on a widefield microscope. Scale bar = 10 microns.*

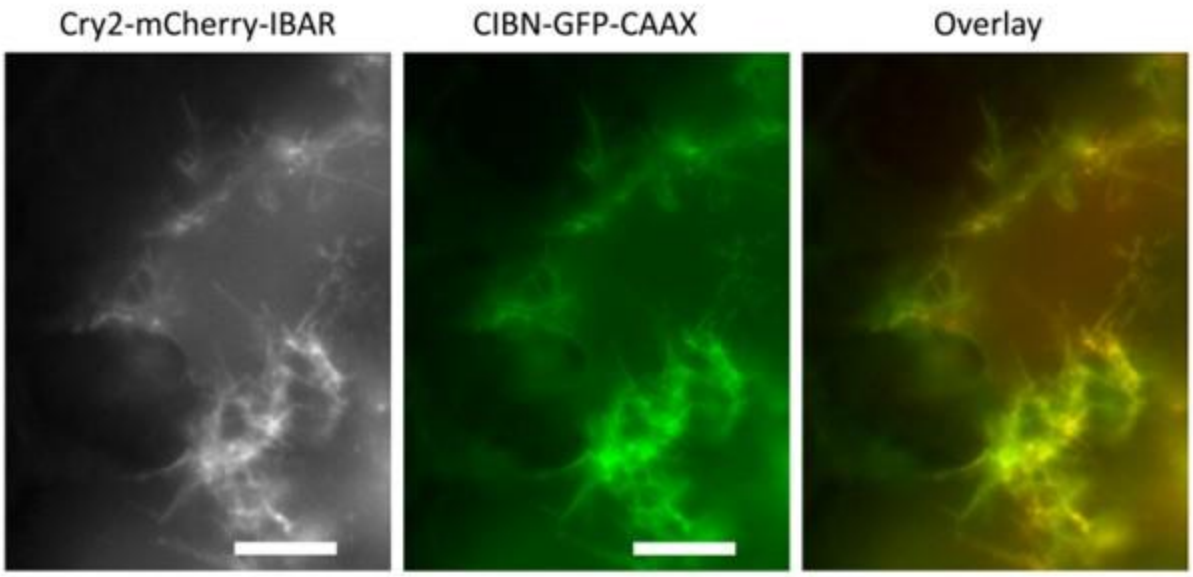

Figure AIII.4*. Dark localization of Cry2-mCh-IBAR and CIB-GFP-CAAX. HEK293T cells transfected with Cry2-mCh-IBAR and CIBN-GFP-CAAX were imaged sequentially (mCherry followed by GFP) to assess their localization patterns prior to light activation of Cry2. Both constructs have similar patterns of plasma membrane localization. Scale bar = 10 microns*

Movie AIII.1A. *Fluorescence widefield microscopy of Cry2-mCh-IBAR light activation in HEK293T cells. Whole cell activation of Cry2-mCh-IBAR results in filopodial clustering and retraction. Images acquired every 30 s (553 nm; 200 ms exposure). Blue light activation (470 nm, 50 ms pulse) protocol: 0:00 to 5:30 min:s (no blue light); 6:00 to 16:30 min:s (blue light pulse every 30 s); 17:00 – end min:s (no blue light)*

Movie AIII.1B*. Fluorescence widefield microscopy of Cry2-mCh-IBAR light activation in HEK293T cells; this movie shows alternate focal plane to highlight filopodial localization. Whole cell activation of Cry2-mCh-IBAR results in filopodial clustering and retraction. Images acquired every 30 s (553 nm; 200 ms exposure). Blue light activation (470 nm, 50 ms pulse)*

protocol: 0:00 to 4:30 min:s (no blue light); 5:00 to 19:30 min:s (blue light pulse every 30 s); 17:00 – end min:s (no blue light)

***Movie AIII.2**. Fluorescence widefield microscopy of Cry2-mCh-IBAR light activation in HEK293T cells; zoomed in region to show clustering at cell edge in detail and reversibility over a longer dark recovery timecourse (30 min) than shown in Movie S1A. Whole cell activation of Cry2-mCh-IBAR results in filopodial clustering and retraction. Images acquired every 30 s (553 nm; 200 ms exposure). Blue light activation (470 nm, 50 ms pulse) protocol: 0:00 to 5:00 min:s (no blue light); 5:30 to 16:00 min:s (blue light pulse every 30 s); 16:30 to 46:00 min:s (no blue light)*

***Movie AIII.3**. Localized Cry2-mCh-IBAR light activation in HEK293T cells with confocal microscope. Three ROIs (shown at beginning of movie) subjected to selective activation with 488 nm laser (5% power). Light pulse applied at 4:00 min:s*

***Movie AIII.4**. Side-by-side movies showing fluorescence widefield microscopy of CRY-BAR(s) light activation in HEK293T cells; whole cell activation results in filopodial clustering and retraction in Cry2-mCh-IBAR (100% observed in 51 cells pooled from 8 replicates) and in IBAR-Cry2-mCh (98% observed in 44 cells pooled from 6 replicates); whereas IBAR-Cry2-mCh-WH2 (96% observed in 52 cells pooled from 7 replicates) remains cytosolic during light activation and does not impact filopodia. Images acquired every 30 s (553 nm; 200 ms exposure). Blue light activation (470 nm, 50 ms pulse) protocol: 0:00 to 5:00 min:s (no blue light); 5:30 to 16:00 min:s (blue light pulse every 30 s); 16:30 to 46:00 min:s (no blue light)*

Movie AIII.5*. Confocal microscopy of Cry2-mCh-IBAR light activation in presence of Actin-GFP in HEK293T cell. Simultaneous activation and imaging of GFP with 488 nm laser (5% power) occurs every 30 s. Rightmost panel shows overlay of Cry2-mCh-IBAR (red) with Actin-GFP (green)*

Movie AIII.6*. Fluorescence widefield microscopy of Cry2-mCh-IBAR/CIBN-GFP-CAAX light activation in neuronal process. Blue light activation (470 nm, 50 ms pulse) protocol: 0:00 to 5:00 min:s (no blue light); 5:30 – end min:s (blue light pulse every 30 s)*

Movie AIII.7*. Fluorescence widefield microscopy of Cry2-mCh-IBAR light activation in neuronal process. Blue light activation (470 nm, 50 ms pulse) protocol: 0:00 to 5:00 min:s (no blue light); 5:30 – end min:s (blue light pulse every 30 s)*

Movie AIII.8*. Localized Cry2-mCh-IBAR light activation in neuronal process with confocal microscope. Three ROIs (shown at beginning of movie) subjected to selective activation with 488 nm laser (5% power). Light pulse applied at 4:00 min:s*